ALGORITHM FOR EARTHQUAKE EARLY WARNING SYSTEM

Ph.D. THESIS

by

RAKHI BHARDWAJ

DEPARTMENT OF EARTHQUAKE ENGINEERING
INDIAN INSTITUTE OF TECHNOLOGY ROORKEE
ROORKEE-247667 (INDIA)
October, 2013

ALGORITHM FOR EARTHQUAKE EARLY WARNING SYSTEM

A THESIS

Submitted in partial fulfilment of the
requirements for the award of the degree
of
DOCTOR OF PHILOSOPHY
in
EARTHQUAKE ENGINEERING

by

RAKHI BHARDWAJ

DEPARTMENT OF EARTHQUAKE ENGINEERING
INDIAN INSTITUTE OF TECHNOLOGY ROORKEE
ROORKEE-247667 (INDIA)
October, 2013

INDIAN INSTITUE OF TECHNOLGY ROORKEE
ROORKEE

CANDIDATE'S DECLARATION

I hereby certify that the work which is being presented in the thesis entitled "**ALGORITHM FOR EARTHQUAKE EARLY WARNING SYSTEM"** in partial fulfilment of the requirements for the award of the Degree of Doctor of Philosophy and submitted in the Department of Earthquake Engineering, Indian Institute of Technology Roorkee, Roorkee is an authentic record of my own work carried out during a period from July, 2009 to October, 2013 under the supervision of Prof. Ashok Kumar and Prof. M. L. Sharma, Department of Earthquake Engineering, Indian Institute of Technology Roorkee, Roorkee.

The matter presented in this thesis has not been submitted by me for the award of any other degree of this or any other Institute.

(RAKHI BHARDWAJ)

This is to certify that the above statement made by the candidate is correct to the best of our knowledge.

(M. L. Sharma)
Supervisor

(Ashok Kumar)
Supervisor

Date: October , 2013

The Ph. D. Viva-Voce Examination of **Ms**. **Rakhi Bhardwaj**, Research Scholar, has been held on ……

Signature of Supervisor's Chairman, SRC Signature of External Examiner

Head of the Department/Chairman, ODC

ABSTRACT

Earthquake Early Warning (EEW) system is considered as one of the real-time earthquake damage mitigation measures, which detects, analyses and transmits information of the impending ground shaking prior to the arrival of seismic waves at the potential user sites. The warning time is used to minimize property damage, loss of lives and to aid emergency response. Such systems can be broadly classified as regional and onsite warning systems. While Regional warning approach is network based, the Onsite warning approach uses single station observations for parameter estimation to provide quick warning. The countries like Japan and Mexico have developed the real-time operating EEW systems and are capable of issuing public warnings. Such systems are in preliminary stage of planning in India albeit having comparable seismic hazard to those countries or regions where such systems have been successfully implemented and functioning. The past and the contemporary seismicity reported from Himalaya region and the risk for the cities falling in the vicinity of this seismically active region implicitly require EEW system for Northern Indian region as a mitigation measure. Hence, an attempt has been made in the present study, to understand EEW, develop new EEW parameters, develop a multi parameter based EEW algorithm for accurate and reliable EEW, size estimation during the issuance of warning and propose EEW system for disaster mitigation in seismically active Northern Indian region.

The basic requirement of an EEW system is the development of a real-time algorithm for fast calculation of earthquake source parameters and the estimation of their reliability. The EEW algorithm automatically detects the P-onset followed by the estimation of location, magnitude and intensity of the event. The instrumentation density deployed in the seismic active area along with the network deign to be used in an EEW system is also an integral part of the system which affects performance of the system. Initially, status of EEW system in different countries with respect to their development, implementation, and social resilience has been studied followed by a detailed review of several EEW parameters, methodologies and systems present worldwide which has helped in marking the research gaps.

In the present study, a new EEW parameter called Root Sum of Squares Cumulative Velocity (RSSCV) has been introduced, which is a function of velocity of the incoming time series and in turn represents the energy component in the time series. The

robustness of this parameter has been shown by detecting the P-onset in real-time based on RSSCV and also using it as one of the parameters for issuing warning. The comparison with classical amplitude based (STA/LTA type) approaches RSSCV has better performed in case of higher magnitudes which supports its use for EEW systems. Therefore, in the developed EEW algorithm, RSSCV parameter has been used for auto P-picking and warning threshold estimation as well.

The strong motion data set for the study compiled from Indian regions reveals the paucity to carry out the regression analysis for development of EEW algorithm. Therefore, data has been imported for the present study from regions like Japan, where K-NET has produced strong motion data from active seismic region having dense network and Pacific Earthquake Engineering Research Centre-Next Generation Attenuation Project Strong Motion Dataset **(**PEER-NGA).

The dataset for development of multi-parameter algorithm taken from K-NET seismic array in Japan consists of 1726 records from 105 events having $5 \leq M \leq 7.2$ with epicentral distance ≤ 60 km. To indigenize the developed EEW algorithm using Japanese dataset, Indian strong motion data has been taken from four different regions namely Region-1: North West Himalaya (Himachal Himalayas); Region-2: Uttarakhand region (Garhwal and Kumaoun Himalaya); Region-3: National Capital Region (consisting of Delhi-Haridwar Ridge region) and Region-4: North East Himalaya (North East Indian region). Indian dataset comprises of 51 digital records of 28 events within epicentral distance upto 60 km and magnitude range varying between 3.3 to 6.8. To further validate the algorithm on worldwide dataset, the data has been taken from countries such as Southern California, Taiwan and Turkey which consists of 219 earthquake records of 14 earthquakes having magnitude range of $4.27 \leq M \leq 7.62$ within 60 km of epicentral distance.

The reliable issuance of warning by EEW system depends upon the accuracy and reliability of predicted parameters used to define the size of the incoming event in real time. Such parameters are estimated using the analyses of initial portion of earthquake records. In the present study, not only the individual parameters such as Maximum Predominant Period (τ_p^{max}), Average Period (τ_c), Peak Displacement (P_d), Cumulative Absolute Velocity (CAV**)** and RSSCV have been used to develop an algorithm but also various combinations have been attempted to issue alarm and estimate magnitude with reliable accuracy in minimal time window. The estimated parameters are empirically

regressed with the apriori known catalogue magnitude of the event at variable time windows starting from 1 sec to 5 sec to determine threshold values for the considered parameters to issue warning for event having $M \geq 6$. For example, for a time window of 4 sec the threshold values of parameters are found to be 1.1 sec for τ_p^{max}, 1.42 sec for τ_c, 0.95 cm for P_d, 23 cm/sec for CAV and 5.2 cm/sec for RSSCV, respectively. The threshold values calculated for issuing warning at different time windows have been compared with the threshold values suggested by other researchers and a close match has been noticed.

The criterion for issuing warning is based on the alarm status of nearest four stations within selected epicentral distance of the event. Out of these four when three stations cross the preset threshold value of an EEW parameter alarm is issued. Based on the correctness of the issued alarm, the efficiency of the system is evaluated by classifying the alarms into Correct Alarm (CA), Missed Alarm (MA), Correct All Clear (CAC) and False Alarm (FA). Further, the developed algorithm also includes the multi-parameter approach for issuing warning. Under this approach, the status of CA/MA/CAC/FA has been tested on various possible combinations of considered parameters. The combinations of EEW parameter preference based approaches include three, four, five and logic combination of EEW parameters preference based approach which has been tested at five different time windows. The three parameter preference based approach has been found to be most efficient at a time window of 4 sec. Under this approach if three out of five EEW parameters show similar alarm status, the event has been marked with the same status.

After issuing the warning for high magnitude event, the algorithm further explores the data for more accurate estimation of magnitude using Brune's model based approach. Brune's model has been fitted on initial P-wave data after P-onset at different time windows starting from 1 sec to 10 sec for estimating spectral parameters such as low frequency spectral level, corner frequency and cutoff frequency for calculating the seismic moment and in turn moment magnitude (M_w). The residuals with respect to window length reveal the direct proportionality of the length with accuracy of magnitude estimation. In case of EEW system, the trade-off between accuracy and time plays an important role where a way has to be adopted that provides reliable magnitude estimation in acceptable limits of time. The study has concluded that a time window of 5 sec gives an uncertainty of ±0.3 in magnitude estimation which is considered to be an optimal time to confirm the magnitude of the issued warning.

The status of seismic hazard in Northern India and the risk associated with the cities around Himalayas reveal that the region between MCT and MBT is the zone of large numbers of seismogenic sources which establish the need for installing an EEW system for Northern India. The instrumentation and network connectivity for the EEW system have also been proposed in the present study followed by the calculation of possible lead time for the cities in northern India such as Dehradun, Hardwar, Roorkee, Muzaffarnagar, Meerut and Delhi. It is found that for all the cities the time available for alarm varies from 5 sec to 90 sec which is substantial time to act for saving human lives and for activation of emergency response measures such as immediate shutdown of industrial units, nuclear power plants, gas lines, pipelines, computers and slow down high speed train. The use of EEW system as a real time risk reduction measures for Northern Indian region for disaster mitigation and management can never be over emphasized. It is envisaged that this work of multi-parameter EEW algorithm will be suitably utilized in EEW systems in India.

ACKNOWLEDGEMENT

The completion of this thesis would not have been possible without the divine grace of **Almighty,** who has given me the strength and determination to carry out this research work. I take this opportunity to thank a number of people who have provided me encouragement during the tough journey of the thesis.

First of all, I would like to express my gratitude to **Prof. Ashok Kumar** and **Prof. M. L. Sharma** for their invaluable supervision, advice, and guidance from the first stage of this research. Above all and most needed, they provided me unflinching support in various ways.

I am deeply grateful to my supervisor **Prof. Ashok Kumar** for his outstanding outlook, wise guidance and invaluable advices. His enthusiastic attitude, ingenious suggestions, hardworking nature and the excellent programming skills have been the backbone of my research work. His constant involvement with complete dedication, constructive comments, pleasant disposition, has inspired me for the successful completion of this thesis. His imagination has nourished and strengthens my logical thinking that I will benefit from, for a long time to come.

I would also like to express my special gratitude to **Prof. M. L. Sharma** for his excellent supervision, liberal guidance and caring parental attitude, which I received so spontaneously and lavishly throughout the work of my thesis. His truly scientific vision, incisive intellect and maestro ability has made him a rich source of new ideas and knowledge, which exceptionally inspired and enriched my growth as a researcher. He always shown persistent zeal for my work and his careful revision of this thesis has improved its quality considerably. I humbly acknowledge a life time's gratitude to him.

A number of people and organizations have provided necessary help and financial support for the completion of this thesis and it gives me great pleasure to thank them.

I wish to thank Head, Department of Earthquake Engineering, IIT Roorkee for providing facilities to conduct this work smoothly. I also gratefully thank **Dr. A. Joshi** and **Dr. S. C. Gupta** for excellent technical advice time to time to improve the quality of this work. I would like to thank **Dr. J. Das**, especially for his kind help and support in GIS plotting.

I would also like to acknowledge **Prof. Ashwani Kumar** and **Dr. J. P. Narayanan,** for their excellent teaching on the subject 'Engineering Seismology', which has helped me a lot to understand the subject thoroughly.

The data used in the present study have been acquired by Indian Institute of Technology Roorkee (IITR) under various project sponsored by Ministry of Earth Sciences, Government of India, Kyoshin Network (K-NET) of Japan and Pacific Earthquake Engineering Research Center-Next Generation Attenuation Project dataset (PEER-NGA). The financial assistance support for carrying out this work from Ministry of Human Resource Department (MHRD) is thankfully acknowledged.

I wish to express my deep regards to all the school teachers, who cemented my steps to make the lucrative triumph possible.

I feel very happy to thank my fellow researchers and friends, Dr. Arjun Kumar, Dr. Ashish Harbindu, Dr. Himanshu Mittal, Dr. Ranjit Das, Rajiv Sachdeva, Pushpa Kumari, Pooja Mishra, Kanika Sharma, Sudesh Bhalothia, Meera Rawat, Priyanka Sharma, Divya Mishra Painuli and Dr. Shashi Chaudhary for their sincere support and encouragement throughout my stay at IITR, Roorkee. I would like to give a special thanks to Shrabony Adhikary for her sincere support and help.

Expression of encomium is due to my guide's family for providing homely ambience and ardent moral support.

I express love and gratitude to my entire family member specially my loving father, S**atya Prakash Sharma** my dear mother, **Veena Sharma** who are the constant source of zeal to make this dream come true. I also wish to thank my elder brother, bhabhi, sister, and in-laws especially my Mother-in-law, **Sharda Devi** for the love, affection, blessings, cooperation, prudence and encouragement in my academic pursuit and blooming future.

I am thankful to my husband, **Praveen Kumar Bhardwaj** for his unending patience, love, understanding and constant motivation during my research work. His sense of humour has always helped me to overcome the difficult phases. He deserves a special mention since his constant support has shown this work the light of the day.

Finally, I would like to thank everybody who directly and indirectly participated in the successful realization of this thesis.

RAKHI BHARDWAJ

CONTENTS

LIST OF FIGURES

LIST OF TABLES

LIST OF NOTATIONS

M_{P_d}	Magnitude calculated using P_d parameter
τ_{i_0}	Time at i_o^{th} instant
τ_i	Average period at i^{th} instant
Δ	Epicentral distance
Δt	Time duration
$\Delta\tau$	Time differences
$A(f)$	Fourier transforms of amplitude time function a(t)
A, B, C, D	Constants
A_{IFL}	Acceleration's constant spectral level at intermediate frequency level
$D(f)$	Fourier transforms of displacement time function d(t)
F	Free surface Amplification
f	Frequency
f_c	Corner frequency
f_{max}	Maximum frequency observed in FAS
j	$(-1)^{0.5}$
M	Magnitude
M_{JMA}	Magnitude scale used by JMA
M_o	Seismic moment
M_w	Moment magnitude
P_d	Peak displacement
P_r	Partition on to the two horizontal components
P_v	Peak velocity
$Q(f)$	Quality factor
$Q_c(f)$	Quality factor estimated using coda waves
Q_o	Quality factor at 1 Hz
$Q_\beta(f)$	Quality factor estimated using Shear waves
R	Distance from the Source (kilometer)
$R_{\theta\varphi}$	Average radiation patter

$S(f)$	Source acceleration spectrum
S/N	Signal to Noise Ratio
S_a	Spectral acceleration
t	Time index
t_i	Time at i^{th} instant
t_{max}	Maximum time
t_{now}	Time at an instant
$V(f)$	Fourier transforms of velocity time function v(t)
v_i	Velocity at i^{th} instant
β	Shear-wave velocity (km/sec)
$\Delta\sigma$	Stress drop
ρ	Density (gm/cm^3)
τ_c	Average period
τ_p^{max}	Maximum predominant period
ω	Angular frequency
$\Omega_{main}(f)$	Recorded spectrum of displacement at distance R
Ω_o	Low frequency Spectral Level
$\Omega_{source}(f)$	Apparent source spectrum of displacement

LIST OF ABBREVIATIONS

AF	Alaknanda Fault
BCAV	Bracketed Cumulative Average Velocity
BCAV-W	Windowed Bracketed Cumulative Average Velocity
BMTPC	Building Materials and Technology Promotion Council
BSL	Berkeley Seismological Laboratory
Caltech	California Institute of Technology
CAV	Cumulative Absolute Velocity
CIRES	Centro de Instrumentacióny Registro Sísmico
CISN	California Integrated Seismic Network
CPC	Central Processing Center
CSMIP	California Geological Survey Strong Motion Instrumentation Program
CWB	Central Weather Bureau of Taiwan
DC	Direct Current
DEQ	Department of Earthquake Engineering
DF	Dhubri Fault
DFZ	Dauki Fault Zone
DI	Destructive Intensity
DNF	Didhnoi Fault
DSHA	Deterministic Seismic Hazard Assessment
DST	Department of Science and Technology
EEW	Earthquake Early Warning
ElarmS	Earthquake Alarm Systems
EPRI	Electric Power Research Institute
ETH	Swiss Institute of Technology Zürich
FREQL	Fast Response Equipment against Quake Load
GMPE	Ground Motion Prediction Equation
GPS	Global Positioning System
GSHAP	Global Seismic Hazard Assessment Program

GSI	Geological Survey of India
HFT	Himalayan Frontal Thrust
IEEWS	Istanbul Earthquake Early Warning System
IERREWS	Istanbul Earthquake Rapid Response and Early Warning System
IITR	Indian Institute of Technology Roorkee
ITSZ	Indus Tsangpo Suture Zone
IV2	Squared Velocity Integral
JMA	Japan Metrological Agency
K-NET	Kyoshin Network
LTA	Long Term Average
MBT	Main Boundary Thrust
MCT	Main Central Thrust
MDF	Mahendragarh-Dehradun Fault
MFT	Main Frontal Thrust
MoES	Ministry of Earth Science (MoES)
NAFZ	North Anatolian Fault Zone
NAT	North Almora Thrust
NCR	National Capital Region
NCT	National Capital Territory
NE	North East
NIED	National Research Institute for Earth Science and Disaster Prevention
NNE	North North East
NRPEEWSA	National Research Project on Earthquake Early Warning System and its Application
NW	North West
PEER-NGA	Pacific Earthquake Engineering Research Center-Next Generation Attenuation
PESMOS	Program for Excellence in Strong Motion Studies
PGA	Peak Ground Acceleration
PGD	Peak Ground Displacement
PGV	Peak Ground Velocity

P-pick	Pick of primary wave
PreSEIS	Pre-SEISmic
PRESTo	Probabilistic and Evolutionary Early Warning System
PSHA	Probabilistic Seismic Hazard Assessment
P-wave	Primary wave
RSSCV	Root Sum of Squares Cumulative Velocity
SAS	Seismic Alert System
SASMEX	Seismic Alert System of Mexico
SASO	Seismic Alert System for Oaxaca City
SE	South East
SMA	Strong Motion Accelerographs
SNF	Sundernagar Fault
SNR	Signal to Noise Ratio
SOESWIN	Seismic Early Warning Information Network
SSW	South South West
STA	Short Term Average
S-wave	Secondary Wave
TF	Tista Fault
TL	Tista Lineament
UrEDAS	Urgent Earthquake Detection and Alarm System
USC	University of Southern California
USGS	United States Geological Survey
VH	Very High Damage Risk
VL	Very Low Damage Risk
VS	Virtual Seismologist
VSN	Virtual Sub-Network

CHAPTER 1

INTRODUCTION

1.1 PREAMBLE

Earthquakes are among the most frightening and destructive phenomena of nature. Due to its complex nature numerous attempts have yielded partial success to understand and predict this natural phenomenon, but most of the time it strikes in different areas at the most unexpected time. Vulnerability of our civilization to natural disasters is rapidly increasing due to unprecedented pace of development going on presently. Today a damaging earthquake may take up millions of lives, cause material damage, render large region uninhabitable and can trigger a localized or regional economic depression. When earthquakes have coincided with human populations they caused some of the deadliest natural disasters in the recorded histories. The 1934 Bihar-Nepal earthquake in India, the 1976 Tangshan earthquake in China, the 2004 Sumatra in Indonesia, the 2005 Pakistan earthquake, the 2010 Haiti earthquake reported causalities around 10700, 250000, 227898, 86000 and 316000, respectively. The precarious condition arising due to earthquakes could be minimized only by making a reliable diagnostics to predict the location, magnitude and time of earthquakes. Over the past few decades, considerable efforts have been focused on obtaining realistic prediction of earthquakes considering the advancement in understanding of earthquake occurrence, its generation mechanism and its real time processing. Thus, the feasibility of *Earthquake Early Warning (EEW)* system comes into existence and serves as a reliable tool for reducing damage and casualties caused from earthquakes. Implementation of EEW system, one of the effective means for seismic risk reduction, has become a major scientific challenge and pressing societal imperative. It works by rapidly detecting the energy radiating from an earthquake rupture and estimating the resulting ground shaking that will occur later in time either at the same location or at some other location. Warning times which are function of the distance of the user from the earthquake epicenter ranges from few seconds to more than a minute. Many countries have succeeded in designing and implementing EEW systems particularly, Japan, Taiwan, Mexico, Romania and Turkey. Japan is the potentate in field of EEW systems; the first country which started the practical application of EEW in early 1990’s for general public.

As far as India is concerned, the seismicity, locations of seismic sources and vulnerable cities in the vicinity of Himalayas tempt scientific community to look for such mitigation remedies like EEW. Tectonically Indian Himalaya is considered as among one of the most seismically active regions in the world. Himalaya is the outcome of convergence of continent-continent boundaries where the Indian plate is under thrusting the Eurasian plate. Many devastating earthquakes have occurred along the Himalayan belt from the ancient times and continuing in recent times as well (for e.g., 1991 Uttarkashi earthquake, 1999 Chamoli earthquake, and 2005 Muzaffarabad Pakistan earthquake in addition to many known Great earthquakes in past history). This has enhanced the perception about the increasing vulnerability that the rapidly growing population in Himalaya is confronted with, and that these earthquakes had significant long term social and economic impact. Thus, it is of paramount interest to have an EEW system for Indian region encompassing the foot hills of Himalaya and cities in which life and structures get affected by the strong motion generated in Himalayas.

In terms of data requirements in such endeavors like EEW system, Himalaya region has a relatively poor strong motion database due late attention made on importance of strong motion seismology and strong motion recordings. Reliable short-time estimation based on huge multi parametric data remaining an intriguing long-term research goal due to non-availability of large magnitude earthquake data. That makes it difficult to calculate relevant parameters from strong ground motions and setting thresholds for issuing warning for strong ground motion associated with the Himalayan earthquakes.

Recent advances in observational seismology especially instrumentation and communication technologies have made inroads for seeking solutions to such problems where huge amount of parameters have to be correlated to the physical phenomenon. The higher sampling rate, larger memory, and faster communications have made it possible to estimate relatively more parameters in real time to be used for earthquake warnings and for the development of rapid and reliable real-time earthquake information systems (Kanamori et al. 1997).

1.2 MOTIVATION BEHIND THE RESEARCH

There is an exponential increase in loss of life and property every year due to earthquakes and rapid increase in population and industrial density around vulnerable areas further enhances the earthquake risk. During the past few decades, the EEW system has

proved to be an efficient, fast and affective real time risk mitigation tool around the world. EEW systems are designed based on different EEW parameters and approaches. It has been found that each parameter has different correct alert capability than other. Therefore, an attempt is required to develop a multi-parameter based EEW algorithm which provides more accurate and reliable EEW.

The studies carried out by various workers for Northern Himalayan region based on the past and the contemporary seismicity in Garhwal Himalaya region, prevalent earthquake occurrence models, plate motions, presently going on deformations in the region and presence of probable locked faults have revealed the region between *Main Central Thrust (MCT)* and *Main Boundary Thrust (MBT)* to be a probable cluster region for any seismogenic source zone in near future earthquake activity. Further, the cities falling in the vicinity of this active region prompt the requirement of an EEW system to be developed for this region. In this context, the present study has been undertaken to understand EEW, develop algorithm for EEW and propose such system for disaster mitigation in this seismically active area.

1.3 EARTHQUAKE EARLY WARNING (EEW) SYSTEM

The rapid advancement in the field of real time transmission and processing of seismological data lead to the development of real time risk mitigation system called EEW system. Its importance is understood by all the seismically active countries to minimize the loss caused by the catastrophic events.

The difference in the speed of non destructive *primary waves (P-wave)*, destructive *secondary waves (S-wave)* and high speed transmission of data (electromagnetic waves) is utilized by EEW algorithms for issuing alarm. Depending upon the distance between the earthquake source and the target site, lead time (i.e., the time between the P-wave detection by a seismic network and the S-wave arrival at the target site) is estimated.

In case of EEW, the warning time is of few seconds. The available few seconds time when wisely used helps in seismic risk reduction (Wieland 2001) by reducing loss of life; property and other resources. A dense network of strong ground motion sensors is required for EEW system instrumentation with real time communication facility. The basic block diagram for an EEW system is shown in Fig. 1.1. The three basic units in an EEW system are as follows:

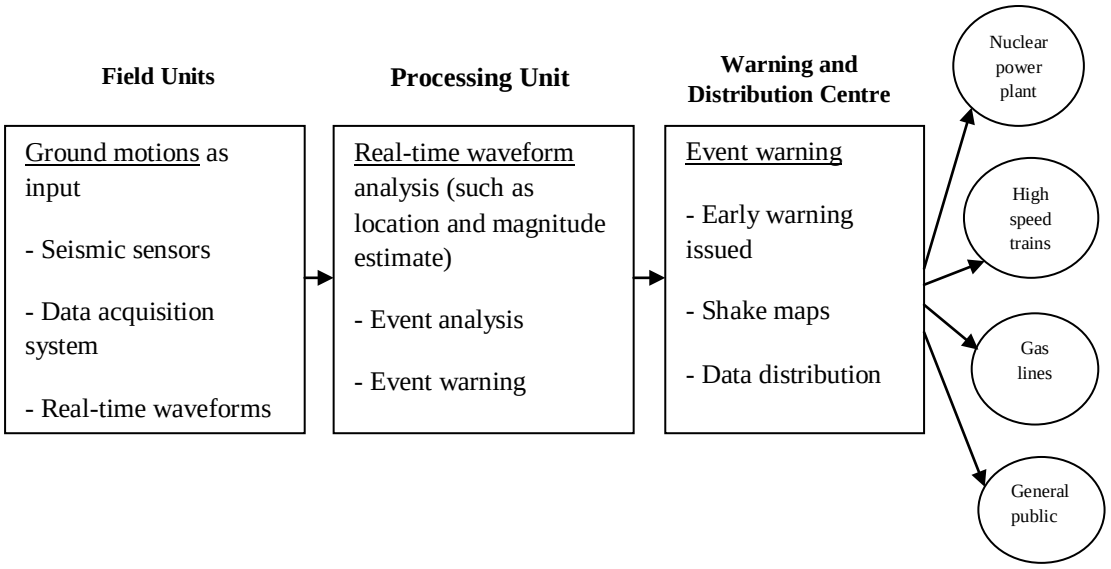

Figure 1.1 Basic components of an EEW system.

Field Units:

Field units are deployed across the seismic-prone regions closely spaced according to the typical depth of their seismic focus. Field units are provided with accelerometers and digital electronics for recording an earthquake's evolution. Ground motions are input signal for field units, which are sensed by seismic sensors. Sensors are analog devices and thus different digital acquisition techniques are applied on sensors output to get digital data at prescribed sampling rate followed by continuous real time streaming of data.

Processing unit:

It can also be termed as processing centre, here the input real time waveforms from the seismic stations connected to it are analyzed in real time and estimation of location, magnitude through EEW parameters are made. Processing centre by making event analysis determines whether the event is large enough to issue a warning or not, to provide reliable information. This unit consists of software and algorithm part of the EEW system which is updated from time to time.

Warning and distribution centre:

This unit distributes EEW among various users such as nuclear power plants, high speed trains to avoid derailment, shutoff of gas pipelines to avoid fire hazards, safe shutdown of computers to avoid loss of database and to general people for personal safety. The shake maps are generated using the estimated magnitude and event location. As stations begin observing ground accelerations, the observations are incorporated into the Shake map/Alert map and the attenuation function is adjusted to best fit the available data. Data distribution is also an integral part of warning and distribution centre, it distributes the data to other stations and units for further analysis.

1.4 RESEARCH GAP

A comprehensive review has been presented in Chapter 3 for EEW systems used worldwide. It reveals that there is further scope to develop such systems in more efficient way for fast and reliable real time disaster mitigation. The development of algorithm and new parameters may increase the efficiency and stability of the EEW system. The better understanding of seismotectonics is required for more realistic designing of an EEW system. The Indian scenario in this regard has been presented in Chapter 2 by revisiting the seismic hazard potential especially in Northern India. The study of tectonic features of Himalayas in Chapter 2 shows that North West Himalaya, Garhwal Himalaya, Kumaoun Himalaya, and North East Himalaya have number of faults, lineaments and discontinuities present in these regions which serve as foci of several devastating earthquakes occurred in the past and has potential of their recurrence in near future. Further, the cities around Himalayas like Dehradun, Hardwar, Saharanpur, Muzaffarnagar, Bijnor, Moradabad, Meerut, Baghpat, Ghaziabad, Gautam Buddha Nagar and Delhi remain in high risk zone due to high seismicity of Himalayas and their vulnerability.

Therefore, there is a prompt requirement to take certain measures for real time risk mitigation viz., EEW system. The development of an efficient EEW algorithm and installation of a strong motion instrumentation network for setting EEW system in India can be a relevant step in lessening the socio-economic loss caused due to earthquakes.

1.5 OBJECTIVE OF THE STUDY

The main objective of the present thesis is to study various parameters used worldwide in EEW system for issuing warning and develop new EEW parameters which are more efficient. In addition to the development of algorithm to logically use EEW parameters for issuing alarms and estimate magnitude of earthquake within few seconds of P-wave onset, the objective also includes developing an algorithm for automatic *pick of primary wave (P-pick)* onset. The final outcome includes suggestion for EEW system in Indian region. The objectives of the thesis can be enumerated as follows:

1) To review the existing EEW systems deployed in various parts of the world.
2) To study various EEW parameters used in EEW systems for issuing warnings.
3) To develop new EEW parameters that can be used in EEW system for issuing warnings.

4) To develop an automatic P-pick algorithm in real time.
5) Estimation of magnitude of the earthquakes from the analysis of initial portion of P-waves.
6) Validating the developed algorithm by worldwide dataset.
7) Suggesting the instrumentation network for EEW system in India and its feasibility for different cities in vicinity of Himalayas in Northern India.

1.6 ORGANISATION OF THE THESIS

This thesis comprises of eight chapters:

Chapter 1 introduces the EEW system and an overview of the research problem, research gaps and objectives has been provided.

Chapter 2 describes the seismotectonics of the four sectors of Himalaya considered in this study. This Chapter also discusses the origin of Himalaya and seismicity of Himalaya. This chapter further reports the seismic hazard and risk associated with the cities around Himalayas.

Chapter 3 presents a brief review of literature about principle and approaches of EEW system, various types of EEW system suggested by different researchers, different procedures to issue warnings. The chapter also reviews the main concerns and challenges of EEW systems.

Chapter 4 presents the methodology for development of an EEW algorithm using EEW parameters. The chapter also explains EEW parameters, automatic P-onset detection, warnings/alarms and magnitude estimation involved in designing EEW algorithm.

Chapter 5 presents a brief description of the three datasets used in the present study namely, Indian dataset, Japanese dataset (*Kyoshin Network, K-NET*) and *Pacific Earthquake Engineering Research Center-Next Generation Attenuation (PEER-NGA)* project strong motion dataset respectively.

Chapter 6 presents the results of automatic P-onset detection using proposed method based on *Root Sum of Squares Cumulative Velocity (RSSCV).* A comparison with the available algorithms has been made using K-NET dataset. The chapter also includes the EEW parameters relations with magnitude to calculate threshold values for issuing alarms. The efficiency of the developed algorithm is tested at individual as well as at different possible combination of EEW parameters, for reliable output at minimal time. EEW parameters have been ranked for various magnitude ranges according to their performance.

The magnitude estimation of the event has been made using Brune's model (1970) based approach. The developed algorithm is validated using Indian and PEER-NGA dataset.

Chapter 7 includes the development of EEW system in Northern India. In this Chapter, the instrumentation with steps required for an EEW system has been explained. Further, the lead times for six cities of Northern India have been calculated and reported using developed EEW algorithm.

Chapter 8 summarizes all the research carried out in the present study. Chapter further highlights the important conclusions drawn from the present study. The chapter also includes the recommendations for future research work.

CHAPTER 2

SEISMIC HAZARD IN NORTHERN INDIA

2.1 INTRODUCTION

The Himalayas are considered to be one of the most seismically active regions of the world. In India, several devastating earthquakes have occurred which have originated from Himalayas. About 60% of Indian geographical region lies in earthquake prone zone and around 75% of all fatalities are due to earthquakes. During earthquakes, death toll rises mainly due to the collapse of non-engineered structures and weak masonry buildings. It is of paramount importance to understand the seismic hazard in a seismically active region to carry out risk mitigation exercises. The understanding of seismogenic sources, their behavior with respect to space and time along with the size distribution in terms of magnitude of the past and probable future earthquakes, lead to better use of the rapid advancement in the field of real time transmission and processing of seismological data which in turn, lead to the development of real time risk mitigation system like EEW system. Thus, risk mitigation and other remedial measures like seismic hazard evaluation, earthquake resistant design of structures and deployment of EEW system are the demand of time in India specifically for active regions like Himalayas and its vicinity.

Many catastrophic earthquakes have been recorded in Himalayan region in the past hundred years namely, 1897 Shilong (M 8.7), 1905 Kangra (M 8.6), 1934 Bihar (M 8.4), 1950 Assam (M 8.7), 1991 Uttarkashi (M 6.8), 1999 Chamoli (M 6.4) and 2005 Muzaffarabad (M 7.6), in which huge loss of life and property took place (Mandal et al. 2000, Mahajan et al. 2011). In the last few decades, pace of urbanization has rapidly increased in Himalayan region and its periphery which has increased the vulnerability many folds. In addition to the classical deterministic and probabilistic seismic hazard assessment methodologies, better estimation of the current Himalayan convergence rate and possible rupture have been found to improve seismic hazard evaluations. In this regard various studies have been carried out regarding the deformations in the Himalayan region (Bhattacharya et al 2012, 2014). However, it is still far to predict the earthquake time and magnitude in a scientific way. Therefore, a different approach as a parallel exercise to these endeavours is also required for risk mitigation. This leads to attempt risk mitigation

techniques like EEW for Himalayan region and its vicinities. This chapter contains a description about the tectonic and seismic characteristics of the regions from where Indian strong motion dataset has been taken in the present study. Further, the description of seismic hazard in cities around Himalayas is also discussed in this chapter.

2.2 THE HIMALAYAN COLLISION ZONE

Himalaya was formed by collision of Indian and Eurasian continents wherein the buoyant crust of the Indian plate was detached from the underlying mantle and its subsequent deformation raised mountain chains. The collision also caused large-scale deformations and high seismicity of vast areas of both continents. The Himalaya occupies the northern part of the Indian subcontinent forming about 400 km wide arcuate bend which is convex to the SSW and runs unbroken for 2400 km between the mountain peaks of Nanga Parbat in the west and Namcha Barwa in the East, each of these peaks being located where the trend of the mountains changes abruptly. It is bounded by Indo-Gangetic plains towards south and the Trans Himalaya ranges towards north. The actual northern boundary may be taken as more or less continuous depression running parallel to the Himalaya trend and containing the valleys in which lie the upper reaches of the Indus and the Tsangpo (named Bhramputra further downstream in Assam). Within the Himalaya, the mountain ranges are arranged in various linear belts; the Trans Himalaya belt, Main Central Crystalline belt which is also called the Great or Higher Himalaya and comprises of high mountain peaks, 30 of which, including Mount Everest, have elevations in excess of 7300 m, the Lesser Himalaya which comprises mostly of the mountains with elevations up to 4500 m and the southernmost outer Tertiary Foot Hill belt with elevations up to 1300 m. The boundaries between the various belts are marked by thrusts. The Great and the lesser Himalaya have also been dissected by transverse deep valleys carrying drainage.

Vast areas of India along the Himalaya and adjoining plains are susceptible to grave earthquake risk. The Himalaya tectonic zone, being a collision plate boundary, is manifested with a number of north dipping thrusts that are exposed at the surface. To explain the cause of occurrence of earthquakes and to understand the seismotectonics of the Himalayan collision zone, various models have been proposed for the evolution of the Himalaya. Among these, two models namely, *Steady-State model* and the *Evolutionary model* have gained considerable importance. Steady state model (Seeber and Armbruster 1981) postulates an active low angle thrust coinciding with the overlying crustal slab, a

portion of which is located between the subducting slab and overlying sedimentary wedge and termed as “Detachment Surface", while the portion between the interacting slabs is termed as the "Basement Thrust". According to this model, the Great Himalayan earthquakes are related to the detachment surface. The evolutionary model (Ni and Barazangi 1984) postulates that zone of plate convergence is progressively shifted south by formation of intra-crustal thrusts and hypothesizes that the MBT is the most active tectonic surface and that the seismicity is concentrated in a 50 km wide zone between the map trace of MCT and MBT. This model suggests that the rupture of Great Himalayan earthquakes may have started in the inter-plate thrust zone, which propagated south along the detachment to the MBT and further south along the detachment to the MBT and further south to the subsidiary blind thrusts. Both these models suggest that the contemporary deformation styles in the Himalaya are guided by the under thrusting of the Indian crust along the detachment surface.

2.3 SEISMOTECTONCIS OF HIMALAYAN REGION

The Himalayas are the result of collision between Indian and Eurasian plate going on since ~55 Ma. The ongoing northward drift of Indian plate makes the Himalayan region geo-dynamically active, with most of the seismic activity concentrated along major thrusts in Himalayas characterized with relatively large magnitudes of earthquakes occurring with longer return periods. Minster and Jordan (1978) estimated the northward motion of the Indian plate relative to the Asian plate as 42 mm/year in the western Himalaya. Later on the basis of geodetic plate model, higher convergence rate of 44 mm/year was observed from west to east Himalayan region (England and Molnar 1997; Wang et al. 2001) and 54 mm/year towards NE (Mahesh et al. 2012). It was concluded that the convergence was absorbed due to (i) shortening of sedimentary strata in the foreland as India under thrusts its cover rocks, (ii) contraction within the collision zone by uplift in the high Himalaya and reactivation of interior thrust faults, and (iii) crustal shortening *via* thickening of the crust and escape-block tectonics along strike slip faults to the north of the collision zone (Molnar and Tapponnier 1975; Molnar and Tapponnier 1977).

In Himalayan arc itself about half of the total convergence of India-Eurasia plate takes place, while remaining half distributes in wide continental range causing deformations (Rastogi 1974). Several researchers have reported convergence rate in different portion of the Himalaya based on the offset of late Pleistocene and Holocene

sediments (Wesnousky et al. 1999; Lave and Avouac 2000; Kumar et al. 2001); contemporary seismicity (Lyon-Caen and Molnar 1985; Leathers 1987; Baker et al. 1988; Avouac and Tapponnier 1993; Powers et al. 1998), convergence rate estimated from analysis of historical earthquakes (Molnar 1990; Gupta et al. 2001) and GPS field survey measurements (Jackson and Bilham 1994; Bilham et al. 1997, 1998; Larson et al. 1999; Banerjee and Burgmann 2002). In Table 2.1 convergence rates of different portions of the Himalaya, as reported by Kumar et al. (2003) have been listed. Due to the high level of tectonic activities in and around the Indian continent innumerable earthquakes have occurred (Fig. 2.1).

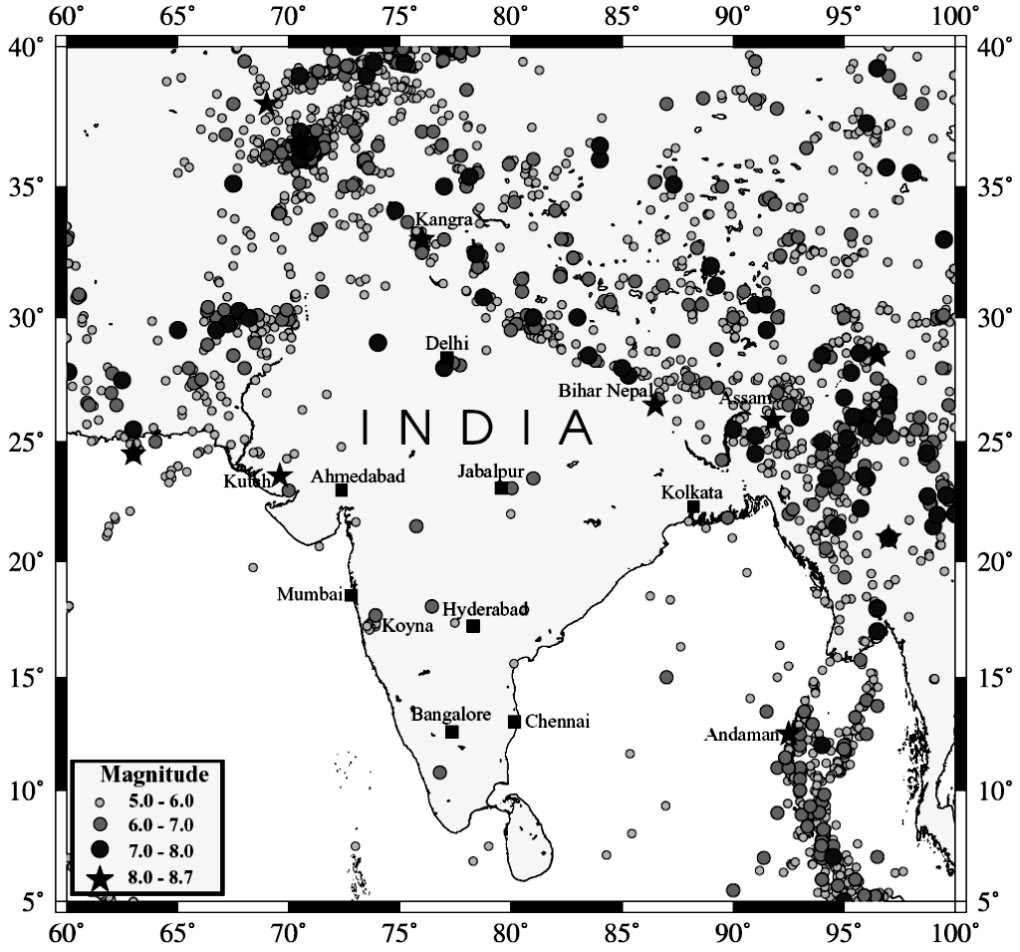

Figure 2.1 Seismicity of the Indian Subcontinent with spatial distribution of earthquakes for the period 1819-1998 (Parvez et al. 2003).

Table 2.1 A compilation of studies reporting convergence rates in Himalayan region modified after Kumar et al. (2003).

Himalayan region	Displacement Measurement Methods	Convergence Rate (mm/yr)	Cited Reference
Soan Syncline, Pakistan	Retro deformation	13-20	Leathers (1987)
Salt Range Thrust, Pakistan	Retro deformation	9-14	Baker et al. (1988)
Eastern Nepal	Well log & earthquake data, sedimentological & provenance data	13±5	Srivastava and Mitra (1994); DeCelles et al. (1998)
Western Nepal	Well log & earthquake data, sedimentological & provenance data	21	Srivastava and Mitra (1994); DeCelles et al. (1998)
HFF in Dehradun	Retro deformation	11±5	Powers et al. (1998)
NW Dehradun	Retro deformation	14±2	Powers et al. (1998)
Entire Himalayan arc	Slip rate	18	Avouac and Tapponnier (1993)
Central/West India	Facies Migration (on lap)	15±5	Lyon-Caen and Molnar (1985)
Indian Himalayan arc	Seismicity, Geodesy	17	Molnar (1990)
Nepal	Seismicity, Geodesy	17.2	Bilham et al. (1997)
Nepal	Seismicity, Geodesy	20±3	Bilham et al. (1998)
Dehra Dun, Central India	Offset Holocene Terraces	13.8±3.6	Wesnousky et al. (1999)
Nepal	Offset late Pleistocene	21±3	Lave and Avouac (2000)
Nepal Himalaya	GPS Field Survey	20	Jackson and Bilham (1994)
Nepal, Assam	Finite Element	18	Peltzer and Soucier (1996)
Nepal Himalaya	GPS Field Survey	18±2	Larson et al. (1999)
Kala Amb, Central/West India	Offset Holocene Terraces	4.8-15.7	Kumar et al. (2001)
Chor Ghalia, Central India	Offset Holocene Terraces	9.8±0.4	Kumar et al. (2003)
NW Himalaya	GPS Field Survey	14±1	Bannerjee and Burgmann (2002)
NW Dehradun	Finite Element	10	Peltzer and Soucier (1996)
Nepal	Finite Element	18	Peltzer and Soucier (1996)
High to sub Himalaya	Retro deformation	7-19	Schelling and Arita (1991)
Hardwar, NE Himalaya	Geological method	10.79±2.23	Parkash et al. (2011)

The northward convergence of Indian plate caused deformation in the northern part of India. The shortening of the Indian crust along the Himalayan thrusts, i.e., the MBT, the MCT and the *Himalayan Frontal Thrust (HFT)* resulted in younger Himalayas. The *Indus Tsangpo Suture Zone (ITSZ)* serves as a plate boundary between the Indian and Asian plates collision area. Fig. 2.2 shows the major faults namely, MBT, MCT faults and its adjoining region such as Indus Suture.

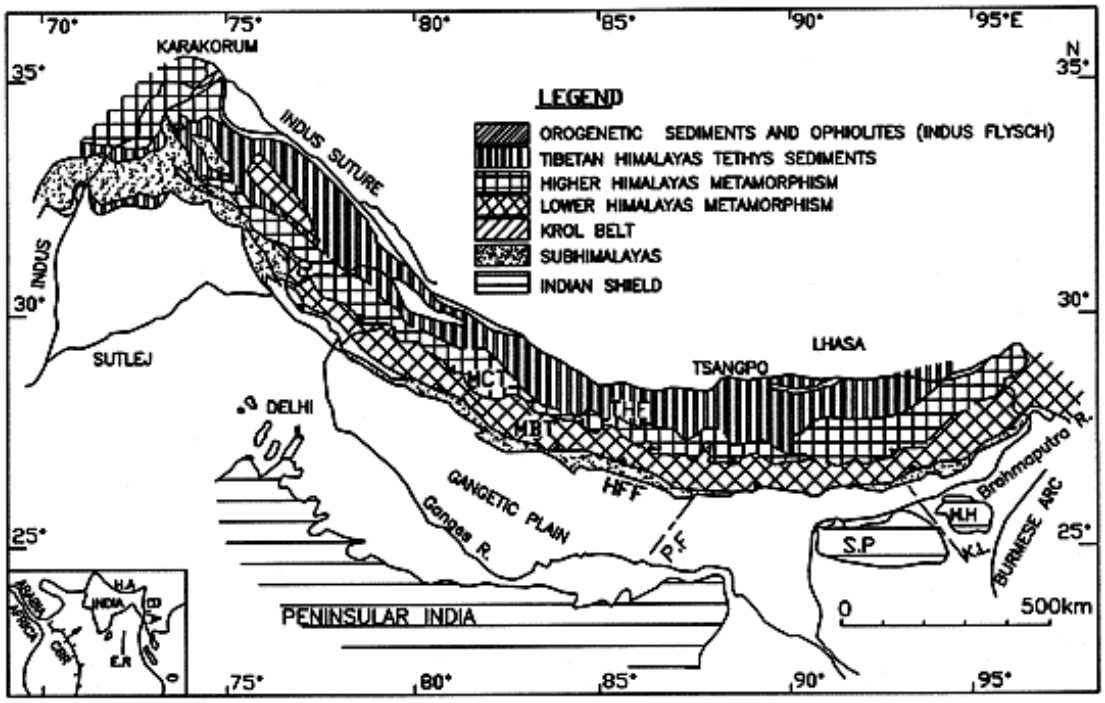

Figure 2.2 Map showing tectonic setup of Himalayas and its adjoining regions and major fault zones (Gansser 1964).

The MCT and northern lesser Himalayan region have instrumental seismicity distributed underneath the topographical front of Higher Himalaya at a depth range of 10 to 20 km covering a distance of about 900 km from Nepal to Indus Kohistan Seismic Zone in Pakistan (Seeber and Armbruster 1981). Himalaya and its surroundings experienced several higher magnitude earthquakes (Srivastava 1988; Srivastava and Rao 1991; Srivastava et al. 2007, 2013) namely, 1897 Shilong (M 8.7), 1905 Kangra (M 7.8), 1934 Bihar-Nepal (M 8.4) and 1950 Assam (M 8.6) in the past that caused enormous loss of life and property as listed in Table 2.2. Estimation showed that 18000 people died during Kangra earthquake, strong ground motion reported at that time exceeds the *Peak Ground Acceleration* (*PGA*) value of 1 g and a heavy destruction occurred. Arya (1990) estimated

that if similar earthquake reoccur in Kangra there would be a four times more loss lives even in the daytime similarly the forecast for the casualty on the reoccurrence of Muzaffarabad earthquake would be 86000. The hike in the estimated number of possible casualty due to impending earthquakes is because of rapidly increasing population, weak and unorganized construction of infrastructure without following any designing seismic code (Chamlagain 2009).

Table 2.2 High magnitude earthquakes reported in Himalaya and its surroundings with number of death casualty reported (Chamlagain 2009, modified). Magnitudes have been taken from IMD.

Place	**Date**	**Magnitude**	**Casualty**
Shillong Plateau	12th June ,1897	8.7	~ 1542
Bihar-Nepal border	1st January,1934	8.3	> 10563
Chamba, India	22nd June, 1945	6.5	~100
Kangra, India	4th April, 1905	8	18000
Quetta, Pakistan	30th May, 1935	7.6	~ 30000
Assam, India	15th August, 1950	8.5	1500
Udayapur, Nepal	20th August, 1988	6.4	~1000
Uttarkashi, India	20th October, 1991	6.6	>2000
Chamoli, India	29th March, 1999	6.8	>150
Hindukush	11th November, 1999	6.2	No death reported
Muzaffarabad, Pakistan	8th October, 2005	7.6	74698

The seismotectonic history of Himalaya reveals that there is a possibility of occurrence of large distributed earthquake with a recurrence interval $\leq$ 500 years (similar to Kangra/Muzaffarabad earthquake) or a mega thrust type earthquake with a recurrence period $\geq$ 1000 years as documented in the paleo-seismological trenches (Kumar et al. 2006; Feldl and Bilham 2006; Sharma and Lindolhm 2012).

Based on the past seismicity, seismic hazard and other considerations which fall in line with the need of EEW system, the Northern Indian region has been selected as the study area for the present research work. This region is part of the seismic gap area between Kangra earthquake and Bihar-Nepal earthquake and lies in Seismic Zone IV and V. The area for EEW has been chosen based on geological and tectonic setting, past seismicity and the location of important cities which are the target region for the EEW system to issue warnings. The area chosen for the study is shown in Fig. 2.3. The area is

already on high probability of occurrence of earthquakes as per many of the studies reported recently.

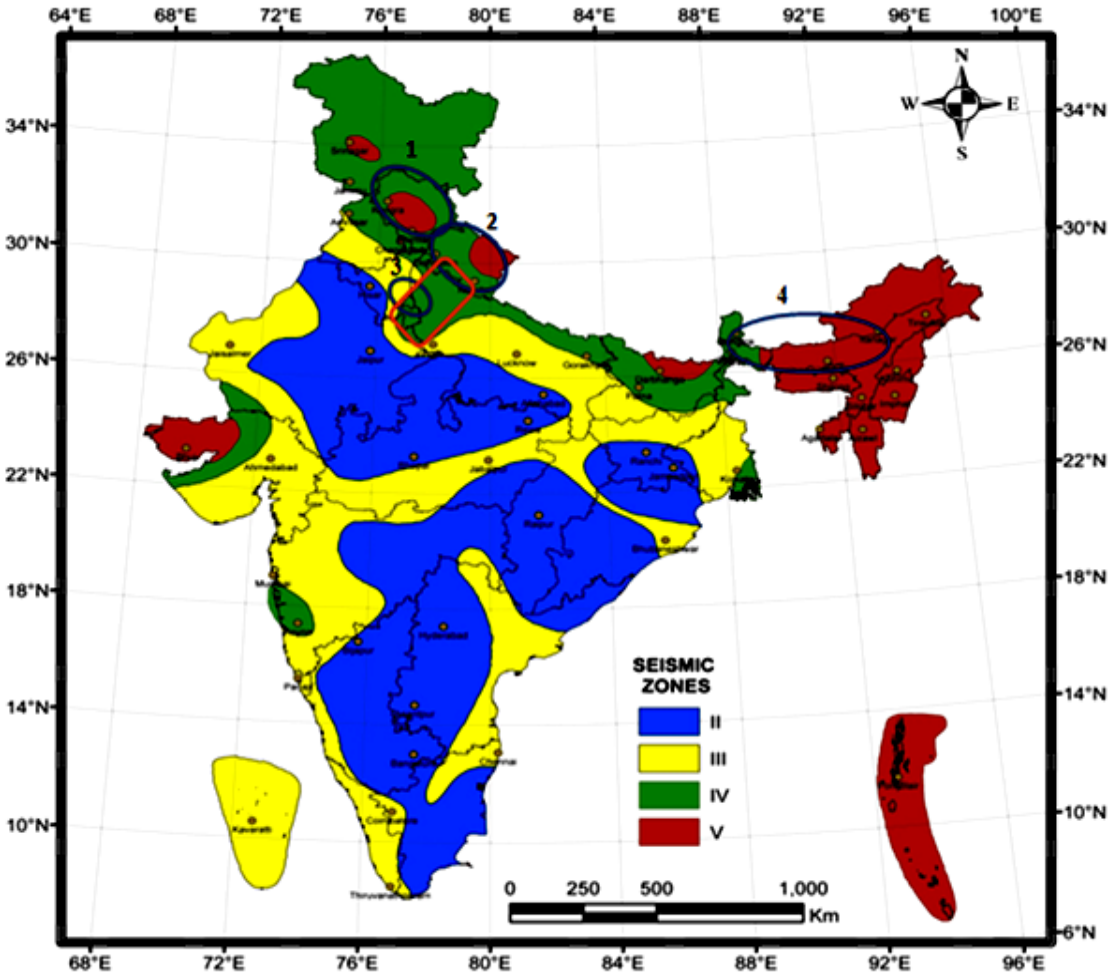

Figure 2.3 Study area (red rectangle) and the regions (1, 2, 3 and 4) from where the strong motion data is selected for validation. Different colors show the Seismic Zones of India as per BIS: 1893-2002.

2.4 SEISMIC HAZARD

The main aim of all types of seismological studies is to develop approaches which can be used for preparedness, evaluation of seismic hazard and to mitigate risk. In seismic hazard and risk analysis, the expected ground shaking or ground failure due to an earthquake at a region is analysed in terms of loss of life and property. Hazard maps are prepared as a result of the estimated affects of the earthquake at the specified regions. Due to varying geology of different regions, the probability of occurrence of potentially damaging earthquake is found to be different. Seismic Zone maps are prepared to

categorize the regions based on their level of seismicity. In India, first Seismic Zone map was issued by Indian Metrology Department (Bureau of Indian Standard) in 1956 (Tandon 1956) having three Seismic Zones. The Seismic Zones were based on the maximum expected MM intensity. The first formal seismic map was included in the Indian standard code (IS: 1893-1962) and it was revised in 1967, 1970 and 1975. The Indian Standard (Part 1) (Fifth Revision) was adopted by the Bureau of Indian Standards, after the draft finalized by the Earthquake Engineering Sectional Committee and had been approved by the Civil Engineering Division Council. IS: 1893-2001 'Recommendations for earthquake resistant design of structures' has been published by BIS and the Seismic Zoning of map India presented in this code is shown in Fig. 2.3 which displays the different seismic prone areas along the Himalayas.

A seismic hazard analysis is based on two approaches, namely: Deterministic and Probabilistic approach. In *Deterministic Seismic Hazard Assessment (DSHA)*, the scenario consists of known specifications like selection of nearest source at the site, selection of distance parameter, selection of controlling earthquake and finally defining the hazard on the basis of controlling earthquake (Kramer 2003). DSHA provides a theoretical framework for estimation of critical ground motions. On the other hand, *Probabilistic Seismic Hazard Assessment (PSHA)* uses the probabilistic approach and considers the uncertainties involved in the input parameters like size, location, recurrence rate and variation in ground motion characteristics (for example-PGA). In India, Khattri et al. (1984) calculated PGA of 0.7 g for 10% probability of exceedance in 50 years for Himalayan region using Probabilistic Seismic Hazard Model which is recalculated as 0.35-0.4 g for 10% probability of exceedance in 50 years by Bhatia et al. (1999) under *Global Seismic Hazard Assessment Programme (GSHAP)*. Sharma and Dimri (2003) reported around 0.35 g PGA for 20% exceedance probability in 50 years (225 years return period) for the Dehradun area. Mahajan et al. (2010) has estimated the probabilistic seismic hazard for the northern Indian region, and the PGA for the approximate Dehradun location was estimated to be about 0.3 g for 10% exceedance in 50 years. For the further improvement of seismic hazard evaluations in the Himalaya two factors are of importance: (i) the development of an attenuation relation specifically derived from sufficient local strong motion data. The attenuation relation and its scatter is decisive for any hazard results, and (ii) the catalog of historical earthquakes cannot compensate for the presently uncertain evaluation of recurrence times and recurrence places for the larger earthquakes in the

Himalayas. An alternative to waiting for the large earthquakes to occur is an improved geodetic monitoring of the main mapped faults around the foothills and the main population centers. When the strain rates on main faults near the urban centers are mapped it will bring significant value to the future seismic hazard evaluations. Kumar (2006) found that for India the conditional probability of occurrence for M > 6 were higher than the ones which were estimated using PSHA. The GPS measurement and neotectonic studies of active faults provided further advancement in the field of seismic hazard. Still a lot of uncertainty regarding Seismic Zones, nature of faults and location of seismic source are present which effect the seismic hazard estimations. However, it can be inferred from the literature review that ongoing northwards drift of Indian plate makes Himalaya geo-dynamically active which has been studied extensively during the past few decades and the seismic hazard estimations made by considering such phenomenon have increased the hazard in long return periods (Shanker and Sharma 1998; Sharma and Tyagi 2010; Sharma and Arora 2005; Sharma and Lindholm 2012). Such conclusions tempt the scientists to work out remedies like EEW systems for risk reduction by estimation of magnitude, location of the impending earthquake and providing warning time of few seconds before the catastrophic event hits the target site.

2.5 STRONG GROUND MOTION DATASET REGIONS IN INDIA

The data requirements in the present study can be categorized in three subsets of data namely: (i) data required for regression analysis to estimate the relevant parameters for EEW to issue warnings, (ii) data required for validation of estimated parameters and developed algorithm for Indian conditions, and (iii) data to check the stability of parameters and the algorithm using worldwide data. Due to paucity of data in the study area, the data has been imported from other regions. The datasets consisting of three main subsets of the data have been selected as follows. The first dataset has been selected from an area where the dataset is good and can be used for regression analysis for estimating EEW parameters and the development of an algorithm based on various EEW parameters. Hence, this dataset has been chosen from K-NET seismic array in Japan where a good number of earthquakes have been recorded in required format. In all 1726 records from 105 events having $5 \leq M \leq 7.2$ with epicentral distance up to 60 km have been selected. To validate and to implement the developed algorithm in Indian conditions, the data has been chosen from Himalayas. About 300 stations of strong motion accelerographs (with inter-

station spacing of about 40 km) have been installed in north and northeastern India by Department of Earthquake Engineering (Kumar et al. 2012) which has recorded a good amount of strong motion data from Himalayan region albeit not sufficient to carry out regression analysis as required in the previous dataset. The second dataset chosen for the present study consists of strong motion records from this array for four regions namely: **Region-1:** NW Himalaya (Himachal Himalayas); **Region-2:** Uttarakhand region (Garhwal and Kumaoun Himalaya); **Region-3:** National Capital Region (consisting of Delhi-Haridwar Ridge region) and **Region-4:** North East Indian region. The areas for data selection along with the target region are shown in Fig. 2.2. All 28 events have been selected from these seismically active regions having 51 digital records from stations having epicentral distance up to 60 km from magnitude range varying from 3.3 to 6.8. To further validate the algorithm on worldwide data, another dataset (not used for regression analysis in the study) has been selected mainly from: Southern California, Taiwan and Turkey. This dataset consists of 219 earthquake records of 14 earthquakes recorded at 174 strong motion stations with magnitude ranging $3.3 \leq M \leq 7.2$ within 60 km of epicentral distance. The more elaborated description of all the datasets considered in the present study is given in Chapter 5. The four regions from which data has been compiled for EEW system are described in details as follows:

2.5.1 Region-1: North West Himalaya (Himachal Himalayas)

The Himachal region is located between 30.3^{o}-33.0^{o} N latitude and 75.6^{o}-9.0^{o} E longitude in the NW Himalayan region of India. The MCT and the MBT are the main tectonic features in this part of Himachal. Besides above tectonic features, the region has also been affected by faults and lineaments and the northerly trending *Sunder Nagar Fault (SNF)* has displaced MCT in dextral sense. Kumar and Mahajan (2001) identified narrow width of Lesser Himalaya in the Chamba-Sundernagar region as well as in NW of Dharmshala which implies that the convergence was accelerated largely by under thrusting of the Lesser Himalaya formation. Fig. 2.4 shows the major tectonic features present in the study area.

The main district head quarters of Himachal region are Chamba, Kangra, Mandi, and Kullu which fall under the Seismic Zone-V with some parts in Seismic Zone-IV as per the BIS code (BIS: 1893-2002). The region has experienced a number of devastating earthquakes which caused enormous damages in the past. Six past earthquakes from this

area have caused considerable damage. The earliest is the Kangra earthquake of 4th April, 1905. This is one of the four great earthquakes of the Himalayan region which took a toll of 20,000 human lives and caused colossal loss in the form of complete damage of buildings and generation of numerous landslides and earth fissures. Kangra earthquake has been discussed in detail by Mahajan et al. (2006) and Srivastava et al. (2010).

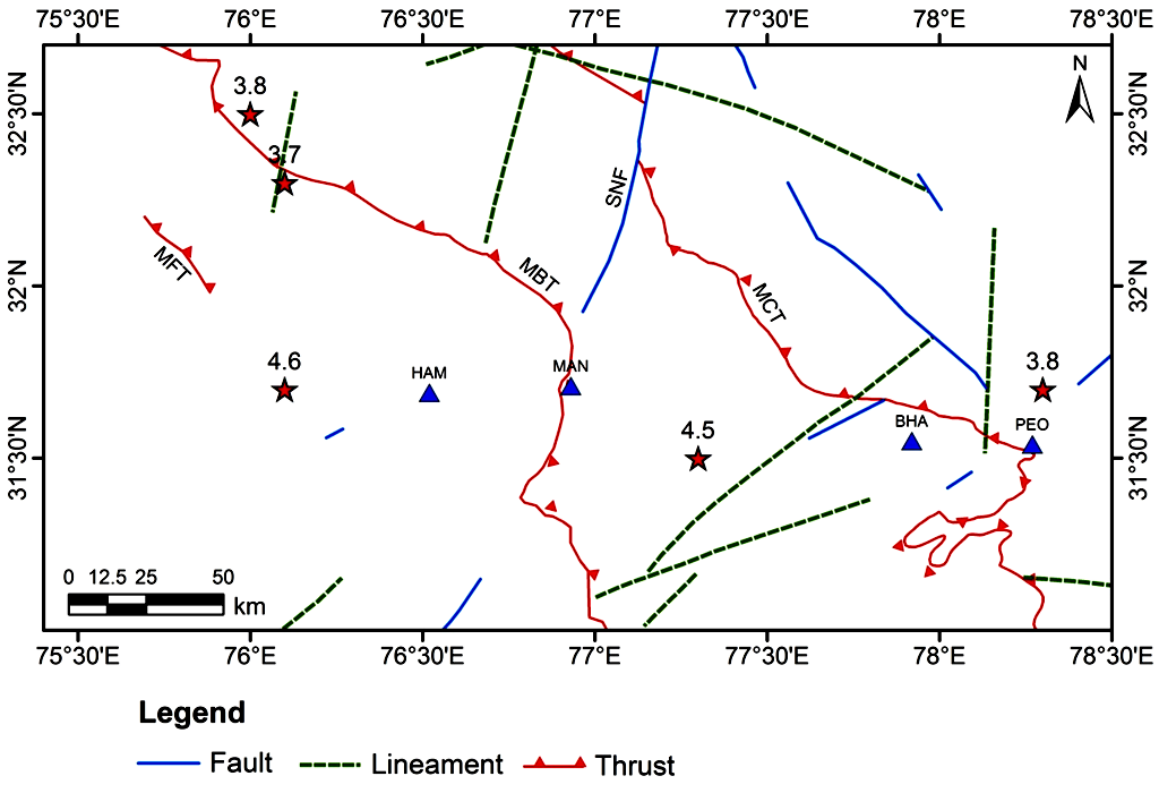

Figure 2.4 Map showing tectonic framework of NW Himalaya along with considered strong motion stations (triangles) and epicenters of earthquakes (stars). MCT-Main Central Thrust, MBT-Main Boundary Thrust, MFT-Main Frontal Thrust and SNF-Sunder Nagar Fault (GSI-2000).

Chamba earthquake of 22nd June, 1945 also caused considerable damage to property. Dharmsala earthquake of 14th June, 1978 had resulted in the development of cracks in a number of buildings in and around Dharmsala town. Minor landslides and earth fissures were also generated. The Dharmsala earthquake of 26th April, 1986 took a toll of three human lives, caused considerable damage to buildings and resulted in the development of earth fissures. Kumar and Mahajan (1990) studied distribution of intensity due to Dharmsala earthquake. Chamba earthquake of 24th March, 1995 caused partial collapse and development of cracks in the buildings.

A catalogue prepared by Szeliga et al. (2010) on intensity, magnitude, location and attenuation of felt earthquake in India since 1762 to 2009 contains at least 7 earthquakes ranging from magnitude 7.8 to 4.5 which have occurred only in Kangra region. Statistical analysis of NW Himalayan earthquake data (Mahajan and Ghosh 2007) and the seismic hazard study by Mahajan et al. (2009) for NW Himalaya, the Kangra region has been assigned as high potential zone. The north western, eastern and central zones of Himachal state are the most seismically active zones.

2.5.2 Region-2: Uttarakhand Region (Garhwal and Kumaon Himalaya)

The Garhwal and Kumaon Himalaya are demarcated by two major thrust planes viz., MCT and MBT. In the south, the young sedimentary Siwalik realm is severed from it by MBT and in the north the MCT delimits the northern boundary of the Lesser Himalaya against the Precambrian high-grade metamorphics of the Great Himalaya. Between these two thrusts, the sprawling Lesser Himalayan subprovince is built up of a number of thrust sheets. The main tectonic units of Garhwal and Kumaon Himalaya are presented in Figs. 2.5 and 2.6.

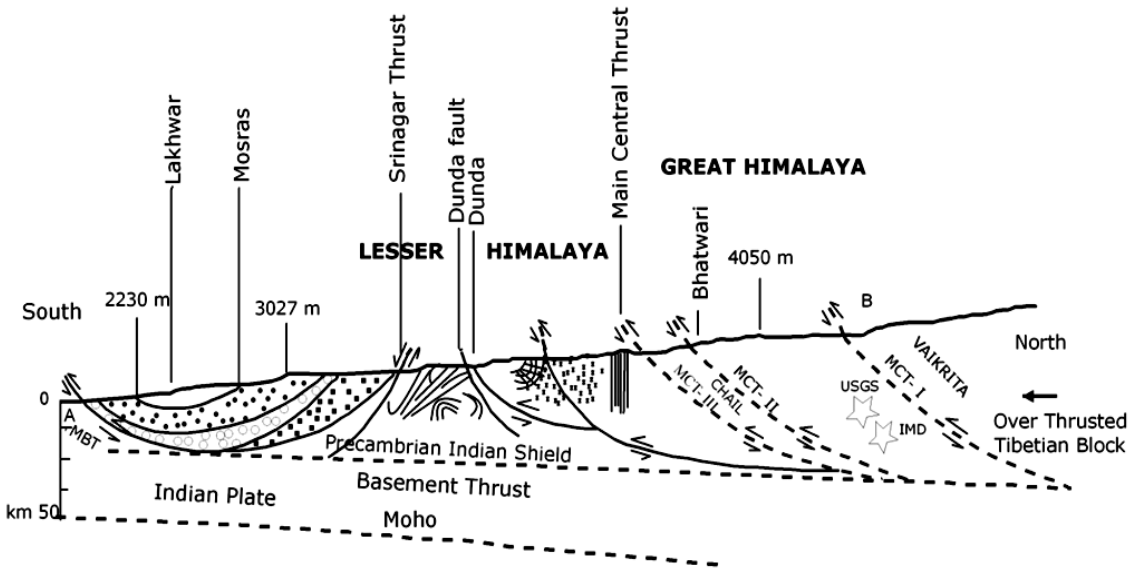

Figure 2.5 Geological cross-sectional view of Garhwal Himalaya showing the various tectonic units (Thakur et al. 1995).

More recently, damaging earthquakes of magnitude 6.6 (Uttarkashi earthquake) and 6.8 (Chamoli earthquake) occurred in the Garhwal-Kumaon Himalayan region on 20th October, 1991 and 29th March, 1999, respectively (Paul et al. 2011). These earthquakes caused widespread damage to poorly constructed buildings killing about 800 persons in Uttarkashi earthquake and 103 in Chamoli earthquake. The earthquake was felt at a far distances including Delhi and maximum ground acceleration of 0.3 g was recorded at Bhatwari. The Chamoli earthquake was also occurred on MCT zone in the east of Uttarkashi. The motion is again thrust type with focal depth of about 20 km (Mahajan and Virdi 2001, Sharma and Dubey 2000, Harbindu et al. 2012).

The seismicity observed in Garhwal and Kumaon Himalaya defines a 50 km wide NW-SE trending belt in the vicinity of the surface trace of MCT. Sharma and Wason (1994) found that in the upper crust of the Garhwal Himalaya shallow depth events have relative low stress drops. Fig. 2.6 shows the location of the considered earthquakes and strong motion stations along with the main tectonic features of the Garhwal and Kumaon region.

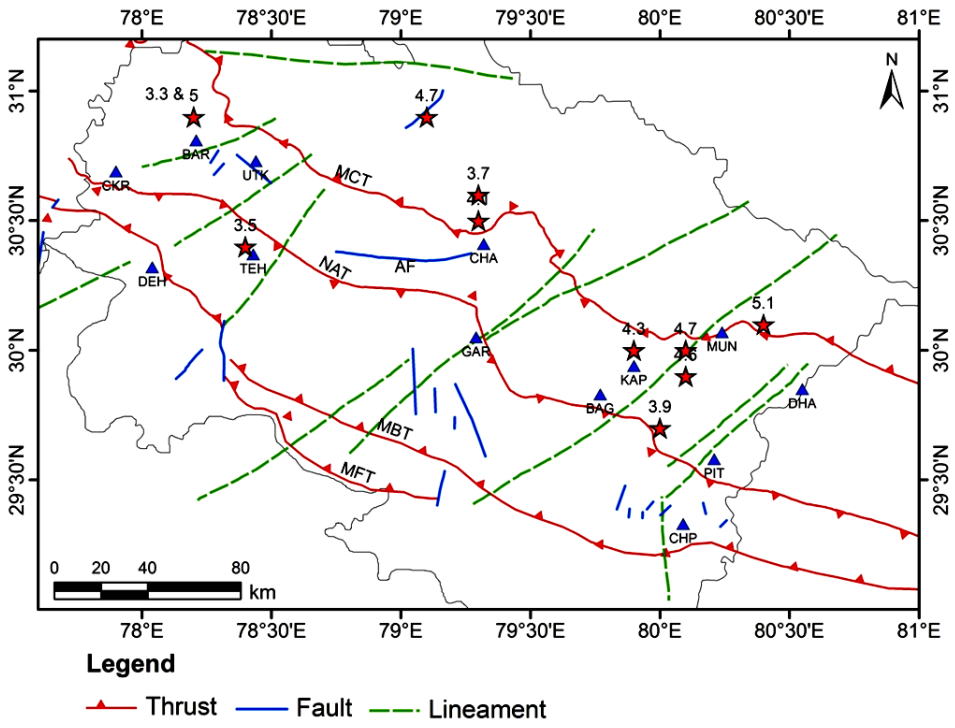

Figure 2.6 Seismotectonic map of Uttarakhand region with several prominent tectonic features present in the region. The triangles and stars represent the strong motion recording stations and the epicenters of the earthquake considered in the present study. MCT, AF-Alaknanda Fault, NAT-North Almora Thrust, MBT and MFT- Main Frontal Thrust (GSI-2000).

2.5.3 Region-3: National Capital Region (Consisting of Delhi and Adjoining Haryana, Rajasthan and Uttar Pradesh)

The *National Capital Region (NCR)* comprises the *National Capital Territory (NCT)* region of Delhi along with many other districts from three neighboring states namely, Haryana, Uttar Pradesh and, Rajasthan, as listed in Table 2.3.

In past, the NCR has experienced many damaging earthquakes having their epicenters in Delhi and surrounding areas such as 1803 Mathura earthquake (Oldham 1883) having M = 7 and 1960 Gurgaon earthquake having M = 6. The earthquake originated in Himalayas also affects the NCR. In Delhi region, the rock type is quartzite of the Alwar series. The terrain of NCR is generally flat except for a low NNE-SSW trending ridge which is an extension of the Aravalli belt (Sharma 2003; Sharma et al. 2003; Sharma et al. 2004).

Table 2.3 States, their cities and the area covered under NCR.

States included in NCR	Cities included in NCR	Area involved (sq. km)
NCT	Delhi, New Delhi	1480
Harayana	Gurgaon, Faridabad, Mewat, Palwal, Rewari, Jhajjar, Rohtak, Sonipat and Panipat	13140
Uttar Pradesh	Gautam Buddha Nagar, Ghaziabad, Bulandshahr and Meerut	10850
Rajasthan	Bhiwadi and Alwar	7830

The main tectonic features of NCR region comprises of Mahendragarh-Dehradun fault analogous to the Delhi-Haridwar ridge, Moradabad fault, Sohna fault and Aravalli fault (Kamble and Choudhary 1979). Joshi and Sharma (2011a, 2011b) the region is also affected by a few faults and lineaments. NCR has moderate seismic intensity and falls in Seismic Zone-IV according to seismic zone map of India (BIS: 1893-2002). In the present study, strong ground motion records of six earthquakes are from NCR region up to an epicentral distance of 60 km (see Fig. 2.7). It has been observed that all the considered events have M < 5.

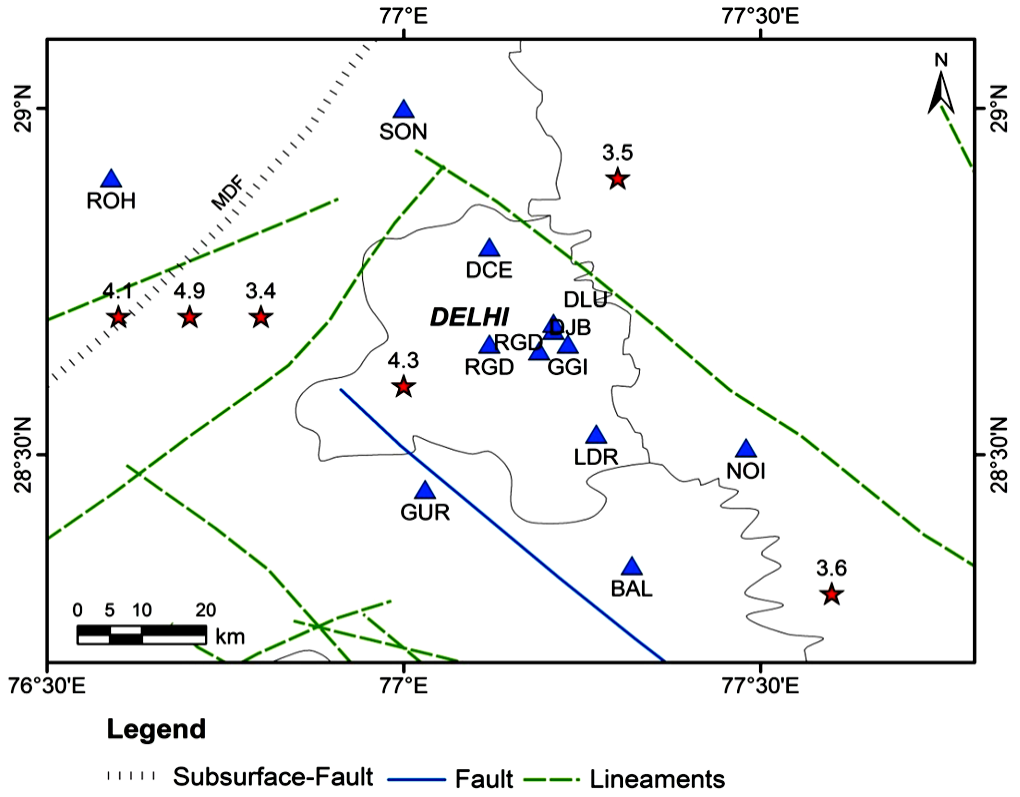

Figure 2.7 Map showing tectonic framework of NCR. Triangles and stars represent the strong-motion stations and the epicenters of the earthquakes considered in the present study with other seismotectonic features present in the region, *MDF-Mahendragarh Dehradun Fault* (GSI-2000).

2.5.4 Region-4: North East Indian Region

The study area in North East Indian region lies between 25^{o} N to 28^{o} N latitude and 88^{o} E to 92^{o} E longitude comprising Himalayan belt, Brahmaputra river basin and Shillong Plateau. This entire NE Indian belt is characterized by high seismic activities as compared to other part of Himalaya. The level of seismicity noticed in this region is a result of Indian and Eurasian plate collision in the north and subduction tectonics along with Indo-Myanmar range (Dewey and Bird 1970; Molnar and Tapponnier 1975, 1977; Kayal 1996, 1998). The NE India falls in Seismic Zone-V due to its high seismicity. In the past many destructive earthquakes which caused heavy loss of life and property have occurred in this region such as Shillong earthquake in 1897 having magnitude of 8.7 in which around 1542 people lost their lives and Assam earthquake in 1950 having magnitude 8.6 in which 1500 fatalities took place.

The tectonic setup of the study area can be divided into three main parts as eastern Himalaya belt, the Brahmaputra basin and the Shillong plateau, as listed in Table 2.4. Figure 2.8 shows the major tectonic features in the study area.

Table 2.4 Classification of NE India based on its various tectonic regions.

Main tectonic region in northeast Himalaya	**Different thrusts, faults and other features present in corresponding region**
Eastern Himalaya	MCT, MBT and their subsidiary thrust, Tista Lineament
Brahmaputra Basin	Atheirkhet Fault, Tista Fault and other faults and lineaments
Shillong Plateau	Dauki Fault Zone, Dudhnoi Fault, Dhubri Fault, other faults and lineaments

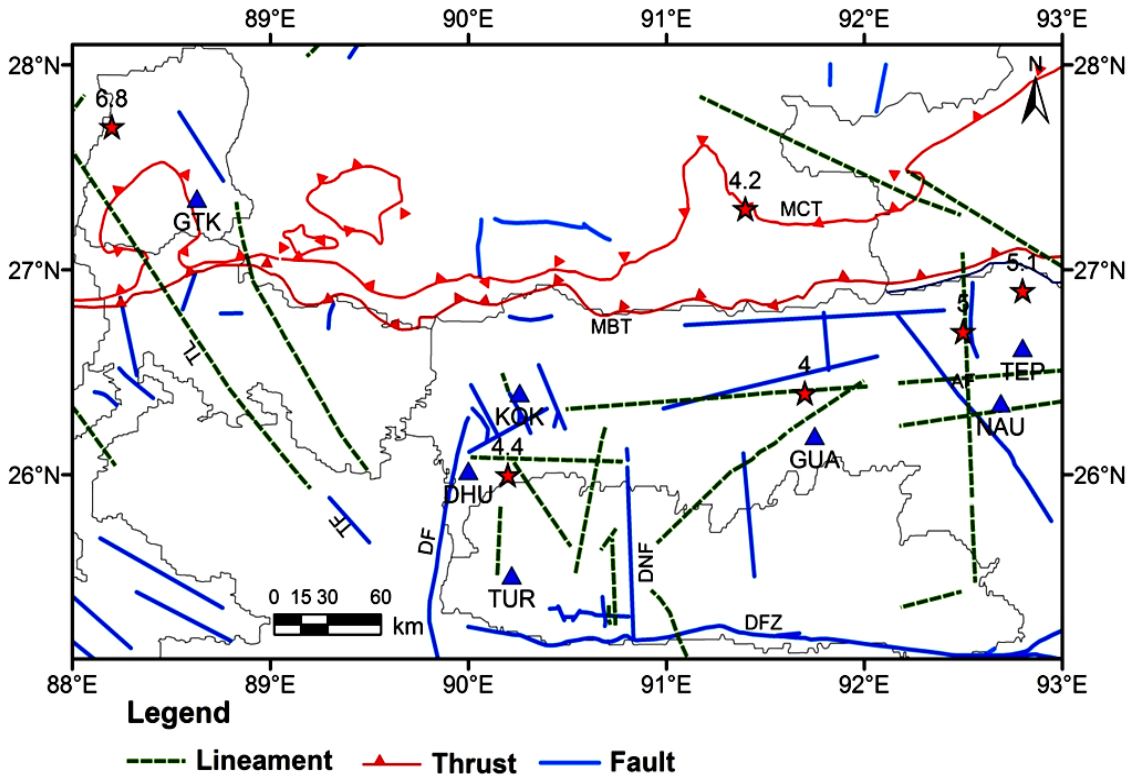

Figure 2.8 Seismotectonic map of NE Indian region showing few prominent tectonics feature of the region. Triangles and stars represent strong motion stations and earthquake epicenters, repectively considered in the present study of the NE Indian region. MCT, MBT, *AF-Atheirkhet Fautl, TL-Tista Lineament, TF-Tista Fault, DF-Dhubri Fault, DNF-Didhnoi Fault, DFZ-Dauki Fault Zone* (GSI-2000).

2.6 RISK IN CITIES AROUND HIMALAYA

It is evident that the seismic hazard in and around Himalaya is high and is of concern not only to the engineers for earthquake resistant design and retrofitting but also to the whole society as it has long lasting effects on the society and economics. It is of paramount importance therefore to seek solutions for mitigation and management of the disaster due to these damaging earthquakes in future. One of the solutions pondered upon in this work is the EEW system.

There are several cities in the vicinity of Himalayas which gets affected by the earthquake having their epicenters in Himalayan region namely: Dehradun, Hardwar, Saharanpur, Muzaffarnagar, Bijnor, Moradabad, Meerut, Baghpat, Ghaziabad, Gautam Buddha Nagar and Delhi. In the past, several destructive earthquake took place in Himalayan region like 1905 Kangra, 1991 Uttarkashi, 1999 Chamoli, 1945 Chamba and 1978 Dharamsala earthquake etc., which not only affected their epicentral area but also adversely affected the cities situated 100's of km away from them.

The risk estimation requires the vulnerability of the built environment and the seismic hazard along with the exposure time. Experience has taught that most of the earthquake-related deaths and injuries during major earthquakes are caused by the partial or complete collapse of structures (e.g., buildings, towers and chimneys). There is a difference between seismic hazard and seismic risk. Seismic hazard describes the potential for dangerous earthquake related physical phenomena such as ground shaking, fault rupture, and liquefaction. These phenomena could result in adverse effects on the society, such as destruction of buildings, dams and loss of life (Deb 2008; Kurian et al. 2006). Seismic risk is the probability of occurrence of these consequences.

A Vulnerability Atlas of India (first revision, 2006) was published by *Building Materials and Technology Promotion Council (BMTPC)*. In this atlas, the earthquake risk has been estimated on the basis of socio-economic loss, casualty, injuries and damage to buildings during earthquake. The hazard and damage risk to housing has been suggested in five damage risk levels for earthquakes based on the given intensity scales such as: **Very High Damage Risk (VH)-** Total collapse of buildings; **High Damage Risk (H)-** Gaps in walls; parts of buildings may collapse, separate parts of the building lose their cohesion, and inner walls collapse; **Moderate Damage Risk (M)-** Large and deep cracks in walls fall of chimneys on roofs; **Low Damage Risk (L)-** Small cracks in walls, fall of fairly

large pieces of plaster, panties slip off, cracks in chimneys, and **Very Low Damage Risk (VL)-** Fine cracks in plaster; fall of small pieces of plaster.

In Table 2.5, the risk for the densely populated cities around Himalayas has been listed on the basis of these different levels of risk such as described in the Atlas. All the cities considered in the study (Dehradun, Hardwar, Saharanpur, Muzaffarnagar, Bijnor, Moradabad, Meerut, Baghpat, Ghaziabad, Gautam Buddha Nagar and Delhi) lies in seismic zone IV based on BIS: 1893:2002. From the Table 2.5, it has been concluded that in Dehradun about 24.4% houses are susceptible to high damage due to type of construction and violation of earthquake resistance designing norms. However, in case of moderate damage Baghpat, Delhi, Ghaziabad, Gautam Budhha Nagar, Muzaffarnagar, Meerut, Bijnor, Hardwar, and Moradabad share 90% to 80% damage of houses. Recently, several software tools have been developed for seismic risk assessment (Lang and Corea 2010, Haldar et al. 2013). However, very few earthquake risk studies are available for the Northern India. Lang et al. (2012) has presented the risk estimate for the city of Dehradun by analytically computing damage and losses based on CSM method (Lang et al. 2008) and have compared it with the previously derived empirical risk estimates.

Thus, if an earthquake of high magnitude occurs in Himalaya or Northern India, a heavy loss of life and property will be unavoidable. Thus, real time risk mitigation feature of EEW system becomes a necessity for this region.

Table 2.5 Cities with percentage of houses under different level of risk around Himalayas (after BMPTC, 2006).

Cities	Percentage of houses under different level of risk			
	High damage	**Moderate damage**	**Low damage**	**Very low damage**
Dehradun	24.4%	69.8%	3%	2.8%
Hardwar	12.6%	82.5%	1.1%	3.7%
Saharanpur	18.2%	77.9%	0.4%	3.5%
Muzaffarnagar	8.6%	89.4%	0.4%	1.6%
Bijnor	15.3%	80.6%	0.4%	3.7%
Moradabad	17.4%	79.2%	0.5%	2.9%
Meerut	6.0%	91.3%	0.8%	1.9%
Baghpat	3.5%	95.6%	0.2%	0.6%
Ghaziabad	5.3%	91.8%	1.1%	1.7%
Gautam Buddha nagar	5.8%	90.4%	0.8%	2.9%
Delhi	4.3%	91.7%	2.0%	1.9%

2.7 SUMMARY

The chapter presents the status of seismic hazard in Northern India. The continent-continent collision has given rise not only to Himalayas but also to the high seismicity to this region. The chapter summarizes the reasons for high seismicity in this region. Further, the details of the area taken up as study area for the current research have also been given in this chapter. The tectonic and geological setup has been described for the four regions from where the Indian strong motion data has been taken for validation.

The chapter further describes possible risk for the cities around Himalayas like Dehradun, Hardwar, Saharanpur, Muzaffarnagar, Bijnor, Moradabad, Meerut, Baghpat, Ghaziabad, Gautam Buddha Nagar, and Delhi.

CHAPTER 3

EARTHQUAKE EARLY WARNING SYSTEM: AN OVERVIEW

3.1 INTRODUCTION

In this chapter, a comprehensive review of different EEW systems, parameters, and methodologies adopted worldwide has been discussed. The chapter mainly presents three sections. The first section consists of the origin, classification and objectives of EEW systems. In the next section, the existing EEW parameters, systems and approaches have been discussed. Finally, the status of EEW system in different countries and the misconceptions, challenges and requirements associated with EEW system have been reviewed in the last section.

3.2 EEW SYSTEM

The rapid increase in population and industrial growth in high hazard and vulnerable areas leads to a continuous rise in expected rate of fatalities every year. Although, the natural phenomena like earthquakes are unpredictable and unavoidable but with the development of real time disaster information system such as EEW system, the risk can be reduced by providing in time warning for disaster mitigation.

The concept of EEW was first put forth by Dr. Cooper around 145 years ago. The basis behind his approach was that the severe damage due to an earthquake is caused by the S-waves which travels at about half the speed of P-waves and much slower than electromagnetic waves. Thus, if the intensity of shaking due to an impending earthquake at the target site can be estimated by the analysis of the initial portion of P-wave and the information about the estimation is transmitted through electronic means, then warning time of few seconds or few tens of seconds can be achieved before the S-wave hit the target site. The effective use of available warning time helps in real time risk reduction and enhances the safety margins from different types of losses by automatic shutdown of nuclear power plants, gas lines, oil lines, industrial units and slow down high speed trains. The basic feature of an EEW system includes real time data transmission, processing and decision making.

The EEW systems can be mainly classified based on the tectonic and seismic environment in the instrumentation region. The EEW is generally classified into two approaches called regional warning approach and onsite warning approach. When the seismic source is present at some distant from the target area/populated area the regional warning approach/front end detection approach is useful. In regional warning approach a dense network of seismic station with a central processing unit is used for estimation of location and magnitude of earthquake and intensity of ground motion at the target site. This warning approach provides a warning time ranging from a few seconds to tens of seconds and is generally used in areas of subducting lithosphere plates. Copper in 1868; first used front end detection approach setup near Hollister for providing warning to San Francisco, California by activating electronic current in an alarm bell on detection of a seismic event in the network region (Copper 1868). Later in Japan, instrumentation at the east coast and along the railway tracks was deployed for long warning time (Nakamura 1984). The *Seismic Alert System (SAS)* used regional warning approach for providing a warning of about 60 sec to Mexico City which is situated around 320 km away from the subduction zone (Espinosa-Aranda et al. 1995). Further, in Bucharest a warning time of about 25 sec was achieved with a seismic instrumentation installed in Vrancea zone about 160 km away from Bucharest (Böse et al. 2007). However, *Istanbul Earthquake Rapid Response and Early Warning System (IERREWS)* is also based on regional warning approach and provide warning time of 8 to 15 sec for Istanbul that is around 486 km away from the Marmara region where the EEW network is installed (Alcik et al. 2009).

The second approach is known as onsite warning approach; it does not require any central processing unit. The warning decision is based on the analysis of initial portion of P-wave observed by the seismic sensor placed directly at the target to issue warning at the same site. This approach is useful in areas where seismic source are present close to the populated areas. In case of onsite approach, the warning time and accuracy in estimation of earthquake parameters are less than the regional warning approach. However, onsite approach is relatively faster, since it makes local measurement of earthquake ground motion and also have small blind zone around the epicenter where no warning can be provided. *Urgent Earthquake Detection and Alarm System (UrEDAS)* (Nakamura 1988), τ_c-P_d method (Wu and Kanamori 2005a, 2005b; Wu et al. 2007; Wu and Kanamori 20008a, 2008b; Böse et al. 2009; Hsiao et al. 2009; Alcik et al. 2011), Compact UrEDAS (Nakamura and Saita 2007b) and *Fast Response Equipment against Quake Load (FREQL)*

(Nakamura and Saita 2007a) are the examples of EEW systems and methodology based on onsite warning approach.

Both the regional and onsite approaches have their own advantages and disadvantages over one another based on reliability and available lead time. It is worth noting that in case of EEW system there is always a tradeoff between the lead time and the reliability of the event information. Analysis based on longer time window length gives more reliable results due to availability of more data after P-onset viz., less number of incorrect alarms but have shorter lead time. Thus, there is a need of a careful selection of EEW approach for an EEW system according to the requirement.

The main objectives of an EEW system is fast, reliable and prompt detection of a damaging earthquake before it actually hits the target site. The objectives of issuing early warning are achieved by employing various algorithms which depends on the approach viz., regional or onsite approach. For example, in case of regional warning approach Heaton (1985), proposed the classical model consisting of four steps: (i) Event identification and estimation of location in real time with high precision, (ii) Magnitude estimation by analyzing the initial portion of the P-wave after P-onset (iii) Intensity estimation at the target site and predicting the peak ground motion with the help of developed attenuation relationships, and (iv) Warning notification based on the calculated source parameter and peak ground estimation for potentially damaging earthquakes.

However, in case of onsite approach, the magnitude and intensity of the event are estimated quickly at the site by analyzing the initial P-arrivals at the same site. Some of the onsite approaches are used to provide support for regional EEW systems in extending their region of applicability (Satriano et al. 2011).

3.3 A REVIEW OF VARIOUS EEW SYSTEMS PARAMETERS

The EEW system generally uses initial portion of P-wave and S-wave to determine location, magnitude and intensity of the impending earthquake for issuing warning. Various EEW parameters have been used in past by analyzing the initial portion P-wave for estimating magnitude of the event such as τ_p^{max}, τ_c, P_d, CAV, BCAV and BCAV-W. This section describes these parameters in details.

τ_p^{max}, i.e., *maximum predominant period* is considered to be the first EEW parameter which utilizes first few seconds of P-wave to calculate the maximum possible

predominant period within a selected time window. Small magnitude earthquake results in slip over a small area of fault and thus results in high-frequency energy, whereas in case of larger magnitude earthquakes larger fault area gets ruptured resulting in lower frequency energy. This difference is used to differentiate between the small and large magnitude earthquakes (Nakamura 1988). In Nakamura's method, a continuous time series of predominant period is determined from the vertical component of the velocity sensor (Nakamura 1984, 1988). τ_p value contains information regarding the frequency content of the entire waveform up to the given point of time and with the increase in time the contribution of given waveform segment decreases. UrEDAS and *Earthquake Alarm Systems (ElarmS)* system uses the τ_p^{max} method for estimation of source parameters (Nakamura 1988; Allen and Kanamori 2003). Nakamura (1988, 1984) and Allen and Kanamori (2003) observed that the logarithmic values of calculated predominant period within 2 to 4 sec from the initial portion of P-waves are linearly related with the earthquake size. Thus, the regression law established between τ_p^{max} and M can be used to determine the impending earthquake magnitude (Lockman and Allen 2005; Wurman et al. 2007; Tsang et al. 2007). Allen and Kanamori (2003) divided the total magnitude range in smaller and larger magnitude range. At small magnitude data, broad band low-pass filter of 10 Hz is applied to estimate the magnitude at 1 sec time window while for higher magnitude data a 3 Hz low-pass filter is applied to get best estimates of magnitude at 4 sec time window. At low magnitude range, τ_p^{max} showed scatter for the lowest magnitude events (Olson and Allen 2005; Wurman et al. 2007). Lockman and Allen (2007) also observed linear relationship between M and τ_p^{max} for circum Pacific belt. On analysing the global dataset from Taiwan, Alaska, Southern California and Japan, Olson and Allen (2005) observed that the scaling relationship remains maintained even for much higher magnitude events such as 8.2. The ElarmS technology has been further extended to Japan to have a state-wide real time system under *California Integrated Seismic Network (CISN)* project in which the offline development of ElarmS in California is combined with error analysis in Japan (Brown et al. 2011).

Another period parameter, τ_c similar to τ_p^{max} was proposed by Kanamori (2005). It is different from τ_p^{max} as follows:

a) τ_p^{max} is calculated from the ratio of velocity and acceleration records, while τ_c is calculated from the ratio of velocity and displacement records.

b) τ_p^{max} determines predominant period of the P-wave, while τ_c represents initial portion of P-wave over a fixed time window i.e., the pulse width of P-wave and it varies according to the size of event thus, used for estimating the event magnitude (Wu et al. 2008a).

Both the τ_p^{max} and τ_c parameters deal with the frequency content present in the initial portion of P-wave and when used together to estimate the magnitude, more accurate results were obtained (Shieh et al. 2008). The τ_c parameter was used by Wu and Kanamori (2005a, 2005b) for the development of onsite EEW system in Taiwan. By using single station, onsite approach a linear correlation between the magnitudes and the logarithmic characteristic periods of the initial P waves for a time window of 3 sec was obtained by Wu et al. (2006) for 46 earthquakes records within 100 km *epicentral distance* (Δ) and M $\leq$ 6.5 in Taiwan. Further, Wu and Kanamori (2008a) analysed 54 events with magnitude range 4 to 8 taken from Taiwan, Japan and Southern California strong ground motion dataset with at least 4 records per event and observed a linear trend on regressing the average τ_c value for each event with corresponding magnitude value at a time window of 3 sec. The τ_c parameter when used in combination with other EEW parameters provides more accurate estimation of magnitude.

Wu and Kanamori (2005a, 2005b) and Wu et al. (2006, 2007) projected another EEW parameter which is based on the maximum amplitude of the displacement time history calculated from the vertical strong ground motion component in a time window of 3 sec after P-onset. *Peak displacement* (P_d) parameter is used to estimate the *Peak ground Velocity (PGV)* i.e., the damageability of the impending earthquake at a site. Wu and Kanamori (2008a) analysed 780 Japanese strong motion vertical records with $\Delta \leq 30$ km and determined a linear relation between P_d and PGV. The relation is used to estimate the shaking intensity of an event using single station observations, whenever $P_d \geq 0.5$ cm, it is estimated that the event has PGV value of more than the damaging level i.e., 20 cm/sec. Wu and Zhao (2006) analysed 25 regional earthquakes of Southern California within 120 km epicentral range and found that attenuation of P_d with the hypocentral distance and M can be used for "P_d magnitude" estimation i.e., magnitude calculated using P_d parameter (M_{P_d}). M_{P_d} values are found to be in a good agreement with the catalogue magnitudes in Southern California with a standard deviation of 0.18 for events having magnitude less than 6.5.

Zollo et al. (2006) further modified P_d parameter approach by introducing two changes during analysis, first a variable time window was used instead of fixed 3 sec

window for P_d calculation and second, modification referred to the use of initial S-wave in (M_{P_d}) calculation. The calculated P_d values were normalised to a common hypocentral distance of 10 km to investigate distance independent relationship. Later, Rydelek et al. (2006), Zollo et al. (2006) and Lancieri and Zollo (2008) observed using Japanese dataset that at different time windows, P_d provides linear relation for moderate to large earthquake but it showed saturation at 2 sec of initial P-wave analysis. The problem of saturation was sorted out by Iervolino et al. (2006) and Lancieri and Zollo (2008) by using Baye's theorem that provides a probabilistic formulation for magnitude estimation by assigning a constant probability for M > 6.5 at 2 sec time window in case of P-wave based P_d estimation. At noisy accelerometers where correct P_d calculation is not possible, peak velocity P_v is found to be more useful (Wurman et al. 2007). P_d parameter based EEW algorithm has been used by several countries like Istanbul (Fleming et al. 2009; Alcik et al. 2011), Japan, China, Hawaii, Italy (Lancieri and Zollo 2008; Satriano et al. 2011), Taiwan (Hsiao et al. 2011) and Southern California (Allen et al. 2009; Böse et al. 2009).

Another EEW parameter is *Cumulative Absolute Velocity (CAV)* which was introduced by Kennedy and Reed (EPRI, 1988) for application in nuclear power plant during a study sponsored by *Electric Power Research Institute (EPRI)*, Palo Alto (California) in 1988. It is defined as the integral of absolute value of ground acceleration over the seismic time history record. It is also defined as the area under the absolute accelerogram and includes the cumulative effects of ground motion duration. The velocity content present in the ground velocity record is found to be associated with the earthquake energy content of the recording site and also used to determine the damage threshold for engineered structures associated with the impeding earthquake. The relation between the CAV and the local intensity was noticed and it is used as a parameter to distinguish a potentially damaging event from a non damaging one at nuclear power plant sites regardless of the response spectral values (EPRI, 1988). CAV is not related with the arrival time of different phases of energy but it is more sensitive to low frequencies (damaging) motions than high frequencies (non-damaging) motion. EPRI (1991) modified the CAV calculation by removing the non damaging accelerations values from the records. The time histories having the maximum acceleration values greater than the predetermined acceleration value (0.025 g) within a selected time domain were considered for calculating modified CAV values and are termed as standardized CAV (*Bracketed Cumulative Average Velocity-BCAV*). Cabanas et al. (1997) stated that the estimation of potential

structural damage for building type structure can be made using CAV and local intensity relation. Later, Kostov (2005) introduced correlation between magnitude and distance parameters correlation with standardized CAV and seismic intensity using European database and concluded that CAV is a better predictor of damage than PGA. EPRI (2006) developed *Ground Motion Prediction Equation (GMPE)* that allows estimation of CAV values directly from physical parameters of an earthquake. Kramer and Mitchell (2006) used another modified CAV parameter i.e., CAV5 (CAV with acceleration values > 0.005g) for measuring the intensity of rock motion. Danciu and Tselentis (2007) and Martinez-Rueda et al. (2008) found that standard deviation in the GMPE for CAV is very small when calculated using Greek and European strong motion database. Alcik et al. (2009) modified BCAV parameter as *Windowed Bracketed Cumulative Average Velocity (BCAV-W)*, the calculation was performed by windowing BCAV calculation on a broader window length (W) basis. BCAV-W parameter along with PGA parameter is used in Istanbul EEW system with more accurate alarms and less false alarms. Campbell and Bozorgnia (2010) analyzed CAV, standardized CAV, CAV5 and found that CAV is more suitable for damage estimation and prediction.

In EEW system, energy content present in the time series is a significant parameter which can be used for automatic P-picking and for estimating size of the event. Therefore, a new approach based on RSSCV parameter (Bhardwaj et al. 2013a) has been considered in which the energy content in the incoming time series is assumed to be present in terms of velocity components in relation to other component of ground motion. Therefore, not only the predominant velocity in the time series is considered but also the cumulative effect is included in terms of its energy component. Its formulation is as simple as CAV and is calculated by taking root of the squared value of velocity vector calculated for a given time window. The RSSCV values calculated have been found to follow more closely the envelop of the incoming time series and hence more efficient parameter for EEW as shown in Fig. 3.1, where it is compared with CAV. RSSCV parameter has its own advantage of providing enhance *Signal to Noise Ratio (SNR)*.

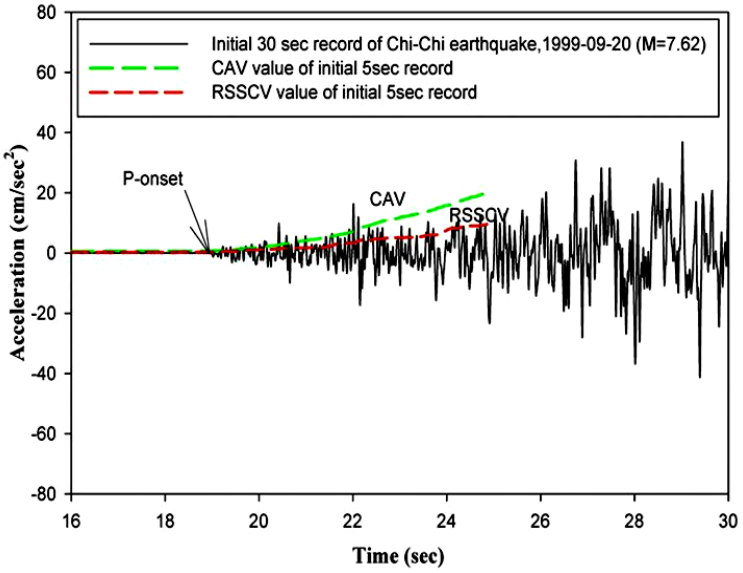

Figure 3.1 Acceleration-time history of initial 30 sec of Chi-Chi earthquake, 1999-09-20 (M = 7.62), where the CAV and RSSCV values are shown as red and green dashed lines, respectively.

3.4 A REVIEW OF VARIOUS EEW SYSTEMS AND METHODOLOGIES

Based on the different types of EEW approaches and available EEW parameters, there are number of EEW systems developed in various countries of the world. The EEW system proposed by Dr. Copper (1868) for San Francisco could never be implemented, but it is considered to be the first conceptual EEW system. Nakamura (1988) introduced **UrEDAS**, the first practically working onsite EEW system in Japan. UrEDAS system was based on τ_p^{max} parameter, calculated for a time window of 3 sec for estimating magnitude of an event. It is an onsite warning approach and uses data from a single 3-component seismometer for magnitude estimation using τ_p^{max} and for estimating event azimuth as well as depth by particle motion. The magnitude and location information are used to trigger an onsite alert based on preset criteria. This system continues to be used along the railway system in Japan (Nakamura 1996, 2004).

After the Kobe earthquake, UrEDAS (Nakamura 1988) was updated and a new version called **Compact UrEDAS** (Nakamura and Saita 2007b), which can issue the alarm by analysing 1 sec of P-wave data has been established. The damaging potential of earthquake is estimated in terms of *Destructive Intensity (DI)*, which is defined as the logarithm of absolute value of the inner product of acceleration and velocity vector. The value of DI is calculated in real time and increases rapidly on P-wave arrival. The maximum value of DI within selected time window after P-onset is used for issuing P-

wave alarm. This system is operational since 1997 as a P-wave detection onsite system along the railroad in Japan (Nakamura and Saita 2007a). A subway Compact UrEDAS was installed in Tokyo metropolitan area in 1998.

The subway Compact UrEDAS was replaced by **FREQL** (Nakamura and Saita 2007a). FREQL was developed to minimize the processing time and issuing fast alarm by combining function of UrEDAS and Compact UrEDAS all together in a small, easy to install and noise proof structure. FREQL estimates the earthquake parameters one second after P-onset faster than UrEDAS and makes warning decision faster than Compact UrEDAS. FREQL functioning remains unaffected by influence of electric thunder noise and can detect the P-wave after a small pre-shock (Nakamura and Saita 2007b).

Mexico City also has operating EEW system similar to Japan and is termed as *Seismic Alert System of Mexico (SASMEX)*. The first *Seismic Alert System (**SAS**)* was developed after the catastrophic event of M 8.1 that occurred off the coast of Michoacan in 1985. In 1991, the system started providing warning to Mexico City subway system and some schools with a warning time of ~60 sec. In 1993, the SAS issued its first public warning for an earthquake of M 6 (Espinosa-Aranda et al. 1995; Espinosa-Aranda et al. 2009). The system consists of a network of 12 accelerometers along the coast of Guerrero. It provides two types of alerts: preventive alert for $5 \leq M < 6$, when two or more station reports moderate earthquake and public alert for $M \geq 6$, when two or more station reports strong earthquake. The basic units of a SASMEX system (Fig. 3.2) were seismic detector system (network of sensor field stations), communication system (radio relay network), central control and registry system (seismic alert issuing control unit) and warning dissemination system (Radio and TV broadcast).

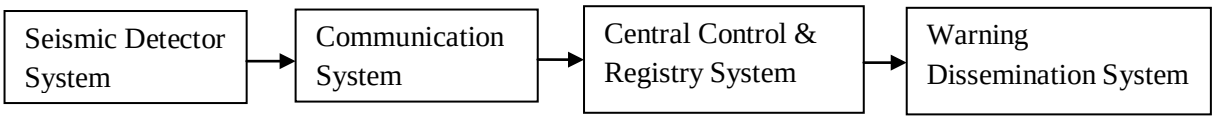

Figure 3.2 Mexican Seismic Alert System (Espiniosa-Aranda et al. 2009, modified).

In 2001 *Centro de Instrumentacióny Registro Sísmico (CIRES)* Civil Association developed the *Seismic Alert System for Oaxaca* City *(**SASO**)*. SASO comprises of 36 seismic stations across Oaxaca with 11 radio relay stations to link its coastal, central, north and isthmus regions. The system modified the SAS system approach because of the shorter

distance between seismic sources and the populated Oaxaca city. Therefore, algorithms based on shorter analyses time of 3 sec are used. Dominant period, peak acceleration and energy are calculated and analysed during the interval from the P to the S-arrival after P-onset. The dominant period of the initial 3 sec of P-wave is also measured when the S minus P time is more than 3 sec. The parameters calculated at two different time windows give empirical relations which are used to estimate the potential of event for issuing preventive and public alerts (Espiniosa-Aranda et al. 2009).

Another flourishing country which is working hard for the development and implementation of an EEW system to mitigate seismic risk is California. ***ElarmS*** which was developed in California (Allen et al. 2009) consisted of ~600 seismic instruments at ~400 sites. ElarmS is based on EEW algorithm which estimates the size of an event by analysing the EEW parameters (τ_p^{max} and P_d) calculated from the initial portion of P-waves after P-onset. In ElarmS magnitude for an event is estimated by linearly averaging the calculated τ_p^{max} and P_d based magnitudes each second. The hypocenter of the event is estimated based on the difference in P-wave arrival times at different stations. The estimated magnitude, hypocenter values and site corrections are then used to calculate attenuation relations to predict the distribution of ground shaking in the region. The system updates every second, providing an "Alert Map" of the predicted ground shaking distribution (Wurman et al. 2007). Fig. 3.3 shows the steps included in the functioning of ElarmS. The main advantage of ElarmS methodology is its ability to provide reliable, accurate and prompt EEW. The EEW parameters used in ElarmS approach provide robust magnitude estimation results because τ_p^{max} is less affected by initial uncertainty in event location, but gets saturated at higher magnitudes while P_d shows less sensitivity to saturation at higher magnitudes and uncertainty in locations but it shows more scatter at low magnitude events.

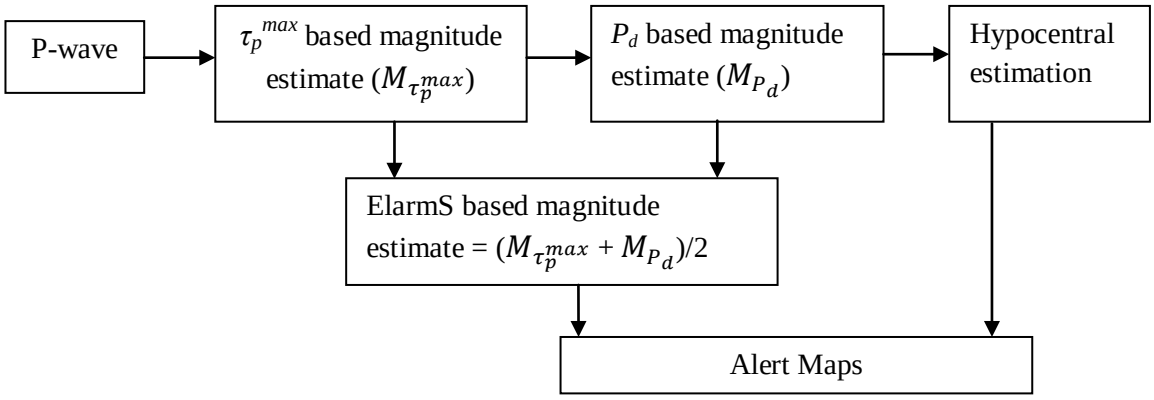

Figure 3.3 Earthquake Alarm Systems in California (Allen et al. 2009).

Wu and Kanamori (2005a, 2005b, 2007, 2008a and 2008b) used τ_c-P_d method for estimating the magnitude and PGV of the event in a time window of 3 sec. Incoming strong motion acceleration signals are recursively converted to ground velocity and displacement. When a P-onset is reported at station, it starts calculating τ_c and P_d values for a time window of 3 sec. For an event, τ_c values are considered from at least four nearest stations to calculate an average value for the event. On regressing the calculated average τ_c values with the catalogue magnitude, a threshold value for a potentially damaging event ($M \geq 6$) is estimated (Bhardwaj et al. 2012a). Similarly, P_d and PGV values are regressed to determine threshold value for P_d for damaging PGV level (20 cm/sec). Wu and Kanamori (2008a) on analyzing 54 events that comprised of 12 events from Taiwan, 26 events from Southern California and 17 events from Japan concluded that when $\tau_c > 1$ sec and $P_d > 0.5$ cm at a site, then the potential of a damaging earthquake striking the site is high. This methodology is widely used in many EEW system used in different countries, namely, Japan, China, California (Böse et al. 2009), Taiwan (Hsiao et al. 2009) and also at the *Pacific Tsunami Warning Centre* in Hawaii.

Earlier, P_d was used for estimating PGV of the event, but later Wu and Zhao (2006) related P_d with hypocentral distance and estimated P_d based magnitude (M_{P_d}) of an event. In a regional warning approach, hypocentral distance is estimated by considering difference in arrival times of P-wave at two or three stations. The EEW parameters are calculated from the initial portion of the P-wave (3 sec) are regressed with hypocentral distance and catalogue magnitude. On applying calculated relations on Southern California

dataset, P_d magnitudes agree with the catalogue magnitudes (M < 6.5) with a standard deviation of 0.18.

Zollo et al. (2006) modified the P_d approach by using initial P and S-wave for estimating the peak displacement scaling relations at variable length time window. They also normalised the observed P_d values to a common reference distance for calculating distance independent relation and concluded that magnitude estimation can be made using both initial P and S wave portion of the event records at the nearest stations. Zollo et al. (2007) and Lancieri and Zollo (2008) have applied the P_d approach on Japan dataset and concluded that at 4 sec time window P-wave and at 1 sec and 2 sec time window S-wave initial portions provides linear relations with magnitude.

Odaka et al. (2003) proposed an approach which was based on single station records, it used a simple exponential function as ($Bt * exp (-At)$) to be fitted in the initial 3 sec portion of P-wave to determine the value of coefficients A and B by least squares fit method. Odaka et al. (2003) concluded that $log\ B$ is inversely proportional to logarithmic of epicentral distance. Thus, after calculating the value of maximum amplitude of P-wave in a time window of 3 sec after P-onset, the event magnitude was estimated by using an empirical magnitude-amplitude relation that included the epicentral distance as a parameter.

A probabilistic approach for the magnitude estimation by using the Baye's theorem was termed as *Virtual Seismologist (VS)* approach and it was proposed by Iervolino et al. (2006) and Cua and Heaton (2007). In this methodology Bayesian approach was used to predict the likelihood of a given magnitude and source location using prior information such as seismicity, long term national hazard maps, known fault traces and the Gutenburg-Richter recurrence relationship (Cua and Heaton 2007). Peak acceleration, velocity and displacement were calculated every second to detect earthquake, locate it, and estimate magnitude to provide more evolutionary framework (Lancieri and Zollo 2008). It was under testing state in California and considered as an effective method of reducing number of false alarms.

In Istanbul, an early warning algorithm based on the exceedance of specified threshold time domain amplitude levels was proposed by Erdick et al. (2003). The bandpass filtered acceleration and CAV parameter values were compared with preset threshold levels. Three different threshold levels were set to issue three alarm levels by

considering nearest three station CAV values. The obtained alarms information needs to be communicated to the appropriate servo shut-down systems.

Alcik et al. (2009) further modified the CAV based approach and set more rational threshold levels based on BCAV-W parameter using Istanbul strong ground motion records. On considering BCAV with 8 sec window length, 1 sec bracket time, preset minimum acceleration level and epicentral distance range up to 100 km threshold levels (0.2, 0.4 and 0.7 m/sec) for three alarm levels to be used in Istanbul EEW system were calculated.

Hsiao et al. (2009) used a *Virtual Sub-Network (VSN)* method in EEW system for Taiwan. After the P-arrival both the VSN algorithm and P-wave method which included three EEW parameters (τ_p^{max}, τ_c and P_d) came in the operational state at the same time. When the average value of P_d calculated from five nearest stations is greater than 0.1 cm then τ_p^{max} and τ_c parameter values are calculated to determine magnitude (M_τ). For an event magnitude estimated from VSN algorithm (M_L) and P-wave method (M_τ) are compared and if both the estimated magnitude values are greater than 6, the event is consider to be potentially damaging and the shake map will be calculated for the EEW report. Warning time of around 10 sec is achieved using this approach in Taiwan EEW system.

The energy radiated in early portion of P and S-wave calculated in terms of S*quared velocity Integral (IV2)* is correlated with event magnitude (Festa et al. 2008). On normalising *IV2* for the rupture area, the energy scaling with the magnitude holds good for a wide magnitude range ($4 < M < 7$). Further, the log ($P_d^2/IV2$) is independent of rupture area, provides information regarding initial slip and has the dimension of squared time thus closely related to τ_c parameter. Therefore, the scaling relation log ($P_d^2/IV2$) and magnitude can be used for EEW system (Festa and Zollo 2009).

In Southern Italy, a probabilistic approach based software tool for EEW system was proposed by Weber et al. (2007) and was termed as *Probabilistic and Evolutionary Early Warning System (PRESTo)*. In this approach, the difference in P-wave arrival times, along with the information of non-triggered stations are used to identify the 3D region where the earthquake focus may be present (Satriano et al. 2008). P_d in a narrow time windows after the observed P and S-wave are used to estimate the earthquake magnitude and predict a peak ground motion parameter at distant target sites by using the empirical attenuation model. On applying the approach on large magnitude events, a significant effect of source fitness is observed (Zollo et al. 2009).

A neural network based approach was introduced by Maren Böse (Böse 2006) and was termed as *Pre-SEISmic* shaking *(PreSEIS)*. It is a fast methodology and is tested at Istanbul and Southern California using synthetic seismograms for finite-fault scenarios and envelope functions of real earthquakes (Böse et al. 2008; Köhler et al. 2009). At a regular interval of time after the triggering of the first station, PreSEIS estimates the most likely source parameters (latitude, longitude, depth, and amplitude of seismic record) of an earthquake using the available information on ground motions at different sensors in a seismic network. Three two-layer Feed Forward Neural Networks are used in PreSEIS methodology for the estimation of location, magnitude and rupture length of an event. The first network uses the information on the time differences ($\Delta\tau$) between the P-wave arrivals at different sensors to estimate the location of the earthquake hypocenter. The second uses the calculated CAV values and estimates hypocenter location to estimate the moment magnitude. The third network, finally, uses the outputs of the other two networks along with the calculated CAV values in order to predict the expansion of the evolving seismic rupture (see Fig. 3.3).

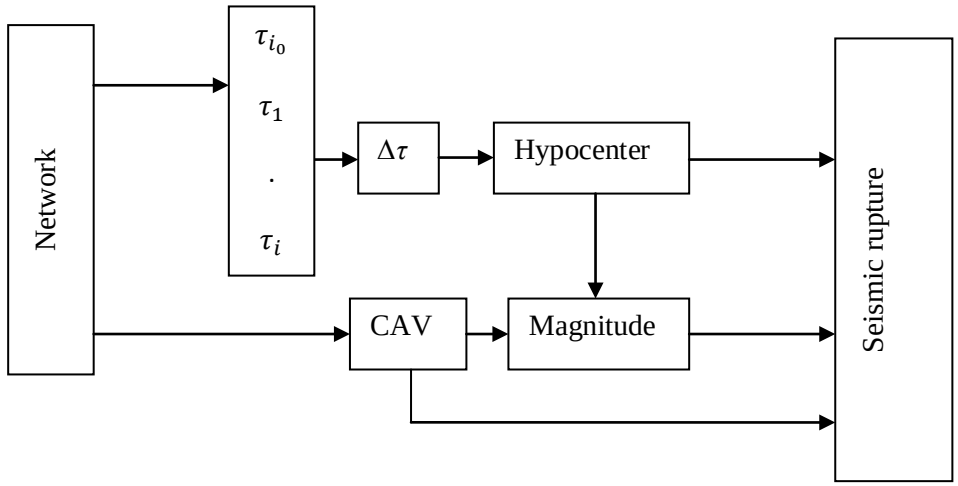

Figure 3.4 Hypocenter, magnitude and seismic rupture estimation using two-layer Feed Forward Neural Network (Böse et al. 2008, modified).

A more advanced early warning information network with no central network processing centre is in testing state in Istanbul (Fleming et al. 2009) and termed as *Self-organizing Seismic Early Warning Information Network (SOESWIN)*. In this network, each station has a sensing node, onsite processing and wireless communication ability to the adjacent stations. Software at each station triggers on P-onset and source parameters such

as arrival time, peak amplitudes and predominant period are calculated at each station and the information is shared to adjacent station. The warning alert is issued on the basis of single station detection and multiple detection stations. This network can use any of the EEW parameter based methodology.

A seismological network based on GPS networking overcome the bandwidth and the dynamic limitations present in conventional seismic network for EEW system. Also, the instruments position, long-term drifts and DC offsets problem are mitigated by GPS instruments. The GPS receiver, unlike the seismometer, measures displacement directly and due to availability of wide dynamic range signal remains unclipped making the system more sensitive to large earthquakes (Crowell et al. 2009).

Caprio et al. (2011) proposed a real time inversion of displacement spectra approach for magnitude estimation in an EEW system. The low frequency plateau of the displacement spectrum is calculated by fitting Brune's ω^2 model in the initial portion of P-wave (Brune 1970). The parameter estimation starts after 1 sec of P-arrival at single station and keeps on updating every second to predict the event magnitude. In starting seconds the event under estimated the predicted magnitude but with increase in time window more data because available and more accurate estimation will be achieved. They concluded that the estimation is stable once the deviation in estimated and network magnitude is within 0.3 units, and at a time window of around 10 sec stable magnitude estimation results for South California and Japanese dataset were obtained.

Böse et al. (2013) developed and implemented the CISN-ShakeAlert EEW demonstration system for California. This system combines three algorithms namely, VS, ElarmS and τ_c-P_d, to estimate various source parameters estimated from the analysis of the initial period of P-wave. The estimated parameters are fed into decision module to generate "ShakeAlert" which includes the most probable estimate of magnitudes, locations, expected seismic intensities and probabilities of correct alarm for an event. At the user's site, the alert messages are received and displayed in real-time via a User's display that runs on user's computer.

3.5 STATUS OF EEW SYTEMS AROUND THE WORLD

The development of EEW system in various countries also depends on the financial, political and sociological support. The requirement of an EEW system includes: liable warning, development of automatic control systems for machines and structures,

training and educational programs for user to respond and integration of EEW system with other system. Development and implementation of EEW systems in the seismic active countries were accelerated after the occurrence of devastating earthquakes in recent past. The seismic hazard levels worked out under the Global Seismic Hazard Assessment Program (GSHAP), a global hazard seismic map (Giardini et al. 1999) shows the levels of hazard in various parts of the world. The seismic hazard in terms of 10% exceedance in 50 years is shown in Fig. 3.4. The high values of seismic hazard are well matched with the countries like Japan, Mexico, Turkey, Taiwan and Romania having operating EEW system and lies in high risk zone having PGA value greater than 1.6 m/sec^2. Other countries like California, Italy, Switzerland and China are also in high risk zone and are actively experimenting and prototyping their EEW systems. Still certain countries which are under high risk zone such as Arabian countries, India, New Zealand, and Indonesia do not have any real time risk mitigation system.

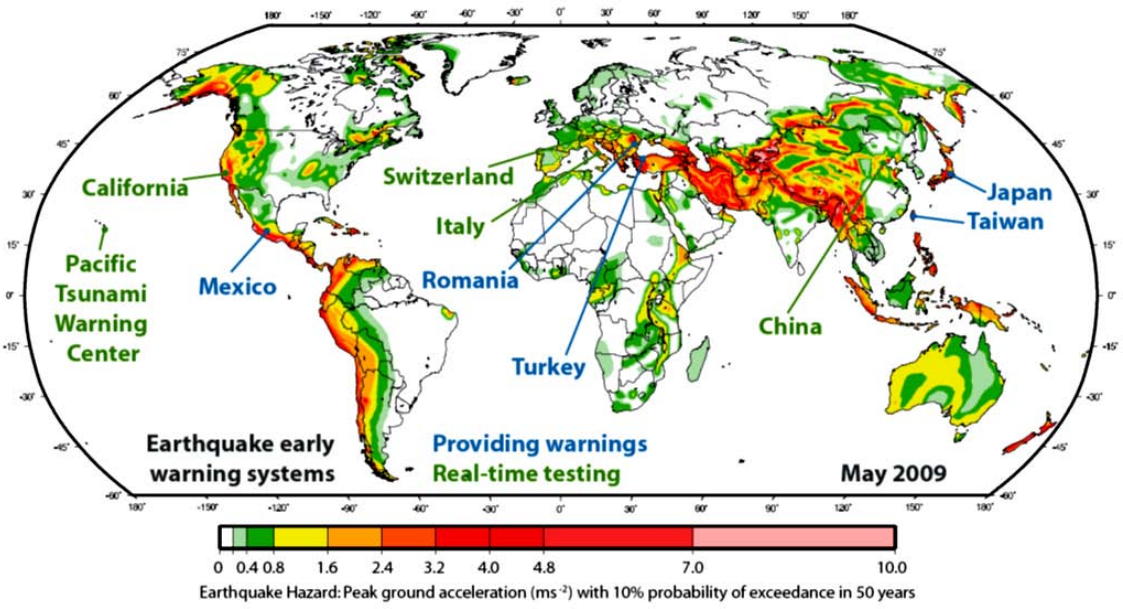

Figure 3.5 Global seismic hazard map showing locations having EEW systems either in real-time testing state (green) or in operational state and provide warning (blue) to potential users (Giardini et al. 1999).

Japan and Mexico are the earliest ones which started using EEW system. Both onsite and regional warning approach are used for EEW in Japan for e.g., in the 2004 Niigata earthquake (M 6.6) the compact UrEDAS system provides onsite warning and prevent derailment of trains in the epicentre region. The regional EEW system provides

warning for multiple earthquakes such as Iwate-Miyagi Nairiku earthquake in 2008 (Kamigaichi et al. 2009). A *National Research Project on Earthquake Early Warning System and its Application (NRPEEWSA)* program was started in Japan as a joint venture by different agencies to enhance the EEW technologies along with a prototype for practical application during 2003-2007. The *Japan Metrological Agency (JMA)* in the year 2007 started issuing public warning to limited users who were trained to take proper action on received EEW. The public warning from JMA are communicated to the users via various broadcasting means such as TV, radio, public loud speakers and cell phones. In Japan: schools, universities, trains, banks, buildings and nuclear power plants are using EEW alerts in day to day life (Kamigaichi et al. 2009).

Mexico is using EEW systems for issuing public warning since 1993 (Espinosa-Aranda et al. 1995). Devastating earthquake in Mexico 1985 of M 8.1 led to the development of SAS system. Earlier in 1991, this system issued warning to limited number of users such as schools, universities, housing complexes and government buildings, but later it started giving public warning using TV channels and radio. SAS system issue public and preventive warning for e.g., for a magnitude range of 4.1 to 7.3 the SAS system issued 13 public and 52 preventive warnings from October 1991 to March 2009. The system consists of 12 accelerometers installed at about 25 km inter-station spacing along the Guerrero. September 14, 1995, SAS system provided a warning time of about 72 sec for an event, due to the large distance available between Mexico City and the seismic source (Espinosa-Aranda et al. 1995; Goltz and Flores 1997). Later, on June 15, 1999, Oaxaca City suffered severe damaged due to earthquake having M 6.7 and lead to the development of SAS system for Oaxaca. The SASO system consists of 29 accelerometers installed in the seismic active regions around Oaxaca City and it has issued five preventive and three public alerts from November 2003 to July 2005 (Espinosa-Aranda et al. 1995).

Other countries like Bucharest, Taiwan, Istanbul, and California have small scale EEW system which provides warning to limited number of users. Bucharest, the capital city of Romania, has noticed severely damaging earthquake from 1940 to 1990 with magnitude ranging from 6.9 to 7.7 with their foci in the seismogeneic Vrancea zone of the Southeastern Carpathians with an average hypocentral distance of around 160 km. A network of three seismic stations based on regional warning approach was installed in the Vrancea region for a warning time of 20 to 25 sec (Wenzel et al. 1999; Böse et al. 2007; Wenzel and Lungu 2000; Wenzel and Marmureanu 2007). This system provides warning

to a nuclear research facility (Ionescu and Marmureanu 2005; Ionescu et al. 2007). Due to small ability of warning time the system cannot issue public alarms but can provide warning to critical units (Marmureanu et al. 2011).

Taiwan is located on the western circum Pacific belt and most of the devastating earthquakes occurred in Taiwan due to the convergence of the Philippine Sea plate and Eurasian plate to the east of it. After the occurrence of three damaging high magnitude earthquakes in Taiwan from 1906 to 1999 (viz., Chi-Chi earthquake) having magnitude range of 7.1 to 7.8, the *Central Weather Bureau of Taiwan (CWB)* led the development of EEW system in Taiwan (Wu et al. 1997, 1998). The system became operational in 2001; it comprised of about 100 seismic stations and used VSN approach for issuing warning for potentially damaging earthquakes by analysing energy present in the initial portion of P and S-wave (Wu and Teng 2002). The system provides a warning time of about 20 sec (Wen et al. 2009). A magnitude-dependent relation between stress parameter and magnitude for reverse faulting spectral models in Taiwan was proposed by Sokolov et al. (2002) followed by time dependent integrated approach to seismic hazard assessment for Taiwan region by using EEW parameter called period of maximum hazard (Sokolov et al. 2004). Also, the regional and onsite warnings are combined together to provide warning to much larger area (Wu and Kanamori 2005a, 2005b). The system provides warning to limited number of users like Bucharest EEW system. No public warning has been issued in the region because no public campaign has been done yet (Hsiao et al. 2009).

The devastating Kocaeli and Düzce earthquakes (M = 7.4 and 7.2) in 1999 that occurred on the strike-slip type *North Anatolian Fault Zone (NAFZ)*, caused severe damage in Istanbul City of Turkey. Due to high population density of Istanbul, a high risk and vulnerability is associated with this city on the occurrence of a high magnitude earthquake. Thus, the IERREWS was installed by the Kandilli Observatory of the Bogazici University for seismic risk reduction in Istanbul and the Marmara region (Erdik et al. 2003). Earlier, EEW system was designed to provide warning to two specific users namely, electric power station and office building. But later the warning is provided for the whole city by using an array of 10 strong motion sensors installed along the coast of the Sea of Marmara which transmit strong ground motion data in real time to the data-centers in Istanbul. There are 100 accelerometers installed in Istanbul, which are operated in dial-up mode for the generation of rapid response information, such as shake maps and loss maps (Erdik et al. 2003). Alcik et al. (2009) introduced a simple and robust algorithm, based on

the exceedance of specified threshold time domain amplitude, CAV and BCAV-W levels. A Neural Network approach (PreSEIS) was also suggested by Böse (2006) to provide fast and accurate warning to Istanbul metropolitan area by estimating source parameters within a few seconds after P-arrival. The system is in operational state and planned to provide warning to more general users such as gas lines, railways, elementary schools and engineering applications (Shieh et al. 2011).

In California many research units and agencies such as *United States Geological Survey (USGS), Berkeley Seismological Laboratory (BSL), California Institute of Technology (Caltech),* the *University of Southern California (USC)* and *Swiss Institute of Technology Zürich (ETH)* are working for development and implementation of EEW system in California since 2007. ElarmS system was developed in California and has been tested using Northern California, Southern California and Japan dataset (Allen and Kanamori 2003; Allen 2007; Wurman et al. 2007; Tsang et al. 2007 and Allen et al. 2009). The algorithm used in ElarmS system for location, magnitude and intensity estimation is updated in 2010-2011 by a direct C++ code (E2 code) for a high performance magnitude, location determination and improved alert modules. The resulting E2 code is fast, efficient and reliable, running continuously in real-time and sending alert messages to CISN ShakeAlert. Further, in 2012 Artificial Neural Network approach was applied in ElarmS processing to improve uncertainties by sorting false alarms prior to transmission to the ShakeAlert Decision Module. ShakeAlert decision is used by various users, display units and engineering applications.

VS is currently operating as a real-time test system in Switzerland. The VS (Iervolino et al. 2006) algorithm was derived and calibrated using Southern California dataset. In Southern Italy PRESTo (Weber et al. 2007) approach is in testing state on the Irpinia Seismic network. The EEW methodologies are in testing state at the Pacific Tsunami Warning Center also using regional seismic network.

Earlier, the researchers were doubtful about the scientific and technical feasibility of EEW approach. As of now, the EEW approach has proved its feasibility both in a regional warning approach such as Mexico City and in onsite warning approach for areas having population centre near to seismic source like Japan. Another misconception about EEW is that a few seconds of apriori information about a large magnitude earthquake may result in panic. Japan and Mexico are the countries which issue public alarms and till now no case of stampedes and traffic accidents due to warning have been noticed. There are

certain challenges related to EEW implementation such as effective use of EEW system by providing information to appropriate users and inclusion of finite sourced detection methods (Heaton 1985; Allen 2006) with magnitude, intensity and location estimation.

3.6 SUMMARY

A detailed review of several EEW parameters (τ_p^{max}, τ_c, P_d, CAV, CAV5, BCAV and BCAV-W), different EEW methodologies and systems such as τ_c-P_d, VS, VSN, PRESTo, PreSEIS, UrEDAS, Compact UrEDAS, FREQL, SAS, SASO, ElarmS has been done in this chapter.

The importance of EEW system has been recognised by different seismic countries around the world as a real-time risk reduction measure. The EEW system provides social safety by providing warning to schools, hospitals, air traffic control and other users unit to take protection measures to remain operational and also minimize the losses that may result from secondary events triggered by large earthquake such as: tsunamis, landslides, train derailment and other accidents.

The status of EEW system in different countries with respect to their development, implementation, and social resilience has been discussed. The requirement of efficient, reliable EEW algorithm and EEW system in other seismically active countries such as Arabian countries, India, New Zealand and Indonesia has been observed.

CHAPTER 4

METHODOLOGY

4.1 INTRODUCTION

The issuance of warning by EEW system depends upon the accuracy and reliability of predicted parameters used to define the size of the incoming event in real time. Various parameters are used for estimation of magnitude and issuing alarm in EEW system worldwide. In the present study, an attempt has been made to combine various EEW parameters to develop an algorithm, which can issue alarm and estimate magnitude with reliable accuracy in minimal time window.

This chapter is divided in three sections. The first section consists of brief discussion of the parameters used in the development of EEW algorithm. The second section describes steps for designing the algorithm, and the last section describes the estimation of magnitude from initial portion of P-waves.

4.2 METHODOLOGY

The early warning methodologies available around the globe can be broadly classified into two approaches (see chapter 3). The first one is regional warning approach, which is based on seismological method of estimating size of earthquake, and prediction of ground motion at other sites. This is a network based approach and processing of data is carried out from a network of seismic instruments. The second approach is termed as onsite warning approach, which is based on the analysis of initial portion of P-wave to estimate seismic parameters. In this approach, the ground motion identified at a site is used to provide warning of coming ground shaking at the same site viz., detect the P-wave, and predict the peak shaking.

Regional warning approach is more reliable than onsite warning approach, as it provides more comprehensive information about the impending earthquake. However, it takes more time for analysis that increases the “blind zone” around the epicenter, where no warning can be provided. In contrast, the onsite warning approach has the potential to increase the

warning time all around, by reducing the radius of the blind zone and potentially provide warning at the epicenter. The combination of these two approaches will result in a more reliable and useful EEW approach. Wu and Kanamori (2005a) in Taiwan have applied this combinational approach. Later, Wu et al. (2007) extended onsite warning to regional warning; they tested 13 events in South California within an epicentral distance of 30 km. To add the regional warning approach, 4 to 6 earliest arrivals were used to locate the magnitude of the event. The event magnitudes were determined from τ_c and P_d parameters by taking the average of P_d values and τ_c values calculated at the considered stations. Obtained magnitude estimates using P_d and τ_c parameters viz., M_{P_d} and M_{τ_c}, respectively, have good agreement with each other as well as with catalogue magnitude. Thus, by using P_d parameter along with τ_c provide better estimate of event magnitude and also, increased the robustness of early warning.

High density seismic networks with real-time data transmission capability are considered to be the primary requisite for an EEW system which is followed by an algorithm for the automatic processing of seismic data, and to retrieve the seismic source parameter information from the processed seismic signal. Thus, the algorithm encompasses the detection of earthquake and determines seismic source parameters to estimate magnitude of the earthquake for issuing warning. Present chapter deals with the algorithm development phase of an EEW system. The automatic P-wave picking algorithm based on Allen (1978) and RSSCV parameter have been discussed in details followed by the comprehensive details of EEW parameters i.e. τ_p^{max}, τ_c, P_d and CAV which are used for estimation of event magnitude and issuing alarms in the specified time interval.

4.3 AUTOMATIC DETECTION OF PRIMARY WAVE ONSET (P-onset)

The first step required for real-time processing of seismic data in an EEW system is automatic detection of P-onset in a continuously streaming data. Traditionally, the auto P-onset detection algorithm is based on *Short Term Average (STA)* and *Long Term Average (LTA)* values (Vanderkulk et al. 1965). Allen (1978) and Magotra et al. (1987) further extended STA/LTA approach in automatic earthquake recognition and source location using single station. Allen's (1978) automatic P-onset detection algorithm is widely used in EEW systems by various countries. The basic requirement of an automatic P-onset detection

algorithm is its ability to distinguish between noise and earthquake signal. Dowla et al. (1990) describes the possible discrimination between natural earthquakes and other source of ground motion signal. There are other approaches available in literature for auto P-onset detection, which are based on data-driven reasoning and pattern recognition (Chiaruttini and Salemi 1993; Joswig 1990). Discrete wavelet transform technique and Higuchis method to characterize and detect P-wave have also been used in EEWS by Colak et al. (2009) and Gonzalo et al. (2012).

The P-onset concept is based on the amplitude variation. However, Allen (1978) included the frequency component by using first order FIR filtering. The LTA was filtered to show the background noise level to its lowest, and the STA was filtered to enhance the signal to noise ratio in the range of frequency component arrivals from a seismic source. The inclusion of filtering in addition to the amplitude monitoring enhanced the efficiency of the phase picker algorithm. Such algorithms were evolved for processing of the data from seismological arrays or networks where location of the earthquakes was of prime importance. In case of EEW, the significance of estimating incoming energy, damageability and the size of earthquake becomes more important in addition to location of the events. Therefore, a new approach has been adopted in which the energy content in the incoming time series has been analyzed online in place of the amplitude or the frequency variation, as was done by Allen (1978). The new approach will help not only in estimating the onset time but also in looking feasibility of using such parameter for issuing warning, as it is proportional to the incoming energy or damageability of the earthquake.

In present chapter, a new approach for automatic P-onset picking, has been used, i.e., RSSCV (Bhardwaj et al. 2013a). RSSCV is simply an advancement of CAV approach, and is defined as:

$$RSSCV = \sqrt{\sum_{i=1}^{n} v_i^2} \tag{4.1}$$

where, v_i is the ith value of the velocity vector calculated by integrating the acceleration time series up to n viz., number of sample present in the selected window length. In RSSCV parameter, the energy content in the incoming time series is assumed to be present more in terms of velocity components in relation to other component of ground motion. Therefore, not

only the predominant velocity in the time series was explored but also the cumulative effect was observed in terms of its energy component.

In RSSCV triggering algorithm, the vertical components of the strong ground motion records are baseline corrected by fitting first degree polynomial on the data. The baseline corrected data is integrated to obtain corresponding velocity record. Velocity values are then filtered with a fifth order high-pass Butterworth filter having cut off frequency 0.075 Hz. Filtering removes the low frequency drift added to the data during integration process. RSSCV vector has been obtained by using a continuous sliding window of 3 sec on velocity record by using Eq. (4.1). The P-onset point is searched in the RSSCV vector by continuously calculating the difference in five samples of RSSCV vector starting from first and fifth samples till the difference of any five samples is found to be ≥ 0.01 cm/sec. The point at which the difference exceeds the preset threshold value, the event is considered to be triggered and the corresponding RSSCV sample is marked as the P-onset point (see Fig. 4.1).

After P-onset detection, the next step is to issue warning for potentially damaging earthquake. RSSCV parameter has its merit of providing estimate of the energy in the signal therefore, it can be used for magnitude estimation of the event too. In view of this the parameter namely, RSSCV can be used for auto P-onset detection as well as for issuing alarms.

4.4 EARTHQUAKE LOCATION DETERMINATION

Earthquake location is another important aspect of an EEW system. In general, hypocenter location is estimated using P and S wave arrivals at three or more seismic sensors distributed around the epicentre. Mohorovicic (1915) and Pujol (2004) used graphical approaches called Encompass circle and Hyperbola method, for determining epicentral position with just two triggered stations. Horiuchi et al. (2005) extended the approach by constraining the hypocentral position by considering non-triggered stations at the time (t_{now}) along with triggered stations. ElarmS approach (Allen 2007) uses the grid search algorithm for event location and origin time. This approach used three or more triggered station for locating an event.

Cua and Heaton (2007) integrated both Horiuchi et al. (2005) and Rydelek and Pujoil (2004) approaches with the concept of Voronoi cells that identify the location with single triggering station. Based on arrival time order and Voronoi diagram, Rosenberger (2009) identified epicentral location more rapidly without using velocity model.

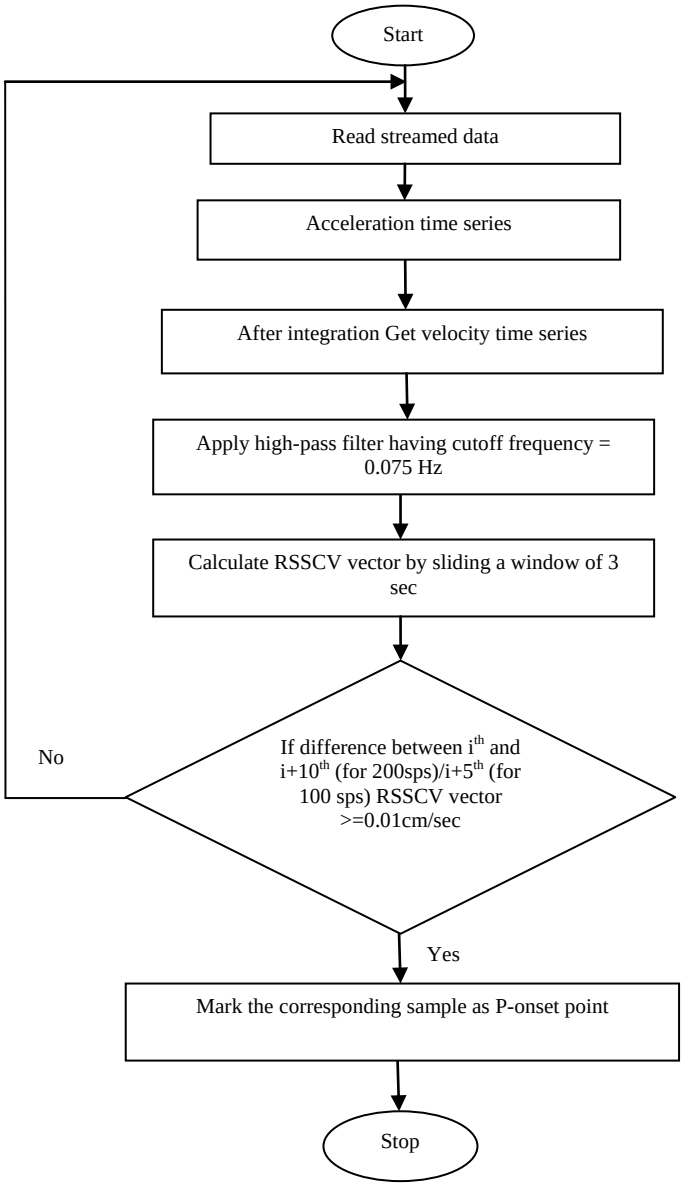

Figure 4.1 Flow chart for automatic P-onset detection algorithm using RSSCV parameter.

UrEDAS, the well-known Japanese EEW system, is also based on single station location approach. For an event, magnitude is estimated by calculating τ_p parameter (Allen and

Kanamori 2003) from the initial portion of P-wave and epicentral azimuth estimation using three components of the single station.

Odaka et al. (2003) presented the single station approach for quick estimation in a different manner. An exponential function $f(t) = Bt * exp(-At)$ was fitted in the initial part of the vertical acceleration waveform envelope; where, t denotes the time, B represents slope of the initial part of P-wave, and A shows amplitude variation with time. A and B are determined through regression from previous events. It was observed that there is an inverse proportionality between $log\ B$ and $log\ \Delta$, where, Δ represents the epicentral distance, and the relation is independent by earthquake magnitude.

Other approaches for real time location identification used in EEW system include VS approach and artificial neural networks approach (Cua 2004 and Böse 2006). In the present study, the locations of the earthquakes are known apriori, and have been taken from the same catalogue which has been used to compile datasets for regression analysis.

4.5 EARTHQUAKE MAGNITUDE

Magnitude estimation in EEW system is generally based on two approaches, first by using the information from the beginning of rupture process, and second by using the initial portion of P-wave for estimating the eventual size of an earthquake. Umeda (1990), Iio (1992, 1995), Ellsworth and Beroza (1995) and Beroza and Ellsworth (1996) in various studies observed that the initial portion of rupture process has the capability to differentiate between large and small earthquake. The nucleation phase model suggests that the initial low amplitude phase tends to last longer for large earthquake. However, Nakatani et al. (2000) has opposed this theory and suggested that micro earthquakes having strong initial rupture tend to grow larger. Mori and Kanamori (1996) and Kilb and Gomberg (1999) found no significant difference between small and large rupture process. Later, Sato and Kanamori (1999) investigated using Griffith's fracture criterion, that variation of fracture toughness near the fault tip can produce variations in P-waves of seismic rupture. But the complexity of rupture process makes it difficult to use initial rupture process for estimating size of an earthquake. The second approach which is based on the initial portion of P-wave for magnitude estimation similar to nucleation phase model but it is conceptually different.

When an earthquake occurs, P and S-waves are generated. Amplitude of P-wave is smaller in comparison to S-wave, however, P-waves have speed approximately twice of S-wave. P-waves are considered as non destructive and carry information about the slip on the fault, while the S-waves are destructive in general and carry information about the energy content in the wave viz., peak ground motion. In EEW system, the initial portion of P-wave over a selected time window after P-onset has been analyzed for retrieving the information about earthquake source parameter. The estimated parameters are empirically regressed with the final magnitude of the event to determine threshold for issuing warning. Five EEW parameters namely τ_p^{max}, τ_c, P_d, CAV, and RSSCV have been used in the present study for development of EEW algorithm. These parameters are described in details as follows.

4.5.1 Maximum Predominant Period (τ_p^{max})

The concept of predominant period (τ_p) has been introduced by Nakamura (1988), where the difference between large and small earthquake has been explained on the basis of frequency content present in the seismic signal. Small earthquakes occurs due to slip in small portion of the fault, and results in high frequency energy. However, large earthquake occurred due to slip in large area of fault resulting in low frequency component and thus, large predominant period.

The parameter, τ_p has been calculated from the vertical component of the acceleration time series for each time step in real time. The recursive relation is defined as:

$$\tau_{p,i} = 2\pi \sqrt{\frac{V_i}{D_i}} \tag{4.2}$$

$$V_i = \alpha V_{i-1} + v_i^2 \tag{4.3}$$

$$D_i = \alpha D_{i-1} + \left(\frac{dv}{dt}\right)_i^2 \tag{4.4}$$

where, v_i is the recorded ground velocity, V_i is the smoothed ground velocity squared, D_i is the smoothed velocity derivative squared, and α is the smoothing parameter ($0 \leq \alpha < 1$). τ_p^{max} is defined as the maximum value of τ_p in the selected time window. In τ_p^{max} calculation, velocity time series are obtained by integrating the acceleration time series. The velocity

records are filtered by applying a high-pass filter Butterworth filter having cutoff frequency of 0.075 Hz and in addition to it a 3 Hz low-pass filter is also applied (Allen and Kanamori 2003). The average of τ_p^{max} value for each event is regressed with respect to magnitude (Wurman et al. 2007) as:

$$log\, \tau_p^{max} = (A * M + B) \pm \sigma_{log\tau_p^{max}} \quad (4.5)$$

where, *A* and *B* are regression coefficients determined from the regression analyses and $\sigma_{log\tau_p^{max}}$ is the standard error associated with the distribution of random variables $log\, \tau_p^{max}$. Further, the determined τ_p^{max}- M regression has been used to estimate the magnitude of the event by calculating τ_p^{max} value from initial portion of P-wave.

The concept of τ_p^{max} was practically first implemented in UrEDAS, the oldest onsite EEW system that used on the tracks of Shinkansen train in Japan (Nakamura 1988, 1989, 1998, 2004; Nakamura and Satia 2007b). Further, Compact UrEDAS uses the same τ_p^{max} concept and provides fast warning by using a time window of 1 sec (Nakamura and Saita 2007b). FREQL is further advanced mobile unit that respond faster than UrEDAS and Compact UrEDAS (Nakamura and Satia 2007b). The ElarmS EEW methodology also founds its basic from the τ_p^{max} concept. It uses 4 sec time window after P-onset for estimating the size of an event (Allen and Kanamori 2003; Olson and Allen 2005; Allen et al. 2009).

4.5.2 Effective (Average) Period (τ_c) of P-wave

Wu and Kanamori (2005a, 2005b) modified Nakamura (1988) approach, and proposed another EEW period parameter τ_c, which is also calculated from the initial portion of the P-wave. The τ_p calculation is recursive, and use acceleration and velocity records, whereas τ_c calculation is done over a fixed interval of time and uses velocity and displacement time records.

For calculating τ_c ground motion displacement $u(t)$ and velocity $\dot{u}(t)$ are obtained by integrating the acceleration records of vertical component:

$$r = \frac{\int_0^{\tau_0} \dot{u}^2(t)\, dt}{\int_0^{\tau_0} u^2(t)\, dt} \quad (4.6)$$

where, 0 to τ_o limits of integration represents time interval selected after the P-onset. Generally τ_o is taken to be 3 sec (Wu and Kanamori 2005a, 2005b; Wu et al. 2006, 2007) and is estimated using Parseval's theorem as follows:

$$r = \frac{4\pi^2 \int_0^\infty f^2 |\hat{u}|^2 df}{\int_0^\infty |\hat{u}|^2 df} = 4\pi^2 \langle f^2 \rangle \tag{4.7}$$

where, $\hat{u}(f)$ is the frequency spectrum of *u(t)*, and $\langle f^2 \rangle$ is the average of f^2 weighed by $|\hat{u}(f)|^2$ then,

$$\tau_c = \frac{1}{\sqrt{\langle f^2 \rangle}} = \frac{2\pi}{\sqrt{r}} \tag{4.8}$$

The parameter τ_c provides the average of initial portion of P-wave in the selected time interval. τ_c symbolize width of the initial portion of P-wave, and its value increases with the increase in magnitude (Wu and Kanamori 2008a). The average τ_c value for each event are then regressed with magnitude to get τ_c - M relation as follows:

$$\log \tau_c = (A * M + B) \pm \sigma_{\log \tau_c} \tag{4.9}$$

where, *A* and *B* are regression coefficients determined from regression analyses, and $\sigma_{\log \tau_c}$ is the standard error associated with the distribution of random variable *log* τ_c. For an event first τ_c values are calculated using initial portion of its P-waves followed by its magnitude estimation by using predetermined τ_c - M empirical relationship.

Since the seismic waves encompass different regions having different properties, the empirical relation between τ_c - M may vary from region to region. In addition to the source and the site effects, the medium characteristics in terms of attenuation of seismic waves play an important role in affecting the amplitude and frequency content of the incoming seismic waves. To investigate medium effect on EEW parameter, attenuation characteristics of a medium which can be described in terms of *Quality factor at 1 Hz* (Q_o) has been included in τ_c - M relation (Bhardwaj et al. 2012b, 2013c). By including Q_o in EEW approach, it gets more enhanced by including effect of medium. The signature of the earthquake is available in the recorded time series convolved with the medium properties. In the present study, τ_c which is a source property is being exploited to mark the difference between two categories of

earthquake, i.e., less than or greater than magnitude 6. The width of τ_c is effected by the medium properties. Therefore, τ_c may be exploited as region dependent property along with source property.

Quality factor is commonly found to be frequency dependent, which is often examined by relaxation processes and scattering. It is given by the relation:

$$Q = Q_o * f^n \tag{4.10}$$

where, Q_o represents heterogeneities and n represents level of tectonic activity of the region. Region with higher n value emphasizes higher tectonic activity (Akinci et al. 1994, Pulli and Aki 1981, Rocker et al. 1982 and Eck 1988).

Quality factor has been estimated from various parts of seismic waves such as Q_c from coda wave, Q_α and Q_β from body wave, respectively. In the present study, Q_c relations calculated by different seismologist for the study regions namely, Northwest Himalaya, Garhwal Himalaya, Kumaon Himalaya, National Capital Region, and Northeast Himalaya have been considered. The Q_o value has been determined using the five frequency dependent Q-relations for the selected regions of India as shown in Table 4.1. Q_c estimated by different researchers for different regions of India: Garhwal Himalaya (Gupta et al. 1995), Kumaun Himalaya (Paul et al. 2003), Northeast Himalaya (Gupta and Kumar 2002), Northwest Himalaya (Kumar et al. 2005), and National capital region (Mohanty et al. 2009) has been plotted in Fig. 4.2. The variation in slopes reveals the different attenuation characteristics of the regions, and the same can be used to represent the region in the empirical relationships between EEW parameters, especially τ_c, M, and the attenuation characteristic in terms of Q_o. As discussed above τ_c value has been calculated for a time window of 3 sec using Eq. (4.8). Then, a regression of τ_c with Q_o and magnitude gives a generalized Eq. as follows:

$$\log \tau_c = A * M + B * \left(\frac{Q_o}{1000}\right) + C \tag{4.11}$$

where, A, B and C are regression coefficients determined from regression analyses. Therefore, by using the empirical relationship the magnitude of an earthquake can be estimated using calculated τ_c and known Q_o value of a region. The estimation of magnitude from such relationship has the advantage that Q studies are generally carried out using low

magnitude earthquakes while prediction of magnitude is done for higher magnitude earthquakes which have not yet occurred in that region.

Table 4.1 List of Q_c relations used in the present study for the five different Indian regions.

Regions	**Q_c relation**	**Reference**
Garhwal Himalaya	$Q = 126 * f^{0.9}$	Gupta et al. (1995)
Kumaon Himalaya	$Q = 92 * f^{0.89}$	Paul et al. (2003)
Northeast Himalaya	$Q = 86 * f^{1.02}$	Gupta and Kumar (2002)
Northwest Himalaya	$Q = 158 * f^{1.05}$	Kumar et al. (2005)
National Capital Regions	$Q = 142 * f^{1.04}$	Mohanty et al. (2009)

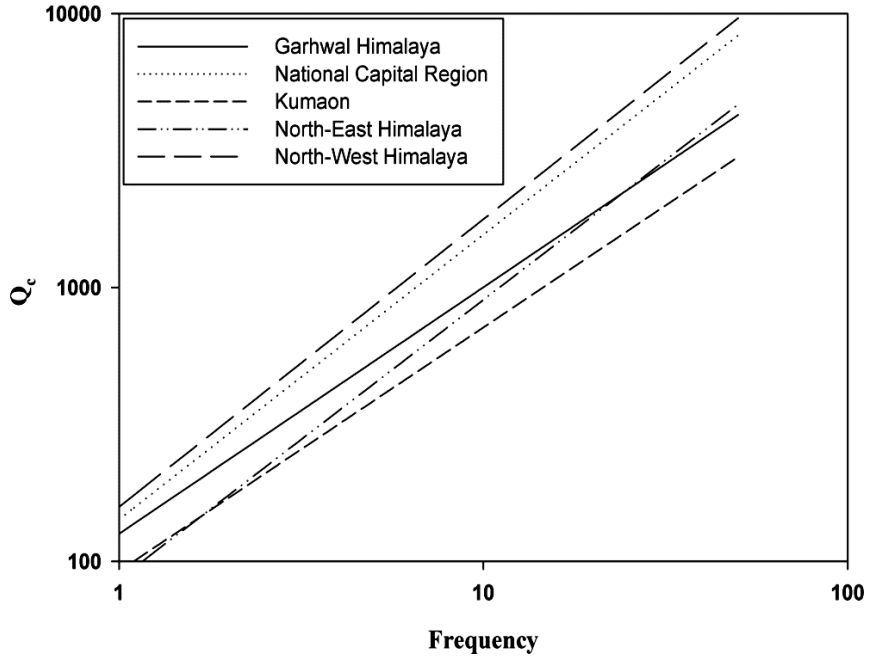

Figure 4.2 Q_c estimated by different researchers for different regions of India: Garhwal Himalaya (Gupta et al. 1995), Kumaun Himalaya (Paul et al. 2003), NE Himalaya (Gupta and Kumar 2002), NW Himalaya (Kumar et al. 2005), and National capital region (Mohanty et al. 2009).

4.5.3 Peak Displacement (P_d)

Another EEW parameter is peak displacement amplitude, measured from the initial portion of P-waves and S-waves (Wu and Zhao 2006; Zollo et al. 2006). P_d value is calculated by finding the maximum value of high-pass filtered vertical displacement amplitude in a selected time window after P-onset. Wu and Zhao (2006) have related P_d with hypocentral distance (R) using relationship that depends on magnitude:

$$\log P_d = A + B * M + C \log R \tag{4.12}$$

where, A, B and C are regression coefficients to be determined from a regression analyses. The event location estimated from the difference in arrival times at stations close to the epicenter provides value of hypocentral distance, which on regression with P_d (Eq. (4.12)) can be used to estimate the event magnitude. Further, Zollo et al. (2006) further modified this approach by normalizing the observed P_d to a common epicentral distance (10 km). The initial portion of both P and S-waves were used for estimating magnitude within a time window of 1 sec. The distance independent relation is defined as:

$$\log P_d = \acute{A} + \acute{B} * M \tag{4.13}$$

where, $\acute{A}$ and $\acute{B}$ are regression coefficients. ElarmS produces an event magnitude by averaging together the magnitudes from ${\tau_p}^{max}$ and P_d. ElarmS magnitude found to be in good agreement with catalogue magnitude, and compensate both the saturation effects of P_d at high magnitudes and the scatter of ${\tau_p}^{max}$ values at low magnitudes (Brown et al. 2009).

The P_d parameter is also used for estimating the shaking intensity of earthquakes. Wu and Kanamori (2005a, 2005b, 2008a) and Wu et al. (2005a) found a linear relation between P_d and PGV and suggested that whenever $P_d \geq 0.5$ cm, the event is most expected to be damaging.

4.5.4 Cumulative Absolute Velocity (CAV)

CAV is another simple and robust EEW parameter. CAV values are highly correlated with physical property damage such as engineered structures and anchored industrial grade

equipment. EPRI (1988) suggested that when CAV is less than 0.3 gsec, the strong ground motion are not damaging for engineered structures.

CAV belongs to integral measurement class of EEW parameters. In Istanbul (Erdik et al. 2003), CAV found its success as an effective EEW parameter as it considered the complexity of short fault distance, and fault rupture process involved. It is a simple preset threshold exceedance approach. CAV is computed by integrating acceleration record *a(t)* to time duration (t_{max}) of record as:

$$CAV = \int_0^{t_{max}} |a(t)|\ dt \tag{4.14}$$

It is also defined as the area under the acceleration curve for time duration (Bhardwaj et al. 2010). The *Istanbul Earthquake Early Warning System* (IEEWS) based on CAV have three alarm levels. An alarm is issued, when CAV value at three stations in a selectable time interval exceed specific threshold values (Alcik et al. 2009).

CAV parameter is further modified to remove its dependence on non-damaging long duration portion of acceleration time history (EPRI 1991), and named as Bracketed Cumulative Absolute Velocity (BCAV) and is defined as:

$$BCAV = \sum \int_{t_i}^{t_i+\Delta t} |a(t)|\ dt \tag{4.15}$$

where, Δt = 1 sec and bracketed interval with one acceleration value greater than 0.025 g (max $|a(t)|$ > 0.025 g). BCAV has been further modified as Windowed Bracketed Cumulative Average Velocity (BCAV-W) to overcome BCAV drawback of false alarms estimation; caused due to accumulation of BCAV values. In BCAV, the CAV calculation is done on a second by second basis for a given time history, while in BCAV-W, the calculation is performed by windowing BCAV on a large window length (W). BCAV-W increases the system robustness, and is calculated as:

$$BCAV - W = \sum_{w=1}^{win\ len} \int_{t_i}^{t_i+\Delta t} |a(t)| dt \tag{4.16}$$

where, a(t) is the acceleration value in a specific bracketed time Δt = 1 sec, and at least one value of acceleration exceeds a predetermine threshold acceleration.

CAV parameter has many other advantages as it has directive effect, and it is sensitive to low frequency motions that are damaging (EPRI 1988). CAV values have a correlation with seismic intensity. Kramer et al. (2003) mentions CAV correlation with pore pressure generation because it gives better results in performance based liquefaction hazard evaluation than any other ground motion parameter.

4.5.5 Root Sum of Squares Cumulative Velocity (RSSCV)

The RSSCV is an EEW parameter which includes the cumulative effect (amplitude and time) of ground motion duration. RSSCV is also an integral EEW parameter same as CAV (Bhardwaj et al. 2013a), and is defined as:

$$RSSCV = \sqrt{\sum_{i=1}^{n} v_i^2} \tag{4.17}$$

where, v_i is the velocity vector calculated by taking integral of strong motion records for n number of samples in the selected window.

RSSCV and CAV parameters are scaled relatively better than peak ground motion and response-spectral parameters. The RSSCV value calculated from the initial portion of P-wave has been found in good agreement with the size of earthquake in near field. *Signal to Noise Ratio* (SNR) is also found to be enhanced using RSSCV parameter which further reduces the standard error. Due to integral process involved in calculation of CAV and RSSCV their peak values appear smoother than peak values for the different slip durations at different time steps. Also, logarithmic CAV is found in good agreement with magnitude for known source to site distance (Böse 2006). The RSSCV is used for automatic P-onset detection as well as in magnitude estimation in an EEW system, which proves it as an important multitasking parameter useful for developing an EEW algorithm.

In the present study, the vertical components of the acceleration time series having a sampling rate of 100 samples per second have been used. The data having higher sampling rate has to be re-sampled using developed MATLAB code. The velocity time series have been obtained by integrating the acceleration strong motion records, and then filtered with a high-pass Butterworth filter having a cutoff frequency of 0.075 Hz to remove the low frequency drift introduced during the integration process. In case of τ_p^{max}, τ_c and P_d parameters the value

is calculated using Eqs. (4.2 and 4.8), and from displacement record in the selected time windows starting from 1 sec, 2 sec, 3 sec, 4 sec and 5 sec. For an event the value of parameters are calculated at each station within 60 km epicenter range in this study. The average value of parameter for each event has been calculated by linear averaging the parameter value at the individual station. The average values of the parameter for different events are then regressed with the magnitude of the events to obtain relations between magnitude and EEW parameter. The general form of empirical regressions between EEW parameter (*P*) and event magnitude are as follows:

$$\log P = A + B * M \tag{4.18}$$

$$M = C + D * P \tag{4.19}$$

where, *A*, *B*, *C* and *D* are the regression coefficients obtained from the regression analyses. After finding the regression relations, one has to decide the threshold for distinguishing a potentially damaging earthquake (M ≥ 6) from a non-damaging one. In Eq. (4.18) on putting M = 6 the respective EEW parameter for an event having magnitude 6 can be obtained, which can be used as a threshold value for issuing warning in an EEW system.

In case of CAV and RSSCV parameters, the threshold values for issuing warning have been determined by analytic study of K-NET data that comprises of 1726 records of 105 earthquakes. All the five EEW parameters τ_p^{max}, τ_c, P_d, CAV, and RSSCV are analyzed at 5 time windows (1sec to 5sec) and specified time domain amplitude level have been estimated for issuing warning for M ≥ 6. In the next Chapter various possible combinations that can be possible for issuing warning in minimum time interval and with reliable accuracy have been described.

4.5.6 Magnitude Estimation: An Automization from P-Wave Time Window Analysis

There are numerous magnitude estimation approaches for EEW around the world. Some are in development, and some are in testing phase like ElarmS (Allen and Kanamori 2003) and Virtual seismologist (Cua et al. 2005) in California and PRESTO (Satriano et al. 2011) in Southern Italy. Japan uses combination of energy and growth rate measure for magnitude estimation, while in Mexico maximum displacement amplitude has been used for

magnitude estimation (Kamigaichi et al. 2009). Both of these approaches are based on empirical relationships, and have more advantages than other magnitude estimation approach. These methods are valid over a wide range of magnitude and are not dependent on correlations calculated between parameters calculated from initial portion of P-waves and the final magnitude (Caprio et al. 2011). In this section a regional EEW approach for magnitude estimation has been discussed. The approach is based on real time automatic computation of acceleration and displacement spectrum for calculating source parameter and estimating magnitude of the event.

The pioneer work of Aki (1967) and Brune (1970) introduces the scaling laws to compute the source parameters using the spectra of seismic waves. These parameters provide a great deal of information about the properties of the earthquake source, and find a large number of applications in seismology and earthquake engineering. In the present study, vertical component of 1726 strong motion records generated from 105 selected earthquakes have been considered. Strong ground motion data after P-onset has been automatically analyzed at variable time window starting from 1 sec to 10 sec to estimate spectral parameters. The DC bias has been removed by fitting polynomial of first degree in the time series. A cosine tapered window has been applied on the baseline corrected data with MATLAB *tukeywin* window function that provides 20% tapering at both the ends to minimize the leakage through side-lobes (Gibbs effect). The windowed time series has been Fourier transformed adopting the standard methodology using the *FFT* function in MATLAB. The corresponding velocity and displacement time series have been obtained from acceleration time series by applying jw and $(jw)^2$ in frequency domain. Since natural frequency of sensors of the considered instruments is quite high, no instrument correction is required. The change in the amplitude and frequency contents of seismic waves on its propagating through the medium between source and site is due to reduction in its energy content. This happens because seismic waves undergoes anelastic attenuation on account of two main factors namely, the geometrical spreading and intrinsic attenuation. Thus, the spectrum is automatically corrected for the attenuation characteristics of the region by taking an average value of the quality factor (Q) with an exponential decay. The geometrical spreading correction has also been made by multiplying the amplitudes by the known hypocentral distance of the station to the source.

Using the Direct method (Sonley and Atkinson 2001), for stations within 70 km of the source, the automatic apparent source spectrum has been expressed as (Atkinson and Boore 1995):

$$\Omega_{source}(f) = \Omega_{main}(f)R * exp(\pi RF/(\beta Q))/S(f) \quad (4.20)$$

where, Ω_{source} (f) is the apparent source spectrum of displacement, Ω_{main} (f) is the recorded spectrum of displacement at distance R, β is the seismic shear-wave velocity at seismogenic depths. When an earthquake occurs seismic waves propagate from the seismic focus. In Present study analysis has been done on the initial portion of the P-waves for estimating the magnitude of the earthquake therefore instead of S-wave velocity, P-wave velocity (Liu and Liu 2012) has been considered in Eq. (4.20). *S(f)* represents the site effects in the near surface materials beneath the recording site (Wen et al. 2008). The Direct method has been used because it can be used for wider frequency range and it is less limited by signal to noise constraints (Sonley and Atkinson 2001). The vertical components were less affected by site effect ($S(f)$ =1) for all frequencies (Sonley and Atkinson 2001) therefore, only vertical components of time series have been considered in the present study (Bhardwaj et al. 2012c, 2013b).

The displacement source spectrum of an earthquake is controlled by the low frequency spectral level, Ω_o, for $f < f_c$, where the spectral amplitudes are almost constant and are dependent on *seismic moment* (M_o). For $f > f_c$, the spectral amplitudes usually decay in a power-law function of the form f^{α}, where 'α' is the exponent representing the spectral decay at high frequencies range above f_c. Commonly accepted power-law functions are of the form f^{-2} or f^{-3} that represent decay of spectral amplitudes at higher frequencies. These two functional forms are referred to as ω^2 and ω^3 models in the literature (Aki 1967; Brune 1970, 1971). Thus, from the earthquake source spectrum following two spectral parameters are estimated: (1) *Low frequency Spectral Level* (Ω_o), and (2) *Corner Frequency* (f_c).

If d(t), v(t) and a(t) are the time functions of the displacement, velocity, and acceleration, their Fourier transforms are *D(f)*, *V(f)*, and *A(f)*, respectively. According to the ω^2 source model, the approximations of the three frequency-dependent functions are:

$$D(f) = \Omega_o/[1 + (f/f_c)]^2 \quad (4.21)$$

$$V(f) = 2\pi f\Omega_o/[1 + (f/f_c)]^2 \quad (4.22)$$

$$A(f) = (2\pi f)^2 \Omega_o / [1 + (f/f_c)]^2 \qquad (4.23)$$

hence, these Eqs. can be individually approximated by automatic fitting a set of two piece-wise linear functions as displayed in Fig. 4.3.

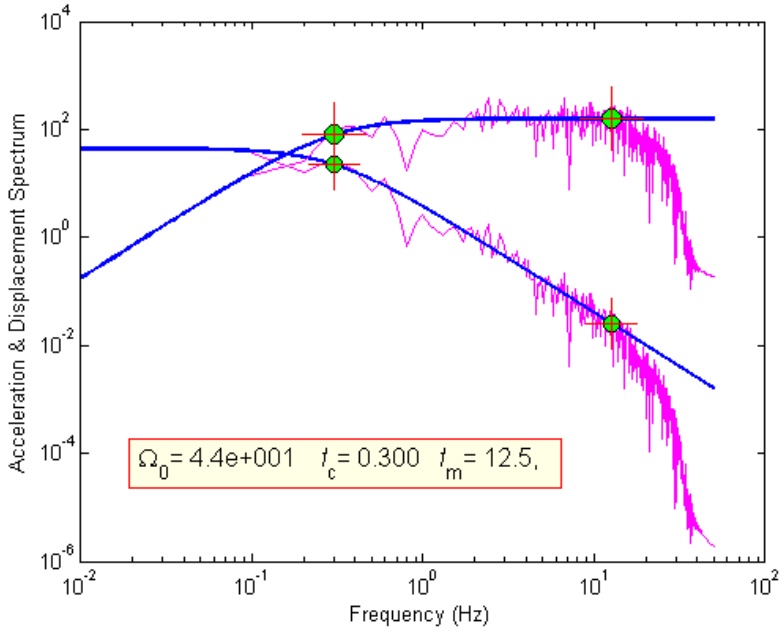

Figure 4.3 Brune's model fitted on acceleration and displacement spectrum and the calculated spectral parameters (Ω_o, f_c, f_{max}).

The f_c value is automatically picked as the index point of maximum absolute velocity. The f_{max} is obtained as the value of frequency at which jounce or snap [$S(f) = \omega^2 A(f)$] has peak amplitude. f_{max} is an important parameter which has been estimated from the acceleration spectrum. As depicted in Fig. 4.4, the theoretical ω^2-spectral model of the seismic source predicts a plateau in the Fourier acceleration spectrum for frequencies above the corner frequency f_c. However, observational data indicates a rapid decay of source spectrum for frequencies higher than f_{max} as shown in Fig. 4.4. Hanks (1982), refers this frequency to f_{max} or simply *cut-off frequency*.

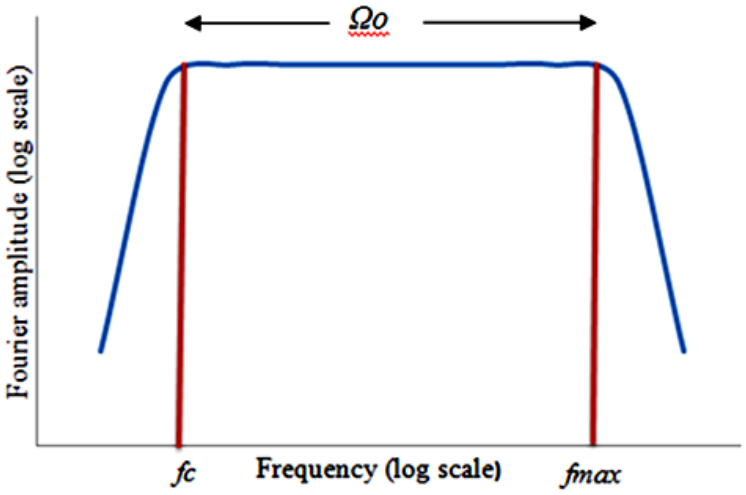

Figure 4.4 Idealized shape of Fourier amplitude spectrum of acceleration time series showing the corner frequency f_c, and cutoff frequency f_{max}.

The third parameter Ω_o is automatically calculated through the value of *acceleration's constant spectral level at intermediate frequency level* (A_{IFL}). A_{IFL} is calculated from the average acceleration amplitude level at intermediate frequencies between f_c and cutoff frequency f_{max}. Since, $A_{IFL} \approx A_\infty$ (Arjun 2011) the Glassmoyer and Borcherdt (1990) relation i.e., $f_c = \frac{1}{2\pi}\sqrt{\frac{A_\infty}{\Omega_0}}$ can be written as:

$$\Omega_o = \frac{A_{IFL}}{(2\pi f_c)^2} \tag{4.24}$$

The relation (Eq. (4.24)) helps in automatic approximation of Ω_o through the value of acceleration's constant spectral level A_{IFL}.

Finally, the seismic moment (M_o) is computed automatically from the spectra of seismic wave using the relation exploded by Keiles-Borok (1959), and modeled by Brune (1970) as follows:

$$M_o = \frac{4\pi\rho\beta^3 R\Omega_o}{R_{\theta\varphi}S_a P_r} \tag{4.25}$$

where, R is the hypocentral distance from the earthquake source to the seismic station, ρ is average density of the medium around the source, β is S-wave velocity of the medium

around the source, $R_{\theta\varphi}$ is a correction to be applied to the observed seismic amplitudes to account for the direction variation of radiation pattern of seismic waves, Ω_o is amplitude at the low frequencies measured from the S-wave spectrum after correcting for the instrument response and attenuation of medium, S_a is a correction for amplification due to free surface effect and P_r is the partition on to the two horizontal components. In this study, we have considered primary wave velocity instead of S-wave velocity for M_o estimation and thus, the parameters are modified accordingly.

After estimating M_o the corresponding moment magnitude (M_w) value is calculated using the relation (Hanks and Kanamori 1979)

$$M_w = \frac{2}{3}(logM_o) - 10.7 \qquad (4.26)$$

In case of EEW system, the main requirement is of real time processing. In the present study, the program is developed in such a way that it produces automatic trigger as soon as it starts receiving strong motion data of the impending earthquake. After P-onset an optimized window length is selected in real time for precise and reliable estimation of the size of earthquake to be used for EEW.

Fig. 4.5 shows the steps involved in designing of EEW algorithm starting from pre-processing of vertical component of time series such as baseline correction, and filtering followed by P-onset picking. After P-onset detection, EEW parameters are calculated at four nearest stations for a selected time window. The calculated EEW parameters are then compared with their preset threshold values. If the calculated parameter has value higher than the corresponding threshold value, an alarm status is set. The alarm is issued for the event only, when a defined number of stations give alarm status. Brune's model based magnitude estimation approach, is simultaneously estimating the magnitude of the event at all the triggered stations at a selected time window after P-onset. The average of event magnitude estimated at the triggered station gives the final magnitude of the event. It may be noted that, the magnitude estimated has been used as information only, and it is not participating in issuance of alarm. It has to be considered after this step whether to confirm the issuance of alarm in next step which is beyond the scope of present work.

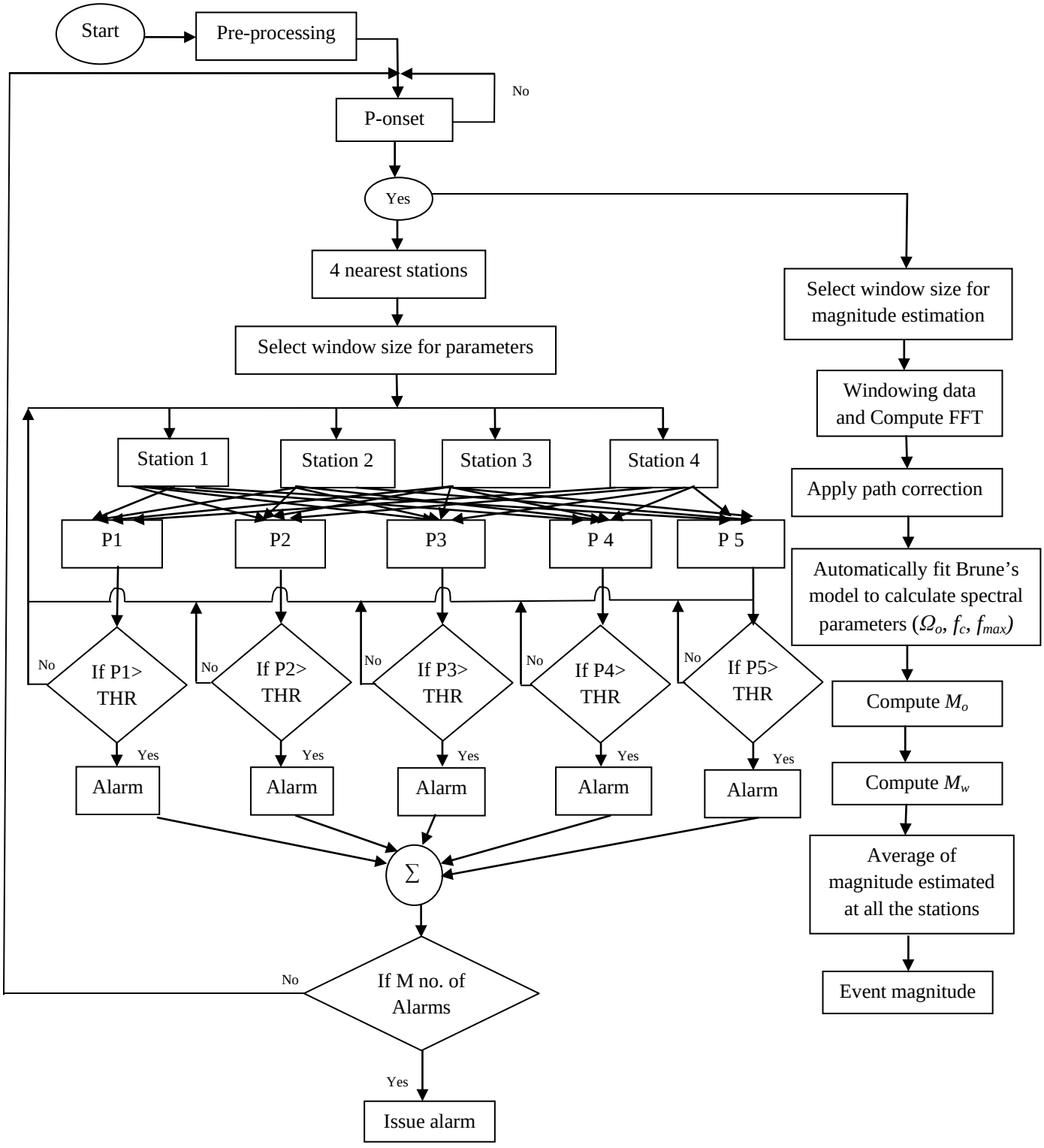

Figure 4.5 Steps involved in designing of EEW algorithm. P1, P2, P3, and P4 represent considered EEW parameters, THR represents the preset threshold values, M represents minimum number of alarm required to issue warning along with estimated magnitude for the event.

Based on the attenuation of strong ground motion with distance, and expected intensity due to the attenuated strong ground motion, the objective of EEW system in terms of the target cities, their distance from the source, and the isoseismal maps showing isoseismals of MSK intensity $\geq$ VI, it has been observed that, a magnitude 6 can be assumed to be a damaging earthquake for EEW system implementation in Northern India (Narayan et al. 2002; Sharma et al. 2013; Paul et al. 1998; Parik and Sharma 2007; Sharma 2001; Sharma and Dubey 2000).

4.6 SUMMARY

The chapter describes the methodology for the development of an EEW algorithm by auto P-onset detection, issuing warning, and magnitude estimation. This chapter consists of brief discussion of the parameters used in the development of EEW algorithm, steps for designing the algorithm and also describes the estimation of magnitude from initial portion of P-waves. The methodology is based on the analysis of initial portion of P-waves for estimation of EEW parameters, i.e., τ_p^{max}, τ_c, P_d, CAV, and RSSCV, respectively, at variable time windows starting from 1sec to 5sec. Further, the chapter also explains the method for obtaining regressions between EEW parameters and magnitude for setting threshold values to issue warning at different time intervals. The magnitude estimation method based on Brune's model has also been discussed in details.

CHAPTER 5

STRONG GROUND MOTION DATASET

5.1 INTRODUCTION

Studies related to hazard estimation or risk mitigation depend on availability of strong ground motion records from earlier earthquakes. The dataset requirements in the present study are: (i) a sufficiently large data required for regression analysis to estimate the parameters and their threshold values for EEW, (ii) validation of parameters and threshold values for the study region, and (iii) to check the stability of parameters using data from other regions which is not used in the regression analysis. The selected datasets consist of three main subsets of the data. This chapter describes these datasets in detail. The main objective of the study being the development of EEW for Indian region, the dataset availability in Indian region has been explored first. Due to paucity of data as per the requirement of the study, other regions have been investigated for such dataset.

5.2 INDIAN STRONG MOTION DATASET

In India, strong motion seismology started in 1980s with the deployment of strong ground motion instruments in the Himalaya. Under the strong motion instrumentation project funded by the *Department of Science and Technology* (DST), Government of India, the *Department of Earthquake Engineering* (DEQ), *Indian Institute of Technology Roorkee* (IITR), *Roorkee*, deployed three strong-motion arrays in the Indian Himalaya, namely, the Kangra array in Himachal Pradesh (NW Himalaya), the Garhwal array in Uttrakhand (North India), and Shilong array in Meghalaya and Assam (NE India). The Kangra array consisted of 50 analog strong-motion accelerographs (SMA 1); the Shilong array, 45; and the Garhwal array, 40. The Kangra array was located in the lesser Himalaya. The first strong motion record obtained in Himalaya was 1986 Dharmsala earthquake (M 5.4). Subsequently, the 1991 Uttarkashi and 1999 Chamoli earthquakes of magnitudes 6.8 and 6.4, respectively, were recorded.

These arrays produced quite good amount of strong-motion data, which are being used at the national and international level by engineers and scientists. These strong-motion instruments performed well up to late 90s and provided good quality recordings. However, due to unavailability of components/spare parts and due to obsolete technology, most of the strong motion accelerographs installed during this program in 1980s are no longer functional.

Recently, IITR completed a project "National Strong Motion Instrumentation Network" funded by Ministry of Earthscience, Government of India in the period 2005 to 2008. Under this program, about 300 state-of-the-art digital strong motion accelerographs were installed in north and northeastern India to record earthquake activities in Seismic Zones IV and V and in some heavily populated cities in Seismic Zone III. This strong motion instrumentation network of IITR covers the Indian Himalayan range from Jammu and Kashmir to Meghalaya and nearby plains. Average station-to-station distance has been kept at between 40 to 50 km, which ensures triggering of at least two or more accelerographs (trigger level of 5 gals) if a magnitude of 5 or larger earthquake occurs anywhere in north and northeastern India. Till date this network has recorded more than 500 records of about 200 earthquakes occurred in this region (Kumar et al. 2012a; Mittal et al. 2012a). All installed strong-motion accelerographs of this network consist of internal AC-63 GeoSIG triaxial force-balance accelerometer and GSR-18 GeoSIG-18 bit digitizer with external GPS. The 12 strong motion accelerographs installed in Delhi are K-2 (Kinemetrics K-2s) with internal accelerometer (model Episensor) and 18-bit digitizer. The recording for all instruments is in trigger mode at a sampling frequency of 200 samples per seconds. The triggering threshold was initially set at 5 gals for all the instruments. However, trigger level of 2 gals was used at many stations where spurious triggers due to local noise were found to be less.

All the processed accelerograms of this strong motion instrumentation network of IITR are available on strong motion data bank *PESMOS* (URL: http:\\www.pesmos.in). The Indian records are available with three components (longitudinal, transverse and vertical component) with a header file of each component. Figure 5.1 shows a typical vertical component file of magnitude 5.1 in Indian data format containing information regarding earthquake, site and acceleration data points etc.

```
Origin Time     04/09/2008 12:53:21     # Origin time of earthquake #
Lat.            30.1°N                  # Epicenter latitude #
Long.           80.4°E                  # Epicenter longitude #
Depth (Km)      10.0                    # Depth #
Magnitude       5.1                     # Magnitude #
Region         INDIA(UTTARAKHAND)-TIBET-BORDER-REGION # Region of Epicenter
Above details taken from IMD

Station Code       MUN                      # Site code #
Station Lat.       30.066                   # Site latitude #
Station Long.      80.237                   # Site longitude #
Station Height(m)  2183.0                   # Site altitude #
Site Class        A  Vs30 between 700 m/sec to 1400 m/sec*   # Site class #
Record Time       04.09.2008 12:53:00.379                  # Recording start time #
Sampling Rate     200 Hz                                   # Sampling frequency #
Record Duration   70.085 Sec.                              # Total recording duration #
Direction         Vert. (Up positive)                      # Type of sensors channel #
Max. Acceleration     -9.464 cm/sec**2                     # Maximum acceleration #

  * For reference see Site Classification link of website

Base Line Corrected and Low Pass Filtered (Cut Off at 35 Hz) Time History
 Acceleration data in cm/sec**2
      -0.002                                              # Acceleration first data point #
      -0.015
       .....
       .....
       0.056
       0.049
       0.025                                              # Acceleration last data point #
```

Figure 5.1 Example of header file of each component for Indian strong motion dataset.

As discussed in Chapter 4, the vertical component of strong ground motion records having magnitude range from 3.3 to 6.8 up to a epicentral distance of 60 km have been downloaded from PESMOS website. The dataset chosen for the present study consists of

strong motion records from the array of four regions namely, Region-1: North West Himalaya having 5 events, Region-2: Uttarakhand region having 11 events, Region-3: National Capital Region having 6 events and Region-4: North East Indian region having 6 events as shown in Fig. 5.4. The seismotectonics description of these regions is given in Chapter 2. Figure 5.2 shows the details of magnitude and corresponding number of earthquake records taken from Indian strong motion dataset from March, 2006 to August, 2012. There are 51 records available within $\Delta \leq 60$ km of 28 earthquake s with magnitude range of 3.3 to 6.8. The distribution of selected events magnitude with epicentral distance has been shown in Fig. 5.3.

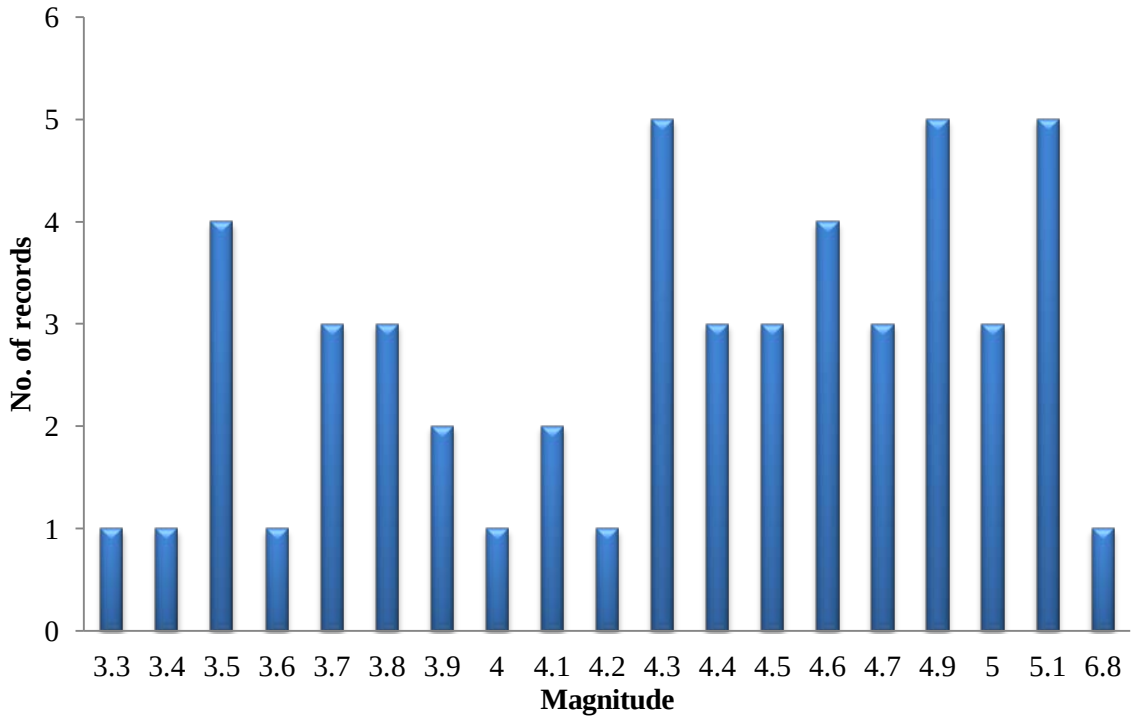

Figure 5.2 Magnitude and corresponding number of earthquake records used from Indian strong motion dataset.

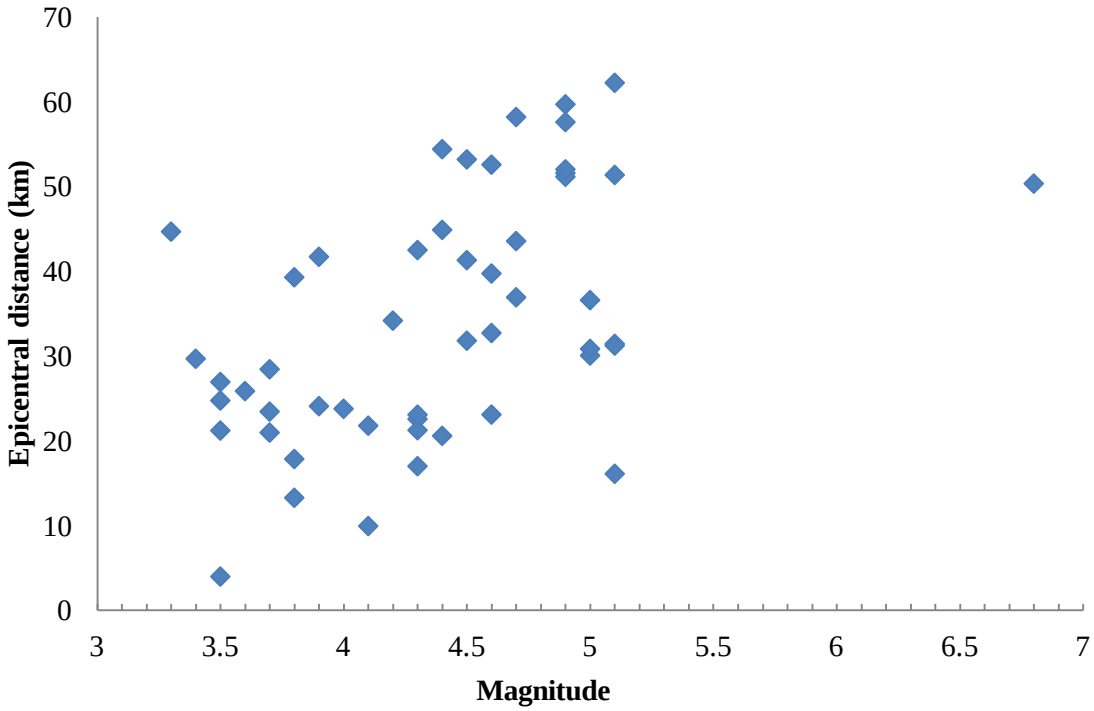

Figure 5.3 Magnitude and epicentral distance distribution of selected Indian strong motion records within 60 km range.

The detail information of the earthquake considered regarding its date, magnitude, location and number of station is given in Table 5.1. The details of the recording stations for these events are given in Appendix (A). The events used for EEW encompass all the four regions 1 to 4. The locations of all the recording stations have been shown in Fig. 5.4. The preliminary data processing has been carried out by using in-house programs for extracting accelerograms from strong motion data of India. The Indian records have been band-pass filtered through lower cutoff frequency of 0.075 Hz and higher frequency of 30 Hz using Butterworth filter. The processed data is then used for calculating different EEW parameters using MATLAB processing. Fig. 5.5 shows a baseline corrected and filtered typical vertical component of M 6.8, Sikkim earthquake recorded at Gangtok.

Table 5.1 Details of the earthquakes recorded in India from March 2006 to August 2012 with epicentral distance ≤ 60 km.

S. No.	Date	Magnitude	Depth (km)	Latitude (^{O}N)	Longitude (^{O}E)	No. of recording stations within Δ ≤ 60 km
1	20090318	3.3	10	30.90	78.20	1
2	20060331	3.4	22	28.70	76.80	1
3	20100503	3.5	8	30.40	78.40	1
4	20120312	3.5	5	28.90	77.30	3
5	20071018	3.6	5	28.30	77.60	1
6	20090225	3.7	10	30.60	79.30	1
7	20090717	3.7	10	32.30	76.10	2
8	20090109	3.8	16	31.70	78.30	2
9	20071004	3.8	10	32.50	76.00	1
10	20100111	3.9	15	29.70	80.00	2
11	20090425	4.0	10	26.40	91.70	1
12	20090515	4.1	15	30.50	79.30	1
13	20060507	4.1	20	28.70	76.60	1
14	20091029	4.2	10	27.30	91.40	1
15	20091003	4.3	15	30.00	79.90	1
16	20071125	4.3	20	28.60	77.00	4
17	20090215	4.4	30	26.00	90.20	3
18	20081021	4.5	10	31.50	77.30	3
19	20100501	4.6	10	29.90	80.10	1
20	20100314	4.6	29	31.70	76.10	3
21	20100222	4.7	2	30.00	80.10	1
22	20090921	4.7	13	27.30	91.50	2
23	20120305	4.9	14	28.70	76.70	5
24	20120209	5.0	10	30.90	78.20	5
25	20120819	5.0	35	26.70	92.50	1
26	20080904	5.1	10	30.10	80.40	3
27	20121002	5.1	35	26.90	92.80	2
28	20110918	6.8	10	27.70	88.20	1

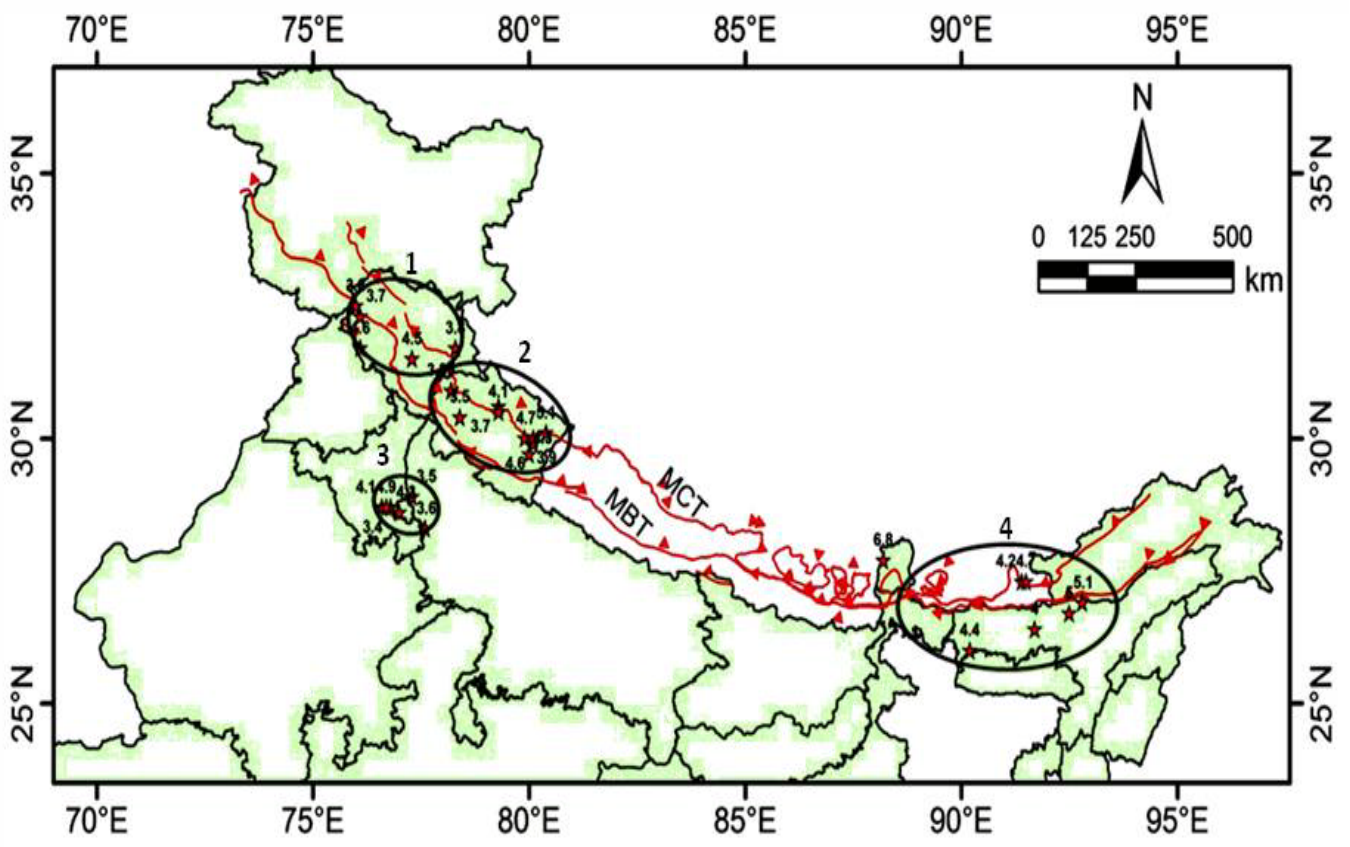

Figure 5.4 Northern Indian region showing location of earthquakes and stations used in the present study with triangles representing the strong motion stations, stars representing the epicenters of the earthquakes and ellipse representing the regions (1, 2, 3 and 4) from where the strong motion data has been selected for validation.

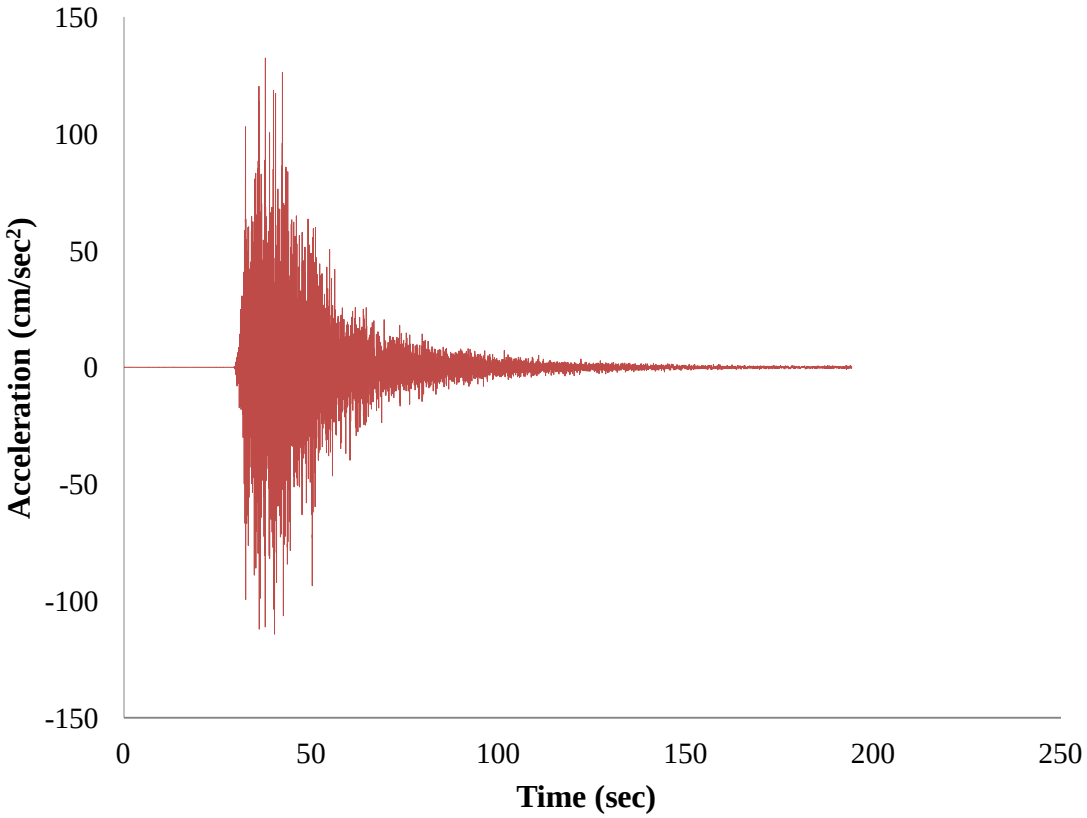

Figure 5.5 Processed vertical component record of 18th September, 2011, Sikkim earthquake having magnitude 6.8 recorded at Gangtok station.

Table 5.1 reveals that Indian dataset has very less number of records for moderate earthquakes with epicentral distance up to 60 km. It may be noted that there is only one earthquake of magnitude 6 and above in this distance range. Therefore, it can be concluded that the dataset is very small and is not sufficient for regression analysis, designing and validation of EEW algorithm. Therefore, region like Japan having rich K-NET strong motion databank has been used in the present study for analysis.

5.3 KYOSHIN NETWORK STRONG MOTION DATASET

Japan, a seismically active region and having state-of-the-art technology, has deployed a dense network for strong motion monitoring. NIED (National Research Institute for Earth Science and Disaster Prevention) installed the K-NET (Kinoshita 1998) that covers uniformly every part of Japan with more than 1000 strong motion accelerometers (~1030) on the ground

surface. The average inter station spacing is 20 km. K-NET95/KNET-02 strong motion accelerometers were installed at each station. K-NET95 has 8 MB and KNET-02 has 512 MB of memory, which can store a total of about 2.5 hours of three component data digitized at a sampling frequency of 100 Hz (Aoi et al. 2004). The data loggers used in K-NET95 have a 24-bit A/D (effective resolution is at least 18-bit) converter and a maximum measurable acceleration of 2000 gals and in case of K-NET-02 it is 4000 gals. Ground motion is stored only if the ground motion satisfies the pre-set trigger condition. The event recording starts at a threshold level of 2 gals and having a minimum recording length of 120 sec. The internal clock used for the recording system (1 ppm precision) is automatically calibrated by a GPS signal every hour with an accuracy of 5 msec. K-NET-02 seismograph connects with the Data Management Center through an ISDN line. It helps in processing of JMA seismic intensity and provides real time data communications. All the data is available through an FTP site (www.k-net.bosai.go.jp). The data on K-NET site is available in a prescribed format with a header of 17 lines containing different information regarding earthquake, recording station and other specifications followed by acceleration values as shown in Fig. 5.6.

Initially, the dataset has been selected from 1996 to 2011 having magnitude greater than 5 and depth ranging up to 20 km. This could fetch 1180 events with 78691 vertical records from the K-NET site. The data have further filtered using constraints for magnitude range and distance range. In this study, a total of 1726 vertical components of earthquake records from 105 earthquakes of Japan (as shown in Fig. 5.7) have been selected from the dataset downloaded from the K-NET website having a magnitude range of 5 to 7.2 with $\Delta \leq$ 60 km. Fig. 5.7 shows the location of selected K-NET events and their corresponding recording stations within desired epicentral range of 60 km. Details of all the earthquakes and recording stations with their latitude, longitude, number of records, depth and station code have been reported in Table 5.2 and Appendix (A).

```
Origin Time        2011/06/23 06:51:00          # Origin time of earthquake #
Lat.               39.9                         # Epicenter latitude #
Long.              142.5                        # Epicenter longitude #
Depth. (km)        20                           # Depth #
Mag.               6.7                          # Magnitude #
Station Code       YMT016                       # Site code #
Station Lat.       38.7895                      # Site latitude #
Station Long.      140.0185                     # Site longitude #
Station Height(m)  25                           # Site altitude #
Record Time        2011/06/23 06:52:10          # Recording start time #
Sampling Freq(Hz)  100Hz                        # Sampling frequency #
Duration Time(s)   60                           # Recording duration time #
Dir.               U-D                          #Number of sensor channels #
Scale Factor       3920(gal)/6182761            # Scale factor #
Max. Acc. (gal)    0.974                        # Maximum acceleration #
Last Correction    2011/06/23 06:52:11          # Time of final correction #
Memo.                                           # Memo #
4123     4154     4127     4096     4106     4126     4095     3998
3837     3634     3507     3536     3629     3706     3814     3942
.....
.....
.....
4145     4249     4188     4130     4135     4148     4166     4147
```

Figure 5.6 Typical data format of K-NET, Japan.

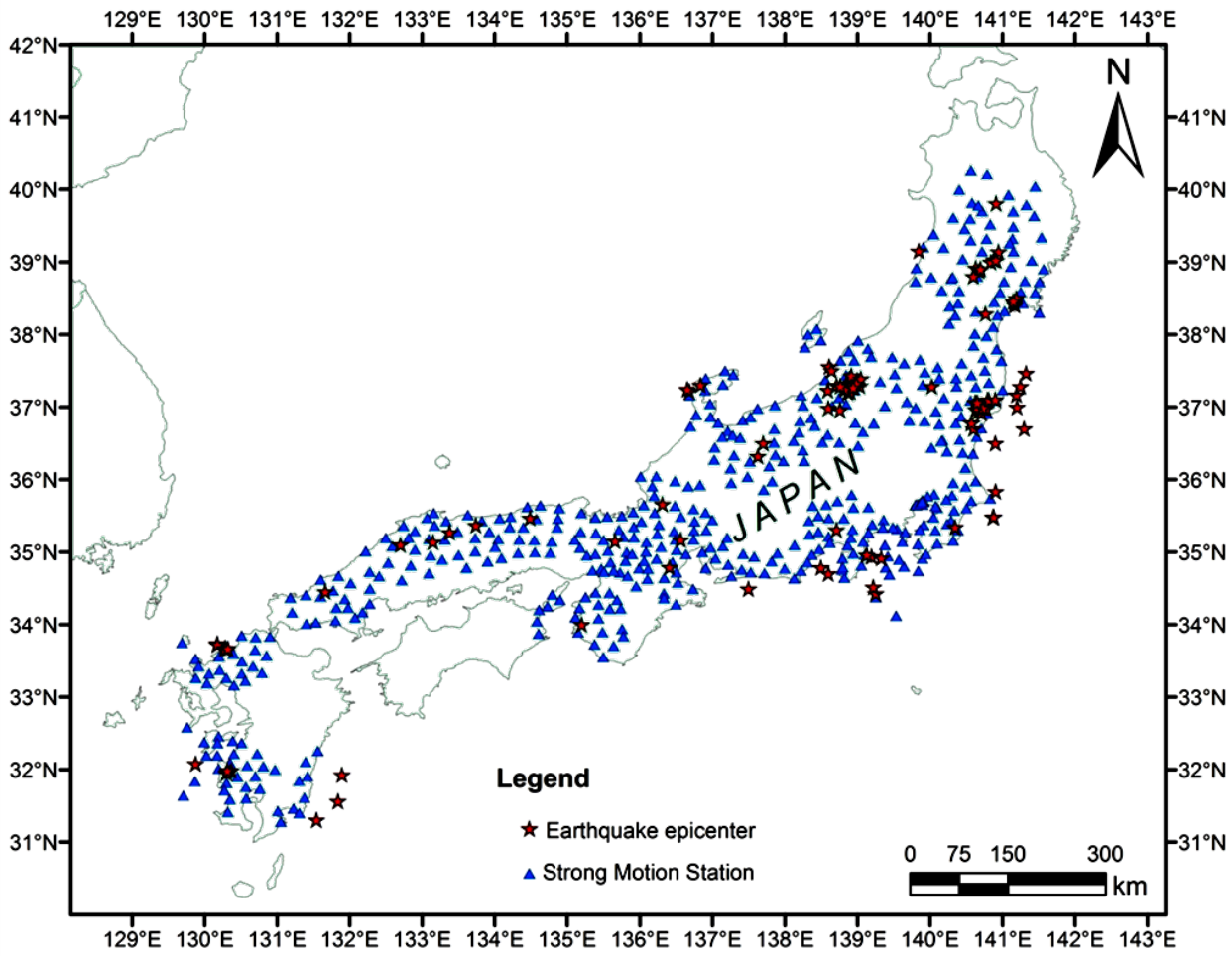

Figure 5.7 Map of Japan showing location of earthquakes and stations used in the present study.

The magnitude with available number of records within $\Delta \leq 60$ km has been shown in Fig. 5.8. It has been observed that small magnitude records were large in number than higher magnitude records due to less availability of higher magnitude near field records. Fig. 5.9 represents the distribution of magnitude up to an epicentral distance of 60 km.

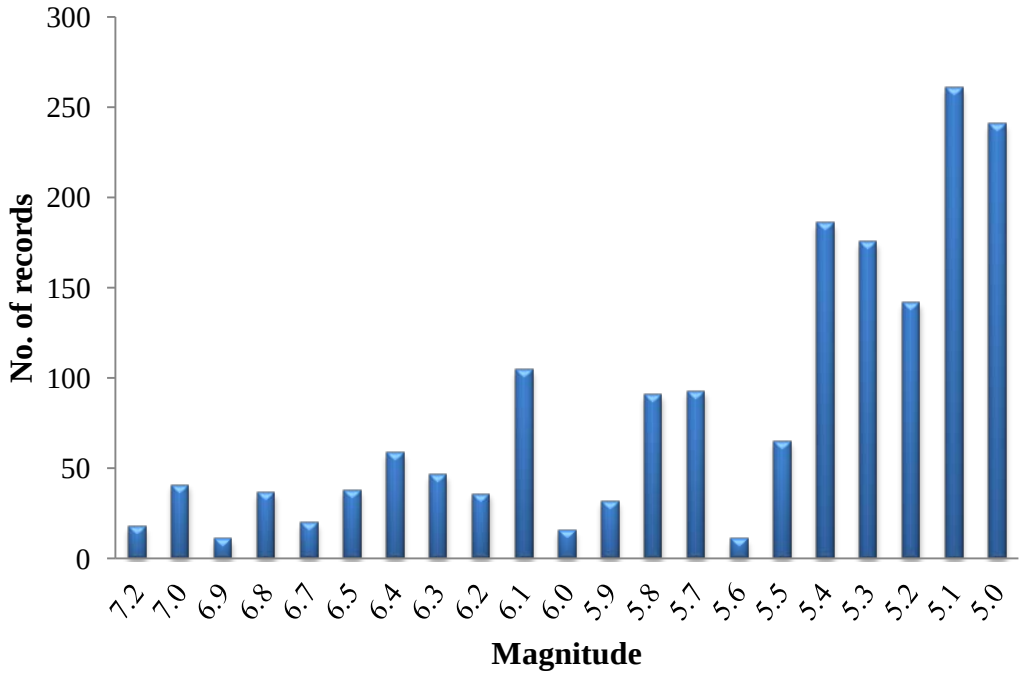

Figure 5.8 Distribution of earthquake magnitude used in present study for Japan region.

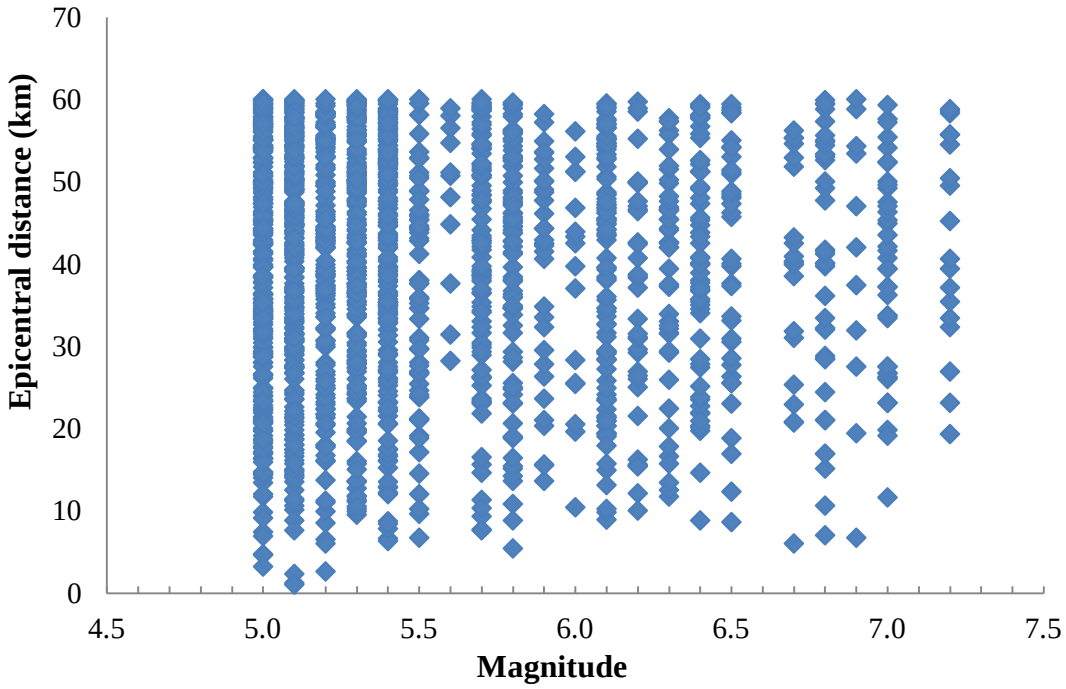

Figure 5.9 Magnitude and epicentral distance distribution of K-NET dataset.

Table 5.2 Details of the 105 earthquakes occurred in Japan from May 1996 to October 2011 with recording stations within 60 km epicentral range.

S. No.	Date	Magnitude	Depth (km)	Latitude (^{o}N)	Longitude (^{o}E)	No. of recording stations within $\Delta \leq 60$ km
1	20080614	7.2	8	39.03	140.88	18
2	20050320	7.0	9	33.74	130.18	15
3	20110411	7.0	6	36.95	140.67	26
4	20070325	6.9	11	37.22	136.69	11
5	20041023	6.8	13	37.29	138.87	19
6	20070716	6.8	17	37.56	138.61	18
7	20110312	6.7	8	36.99	138.60	20
8	20090811	6.5	23	34.79	138.50	21
9	20041023	6.5	14	37.31	138.93	17
10	20110315	6.4	14	35.31	138.71	30
11	20110412	6.4	15	37.05	140.64	20
12	20110412	6.4	26	35.48	140.87	9
13	20000715	6.3	5	34.43	139.25	7
14	19970326	6.3	8	31.99	130.37	22
15	20041023	6.3	9	37.35	138.98	18
16	19970513	6.2	8	31.95	130.30	21
17	20030726	6.2	12	38.41	141.17	15
18	20110319	6.1	5	36.78	140.57	20
19	20110316	6.1	10	35.84	140.91	9
20	19980903	6.1	10	39.80	140.91	23
21	20041027	6.1	12	37.29	139.03	19
22	19970625	6.1	12	34.45	131.67	18
23	20110801	6.1	20	34.70	138.60	16
24	20110323	6.0	8	37.08	140.79	16
25	19960811	5.9	7	38.92	140.63	14
26	20110411	5.9	11	36.97	140.63	18
27	20060421	5.8	7	34.94	139.20	28
28	20050420	5.8	14	33.68	130.29	20
29	20041025	5.8	15	37.33	138.95	16

S. No.	Date	Magnitude	Depth (km)	Latitude (^{o}N)	Longitude (^{o}E)	No. of recording stations within $\Delta \leq 60$ km
30	20070716	5.8	23	37.50	138.64	18
31	20050531	5.8	29	31.31	131.55	5
32	20110317	5.8	30	36.70	141.30	4
33	20110413	5.7	5	36.92	140.71	17
34	20080614	5.7	6	38.88	140.68	19
35	20100929	5.7	8	37.29	140.03	23
36	19960811	5.7	10	38.90	140.70	16
37	20041023	5.7	12	37.30	138.88	18
38	20110604	5.6	20	37.00	141.20	7
39	20090405	5.6	28	31.93	131.89	4
40	20110323	5.5	7	37.10	140.80	15
41	2001008	5.5	8	35.14	133.15	18
42	19970403	5.5	9	31.99	130.32	18
43	20030726	5.5	12	38.43	141.16	14
44	20110411	5.4	5	37.06	140.62	19
45	19980816	5.4	5	36.32	137.63	17
46	19980422	5.4	10	35.17	136.56	29
47	20010112	5.4	10	35.47	134.49	18
48	19960811	5.4	10	38.90	140.70	13
49	20110705	5.4	10	34.00	135.20	23
50	20110414	5.4	11	36.98	140.77	17
51	20050322	5.4	11	33.73	130.18	11
52	20070415	5.4	16	34.79	136.41	31
53	20110423	5.4	21	37.17	141.19	8
54	20041110	5.3	5	37.37	139.00	18
55	20000911	5.3	9	34.52	139.22	10
56	20110921	5.3	10	36.70	140.60	18
57	20020916	5.3	10	35.37	133.74	20
58	20111005	5.3	10	36.50	137.70	23
59	20041025	5.3	10	37.20	138.87	12
60	20080616	5.3	11	39.00	140.84	18

S. No.	Date	Magnitude	Depth (km)	Latitude (^{o}N)	Longitude (^{o}E)	No. of recording stations within $\Delta \leq 60$ km
61	20030726	5.3	12	38.50	141.19	15
62	20070325	5.3	11	37.30	136.84	9
63	20041023	5.3	16	37.31	138.86	4
64	20041023	5.3	20	37.32	138.91	11
65	19970524	5.3	22	34.50	137.50	10
66	20110413	5.3	27	35.49	140.88	8
67	20110506	5.2	6	37.10	140.81	14
68	19970904	5.2	6	35.27	133.38	19
69	20100704	5.2	7	39.02	140.91	18
70	20090218	5.2	9	35.66	136.31	23
71	20080614	5.2	11	39.14	140.94	15
72	20110426	5.2	13	37.29	141.25	6
73	20041104	5.2	18	37.43	138.92	18
74	20070818	5.2	20	35.34	140.35	29
75	20091218	5.1	5	34.96	139.13	26
76	20041108	5.1	6	37.39	139.05	16
77	20110414	5.1	9	36.78	140.57	20
78	20110525	5.1	10	37.10	140.90	11
79	20110604	5.1	10	35.10	132.70	19
80	20010825	5.1	10	35.15	135.66	33
81	20111005	5.1	10	36.50	137.70	23
82	20110411	5.1	12	36.99	140.73	18
83	20060204	5.1	12	32.08	129.88	14
84	20050420	5.1	13	33.68	130.28	20
85	20010104	5.1	14	36.96	138.76	22
86	20060502	5.1	15	34.92	139.33	31
87	19990226	5.1	19	39.15	139.85	8
88	20050410	5.0	5	33.67	130.28	14
89	20070611	5.0	7	37.24	136.65	9
90	20041101	5.0	8	37.21	138.90	16
91	20041228	5.0	8	37.32	138.98	17

S. No.	Date	Magnitude	Depth (km)	Latitude (^{o}N)	Longitude (^{o}E)	No. of recording stations within $\Delta \leq 60$ km
92	19960813	5.0	10	38.80	140.60	12
93	20110531	5.0	10	36.50	140.90	8
94	20041024	5.0	11	37.25	138.83	12
95	20110412	5.0	11	37.06	140.65	19
96	20050502	5.0	11	33.67	130.32	18
97	19980915	5.0	13	38.29	140.76	17
98	20000211	5.0	13	39.03	140.91	15
99	20030728	5.0	14	38.46	141.15	13
100	20041023	5.0	15	37.27	138.94	10
101	20050620	5.0	15	37.23	138.59	17
102	20050821	5.0	17	37.30	138.71	16
103	19980221	5.0	21	37.29	138.76	16
104	20040421	5.0	25	31.56	131.84	5
105	20110411	5.0	29	37.47	141.32	7

The type of magnitude scale used by JMA in Japan is M_{JMA}, i.e, magnitude estimated by JMA as mentioned at line no. 5 of Fig. 5.6. It was found by Katsumata (1996) that the average difference between M_{JMA} and M_w is not significant for earthquakes in the magnitude range from 4.5 to 7.5. The magnitudes considered in this study lies within this range therefore no magnitude conversion has been needed in the present study.

The preliminary data processing has been carried out on downloaded vertical components using in-house developed programs. The raw data available in terms of counts in the data format of K-NET (as shown at line number 18 in Fig. 5.6) has been converted into acceleration records in cm/sec^2 using the scale factor given in the header of data at line number 14, Fig. 5.6. As natural frequencies of all accelerographs were very high (about 200 Hz), there was no need of instrument response correction. A baseline correction of all acceleration time series have been performed using the least square line of the time series. Corrections have also been applied in frequency domain by filtering high and low frequency components of the accelerograms. All accelerograms were band-pass filtered by removing frequencies below 0.075 Hz and frequencies above 30 Hz. A fifth order Butterworth band-pass

filter has been used for the above filtering operation. The multi events reported in one file have been removed by manually viewing all the vertical component of downloaded earthquake records. Finally 1726 time histories were used for the present study from K-NET dataset. Also the P-onset points have been manually marked in the present study for further analysis.

5.4 PEER-NGA STRONG MOTION DATASET

The next data requirement to meet the objectives of the study is for checking the stability of parameters using data from other regions which is not used in the regression analysis. For this purpose Pacific Earthquake Engineering Research Center - Next Generation Attenuation **(**PEER-NGA) project strong motion dataset has been used. PEER-NGA dataset is an updated and expanded version of PEER strong motion database (Chiou et al. 2008). The PEER-NGA dataset includes 173 shallow crustal earthquakes with 1456 recording stations and 3551 multicomponent recordings obtained from about 35 agencies. This dataset comprises of earthquakes from different active tectonic regions worldwide with magnitude ranging from 4.2 to 7.9.

The strong motion records available on PEER-NGA dataset are taken from the strong motion networks operated by the CWB, the *California Geological Survey Strong Motion Instrumentation Program* (CSMIP) and the *United States Geological Survey (USGS)*. The available dataset is rich in site characterizations and contains information about faulting mechanism, occurrence of primary rupture surface, dimension of fault rupture, depth to the top of rupture and tectonic environment. The source, station, propagation path, ground motion parameter flat file and PEER record processing parameter tables are shown in Fig. 5.10 as the record file. Each record file has a unique station sequence number for e.g., NGA 1868 (Fig. 5.10) contains information about the seismic source, origin time, seismic moment, moment magnitude, hypocenter location, fault information, station specifications, various distances, PGA, PGV, *Peak Ground Displacement (PGD)* and type of filtering used for processing

Record Number NGA1868

Earthquake: Big Bear-02 2001-02-10 # Name of earthquake #
Magnitude: 4.53 # Moment magnitude #
Mo: 6.9984E+22 # Seismic moment #
Mechanism: 0 # Earthquake mechanism based on rake angel #
Hypocenter Latitude: 34.2895 | Longitude: -116.946 | Depth: 9.1 (km) # Earthquake parameters #
Fault Rupture Length: | Width: # Fault dimension #
Average Fault Displacement: # The average amount of slip over the rupture #
Fault Name: # Fault name#
Slip Rate:

Station: CDMG 23788 Colton - Hospital Complex FF # Name of station#
Latitude: 34.0740 | Longitude: -117.350 # Station location parameters #
Geomatrix 1: I | Geomatrix 2: H | Geomatrix 3: D # Site classifications #
Preferred Vs30: 271.40 (m/s) | Alt Vs30: # Average shear wave velocity to 30 m depth#
Instrument location: # Instrument location #

Epicentral Distance: 44.27 (km) | Hypocentral Distance: 45.19 (km) | Joyner-Boore Distance:
Campbell R Distance: | RMS Distance: | Closest Distance: # Various distances #
PGA: 0.0020 (g) # Peak ground acceleration #
PGV: 0.1300 (cm/sec) # Peak ground velocity #
PGD: 0.0100 (cm) # Peak ground displacement #

PEER record processing#

ATH	PGA (g)	PGV (cm/s)	PGD (cm)	Filter	nPass	nRoll	HP	LP	Lowest Usable Frequency
BEARAFT/788BY360				C	1		0.3	40	0.39
BEARAFT/788BY090							0.3	40	0.39
BEARAFT/788BYUP1									

Figure 5.10 Header of record file NGA1868 of Big Bear-02 earthquakes, dated 10th February, 2010 containing information regarding seismic source, location, fault information, station specifications, distances, ground motion period parameters and record processing.

In case of PEER-NGA dataset the prescribe format of data consists of a header of 4 lines followed by acceleration values are shown in Fig. 5.11. In the present study, a total of 219 earthquake records of 14 earthquakes have been taken from PEER-NGA database. The records are downloaded from PEER-NGA website (http://peer.berkelet.edu/nga/search.html) with specification of $4.5 \leq M \leq 8$ and having records within 60 km epicentral range. The dataset comprised of events taken from South California- 6 events, Turkey- 2 events and Taiwan- 6 events. The magnitude and corresponding number of records considered in the present study has been shown in Fig. 5.12. In Fig. 5.13 the magnitude and epicentral distance distribution has been shown with the help of a scatter plot. The locations of considered earthquakes and recording stations taken from South California, Turkey and Taiwan have been shown in Fig. 5.14.

```
PEER NGA STRONG MOTION DATABASE RECORD                    # Database name #
BIG BEAR 02/10/01, COLTON-3-BLDG HOSPITAL COMPLEX  # Earthquake and station name #
ACCELERATION TIME HISTORY IN UNITS OF G  # Acceleration time history specifications #
3700    0.0100    NPTS, DT                # no. of acceleration points and time interval #
-0.927925E-06  -0.117306E-05  -0.689511E-06  -0.148454E-06 # Acceleration data #
0.346713E-06
-0.122988E-05  -0.262599E-05  -0.448964E-05  -0.483004E-05   0.492505E-05
.....
.....
.....
0.126116E-05   0.130301E-05   0.134413E-05   0.138460E-05
0.142424E-05
```

Figure 5.11 Typical data format of PEER-NGA dataset.

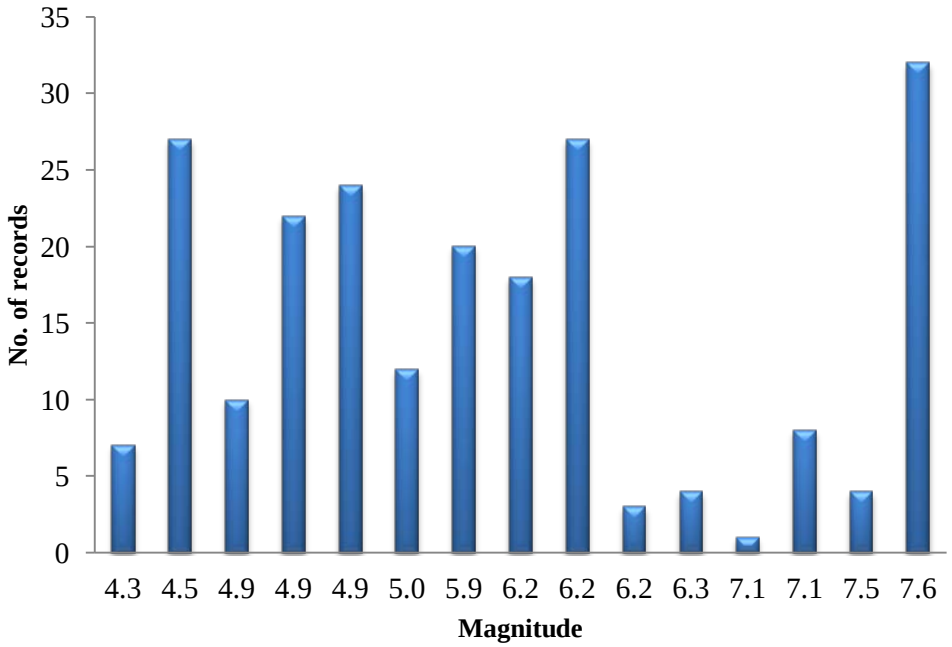

Figure 5.12 Distribution of earthquake magnitude used in present study for South California, Turkey and Taiwan region.

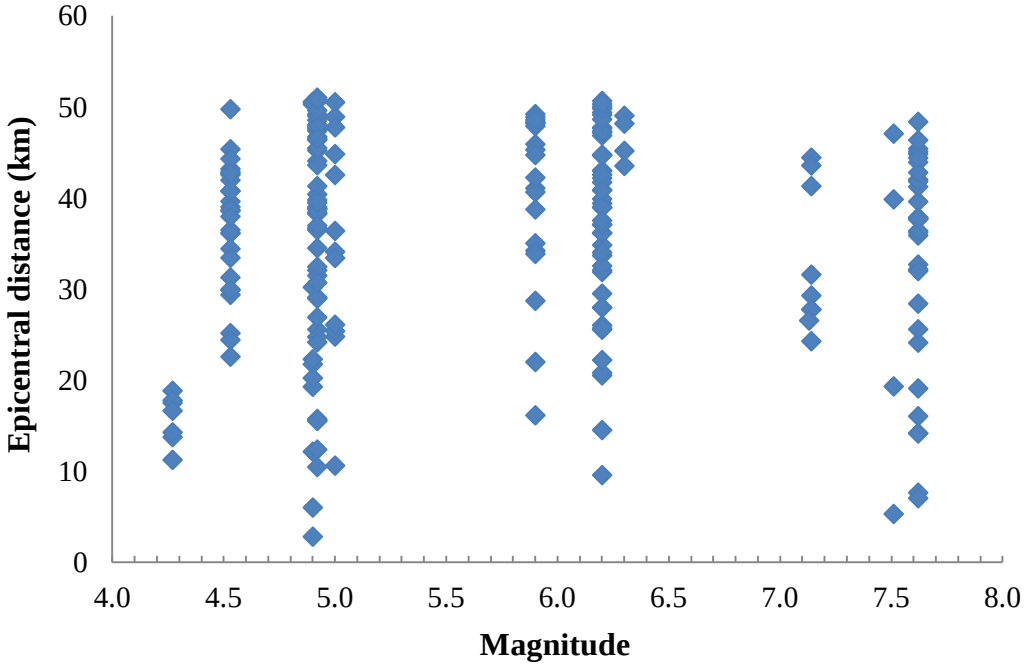

Figure 5.13 Magnitude and epicentral distance distribution of PEER-NGA dataset.

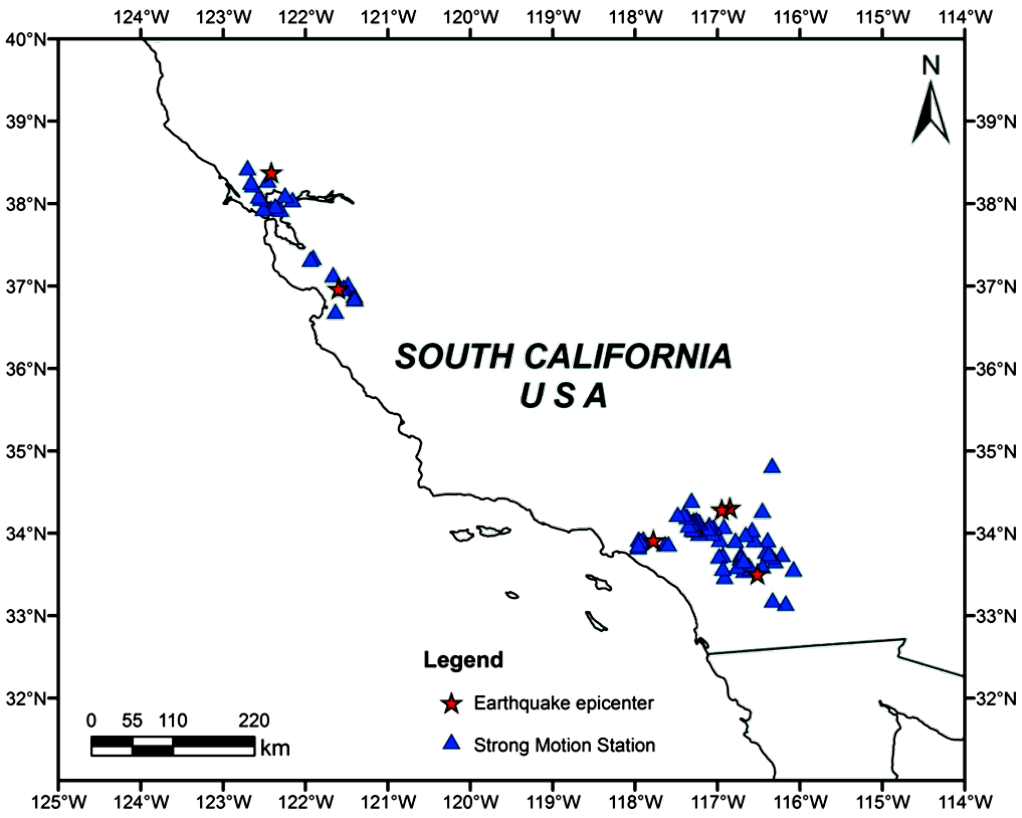

(a)

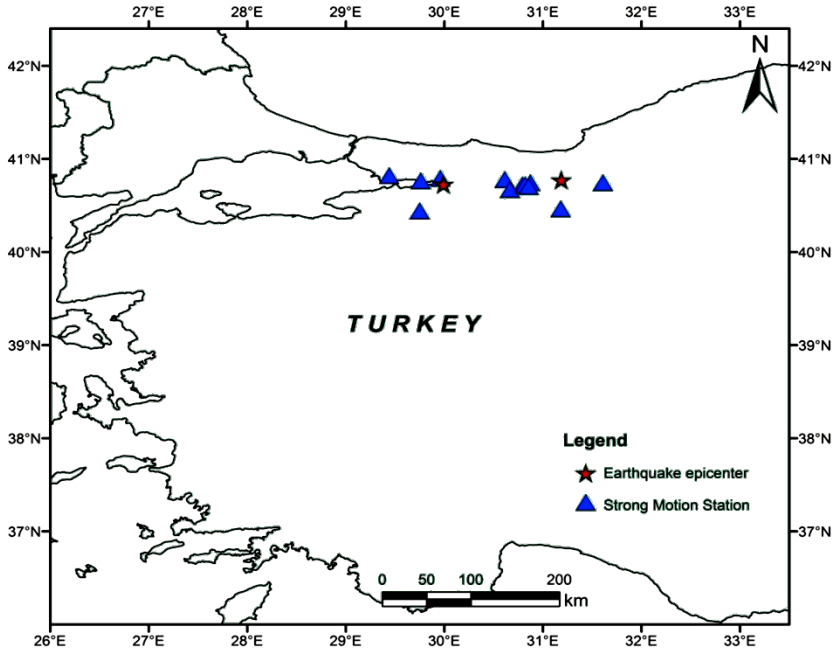

(b)

Figure 5.14 Location of earthquakes and stations in (a) South California, (b) Turkey and (c) Taiwan.

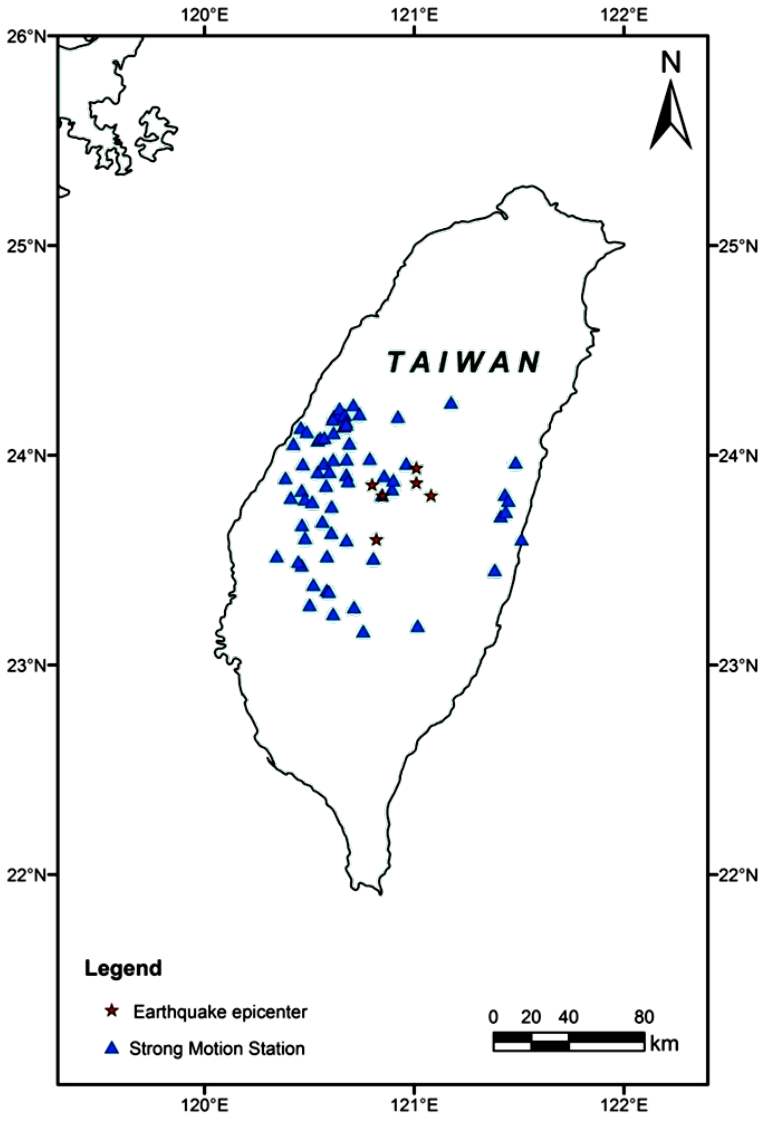

(c)

Figure 5.14 (Continued)

Details of all the earthquakes with source latitude, longitude, number of records and depth have been reported in Table 5.3 in which Yorba Linda, Big Bear City -02, Big Bear City, Gilroy, Anza and Yountville earthquake belongs to Southern California. Chi-Chi, Chi-Chi-02, Chi-Chi-03, Chi-Chi-04, Chi-Chi-05 and Chi-Chi-06 earthquake belongs to Taiwan. The Duzce and Kocaeli earthquake belong to Turkey region.

Table 5.3 Details of the 14 earthquakes occurred in South California, Turkey and Taiwan from August 1999 to February 2003, and recorded on recording stations within 60 km epicentral range.

S. No.	Date	Earthquake name	Magnitude	Depth (km)	Latitude (^{o}N)	Longitude (^{o}E)	No. of Recording Stations with $\Delta \leq 60$ km
1	20020903	Yorba Linda	4.3	7	33.92	-117.78	7
2	20010210	Big Bear-02	4.5	9	34.29	-116.95	27
3	20020514	Gilroy	4.9	10	36.97	-121.60	10
4	20030222	Big Bear City	4.9	6	34.31	-116.85	22
5	20011031	Anza	4.9	15	33.51	-116.51	24
6	20000903	Yountville	5.0	10	38.38	-122.41	12
7	19990920	Chi-Chi, Taiwan-02	5.9	8	23.94	121.01	20
8	19990920	Chi-Chi, Taiwan-03	6.2	8	23.81	120.85	18
9	19990920	Chi-Chi, Taiwan-04	6.2	18	23.60	120.82	27
10	19990922	Chi-Chi, Taiwan-05	6.2	10	23.81	121.08	3
11	19990925	Chi-Chi, Taiwan-06	6.3	16	23.87	121.01	4
12	19991112	Duzce, Turkey	7.1	10	40.77	31.19	8
13	19990817	Kocaeli, Turkey	7.5	15	40.73	29.99	4
14	19990920	Chi-Chi, Taiwan	7.6	7	23.86	120.80	32

Further, the information regarding the considered recording stations in the present study comprises of station name and location information as shown in Appendix (A). The records from 174 recording stations have been considered in case of PEER-NGA dataset.

The PEER-NGA datasheet as shown in Fig. 5.10 has been processed using developed in-house program. The 219 vertical components of 14 earthquakes have been baseline corrected and then band-pass filtered in a frequency range of 0.075 to 30 Hz using Butterworth filter and finally the processed data has been used for calculating different EEW parameters using MATLAB processing.

5.5 SUMMARY

The chapter describes the strong motion dataset for the development of EEW system vis-a-vis the availability from Indian regions. The dataset available is concluded to be not sufficient for such endeavors and therefore, an attempt has been made to import data from well instrumented seismically active regions. The present chapter describes the three datasets used in the study (Indian, K-NET and PEER-NGA) that covers five countries namely, India, Japan,

Southern California, Turkey and Taiwan. A total of 1996 acceleration records of 147 earthquakes recorded at 697 strong motion stations have been considered in the present study.

The chapter provides information regarding earthquake magnitude, location, depth with their recording station code, name and location. Further, the chapter describes the different data formats and processing programs developed in-house for calculating various EEW parameters using datasets from PESMOS, K-NET and PEER-NGA.

CHAPTER 6

ANALYSES AND RESULTS

6.1 INTRODUCTION

The methodology as reported in the earlier chapters has been used to analyze the data to achieve the objectives of the present study. In this chapter automatic P-onset detection, development of EEW algorithm and magnitude estimation has been discussed using K-NET strong motion data having magnitude range of 5.0 to 7.2 within an epicentral distance of 60 km. In the starting phase, automatic P-pick has been carried out using RSSCV and Allen's 1978 algorithms. In the next phase development of EEW algorithm using EEW parameters (τ_p^{max}, τ_c, P_d, CAV and RSSCV) has been analysed which is followed by the magnitude estimation of the event. Regression relations have been established between various EEW parameters and magnitude to determine the threshold values for issuing warning for the events having $M \geq 6$. The threshold values have been determined for different time windows. Further, the efficacy of the algorithm has been tested for various possible combinations of EEW parameters at different time windows to get reliable and fast warning. Finally, Indian strong motion dataset and PEER-NGA dataset (which comprises of data taken from Southern California, Turkey and Taiwan) have been used for the adoption to Indian context and validation of the algorithm using worldwide data set, respectively.

6.2 AUTOMATIC P-ONSET

The classical concept of P-onset is based on the amplitude variation, which is modified by Allen (1978) with the inclusion of frequency component and filtering concept. The STA filtering enhances the signal strength while LTA filtering is made to show the background noise level to its lowest. Thus, an enhanced signal to noise ratio is achieved in the range of frequency component arrivals from a seismic source. Allen used first order FIR filter along with amplitude check to enhance the efficiency of the phase picker. For EEW system, auto P-onset picking as well energy estimation in the time series is important. Therefore, in the present study, RSSCV approach was adopted in which the energy content in the incoming seismic signal was assumed to be present more in terms of

velocity components in relation to other ground motion components. RSSCV parameter provides information about the predominant velocity in the time series and the cumulative effect observed in terms of energy component. The following sub sections report the automatic P onset carried out on the three datasets.

6.2.1 K-NET Dataset

On applying the RSSCV and Allen's P-onset algorithm (as discussed in Chapter 4) on K-NET data a good matching has been achieved between manually marked (assumed to be correct) and calculated P-onset from the two algorithms. Table 6.1 and Fig. 6.1 shows time difference between manually marked and calculated P-onset point using RSSCV and Allen's algorithm. The difference is calculated in terms of number of records and percentage of records having P-onset value different from manually marked P-onset points. In case of RSSCV algorithm out of 1726 records there are 1273 records having time difference varying from 0 to 0.2 sec, 198 records having time difference varying from 0.21 to 0.4 sec, 67 records having time difference varying from 0.41 to 0.6 sec, 35 records having time difference varying from 0.61 to 0.8 sec, 27 records having time difference varying from 0.81 to 1.0 sec and 126 records having time difference greater than 1 sec. However in case of Allen's algorithm out of 1726 records there are 1454 records having time difference varying from 0 to 0.2 sec, 150 records having time difference varying from 0.21 to 0.4 sec, 20 records having time difference varying from 0.41 to 0.6 sec, 9 records having time difference varying from 0.61 to 0.8 sec, 8 records having time difference varying from 0.81 to 1.0 sec and 85 records having time difference greater than 1 sec. Allen's algorithm is found to have better performance than RSSCV algorithm as it has 84% records having time difference between 0 to 0.2 sec, while in case of RSSCV algorithm it is 74%. The comparison of marking the triggered events as seismic events shows that in case of K-NET dataset on analyzing 1726 records of 105 earthquakes, Allen's algorithm provides P-onset picking results more close to the manual marked P-onset point.

Fig. 6.1 shows example of the event dated 15th April, 2007 displaying starting portion i.e., 3 sec strong ground motion data. The vertical lines are drawn at the corresponding samples, at which the manual analysis (M), Allen's algorithm (A) and RSSCV (R) algorithm, have marked the P-onset. The differences between the picks by the corresponding procedures are very small as noticed from Fig. 6.1.

Table 6.1 Time difference between manually marked and calculated P-onset using RSSCV and Allen's algorithm in terms of number of records and percentage of matching obtained in case of K-NET dataset.

Time difference	Number of records		Percentage of records	
	RSSCV	**Allen (1978)**	**RSSCV**	**Allen (1978)**
0-0.2 sec	1273	1454	73.75%	84.24%
0.21-0.4 sec	198	150	11.47%	8.69%
0.41-0.6 sec	67	20	3.88%	1.16%
0.61-0.8 sec	35	9	2.03%	0.52%
0.81-1.0 sec	27	8	1.56%	0.46%
>1 sec	126	85	7.30%	4.92%

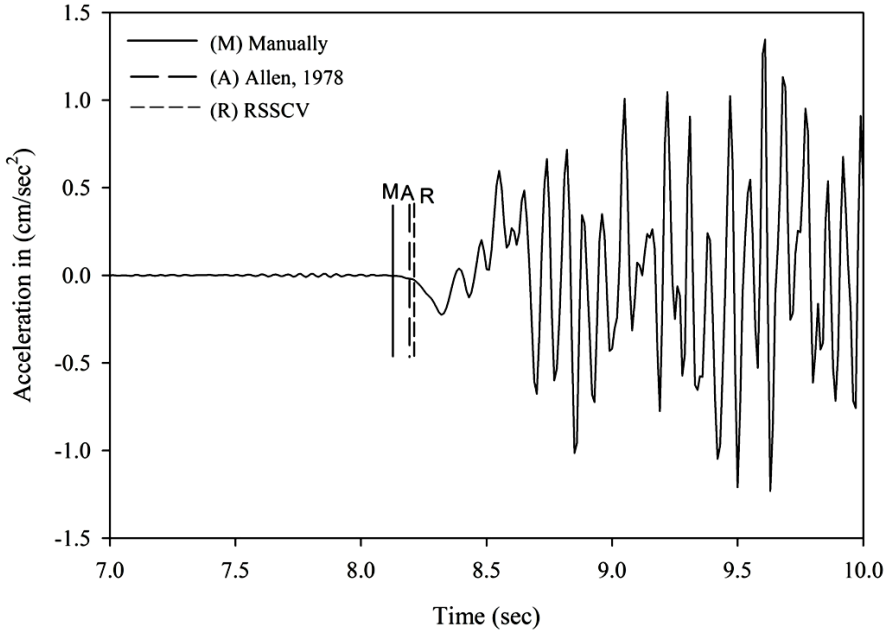

Figure 6.1 Example of different P-onset picking in starting portion 3 sec of an event recorded at GIF022 (KAMIISHIDU) station dated 15th April, 2007 having magnitude 5.4. The manually (M), Allen's (A) and RSSCV (R) algorithm pick are represented by solid, long dash and small dash lines, respectively.

6.2.2 Indian Dataset

The RSSCV algorithm has been applied on Indian strong motion dataset that comprises of 51 records of 28 earthquakes having magnitude range varying from 3.3 to 6.8. Table 6.2 shows time difference between manually marked and calculated P-onset point using RSSCV and Allen's algorithm. The difference is calculated in terms of number

of records and percentage of records having P-onset value different from manually marked P-onset points. In case of RSSCV algorithm there are 36 records having time difference varying from 0 to 0.2 sec out of 51 records, while no records were found having time difference varying from 0.21 to 0.4 sec and 0.41 to 0.6 sec. Single- single record having time difference varying from 0.61 to 0.8 sec and from 0.81 to 1.0 sec, respectively, have found. Also, there are and 13 records having time difference greater than 1 sec was found. However, in case of Allen's algorithm out of 51 records there are 37 records having time difference varying from 0 to 0.2 sec, 7 records having time difference varying from 0.21 to 0.4 sec, 5 records having time difference varying from 0.41 to 0.6 sec, single record having time difference varying from 0.61 to 0.8 sec, no record having time difference varying from 0.81 to 1.0 sec and single record having time difference greater than 1 sec. Allen's algorithm is found to have superior performance than RSSCV algorithm as it has 73% records having time difference between 0 to 0.2 sec, while in case of RSSCV algorithm it is 71%. In case of RSSCV algorithm, the difference between manually marked P-onset point and P-onset point pick using the algorithm is found to be more as there are 13 records having a time difference greater than of 1 sec, while there is only one record in case of Allen's algorithm having a time difference greater than 1 sec which shows that a difference of greater than 100 samples in the P-picking. Allen with less number of sample differences proves to give more accurate P- picking results.

Table 6.2 Time difference between manually marked and calculated P-onset using RSSCV and Allen's algorithm in terms of number of records and percentage of matching obtained in case of Indian dataset.

Time difference	Number of records		Percentage of records	
	RSSCV	Allen (1978)	RSSCV	Allen (1978)
0-0.2 sec	36	37	70.59%	72.55%
0.21-0.4 sec	0	7	0%	13.73%
0.41-0.6 sec	0	5	0%	9.80%
0.61-0.8 sec	1	1	1.96%	1.96%
0.81-1.0 sec	1	0	1.96%	0.00%
>1 sec	13	1	25.49%	1.96%

6.2.3 PEER-NGA Dataset

The PEER–NGA dataset which consist of strong ground motion records of various countries for example South California, Turkey and Taiwan (see chapter 5) has been used

to validate the automatic P-picking algorithms. Total 219 records of 14 earthquakes having magnitude range of 4.27 to 7.62 within 60 km epicentral distance have been analyzed. Table 6.3 shows the time difference in the manually marked P-onset time and P-onset point marked by using RSSCV based algorithm and Allen's algorithm. The difference is calculated in terms of number of records and in percentage of records having P-onset value different from manually marked P-onset points. In case of RSSCV algorithm out of 219 records there are 169 records having time difference varying from 0 to 0.2 sec, 19 records having time difference varying from 0.21 to 0.4 sec, 10 records having time difference varying from 0.41 to 0.6 sec, 2 records having time difference varying from 0.61 to 0.8 sec, 2 records having time difference varying from 0.81 to 1.0 sec and 17 records having time difference greater than 1 sec. However, in case of Allen's algorithm out of 219 records there are 154 records having time difference varying from 0 to 0.2 sec, 11 records having time difference varying from 0.21 to 0.4 sec, 13 records having time difference varying from 0.41 to 0.6 sec, 11 records having time difference varying from 0.61 to 0.8 sec, 5 records having time difference varying from 0.81 to 0.1 sec and 25 records having time difference greater than 1 sec.

Table 6.3 Time difference between manually marked and calculated P-onset using RSSCV and Allen's algorithm in terms of number of records and percentage of matching obtained in case of PEER-NGA dataset.

Time difference	Number of records		Percentage of records	
	RSSCV	**Allen (1978)**	**RSSCV**	**Allen (1978)**
0-0.2 sec	169	154	77.17%	70.32%
0.21-0.4 sec	19	11	8.68%	5.02%
0.41-0.6 sec	10	13	4.57%	5.94%
0.61-0.8 sec	2	11	0.91%	5.02%
0.81-1.0 sec	2	5	0.91%	2.28%
>1 sec	17	25	7.76%	11.42%

The phase-picking is based on the amplitude and frequency variation which is not of direct use in EEW system. Therefore, it is necessary to search for some common parameters for P-picking as well as to estimate the incoming energy for the purpose of EEW. In view of this the parameter namely, RSSCV has been chosen for autopicking of P-onsets and issuing warning in EEW system. The comparison has been made for the results obtained on the P-picks based on Allen's algorithm and the RSSCV parameters. Based on

the comparison, it has been observed that the absolute difference in automatic P-onset picking can be adjusted towards having more false alarms without compromising the missing of actual P-onsets. This may have almost nil effect on the type of P-pick onset being used. In the present study, on comparing the automatic P-onset pick algorithms, it has been found that Allen's algorithm provides better accuracy in case of K-NET and Indian dataset. However, in case of PEER-NGA dataset RSSCV algorithm provides better P-pick results.

6.3 ESTIMATION OF PARAMETER'S THRESHOLD VALUES FOR ISSUING EEW

The determination of the size of the earthquake viz., magnitude based on the amplitudes of ground motion is a complex task. In case of EEW system automatic, reliable and robust estimates of the earthquake parameters viz., magnitude can be obtained by continuously updating the EEW parameters (τ_p^{max}, τ_c, P_d, CAV and RSSCV) for issuing warning and for emergency preparations and management. In the present study, K-NET strong motion dataset has been used in the analysis due to its high spatial density of the network in the source region. Also, EEW parameters threshold values for issuing EEW have been obtained by calculating the correlations between the calculated EEW parameters value after P-onset with magnitude at different time windows.

6.3.1 τ_p^{max} - Magnitude Relation

For determining the scaling relationship between τ_p^{max} and magnitude, the τ_p^{max} values have been calculated at each station using Eq. (4.2). The regression has been based on the average of τ_p^{max} value for each event. The calculation of average value of τ_p^{max} includes the value of τ_p^{max} calculated at nearest four stations up to 60 km epicentral distance. The τ_p^{max} values have been calculated at different window lengths starting from 1 sec to 5 sec. The longer the duration, the more accurate and reliable will be the EEW system estimation. Thus, to search for the accurate and minimal time window the analysis has been carried out at five windows (1 sec, 2 sec, 3 sec, 4 sec and 5 sec) as shown in Fig. 6.2. In the present study separate scaling relations for each time window has been calculated. The least square fit to the data at different time windows produces scaling relations as shown in Table 6.4.

Table 6.4 Scaling relation obtained between τ_p^{max} and magnitude at different window lengths.

Time window	**Obtained scaling between τ_p^{max} and magnitude**	**Conversely, in terms of magnitude**
1 sec	$log\,\tau_p^{max} = (0.1832M - 1.1208) \pm 0.1161$	$M = 6.080 + 3.5542\,log\,\tau_p^{max}$
2 sec	$log\,\tau_p^{max} = (0.2107M - 1.2614) \pm 0.0700$	$M = 5.990 + 4.1542\,log\,\tau_p^{max}$
3 sec	$log\,\tau_p^{max} = (0.2156M - 1.2698) \pm 0.0775$	$M = 5.878 + 4.846\,log\,\tau_p^{max}$
4 sec	$log\,\tau_p^{max} = (0.2183M - 1.2708) \pm 0.0733$	$M = 5.802 + 5.312\,log\,\tau_p^{max}$
5 sec	$log\,\tau_p^{max} = (0.2226M - 1.2751) \pm 0.0728$	$M = 5.680 + 5.3634\,log\,\tau_p^{max}$

The observed τ_p^{max} values at each station have been plotted in Fig. 6.2 against the catalogue magnitude at each event. The least square fit to the average values of τ_p^{max} and magnitude have shown by solid lines and the two dashed lines show the range of standard deviation. τ_p^{max} values are not so sensitive to time window but from Fig. 6.2 it has been observed that with increase in time there has been a slight increase in slope and improvement in magnitude estimate with additional seconds of data. The magnitude estimation of large events in particular improves with additional seconds. The slope at 4 sec and 5 sec were almost same. Thus, 4 sec is the optimal time window, providing good estimate of earthquake magnitude. Also, the scattering effect of τ_p^{max} at lower magnitudes gets reduced with increase in window length which verifies Brown et al. (2009) observation.

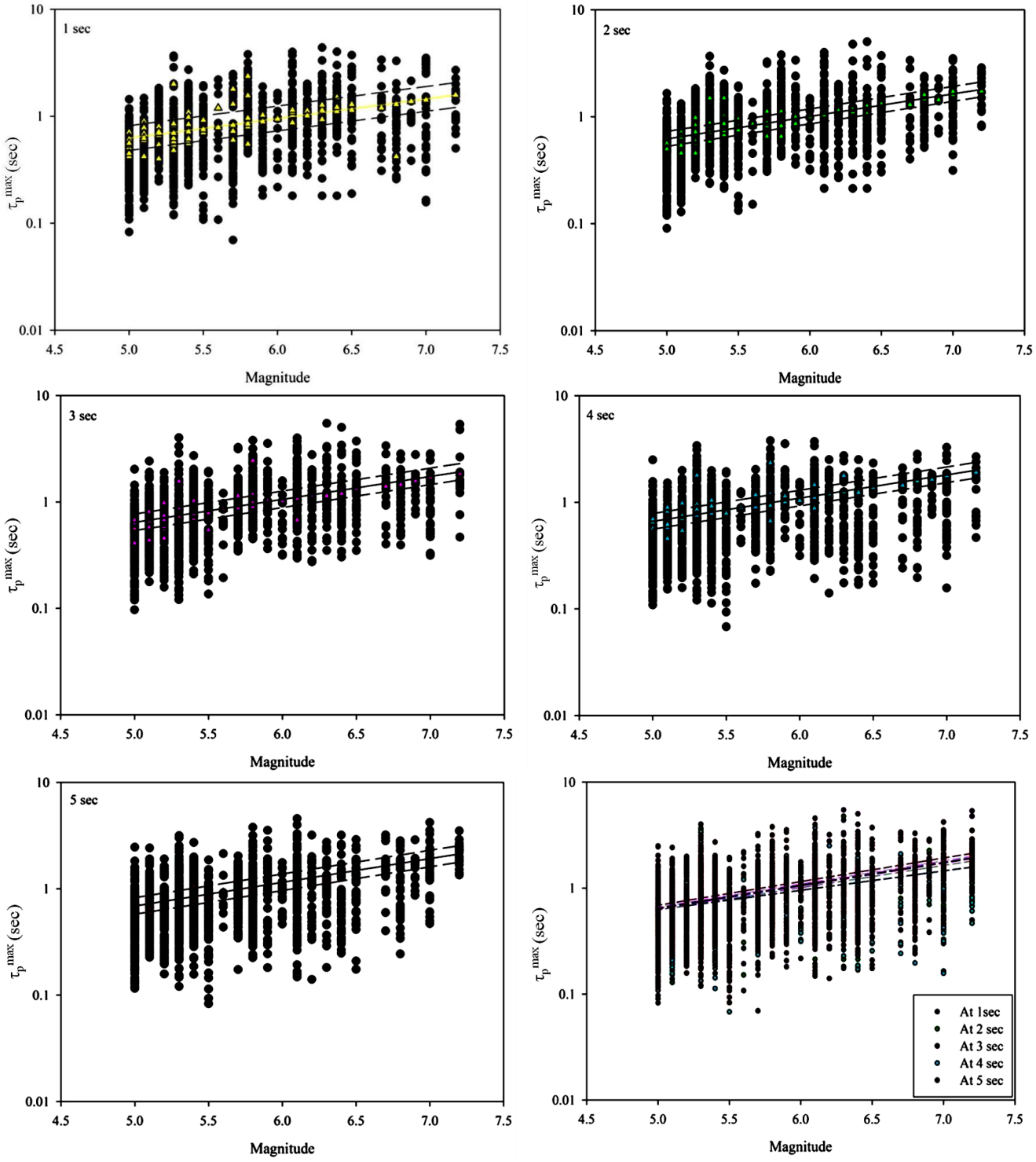

Figure 6.2 Effect of number of seconds of P-wave data on scaling relations between τ_p^{max} and magnitude. Circles are observation at individual stations, triangles are average of events, and lines are linear best fit scaling relations to triangles of the same color. Combined effect of all the five time windows (1 sec, 2 sec, 3 sec, 4 sec and 5 sec) shows the rise in slope with each additional second of data.

Five threshold values of τ_p^{max} have been determined at five different time windows for issuing warning for event having M ≥ 6, as discussed in chapter 4 (section 4.5.6). Based on the attenuation of strong ground motion with distance and expected intensity due to the attenuated strong ground motion, the objective of EEW system in terms of the target cities, their distance from the source and the isoseismal maps showing isoseismals of MSK intensity ≥ VI, it has been observed that a magnitude 6 can be assumed to be a damaging earthquake for EEW system implementation in Northern India (Narayan et al. 2002; Sharma et al. 2013; Paul et al. 1998; Parik and Sharma 2007; Sharma 2001; Sharma and Dubey 2000). Therefore, the warning threshold has been calculated for M ≥ 6 because it has been considered to be potentially damaging magnitude level. From the calculated scaling relation (Table 6.4), the estimated threshold values for issuing warning have been listed in Table 6.5.

Table 6.5 Threshold values calculated for issuing warning for an event having M ≥ 6, at different time windows.

Time window	**Threshold values of τ_p^{max} (sec) for issuing warning (M ≥ 6)**
1 sec	0.95
2 sec	1
3 sec	1.06
4 sec	1.1
5 sec	1.14

6.3.2 τ_c - Magnitude Relation

τ_c values, which represent the average value of the initial portion of P-wave (Wu and Kanamori 2005a), are used to estimate the magnitude of an event. In the present study, τ_c values have been calculated for 1726 records of 105 earthquake event using Eq. (4.8) under the condition that for each event at least four measurement should be available within 60 km epicentral range. The regression has been calculated at the average τ_c values of 105 event and the catalogue magnitude of each event. The scaling relations obtained at five different time windows have been given in Table 6.6. The standard deviation obtained is found to be comparable with other studies (Wu and Kanamori 2008a) carried out on K-

NET dataset. Event having M < 5 scatter is relatively more due to low SNR (Wu et al. 2007).

Table 6.6 Scaling relation obtained between τ_c and magnitude at different window lengths.

Time window	**Obtained scaling between τ_c and magnitude**	**Conversely, in terms of magnitude**
1 sec	$\log \tau_c = (0.2848M - 1.6982) \pm 0.1002$	$M = 5.967 + 3.213\, log\, \tau_c$
2 sec	$\log \tau_c = (0.2963M - 1.7088) \pm 0.1211$	$M = 5.7738 + 3.283\, log\, \tau_c$
3 sec	$\log \tau_c = (0.2994M - 1.7167) \pm 0.1229$	$M = 5.737 + 3.312\, log\, \tau_c$
4 sec	$\log \tau_c = (0.3142M - 1.7321) \pm 0.1252$	$M = 5.485 + 3.3719\, log\, \tau_c$
5 sec	$\log \tau_c = (0.3217M - 1.7385) \pm 0.1300$	$M = 5.3427 + 3.4334\, log\, \tau_c$

Fig. 6.3 shows a good linear trend between τ_c and magnitude determined from the K-NET dataset. The τ_c - M slope is more than τ_p^{max}- M slope which shows that the average value of initial portion is higher than maximum predominant period for the initial portion of P-wave. At 1 sec, data results in smaller slope to the scaling relation leading to systematic underestimation of magnitude for large events due to saturation at higher magnitude (Kanamori 2005). But by the addition of more seconds to data the increase in slope and improves the magnitude estimate for larger events.

The τ_c calculation is effected by the double integration used in its calculation which results in long-period drift which can be removed by using Butterworth filter whose order also effects the slope and scattering of data. In the present study, fifth order Butterworth filter having cutoff frequency of 0.075 Hz (Wu and Kanamori 2008a) has been used.

Five threshold values of τ_c have been determined at five different time windows, for issuing warning for event having M ≥ 6. From the calculated scaling relation (Table 6.6) the estimated thresholds for issuing warning have been listed in Table 6.7. The calculated threshold values have τ_c values approximately greater than 1 at each time window for issuing warning for M ≥ 6 which verify the results with studies carried out by Wu and Kanamori (2005a); Wu et al. (2007); Wu and Kanamori (2008a); Hsiao et al. (2009) and Alcik et al. (2011). Thus, the estimated threshold values decides the warning criteria for damaging earthquake and it has been consider that 4 sec time window maximizes data availability and timeliness.

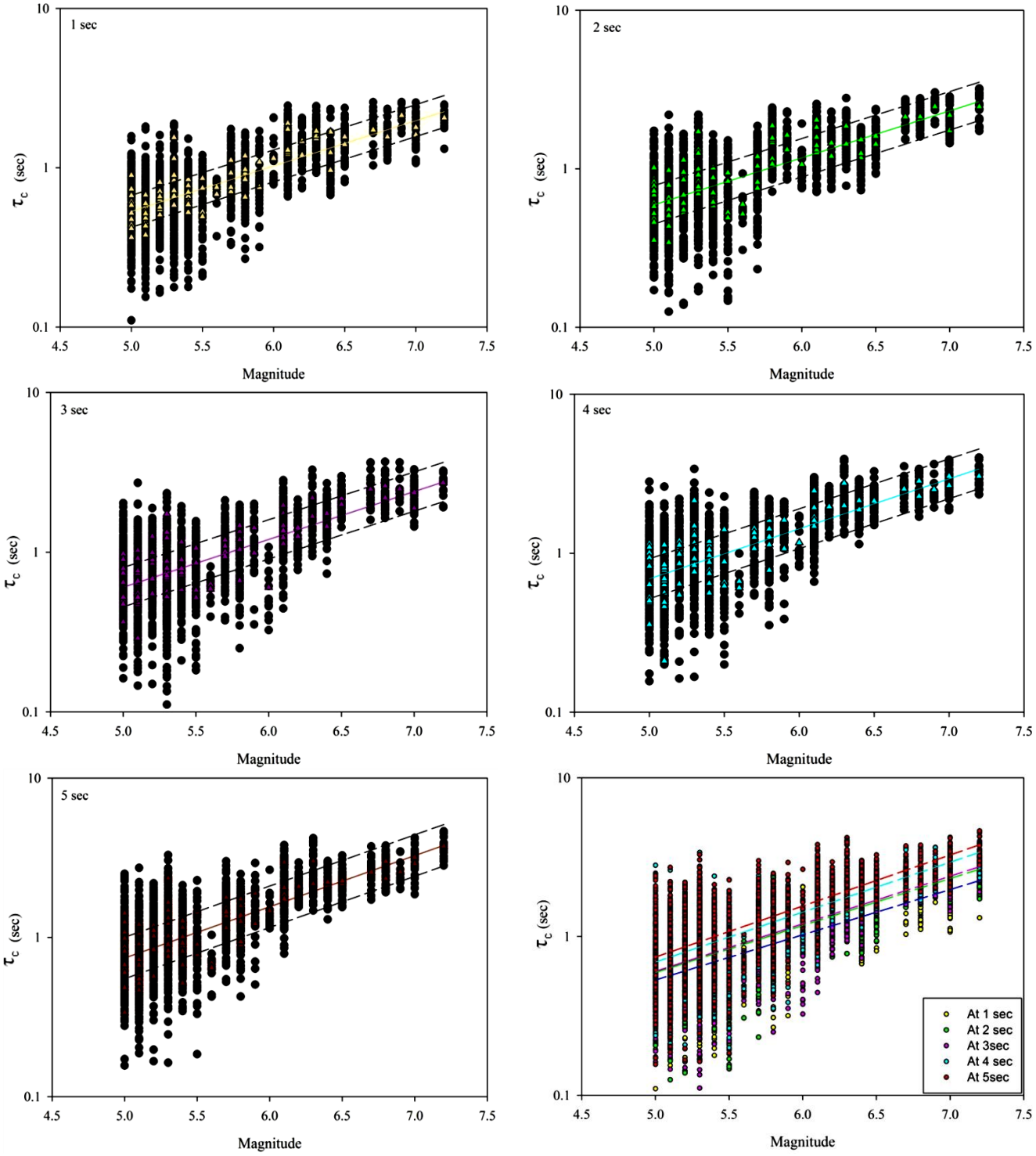

Figure 6.3 Effect of number of seconds of P-wave data on scaling relations between τ_c and magnitude. Circles are observation at individual stations, triangles are average of events, and lines are linear best fit scaling relations to triangles of the same color. Combined effect of all the five time windows (1 sec, 2 sec, 3 sec, 4 sec and 5 sec) shows the rise in slope with each additional second of data.

Table 6.7 Threshold values calculated for issuing warning for an event having M ≥ 6, at different time windows.

Time window	Threshold values of τ_c (sec) for issuing warning (M ≥ 6)
1 sec	1.02
2 sec	1.17
3 sec	1.20
4 sec	1.42
5 sec	1.55

6.3.3 P_d - Magnitude Relation

P_d is an important EEW parameter which depends on the initial rupture process of an event and is less affected by the scattering that occurs due to the complex velocity structure in other EEW parameters like τ_p^{max}, CAV and RSSCV (Wu and Kanamori 2008a; Wu et al. 2007; Wu and Zhao 2006). Peak displacement is measured from the initial portion of the P-wave, by double integrating the vertical component of acceleration record and filtering it with a high-pass filter. Wu and Zhao (2006) proposed a relation between P_d, hypocentral distance and magnitude to study attenuation of P_d with the hypocentral distance using a relationship that depends on magnitude. In this study the regression of P_d, hypocentral distance and magnitude using K-NET dataset for five different time windows have been shown in Table 6.8.

Table 6.8 List of scaling relation obtained between P_d, hypocentral distance and magnitude at different window lengths.

Time window	Obtained scaling between P_d, hypocentral distance and magnitude
1 sec	$\log \mathrm{P_d} = (0.3817\mathrm{M} - 1.5603 \log \mathrm{R} - 1.6421) \pm 0.4699$
2 sec	$\log \mathrm{P_d} = (0.5187\mathrm{M} - 1.6497 \log \mathrm{R} - 2.0705) \pm 0.4113$
3 sec	$\log P_d = (0.6127M - 1.8471 \log R - 2.149) \pm 0.3719$
4 sec	$\log P_d = (0.6852M - 2.0767 \log R - 2.0767) \pm 0.3403$
5 sec	$\log P_d = (0.7158M - 2.1850 \log R - 1.9883) \pm 0.3289$

The standard deviation at 1 sec and 2 sec is observed to be relatively higher i.e., around 0.5 and 0.4 which get reduce with addition of more seconds up to 0.33. Further, Zollo et al. 2006 modified the regression relation by normalizing the observed P_d to a reference distance of 10 km and calculate the distance independent relation. The calculated P_d values have also been normalized to 10 km and the scaling relation obtained using the 105 earthquake events between P_d and the catalogue magnitude have been given in Table 6.9.

Table 6.9 List of scaling relation obtained between P_d and magnitude at different window lengths.

Time window	**Obtained scaling between P_d and magnitude**	**Conversely, in terms of magnitude**
1 sec	$\log P_d = (0.3888M - 3.2111) \pm 0.3451$	$M = 6.7028 + 0.8\, log\, P_d$
2 sec	$\log P_d = (0.5169M - 3.6761) \pm 0.298$	$M = 6.6501 + 1.12\, log\, P_d$
3 sec	$\log P_d = (0.6094M - 3.9492) \pm 0.2636$	$M = 6.3426 + 1.17\, log\, P_d$
4 sec	$\log P_d = (0.6790M - 4.0942) \pm 0.2181$	$M = 6.0251 + 1.2\, log\, P_d$
5 sec	$\log P_d = (0.7073M - 4.1051) \pm 0.2098$	$M = 5.8201 + 1.3\, log\, P_d$

In Fig. 6.4 separate scaling relations for 1 sec to 5 sec show that, with increase in time window, the slope of the best fit line increases. At 1 sec and 2 sec, a saturation effect is observed for higher magnitude earthquake. Small P_d values for a large earthquake with a long rupture length are observed because P_d values are calculated from seismic signals generated close to earthquake initials (Huang et al. 2009). Thus, at small time windows higher magnitude events are underestimated due to saturation of P-wave amplitudes and also due to distant location of larger events. Error in estimation of epicentral distance effects magnitude estimation using P_d (Brown et al. 2009). However, the higher slope of 4 sec and 5 sec shows the improvement in magnitude estimate for lager events at long time windows. For each time window, thresholds for issuing warning has been calculated from the scaling relation between P_d and magnitude as listed in Table 6.9. The threshold value of P_d increases from 0.13 to 1.38 for time window 1 sec to 5 sec, as listed in Table 6.10.

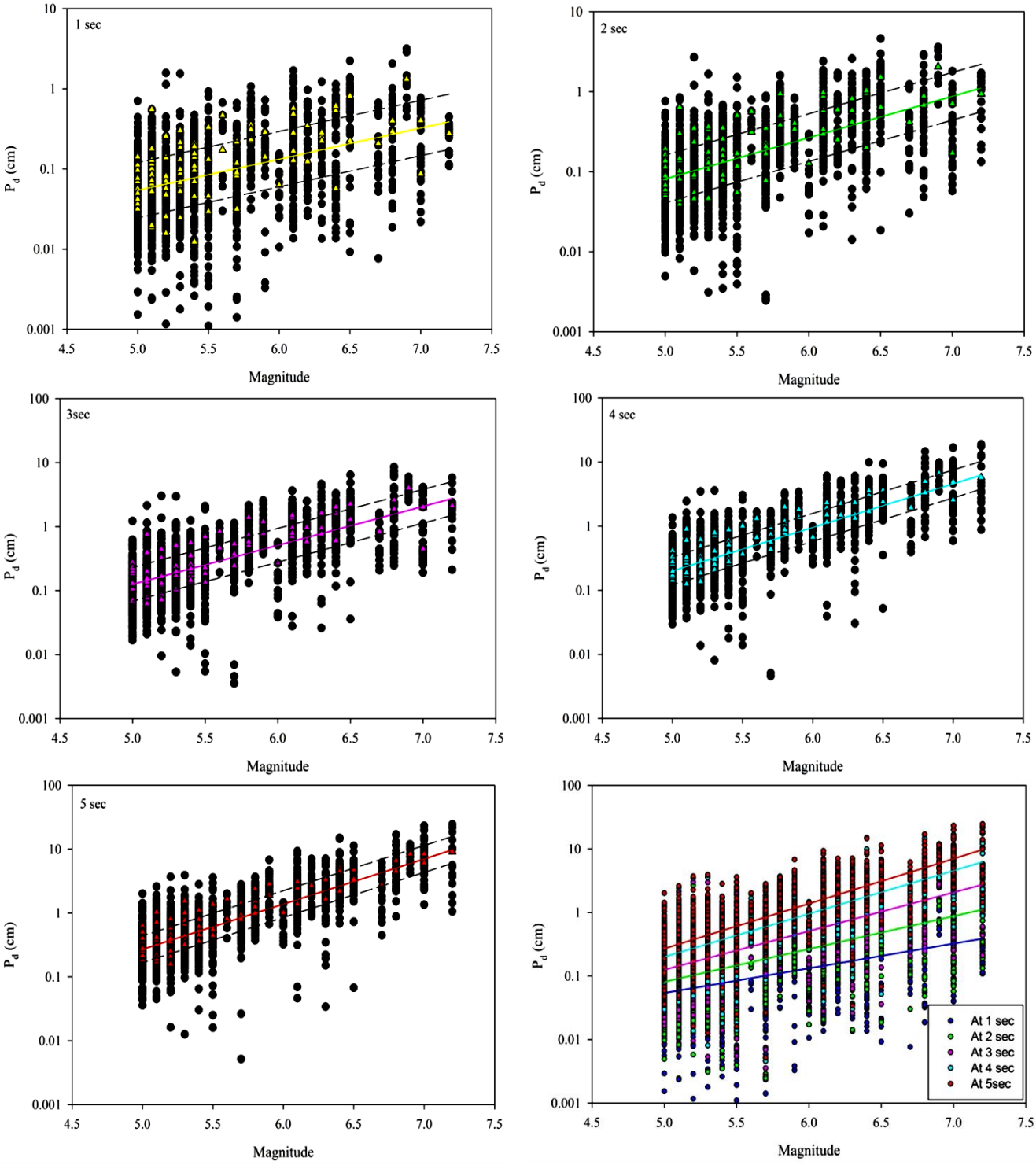

Figure 6.4 Effect of number of seconds of P-wave data on scaling relations between P_d and magnitude. Circles are observation at individual stations, triangles are average of events, and lines are linear best fit scaling relations to triangles of the same color. Combined effect of all the five time windows (1 sec, 2 sec, 3 sec, 4 sec and 5 sec) shows the rise in slope with each additional second of data.

Table 6.10 Threshold values calculated for issuing warning for an event having M ≥ 6 using P_d at different time windows.

Time window	Threshold values of P_d (sec) for issuing warning (M ≥ 6)
1 sec	0.13
2 sec	0.27
3 sec	0.51
4 sec	0.95
5 sec	1.38

6.3.4 CAV - Magnitude Relation

CAV is another EEW parameter used to determine threshold for issuing warning for potentially damaging events. CAV values are highly correlated with physical property damage such as engineered structures. In Istanbul, a simple CAV based threshold exceedance approach has been used in EEW system (Alcik et al. 2009).

In the present study, the CAV values have been calculated from 1726 records of 51 earthquakes using Eq. (4.14). The threshold values for five time windows have been calculated by manually observing the best fit on the records as shown in Fig. 6.5. The individual station records are marked by cross and average of event is marked with plus. The solid horizontal line represents the specified threshold value for the particular time window best obtained after analysis.

CAV describes the cumulative effect of generated ground signal in the selected time thus used to differentiate between a damaging and non-damaging event. In Fig. 6.5 it has been clearly shown that, at 1 sec and 2 sec, some of the events with higher magnitude are below the specified threshold level thus, considered as missed alarm. But with the increase in data availability with time, rate of correct alarm get increased. It has been observed that 3 sec onwards there have been less number of individual records and no average of event below the specified threshold level viz., reduction in number of false and missed alarms. Thus, for a potentially damaging earthquake of M ≥ 6 correct alarms have been issued with good accuracy using CAV as an EEW parameter.

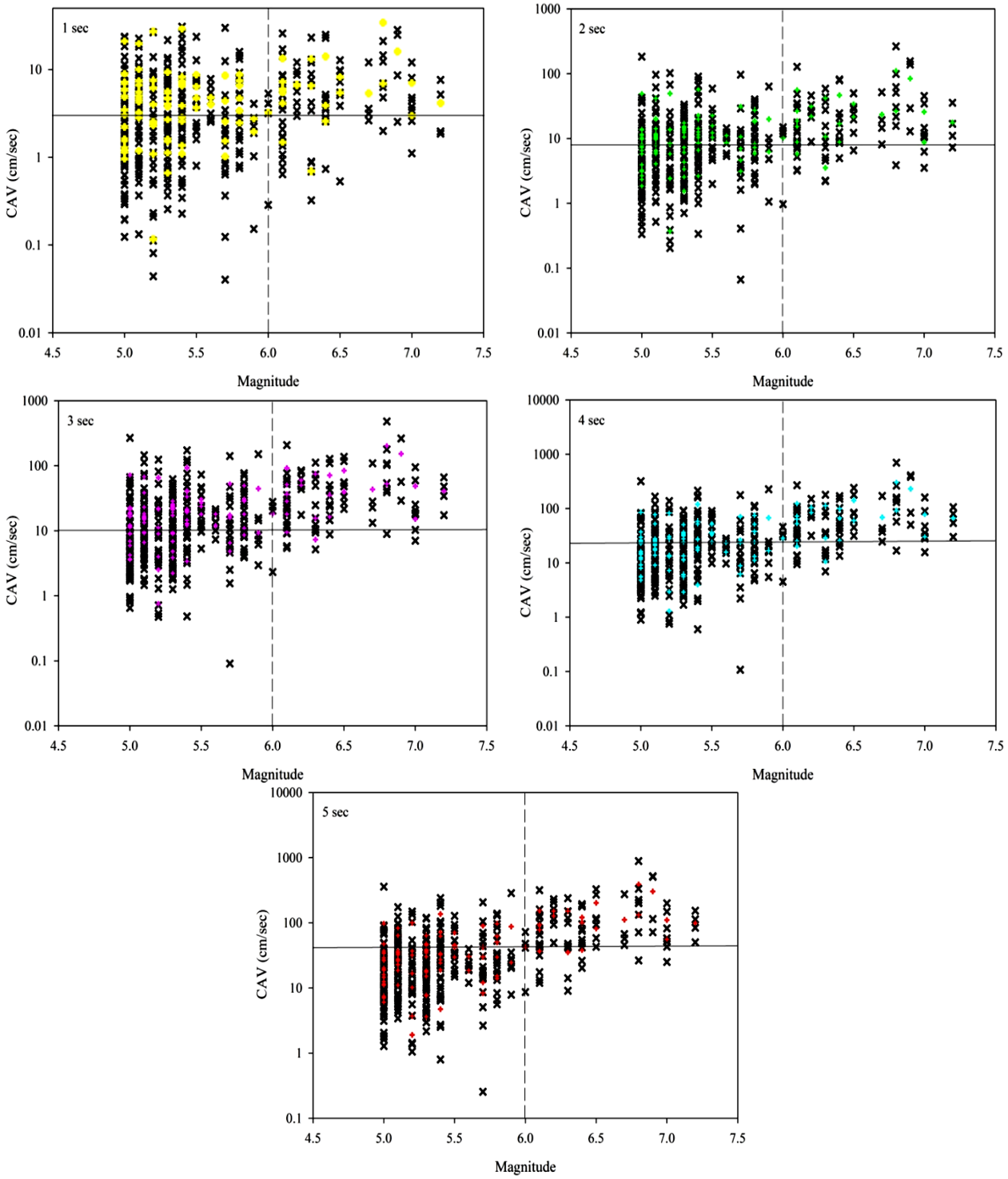

Figure 6.5 Specified threshold values of CAV for all the five time windows (1 sec, 2 sec, 3 sec, 4 sec and 5 sec). 1726 records are marked with cross and plus represents the average CAV value of 105 earthquake events. Solid horizontal line represents best fit threshold value and dashed vertical line is marked at M = 6. The CAV values scatter gets reduce with increasing time window with a rise in correct alarm rate.

Table 6.11 shows the observed threshold values obtained from the analysis of the dataset at five time windows starting from 1 sec to 5 sec. The suggested CAV threshold values are found to be in close agreement with the threshold values suggested by Alcik et al. (2009) for three selectable alarm levels within a time period of 5 sec to 10 sec (20 cm/sec, 40 cm/sec and 70 cm/sec).

Table 6.11 Threshold values for issuing warning for an event having M ≥ 6 using CAV at different time windows.

Time window	Threshold values of CAV (cm/sec) for issuing warning (M ≥ 6)
1 sec	3.0
2 sec	8.0
3 sec	10.0
4 sec	23.0
5 sec	41.0

6.3.5 RSSCV - Magnitude Relation

RSSCV is another EEW parameter which includes the cumulative effect (amplitude and time) of ground motion duration (Bhardwaj et al. 2013a). RSSCV helps in enhancing the SNR and reduces the standard error in observational seismology. In the present study, RSSCV proved to be an important EEW parameter, as it has been used for automatic P-pick and also for issuing warning for potentially damaging earthquakes. The RSSCV parameter values are calculated from the initial portion of the P-waves using Eq. (4.17).

In Fig. 6.6 the RSSCV values are calculated for 1726 records of 105 earthquakes and have been plotted against the catalogue magnitude, the average value of RSSCV for an event have also been plotted on the same plot for the selected time window. The threshold values of RSSCV for five different time window (1 sec, 2 sec, 3 sec, 4 sec and 5 sec) are decided by the analysis of calculated RSSCV values. It has been observed from the plots in Fig 6.8 that with the addition in time RSSCV gives more accurate warning estimate required for an EEW system. The threshold values have underestimated the calculated RSSCV values at 1 sec and 2 sec but the scattering in the data reduced at 3 sec, 4 sec and 5 sec and most of the RSSCV values lies in the vicinity of the calculated specified threshold levels at each time window. Thus, it reveals that this parameter gives more accurate

estimation of higher magnitude event for issuing warning with the increase in window length. The specified threshold value for RSSCV at five different time windows has been given in Table 6.12 which states that with the rise in available time the threshold values also increases from 0.3, 1.0, 1.7, 5.2 and finally to10 cm/sec.

Table 6.12 Threshold values for issuing warning for an event having M ≥ 6 using RSSCV at different time windows.

Time window	**Threshold values of RSSCV (cm/sec) for issuing warning (M ≥ 6)**
1 sec	0.3
2 sec	1.0
3 sec	1.7
4 sec	5.2
5 sec	10.0

All the above discussed EEW parameters (τ_p^{max}, τ_c, P_d, CAV and RSSCV) have their own advantages and efficiencies to be used in designing of an EEW algorithm. However, if different combinations of these EEW parameters have been used an accurate and fast warning EEW algorithm can be designed.

It may be concluded from Figs. 6.2, 6.3, 6.4, 6.5 and 6.6 that with each additional second scattering in the data gets reduced and better estimation of magnitude for large events can be achieved. This verifies the finding of Allen and Kanamori (2003) that the initial magnitude estimate using 1 sec data is a minimum estimate and it gets improved with each additional second of data, but with a reduction in warning time. The magnitude estimation also depends on number of station reporting triggers for an event (Brown et al. 2009). Therefore, in the present study the designed EEW algorithm considers nearest four stations within 60 km epicenter range that gets triggered for an event for estimating different alarms. Use of closest station reduces the scattering in the data by reducing individual and average error of magnitude estimation.

In Table 6.13, a comparison of all the threshold values of the five EEW parameters calculated at different time windows have been listed. Further, it has been observed that with the increase in time window, the amplitude of all the threshold values increases.

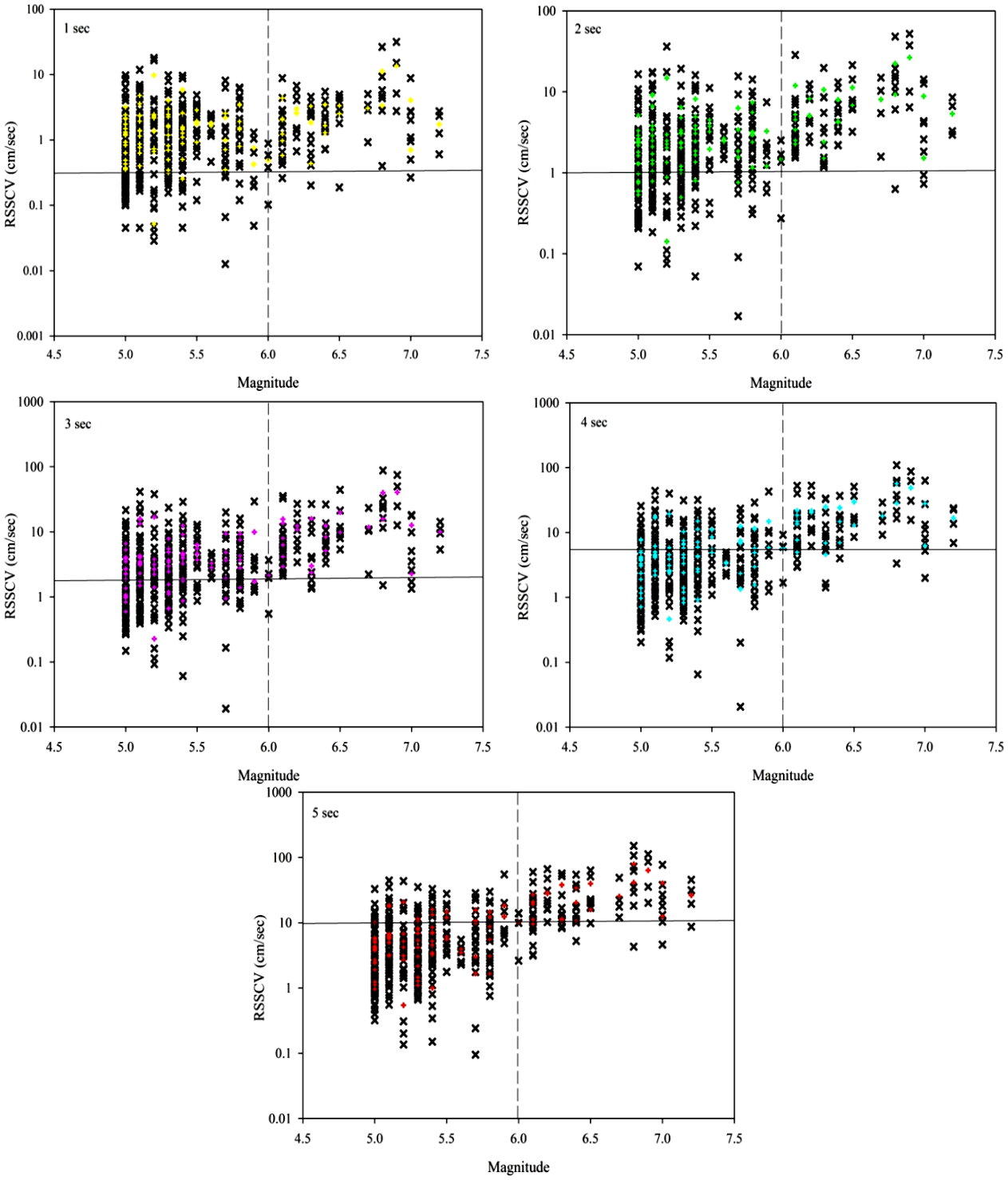

Figure 6.6 Specified threshold values of RSSCV for all the five time windows (1 sec, 2 sec, 3 sec, 4 sec and 5 sec). 1726 records are marked with cross and plus represents the average RSSCV values of 105 earthquake events. Solid horizontal line represents best fit threshold value and dashed vertical line is marked at M = 6. The RSSCV values scatter gets reduce with increasing time window with a rise in correct alarm rate.

Table 6.13 Comparison of threshold values of different EEW parameter for issuing warning for an event having M ≥ 6 at different time windows.

Parameters	Time Window				
	1 sec	**2 sec**	**3 sec**	**4 sec**	**5 sec**
τ_p^{max} **(sec)**	0.95	1.00	1.06	1.10	1.14
τ_c **(sec)**	1.02	1.17	1.20	1.42	1.55
P_d **(cm)**	0.13	0.27	0.51	0.95	1.38
CAV (cm/sec)	3.00	8.00	10.00	23.00	41.00
RSSCV (cm/sec)	0.30	1.00	1.70	5.20	10.00

6.3.6 Comparison of Regression Relationships for Magnitude Prediction

The regression relations obtained between the various EEW parameters and magnitude using K-NET dataset at different time windows have been compared with the regression relations obtained by other researchers using dataset from different regions in Table 6.14. In the present study, the threshold values calculated for issuing warning for events having M ≥ 6 at different time windows as listed in Table 6.13 have been compared with the threshold values suggested by other researchers and good similarity have been obtained. For example, at 3 sec time window, the threshold value for τ_c is 1.2 sec in the present study, while it is approximately 1.63 sec, 1.69 sec, 1.15 sec, 1.3 sec, 2.38 sec and 1.15 sec in other studies (Wu and Kanamori 2005a; Wu et al. 2006; Wu and Kanamori 2008a; Sokolov et al. 2009; Alcik et al. 2011; Zollo et al. 2010). The higher value of τ_c may be due to difference in SNR, especially for small earthquakes and due to long-period drift due to integration process involved in τ_c calculation. Similarly, the threshold value, obtained in the present study, for τ_p^{max} at 4 sec time window is 1.1 sec and in other studies it is reported as 1.03 sec, 1.32 sec and 1.1 sec (Allen and Kanamori 2003; Wurman et al. 2007; Brown et al. 2009). Further, on comparing the calculated P_d value viz., 0.95 cm at 4 sec with value estimated by Brown et al. (2009) which is 0.87 cm, a good matching has been achieved.

Table 6.14 List of different regressions developed using different datasets.

References	Types	Events	Regression relations
Wu and Kanamori (2005a)	τ_c-M	Taiwan - 26 events	$log\ \tau_c = 0.221*M_w - 1.113$
			$M_w = 4.525*\ log\ \tau_c + 5.036$
Wu et al. (2006)	τ_c-M,	Taiwan - 46 events	$M_w = 3.088*\ log\ \tau_c + 5.300 \pm 0.57$
	P_d-M		$log\ P_d = -3.801 + 0.722*M - 1.444*\ log\ R \pm 0.29$
Wu and Kanamori (2008a)	τ_c-M	Taiwan, Southern California and Japan - 54 events	$log\ \tau_c = 0.296*M_w - 1.716 \pm 0.122$
			$M_w = 3.373*\ log\ \tau_c + 5.787 \pm 0.412$
Sokolov et al. (2009)	τ_c-M	Japan and Taiwan - 110 events	$log\ \tau_c = 0.293*M_w - 1.644 \pm 0.152$
Alcik et al. (2011)	τ_c-M	Istanbul - 12 events	$log\ \tau_c = 0.142*M_w - 0.475 \pm 0.1433$
			$M_w = 7.042*\ Log\ \tau_c + 3.345 \pm 1.009$
Zollo et al. (2010)	τ_c-M	Japan, Taiwan and Central Italy - 296 events	$log\ \tau_c = 0.21(\pm 0.01)*M_w - 1.2\ (\pm 0.07)$
Wu and Zhao (2006)	P_d-M	Southern California - 25 events	$logP_d = -3.463 + 0.729*M - 1.374*\ log\ R \pm 0.305,$
			$M_{P_d} = 4.748 + 1.371*\ log\ P_d + 1.883\ *log\ R$
Hsiao et al.(2011)	P_d-M	Taiwan - 186 events	$log\ P_d = -1.777 + 0.455*M - 1.23*\ log\ R,\ SDV = 0.362,$
			$M_{P_d} = 3.905 + 2.198*\ log\ P_d + 2.703*\ log\ R$
Allen and Kanamori (2003)	τ_p^{max}-M	Southern California- 53 events	$M_w = 7.0*\ log\ \tau_p^{max} + 5.9,\ SDV = 0.67$
Wurman et al. (2007)	τ_p^{max}-M	Northern California - 43 events	$log\ \tau_p^{max} = 0.15*M_w - 0.78,$
	P_d-M		$M = 5.22*\ log\ \tau_p^{max} + 6.66,$
			$logP_d = 0.73\ *\ M_w - 3.77$
Brown et al. (2009)	τ_p^{max}-M,	Japan - 84 events	$log\ \tau_p^{max} = 0.21*M_L - 1.22$
	P_d-M		$logP_d = 0.66\ *\ M_L - 4.02$

6.4 EEW ALGORITHM

The EEW algorithm has been designed using K-NET dataset (see chapter 5) which is based on five EEW parameters (τ_p^{max}, τ_c, P_d, CAV and RSSCV) as discussed in chapter 4. The EEW parameters have a close relation with the magnitude of the events as shown by the scaling relations obtained between EEW parameters and the magnitude (see Table 6.4, 6.6 and 6.9). All the EEW parameters used are based on their empirical formulations. The EEW parameter regressed with the catalogue magnitude results in estimation of specified threshold value at different time windows. The calculated threshold values of different EEW parameters (see Table 6.13) for five different time windows have been used in the developed algorithm for issuing various alarms.

The algorithm considers the four nearest stations within 60 km which get triggered on the onset of the event. The five EEW parameters value have been calculated using the empirical formulae as discussed in chapter 4 at each station after P-onset. Then, the calculated values are compared at different time windows (1 sec, 2 sec, 3 sec, 4 sec and 5 sec) with the specified threshold values. If the calculated EEW parameter value at the considered station exceeds the preset threshold value, it is considered as a vote for the event. If out of four nearest stations, three gives vote within the selected time window then the EEW algorithm will issue alarm for that event.

The alarm in the present study has been classified in four categories as:

(a) *Correct Alarm (CA)* means issuing alarms where alarm needs to be issued and have been issued

(b) *False Alarm (FA)* means no alarm needs to be issued but issued

(c) *Correct All Clear (CAC)* means no alarm needs to be issued and also not issued

(d) *Missed Alarm (MA)* means issuing alarm where alarm need to be issued but not issued

The concept of these alarms has been described with the help of Fig. 6.7 in which cross represents the calculated EEW parameter values for example RSSCV value calculated at 5 sec time window and solid horizontal line represents the specified threshold value. The CA, MA, CAC and FA zones are represented by Quarter-I, Quarter -II, Quarter -III and Quarter -IV in Fig. 6.7.

Q-I represents zone of correct alarms, where alarm needs to be issued and have been issued by the system. Q-II represents false alarm zone, where no alarm is required but issued. Q-III represents correct all clear zone, where no alarm need to be issued and also not issued. Moreover, Q-IV represents missed alarm zone, where alarm need to be issued

but not issued. Further, CA and CAC are together termed as the correct detection (CD) while the FA and MA are the undesired alarms and together called as incorrect alarms (ICA).

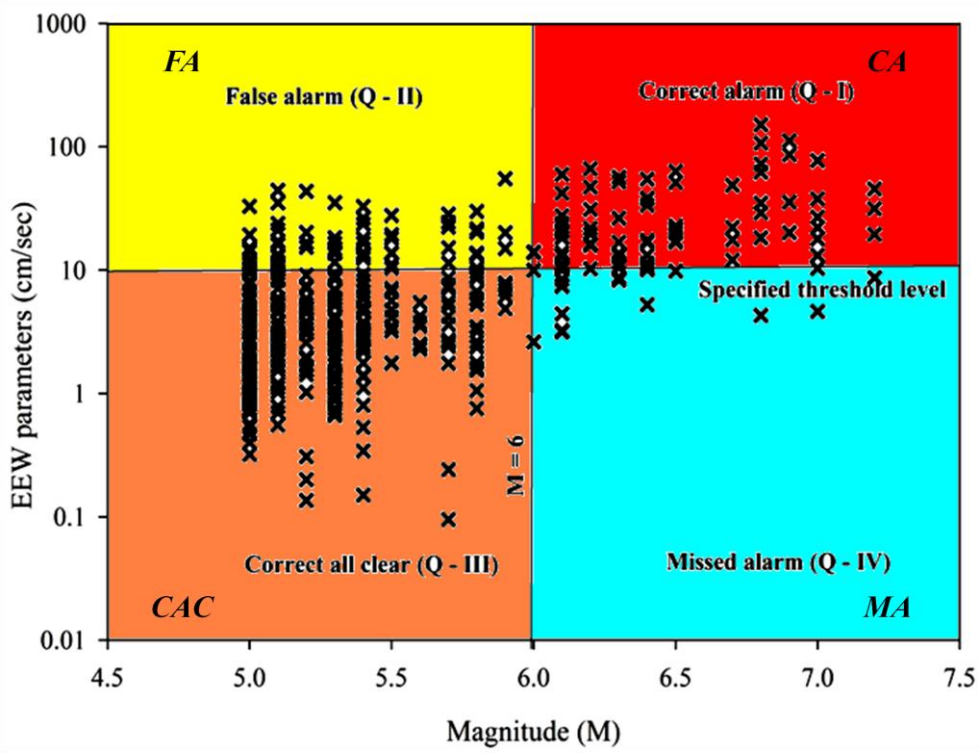

Figure 6.7 Four different alarm zones as CA, FA, CAC and MA with cross represents the EEW parameter value calculated at individual stations. The horizontal line represents the specified threshold level and the vertical line represents the line at M = 6.

The efficiency of individual EEW parameter has been calculated in terms of number as well as percentage of CA, MA, CAC, FA, CD and ICA. Further, to provide reliable and accurate warning results in minimal time length, the search for best possible combination of EEW parameters has been carried out.

6.4.1 Calculation of Efficiency of the Algorithm using Individual EEW Parameter

There are five EEW parameter (τ_p^{max}, τ_c, P_d, CAV and RSSCV) on which the efficiency of the desired algorithm depends. In this section, the efficiency of individual EEW has been discussed.

On the analysis of 1726 records of 105 events the EEW parameters gives different efficiencies based on the number of CA, MA, CAC and FA. The more will be the number

of CA and CAC, the better will be the efficiencies of the algorithm. MA and FA are the undesired alarms and reduce the efficiency. Thus, in a reliable and accurate EEW algorithm it is required that CD number should be more than ICA.

In the selected dataset, there are 105 earthquakes out of which there are 24 earthquakes having $M \geq 6$ for which warning need to be issued. There are 81 earthquakes having $M \leq 5.9$ for which warning need not to be issued because for the present study warning threshold has been set at $M \geq 6$. The number of CA and MA are calculated out of 24 earthquakes and CAC and FA are calculated out of 81 earthquakes. While, CD and ICA values are calculated from total 105 earthquakes.

Time taken by the algorithm for the accurate and correct warning is also an important point of concern in an EEW algorithm. Thus, the efficiency of the algorithm has been checked at five different time windows (1 sec to 5 sec) to find out the appropriate time window for issuing reliable warning.

6.4.1.1 τ_p^{max} *Based Algorithm*

In case of τ_p^{max} the efficiency of algorithm in terms of number of different alarms at different time windows has been listed in Table 6.15. In Table 6.15, it has been observed that from 1 sec to 5 sec the percentage of CA and CAC increases from 83.33% to 100% and 96.3% to 93.83%. However, in case of MA and FA with increase in time window length there is a variation from 16.67% to 0% and 3.7% to 6.17% which shows that τ_p^{max} is an efficient EEW parameter.

Table 6.15 Number and percentage of CA and MA obtained from 24 events having $M \geq 6$, while CAC and FA obtained from 81 events having $M < 6$, using τ_p^{max}.

Time	**CA**		**MA**		**CAC**		**FA**	
window	Numbers	%	Numbers	%	Numbers	%	Numbers	%
1 sec	20	83.33%	4	16.67%	78	96.30%	3	3.70%
2 sec	23	95.83%	1	4.17%	56	69.14%	25	30.86%
3 sec	24	100%	0	0%	73	90.12%	8	9.88%
4 sec	22	91.67%	2	8.33%	76	93.83%	5	6.17%
5 sec	24	100%	0	0%	76	93.83%	5	6.17%

Further, the results have been illustrated in terms of CD and ICA in Fig 6.8. In Fig 6.8 at 1 sec out of 105 events, 98 events are correctly detected while 7 events are wrongly interpreted. At 2 sec window, there is a sudden increase in number of ICA with decrease in number of CD because the preset threshold value has been crossed by the some events having M ≤ 6. However, from 2 sec onwards i.e. 3 sec, 4 sec and 5 sec, there has been a continuous increase in CD and decrease in ICA.

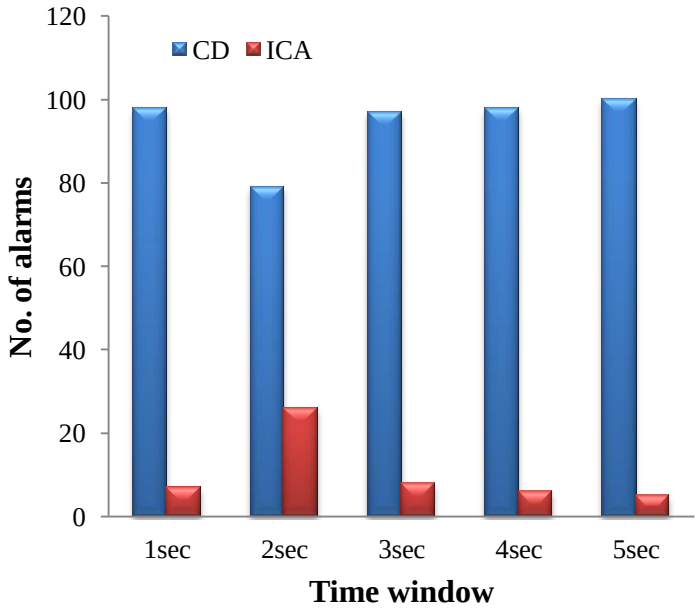

Figure 6.8 Number of CD and ICA obtained from 105 events at different time windows. Blue bars in the histogram represent the number of correct detection made by the algorithm using τ_p^{max} and red bars represent the erroneous alarms.

6.4.1.2 τ_c *Based Algorithm*

The average period of the initial portion of P-wave has a linear relation with the magnitude of the event as shown in Fig 6.3 at different time windows. The efficiency of the algorithm based on τ_c has been calculated at five different time windows in terms of CA, MA, CAC and FA.

In Table 6.16 it has been observed that from 1 sec to 5 sec the number/ percentage of CA and CAC increases from 22 (91.67%) to 23 (95.83%) and 78 (96.3%) to 78 (98.77%), respectively. However, in case of MA and FA with increase in time window length there is a decrease from 2 (8.33%) to 1 (4.17%) and 3 (3.7%) to 1 (1.3%), repectively, which implies that τ_c is a proficient EEW parameter. On comparing τ_p^{max} and τ_c

it has been found that τ_c performance is more consistent than τ_p^{max}. The percentage of MA and FA at each time window continuously decreases in case of τ_c, while in case of τ_p^{max} the decrease is not consistent.

Table 6.16 Number and percentage of CA and MA obtained from 24 events having M ≥ 6, while CAC and FA obtained from 81 events having M < 6, using τ_c.

Time	**CA**		**MA**		**CAC**		**FA**	
window	Numbers	%	Numbers	%	Numbers	%	Numbers	%
1 sec	22	91.67%	2	8.33%	78	96.30%	3	3.70%
2 sec	23	95.83%	1	4.17%	75	96.30%	6	7.41%
3 sec	21	87.50%	3	12.50%	77	95.06%	4	4.94%
4 sec	22	91.67%	2	8.33%	77	95.06%	4	4.94%
5 sec	22	95.83%	2	4.17%	78	98.77%	1	1.23%

Further, in terms of CD and ICA the performance of τ_c has been shown in Fig. 6.9 where out of 105 events at 1 sec 100 events are correctly detected while 5 events are interpreted wrongly. At 2 sec and 3 sec time window there is a sudden increase in number of ICA with decrease in number of CD because the preset threshold value has been crossed by the some events having M ≤ 6. From 3 sec onwards viz., 4 sec and 5 sec there is a continuous increase in CD with decrease in ICA.

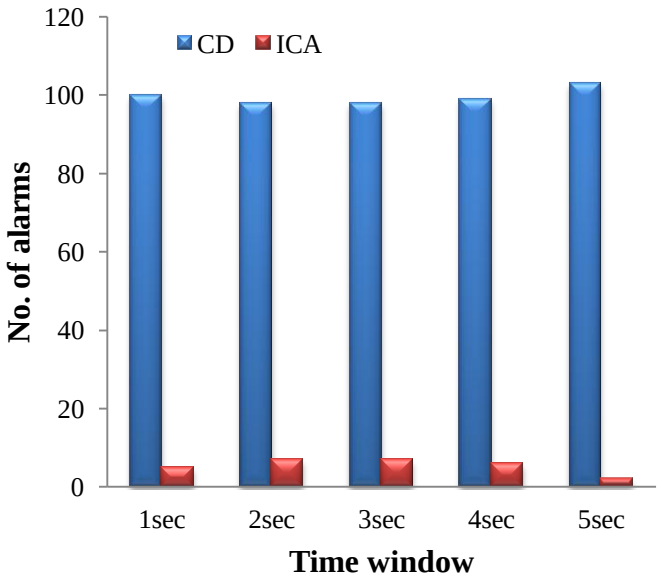

Figure 6.9 Number of CD and ICA obtained from 105 events at different time window using τ_c.

The propagation path of the seismic waves also plays an integral role in affecting the amplitude and frequency content of the incoming seismic waves. Thus, in addition to the source and the site effects, the medium characteristics in terms of attenuation of seismic signal generally described in terms of quality factor at 1 Hz (Q_o) has been included in τ_c-M relation. The analysis has been carried out on Indian dataset (discussed in Chapter 5). Q_c relation estimated by different researchers for different regions of India: Garhwal Himalaya (Gupta et al. 1995), Kumaun Himalaya (Paul et al. 2003), Northeast Himalaya (Gupta and Kumar 2002), Northwest Himalaya (Kumar et al. 2005) and National capital region (Mohanty et al. 2009) have been used in the present study. On calculating the τ_c for a time window of 3 sec using Eq. (4.8) and regressed it with the Q_o and magnitude gives the following relation:

$$\log \tau_c = 0.2268M + 1.0325\left(\frac{Q_o}{1000}\right) - 1.465 \qquad (6.1)$$

The standard deviation in Eq. (6.1) is 0.2563. Linear relation has been obtained between τ_c and magnitude for different regions having Q_o ranging from 100 to 1000. Fig. 6.10 (a) and (b) reveal the dependency of τ_c on magnitude and Q_o. For example in Fig 6.10 (a), on putting of M = 6, it has been found that τ_c varies between 0.99 to 8.47 having a mean value of 3.6 and standard deviation of 2.5 for a change in value of Q_o from 100 to 1000. Similarly, in Fig. 6.10 (b), for a value of Q_o = 600, τ_c varies between 1.9431 to 9.3089 having a mean value of 4.9 and standard deviation of 2.7 for magnitude range 5 to 8. The high value of standard deviation from mean value of τ_c for different Q_o values shows that τ_c is not only the function of magnitude but it is dependent on attenuation characteristic of the medium also.

For Indian region due to highly heterogeneous medium and scarcity of higher magnitude strong motion records, the correlation between τ_c and magnitude with Q_o may give better estimations of magnitude making it more region specific. But the effect of medium is not observed to be so significant and require more data to conclude such studies. Therefore, in the present EEW algorithm, this effect has not been considered.

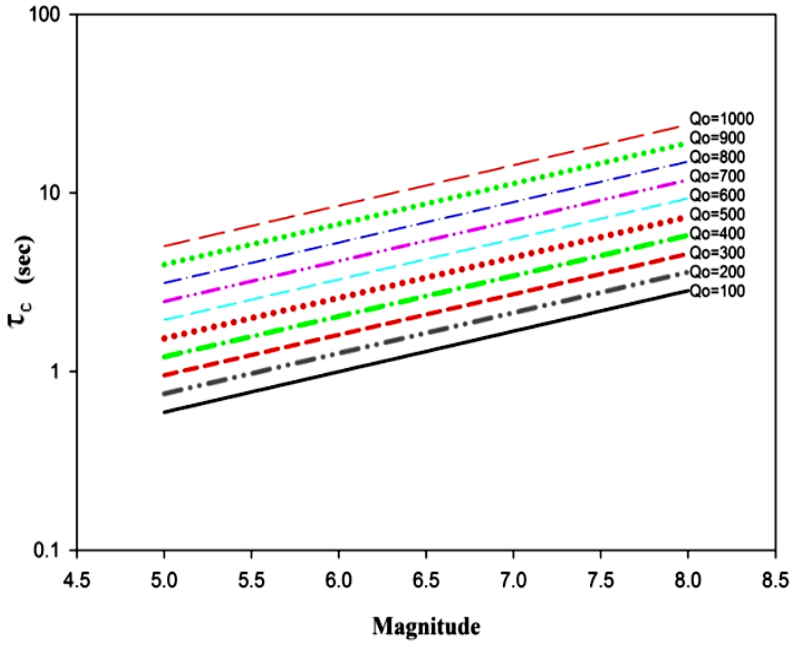

(a)

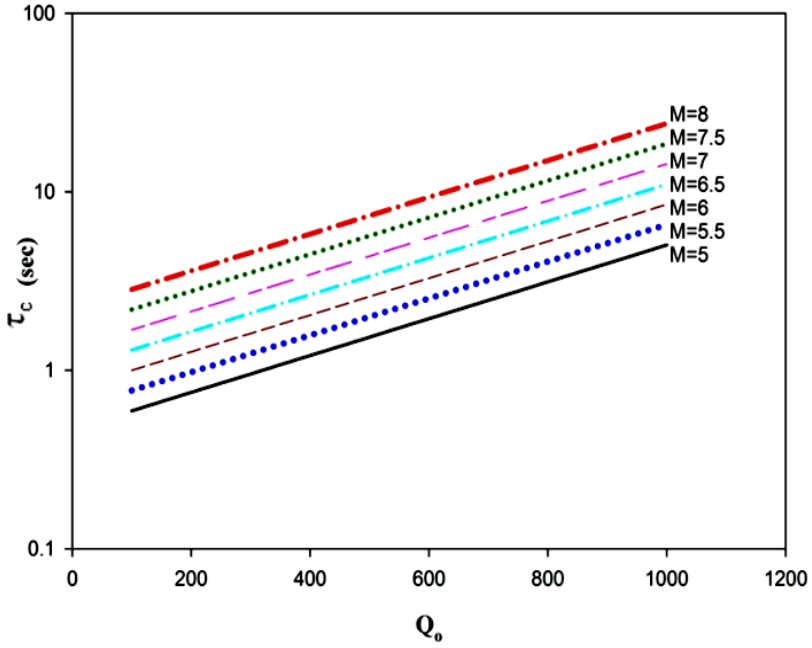

(b)

Figure 6.10 Plot showing dependency of τ_c on magnitude and Q_o (a) shows linear relation between τ_c and magnitude for Q_o of different regions (100 to 1000), (b) shows linear relationship between τ_c and Q_o for magnitude ranges (5 to 8).

6.4.1.3 *P_d Based Algorithm*

Peak displacement calculated from the initial portion of P-wave has been considered as a robust and an important EEW parameter for magnitude estimation. In the

present study, P_d has also been used in issuing warning for higher magnitude earthquake. The τ_p^{max} and τ_c parameters efficiency as discussed in above section have found to be quite good. Inclusion of P_d in the algorithm with τ_p^{max} and τ_c provide more promising results because it shows less scattering in comparison to other EEW parameters (see Fig. 6.4).

Table 6.17 represents the performance of P_d in terms of different types of alarm, at different time windows. It has been observed that from 1 sec to 5 sec the number/percentage of CA and CAC increases from 17 (70.83%) to 24 (100%) and 73 (90.12%) to 79 (97.53%), respectively. However, in case of MA and FA with increase in time window length there is a decrease from 7 (29.17%) to 0 (0%) and 8 (9.88%) to 2 (2.47%), respectively, which shows that P_d is a competent EEW parameter.

From the efficiency analysis of τ_p^{max}, τ_c and P_d, it has been concluded that all the three parameters have their advantages and the combination of these parameters, when used for issuing warning, provide a robust, reliable and accurate EEW algorithm.

Table 6.17 Number and percentage of CA and MA obtained from 24 events having M ≥ 6, while CAC and FA obtained from 81 events having M < 6, using P_d.

Time	**CA**		**MA**		**CAC**		**FA**	
window	Numbers	%	Numbers	%	Numbers	%	Numbers	%
1 sec	17	70.83%	7	29.17%	73	90.12%	8	9.88%
2 sec	19	79.17%	5	20.83%	74	91.30%	7	8.64%
3 sec	19	79.17%	5	20.83%	75	92.60%	6	7.41%
4 sec	23	95.83%	1	4.17%	79	97.53%	2	2.47%
5 sec	24	100%	0	0.00%	79	97.53%	2	2.47%

The results of P_d algorithm have been analyzed in terms of CD and ICA as shown in Fig. 6.11. In Fig. 6.11 out of 105 events 90 events are correctly detected at 1 sec while 15 events are wrongly interpreted. At 2 sec there are 93 CD and 15 ICA, at 3 sec there are 94 CD and 11 ICA, at 4 sec there are 102 CD and 3 ICA similarly at 5 sec there are 103 CD and 2 ICA. Thus, with the increase in time window, the number of CD is continuously increasing with a simultaneous decrease in ICA.

The consistent increase in CD that has been observed in case of P_d could not be seen in case of τ_p^{max} and τ_c (see Figs. 6.11 and 6.12). In case of τ_p^{max}, there is sudden dip in

the value of CD at 2 sec. While in case of τ_c, at 2 sec and 3 sec, the rate of CD remains constant and starts linearly rising with 3 sec time window onwards.

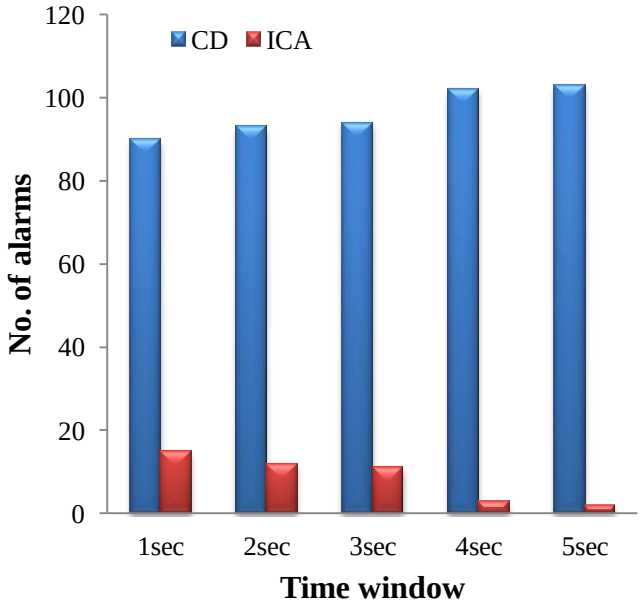

Figure 6.11 Number of CD and ICA obtained from 105 events at different time windows using P_d.

6.4.1.4 *CAV Based Algorithm*

Cumulative Absolute Velocity is another EEW parameter which has been used for issuing warning for higher magnitude earthquake. It is an integral measurement of the acceleration records within a defined time period (see Chapter 4, Eq. (4.14)). The threshold levels for the damaging earthquake at five different time windows have been estimated (see Table 6.11) by analytic study on K-NET dataset. The efficiency of algorithm in terms of number of different alarms at different time windows is shown in Table 6.18.

In Table 6.18, it has been observed that 1 sec to 5 sec the number/percentage of CA and CAC increases from 18 (75%) to 24 (100%) and 57 (70.37%) to 74 (91.36%), repectively. However, in case of MA and FA with increase in length of time window there is a decrease from 6 (25%) to 0 (0%) and 24 (29.63%) to 7 (8.64%), respectively, which shows that CAV is also an effective EEW parameter.

In case of CAV the number of FA have observed to be high but the event having FA are generally of M = 5.9, 5.8 and 5.7. The FA at M = 5.9 and 5.8 is not the point of much apprehension because earthquakes with small focal depth and having magnitude around 5.9, 5.8 and 5.7 may also lead to high damage similar to M = 6 earthquake.

Table 6.18 Number and percentage of CA and MA obtained from 24 events having M ≥ 6, while CAC and FA obtained from 81 events having M < 6, using CAV.

Time	CA		MA		CAC		FA	
window	Numbers	%	Numbers	%	Numbers	%	Numbers	%
1 sec	18	75.00%	6	25.00%	57	70.37%	24	29.63%
2 sec	21	87.50%	3	12.50%	57	70.37%	24	29.63%
3 sec	22	91.67%	2	8.33%	54	66.67%	27	33.33%
4 sec	23	95.83%	1	4.17%	66	81.48%	15	18.52%
5 sec	24	100.00%	0	0.00%	74	91.36%	7	8.64%

The CAV algorithm has been analyzed in terms of CD and ICA for looking into its efficacy as shown in Fig. 6.12. In Fig. 6.12 it has been observed that out of 105 events, 75 events are correctly detected at 1 sec, while 30 events are wrongly interpreted. At 2 sec there are 78 CD and 27 ICA, at 3 sec there are 76 CD and 29 ICA, at 4 sec there are 89 CD and 16 ICA similarly at 5 sec there are 98 CD and 7 ICA. Thus, it has been concluded that with the increase in time window length, the results becomes more accurate. But in case of CAV, at 3 sec there is a sudden rise in incorrect alarms with decrease in correct once. Further, at 4 sec and onwards there is a constant rise in CD rate with decrease in ICA. The results of CAV at 4 sec and 5 sec are in comparable state with τ_p^{max}, τ_c and P_d. Thus, 4 sec window has been selected for obtaining stable results.

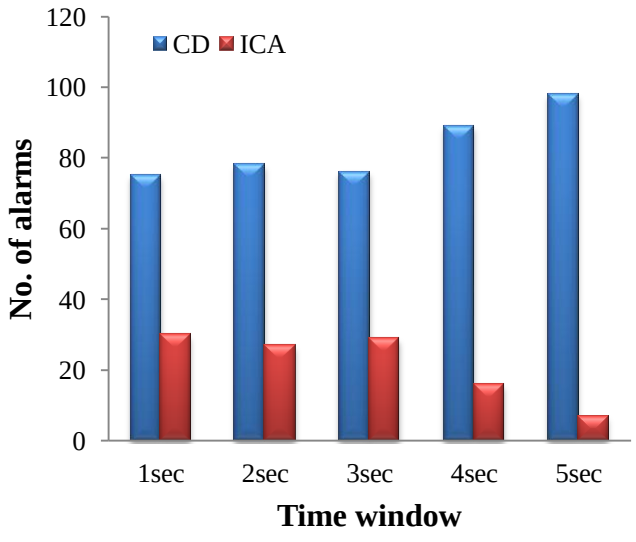

Figure 6.12 Number of CD and ICA obtained from 105 events at different time window using CAV.

6.4.1.5 *RSSCV Based Algorithm*

In the present study, Root Sum of Squares Cumulative Absolute Velocity parameter have been used for auto P-pick algorithm as well as for issuing warning for potentially damaging earthquakes (see section 6.2 and 6.3.5). Five threshold levels at five different time windows have been calculated and used to calculate different alarms for determining the efficiency of the algorithm. The efficiency of the algorithm in terms of number of CA, MA, CAC and FA have been calculated and shown in Table 6.19.

Table 6.19 Number and percentage of CA and MA obtained from 24 events having M ≥ 6, while CAC and FA obtained from 81 events having M < 6, using RSSCV.

Time	**CA**		**MA**		**CAC**		**FA**	
window	Numbers	%	Numbers	%	Numbers	%	Numbers	%
1 sec	23	95.83%	1	4.17%	29	35.80%	52	64.20%
2 sec	23	95.83%	1	4.17%	30	37.04%	51	62.96%
3 sec	24	100%	0	0%	43	53.09%	38	46.91%
4 sec	24	100%	0	0%	71	87.65%	10	12.35%
5 sec	24	100%	0	0%	73	90.10%	8	9.90%

In Table 6.19 it has been observed that from 1 sec to 5 sec the number/percentage of CA and CAC increases from 23 (95.83%) to 24 (100%) and 29 (35.8%) to 73 (90.1%), respectively. However, in case of MA and FA with increase in time window length there is a reduction from 1 (4.17%) to 0 (0%) and 52 (64.2%) to 8 (9.9%), respectively, which shows that CAV is also an important EEW parameter.

In case of RSSCV the numbers of CA and MA are comparable with other EEW parameters such as τ_p^{max}, τ_c, P_d and CAV, respectively. However, the rates of CAC and FA have been observed poor, at small time windows i.e., 1 sec, 2 sec and 3 sec, but for higher time window (4 sec and 5 sec) the improvement in rate of CAC and FA takes place.

From Fig. 6.13, it has been observed that with each second of increase in time window, the percentage of issuing correct alarms have been increasing continuously. The consistent increase in CD has been observed in RSSCV and P_d parameter only. However, in case of τ_p^{max}, τ_c and CAV, there is a sudden dip in the value of correct detection at different time windows below 4 sec.

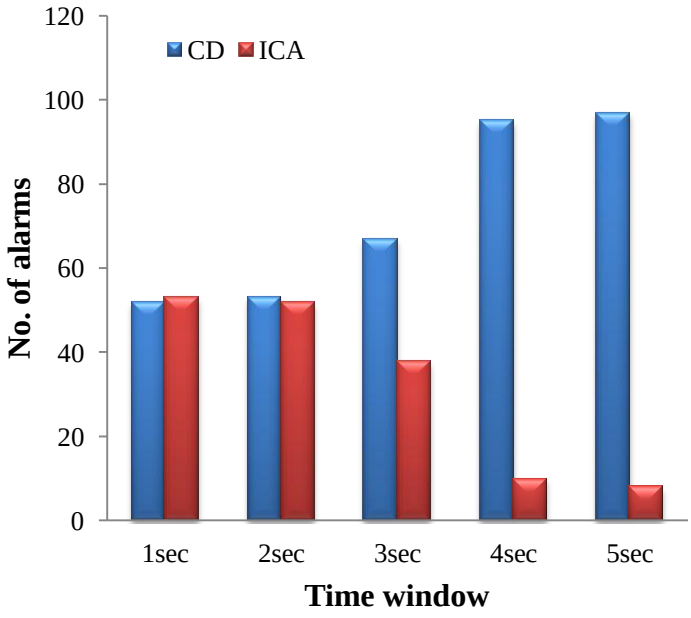

Figure 6.13 Number of CD and ICA obtained from total 105 events at different time window using RSSCV.

The analysis of all the five EEW parameters (τ_p^{max}, τ_c, P_d, CAV and RSSCV) considered in the present study have their own rate of correct and incorrect alarms as discussed above at different time windows. In starting 2 sec, the results obtained by the EEW parameters are not consistent and reliable, but at 3 sec and above, the results gets stabilized. It has been observed that at 4 sec and above, the performance level of all the five EEW parameters attains its reliable and fairly accurate state. Further, in the present study, the next step is to search the best possible combination of EEW parameter that gives most accurate and reliable results in all the five time windows.

6.4.2 Search for the Best EEW Parameters Combination

In the present study, five parameters (τ_p^{max}, τ_c, P_d, CAV and RSSCV) have been considered. There have been different possible combinations of the parameters that could be possible for the selection of accurate and fast warning EEW algorithm. The Four possible combinations which have been analyzed in the present study for the search of best EEW algorithm have been discussed below.

6.4.2.1 *Three EEW Parameters Preference Based Approach*

In the present study, the analysis is made over 105 K-NET earthquakes, which comprised of 1726 records. The nearest four stations within 60 km epicentral distance of each event have been considered. In the selected dataset, there are 24 earthquakes having $M \geq 6$, for which warning need to be issued (CA/MA), while 81 earthquakes having $M < 6$ for which warning need not to be issued (CAC/FA). CD and ICA values are calculated from a total of 105 earthquakes.

Five EEW parameters values have been calculated for five different time windows at stations. Out of four, when three stations cross the preset threshold value of an EEW parameter alarm (CA/ MA/ CAC/FA) has been marked for that event at that particular time window. Further, whenever for an event three out of five EEW parameters shows similar alarm status, the event has been marked with the same status. For example, for an event of M = 7.2, at a time window of 2 sec if CAV parameter shows CA, RSSCV shows MA, τ_p^{max} shows CA, τ_c shows CA and P_d shows CA then the event output of the algorithm will be a CA. In Table 6.20 the number of different alarms obtained by the three parameter preferences based approach at different time window has been listed.

Table 6.20 Number and percentage of CA and MA obtained from 24 events having $M \geq 6$, while CAC and FA obtained from 81 events having $M < 6$, for a three EEW parameter preference based approach.

Time	**CA**		**MA**		**CAC**		**FA**	
window	Numbers	%	Numbers	%	Numbers	%	Numbers	%
1 sec	22	91.67%	2	8.33%	77	95.06%	4	4.94%
2 sec	23	95.83%	1	4.17%	73	90.12%	8	9.88%
3 sec	24	100%	0	0%	77	95.06%	4	4.94%
4 sec	24	100%	0	0%	80	98.77%	1	1.23%
5 sec	24	100%	0	0%	81	100%	0	0%

In Table 6.20 it has been observed that from 1 sec to 5 sec the number/percentage of CA and CAC increases from 22 (91.67%) to 24 (100%) and 77 (95.06%) to 81 (100%), respectively. However, in case of MA and FA with increase in time window length there is decrease from 2 (8.33%) to 0 (0%) and 4 (4.94%) to 0 (0%), respectively. Thus, the

percentage of correct number of alarms have been found quite high by giving preference to any three similar output EEW parameters out of five.

From Fig. 6.14 it has been observed that the number of CD increases from 99 to 104 and remains constant after 4 sec. Also, the number of ICA reduces from 6 to 1 for time window of 1 sec to 4 sec. The CD of 104 events out of 105 shows that three parameter preference based approach is quiet effective for an EEW algorithm.

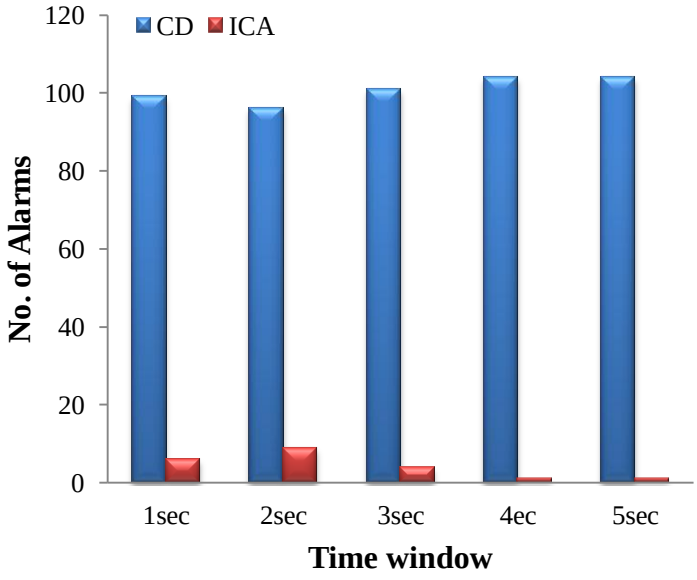

Figure 6.14 Number of CD and ICA obtained from total 105 events at different time window using three EEW parameter preference based approach.

6.4.2.2 *Four EEW Parameters Preference Based Approach*

Other considered approach has been termed as four parameter preference based approach. In four parameter preference based approach, whenever for an event four out of five parameters have common alarm status, the event has been marked with the same status. For an event of M = 7.2, at a time window of 2 sec if CAV parameter shows CA, RSSCV shows MA, τ_p^{max} shows CA, τ_c shows CA and P_d shows CA then for the event output of the algorithm will be a CA.

In Table 6.21 it has been observed that from 1 sec to 5 sec, the number/percentage of CA and CAC increases from 19 (79.17%) to 24 (100%) and 50 (61.73%) to 74 (91%), respectively. However, in case of MA and FA with increase in time window length there is a decrease from 5 (20.83%) to 0 (0%) and 31 (38.27%) to 7 (9%), respectively. The

percentage of correct number of alarms has observed to be quite good. But on comparing four parameter preference based approach results from three parameter based approach it has been observed that three parameter based approach provides more accurate results at each time window starting from 1 sec to 5 sec in terms of all the four alarms.

Table 6.21 Number and percentage of CA and MA obtained from 24 events having $M \geq 6$, while CAC and FA obtained from 81 events having $M < 6$, for four EEW parameter preference based approach.

Time	**CA**		**MA**		**CAC**		**FA**	
window	Numbers	%	Numbers	%	Numbers	%	Numbers	%
1 sec	19	79.17%	5	20.83%	50	61.73%	31	38.27%
2 sec	23	95.83%	1	4.17%	48	59.26%	33	40.74%
3 sec	22	92%	2	8.33%	50	61.73%	31	38.27%
4 sec	22	92%	2	8.33%	71	87.65%	10	12.35%
5 sec	24	100%	0	0%	74	91%	7	9%

From Fig. 6.15 it has been observed that the number of CD increases from 1 sec to 5 sec i.e., 69 in 1 sec and 98 in 5 sec. The number of ICA also decreases from 1 sec to 5 sec such as 36 to 7. A comparison has been drawn between the results of four parameter preference based approach with three parameter preference based approach. The CD rate at each time window in three parameter preference based approach is found to be higher than four parameter preference based approach.

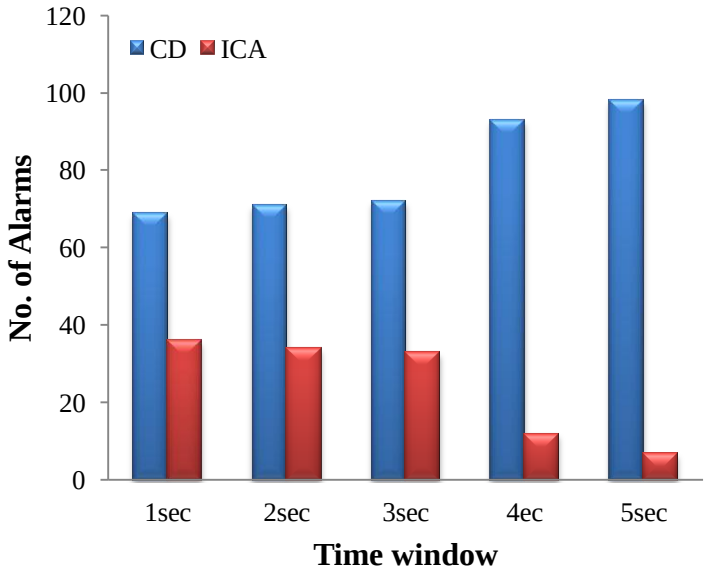

Figure 6.15 Number of CD and ICA obtained from total 105 events at different time window using four EEW parameter preference based approach.

6.4.2.3 *Five EEW Parameters Preference Based Approach*

Another EEW parameters combination has been termed as five EEW parameters preference based approach. In five EEW parameters preference based approach, event decision is based on all the five parameters. For an event if all the five EEW parameter have common alarm status, then only the event has been marked with the same status. For example, if for an event having M = 7.2, at time window of 2 sec if CAV parameter shows CA, RSSCV shows MA, τ_p^{max} shows CA, τ_c shows CA and P_d shows CA then for the event output of the algorithm will be a MA.

In Table 6.22 it has been observed that from 1 sec to 5 sec the number/percentage of CA and CAC increases from 12 (50%) to 23 (95.83%) and 26 (32.1%) to 65 (80.25%), respectively. However, in case of MA and FA with increase in time window length there is a decrease from 12 (50%) to 1 (4.17%) and 55 (67.9%) to 16 (19.75%), respectively. The percentage of correct number of alarms has found to be quite poor in the starting 1 sec but latter from 3 sec onward it gets modified and reaches to 95.83% in 5 sec. Similarly, in case of ICA, MA and FA, quite reliable efficiency has been achieved at higher time windows.

Table 6.22 List of number and percentage of CA and MA obtained from 24 events having M ≥ 6, while CAC and FA obtained from 81 events having M < 6, for five EEW parameter preference based approach.

Time	CA		MA		CAC		FA	
window	Numbers	%	Numbers	%	Numbers	%	Numbers	%
1 sec	12	50.00%	12	50.00%	26	32.10%	55	67.90%
2 sec	15	62.50%	9	37.50%	27	33.33%	54	66.67%
3 sec	17	71%	7	29.17%	37	45.68%	44	54.32%
4 sec	20	83%	4	16.67%	55	67.90%	26	32.10%
5 sec	23	95.83%	1	4.17%	65	80.25%	16	19.75%

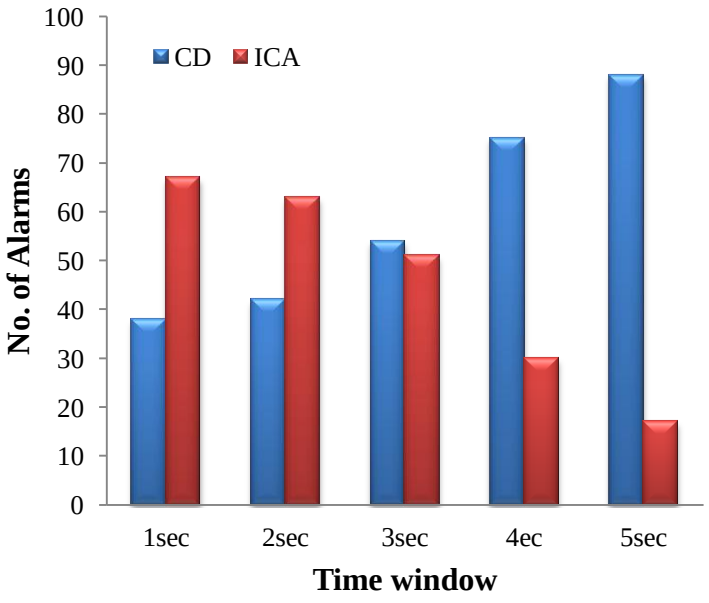

Figure 6.16 Number of CD and ICA obtained from total 105 events at different time window using five EEW parameter preference based approach.

From Fig. 6.16 it has been observed that the number of CD increases from 38 to 88 on a time window variation of 1 sec to 5 sec, while the rate of ICA decreases from 67 at 1 sec to 17 at 5 sec. The number of CD has found to be very small approximately half than the ICA in 1 sec. It implies that the five parameter preference based approach has poor performance at small time windows (1 sec, 2 sec and 3 sec). On comparing the obtained result with three and four parameter preference based approach it has been observed that

the best result in terms of maximum CD and minimum ICA has been obtained using three parameter preference based approach.

6.4.2.4 *Logic Combination of EEW Parameters Preference Based Approach*

In the previous study, different possible combinations of EEW parameter were discussed as three, four and five parameter preference based approach. One more approach has been discussed in this section which comprised of the combination of similar types of EEW parameters and is logically represented as:

$$(\tau_p^{max} \textbf{ OR } \tau_c) \textbf{ AND } (\text{CAV } \textbf{OR } \text{RSSCV}) \textbf{ AND } P_d \tag{6.2}$$

From Eq. (6.2) it has been observed that the time parameters (τ_p^{max} and τ_c) and velocity parameters (CAV and RSSCV) are combined together using OR gate and finally the AND gate is applied on time, velocity and displacement (P_d) parameters based alarms to find out the resultant alarm. For example for an event of M = 7.2 at a time window of 2 sec, if CAV parameter shows CA, RSSCV shows MA, τ_p^{max} shows CA, τ_c shows CA and P_d shows CA, then on applying logical operation with assumption that CA and CAC represents 1 and MA and FA represent 0, the processing is as follows:

$$\tau_p^{max} \textbf{ OR } \tau_c = 1+1=1 \tag{6.3}$$

$$\text{CAV } \textbf{OR } \text{RSSCV}=1+0= 1 \tag{6.4}$$

$$(\tau_p^{max} \textbf{ OR } \tau_c) \textbf{ AND } (\text{CAV } \textbf{OR } \text{RSSCV}) \textbf{ AND } P_d = 1*1*1=1 \tag{6.5}$$

Therefore, from Eqs. (6.3, 6.4 and 6.5) it have been observed that the output of the event has found to be 1 (see Eq. (6.5)) that is CA. Due to the inclusion of logic operators in the present approach it is termed as logic combination of EEW parameters preference based approach. On applying this approach on K-NET dataset, the number of different alarms obtained for 105 events have been listed in Table 6.23.

Table 6.23 List of number and percentage of CA and MA obtained from 24 events having $M \geq 6$, while CAC and FA obtained from 81 events having $M < 6$, for logic combination of EEW parameters preference based approach.

Time	**CA**		**MA**		**CAC**		**FA**	
window	Numbers	%	Numbers	%	Numbers	%	Numbers	%
1 sec	17	70.83%	7	29.17%	52	64.20%	29	35.80%
2 sec	19	79.17%	5	20.83%	51	62.96%	30	37.04%
3 sec	19	79.17%	5	20.83%	52	64.20%	29	35.80%
4 sec	21	87.50%	3	12.50%	70	86.42%	11	13.59%
5 sec	24	100%	0	0%	72	88.89%	9	11.11%

In Table 6.23, it has been observed that from 1 sec to 5 sec the number/percentage of CA and CAC increases from 17 (70.83%) to 24 (100%) and 52 (64.2%) to 72 (88.89%), respectively. However, in case of MA and FA with increase in time window length there is a decrease from 7 (29.17%) to 0 (0%) and 29 (35.8%) to 9 (11.11%), respectively. The results obtained using logic combination of EEW parameters preference based approach shows that the number of CA, MA, CAC and FA have comparability with the results obtained from three and four parameters preference based approach. Further, the results of logic combination of EEW parameters preference based approach have more number of CA, MA, CAC and FA than five parameters preference based approach.

From Fig. 6.17 it has been observed that the rate of CD increases from 69 at 1 sec to 96 at 5 sec, while the number of ICA decreases from 36 at 1 sec to 9 at 5 sec. The number of CD in case of logic combination of EEW parameters preference based approach is better than five parameters preference based approach, comparable with four parameters preference based approach and poorer than three parameters preference based approach.

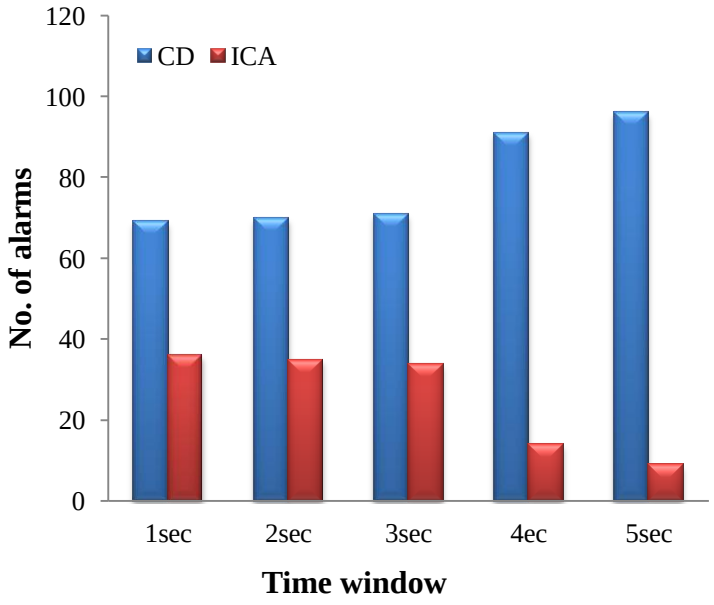

Figure 6.17 Number of CD and ICA obtained from total 105 events at different time window using logic combination of EEW parameters preference based approach.

From Table 6.24, it has been concluded that on comparing the number of CD obtained by all the possible four approaches, it has been found that at a time window of 4 sec, three parameter preference based approach provides the efficient, accurate and reliable results.

Table 6.24 Comparison in number of CD achieved out of 105 events using various EEW parameter preferences based approaches.

No. of CD by EEW Parameter preference based approaches	**Time window**				
	1 sec	**2 sec**	**3 sec**	**4 sec**	**5 sec**
Three parameters	99	96	101	104	104
Four parameters	69	71	72	93	98
Five parameters	38	42	54	75	88
Logic combination of EEW parameters	69	70	71	91	96

6.4.3 Ranking of Different EEW Parameters

In the present study, five EEW parameters (τ_p^{max}, τ_c, P_d, CAV and RSSCV) have been used for issuing warning for earthquakes having $M \geq 6$. Further, from the search of best combination of EEW parameter and the minimal time window it has been observed that at 4 sec, three parameter preference based approach provides best results. All the EEW parameters considered in the present study have their own advantages. However, for ranking EEW parameters the dataset has been classified in three categories: **(a)** For $6 \leq M \leq 7.2$; **(b)** For $5 \leq M \leq 5.9$; **(c)** For $5 \leq M \leq 7.2$. The search for the ranking of each attribute has been made at five different time windows (1 sec, 2 sec, 3 sec, 4 sec and 5 sec) for three ranges of magnitude ($6 \leq M \leq 7.2$, $5 \leq M \leq 5.9$ and $5 \leq M \leq 7.2$). It has been observed that in magnitude range of $6 \leq M \leq 7.2$ there are total 24 events, in $5 \leq M \leq 5.9$ there are 81 events and in $5 \leq M \leq 7.2$ there are 105 events for which CD is required. The CD has been done by using three parameter preference based approach at different time windows. For each EEW parameter, analysis has been done in terms of number of correct alarms, percentage of correct alarms and thus, ranking of each parameter at each time window has been decided. Finally, the overall ranking of parameters at all time windows has been calculated as shown in Table 6.25.

It has been observed from Table 6.25 (a) that for higher magnitude range ($6 \leq M \leq 7.2$) RSSCV has highest ranking because it does not saturate at higher magnitude, but for low magnitude range ($5 \leq M \leq 5.9$) it is not providing good results, while τ_c have highest ranking in this range (as shown in Table 6.25 (b)). However, when entire magnitude range has been considered ($5 \leq M \leq 7.2$) τ_c come up with the highest ranking followed by τ_p^{max}, P_d, CAV and RSSCV (see Table 6.25 (c)).

Table 6.25 List of number of correct detection, percentage of correct detection and ranking of each EEW parameter at different time window and for different magnitude ranges (a) $6 \leq M \leq 7.2$ (b) $5 \leq M \leq 5.9$ and (c) $5 \leq M \leq 7.2$.

(a)

For $6 \leq M \leq 7.2$

In terms of correct no. of alarms

Time window	1 sec	2 sec	3 sec	4 sec	5 sec
CAV	18	21	23	23	24
RSSCV	23	23	24	24	24
τ_p^{max}	20	23	24	22	24
τ_c	22	23	21	22	23
P_d	17	19	19	23	24

In terms of percentage of correct no. of alarms

Time window	1 sec	2 sec	3 sec	4 sec	5 sec
CAV	75.00%	87.50%	95.83%	95.83%	100%
RSSCV	95.83%	95.83%	100%	100.00%	100%
τ_p^{max}	83.33%	95.83%	100%	91.67%	100%
τ_c	91.67%	95.83%	87.50%	91.67%	95.83%
P_d	70.83%	79.17%	79.17%	95.83%	100%

Ranking in terms of correct no. of alarms

Time window	1 sec	2 sec	3 sec	4 sec	5 sec	Total ranking
CAV	IV	IV	III	II	I	III
RSSCV	I	I	I	I	I	I
τ_p^{max}	III	I	I	IV	I	II
τ_c	II	I	IV	IV	V	IV
Pd	V	V	V	II	I	V

(b)

For $5 \leq M \leq 5.9$

In terms of correct no. of alarms

Time window	1 sec	2 sec	3 sec	4 sec	5 sec
CAV	57	57	54	66	74
RSSCV	29	3	43	71	73
τ_p^{max}	78	74	73	76	76
τ_c	78	75	77	77	80
P_d	73	74	75	79	79

In terms of percentage of correct no. of alarms

Time window	1 sec	2 sec	3 sec	4 sec	5 sec
CAV	70.37%	70.37%	66.67%	81.48%	91.36%
RSSCV	35.80%	37.04%	53.09%	87.65%	90.12%
τ_p^{max}	96.30%	91.36%	90.12%	93.83%	93.83%
τ_c	96.30%	92.59%	95.06%	95.06%	98.77%
P_d	90.12%	91.36%	92.59%	97.53%	97.53%

Ranking in terms of correct no. of alarms

Time window	1 sec	2 sec	3 sec	4 sec	5 sec	Total ranking
CAV	IV	IV	IV	V	IV	IV
RSSCV	V	V	V	IV	V	V
τ_p^{max}	I	II	III	III	III	III
τ_c	I	I	I	II	I	I
P_d	III	II	II	I	II	II

(c)

For $5 \leq M \leq 7.2$

In terms of correct no. of alarms

Time window	1 sec	2 sec	3 sec	4 sec	5 sec
CAV	75	78	77	89	98
RSSCV	52	53	67	95	97
τ_p^{max}	98	97	97	98	100
τ_c	100	98	98	99	103
P_d	90	93	94	102	103

In terms of percentage of correct no. of alarms

Time window	1 sec	2 sec	3 sec	4 sec	5 sec
CAV	71.43%	74.29%	73.33%	84.76%	93.33%
RSSCV	49.52%	50.48%	63.81%	90.48%	92.38%
τ_p^{max}	93.33%	92.38%	92.38%	93.33%	95.24%
τ_c	95%	93.33%	93.33%	94.29%	98.10%
P_d	85.71%	88.57%	89.52%	97.14%	98.10%

In terms of percentage of correct no. of alarms

Time windows	1 sec	2 sec	3 sec	4 sec	5 sec	Total ranking
CAV	IV	IV	IV	V	IV	IV
RSSCV	V	V	V	IV	V	V
τ_p^{max}	II	II	II	III	III	II
τ_c	I	I	I	II	I	I
P_d	III	III	III	I	I	III

6.5 MAGNITUDE ESTIMATION

In the earlier section of the present chapter, different EEW parameters have been discussed, their relations with magnitude have been calculated, different thresholds for automatic P-pick and issuing warning for potentially damaging earthquakes ($M \geq 6$) have been made. Estimation of magnitude to issue warning for an event within a few seconds after it originates is integral task of an EEW algorithm.

After issuing the warning for $M \geq 6$, the algorithm further explores the data for more accurate magnitude determination. Brune's model has been used to fit on P-wave data after P-onset at different time window lengths starting from 1 sec to 10 sec for estimating spectral parameters (Bhardwaj et al. 2012c, 2013b). Fig. 6.18 shows the source

displacement and acceleration spectra fitted with Eqs. (4.21 and 4.23) to calculate three spectral parameters at 5 sec time window for different magnitudes 5.0, 5.5, 6.0, 6.5 and 7.0 respectively. The best fit Brune's displacement and acceleration spectra on the source displacement and acceleration spectra yield calculation of three spectral parameters Ω_o, f_c and f_{max} which is used for calculating source parameter that is, seismic moment using Eq. (4.24).

The estimated M_o gives the value of M_w which is comparable with the catalogue magnitude of the earthquake. The plot of computed magnitude v/s catalogue magnitude shows a linear relationship, as shown in Fig. 6.19. There are 105 individual earthquake points (marked by cross) and 12 earthquake points which represent the average of the earthquakes having same magnitude (marked by solid diamond). For example, in the selected dataset, there are 18 earthquakes having magnitude 5 represented by cross and the average of these 18 earthquakes are represented by solid diamond in Fig. 6.19. The plots in Fig. 6.19 reveal that at short time window lengths of 1 sec, 2 sec, 3 sec and 4 sec large scattering at higher magnitudes have been observed, but at large windows this scattering gets reduced. To quantify the goodness of fit between the computed magnitude and the catalogue magnitude, residuals have been calculated at different window lengths. The residuals are defined as the difference between the computed and catalogue magnitudes. Residual and magnitude plots are shown in Fig. 6.20, at 1 sec window for magnitude 7.2 the residual is found to be -1.6, but at 5 sec it reduces to -0.06. Thus, by increasing window length higher precision in estimating magnitude of an earthquake is achieved.

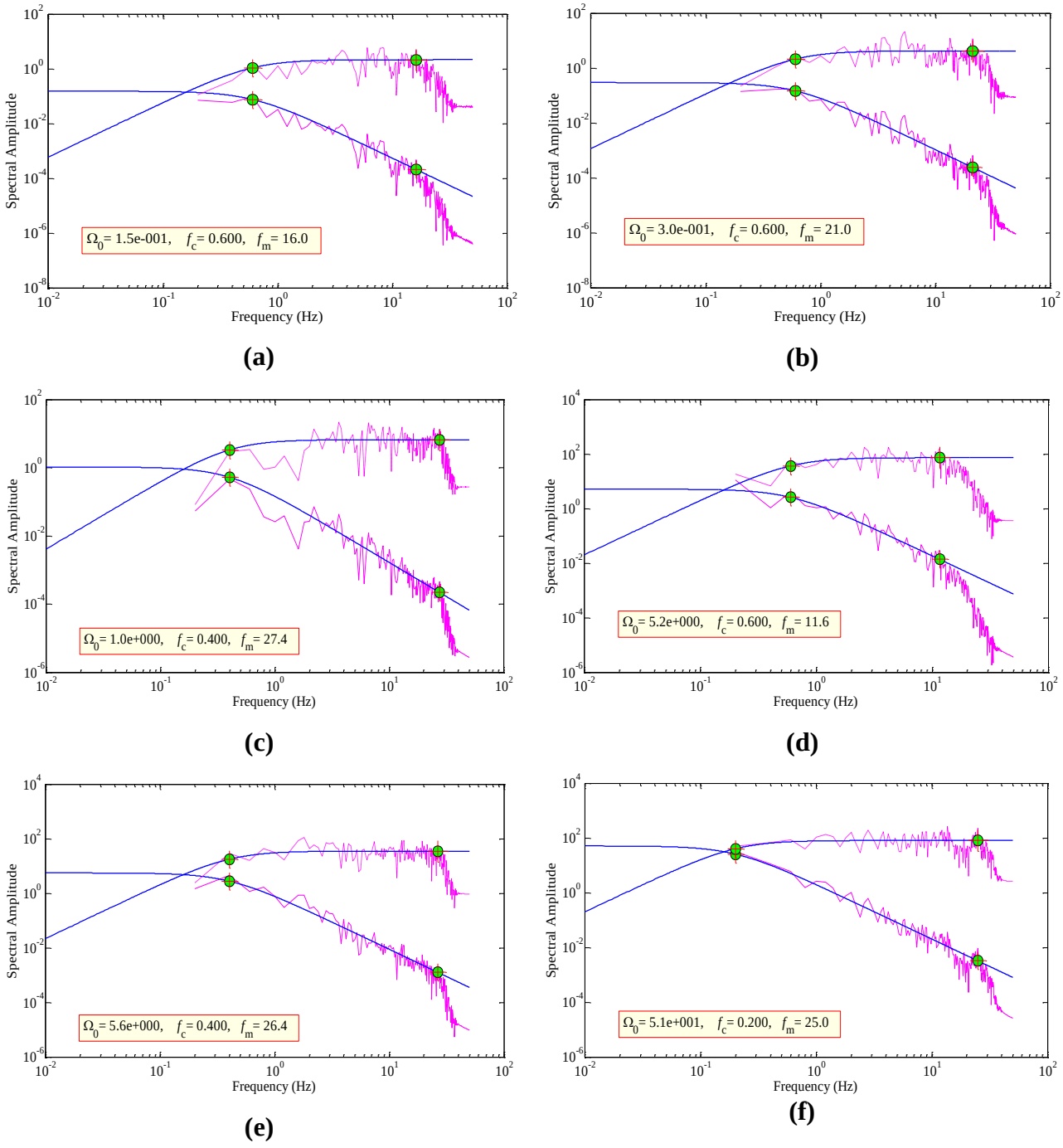

Figure 6.18 Source displacement (continuous curves) and acceleration (dashed curves) spectra fitted with theoretical Brune's spectra (continuous smooth lines represent Brune's displacement and acceleration spectra) for computation of spectral parameters (Ω_o, f_c and f_{max}) for different magnitudes (a) M = 5, (b) M = 5.5, (c) M = 6, (d) M = 6.5, (e) M = 7 and (f) M = 7.2. The encircle plus point represent the f_c and f_{max} position in spectra.

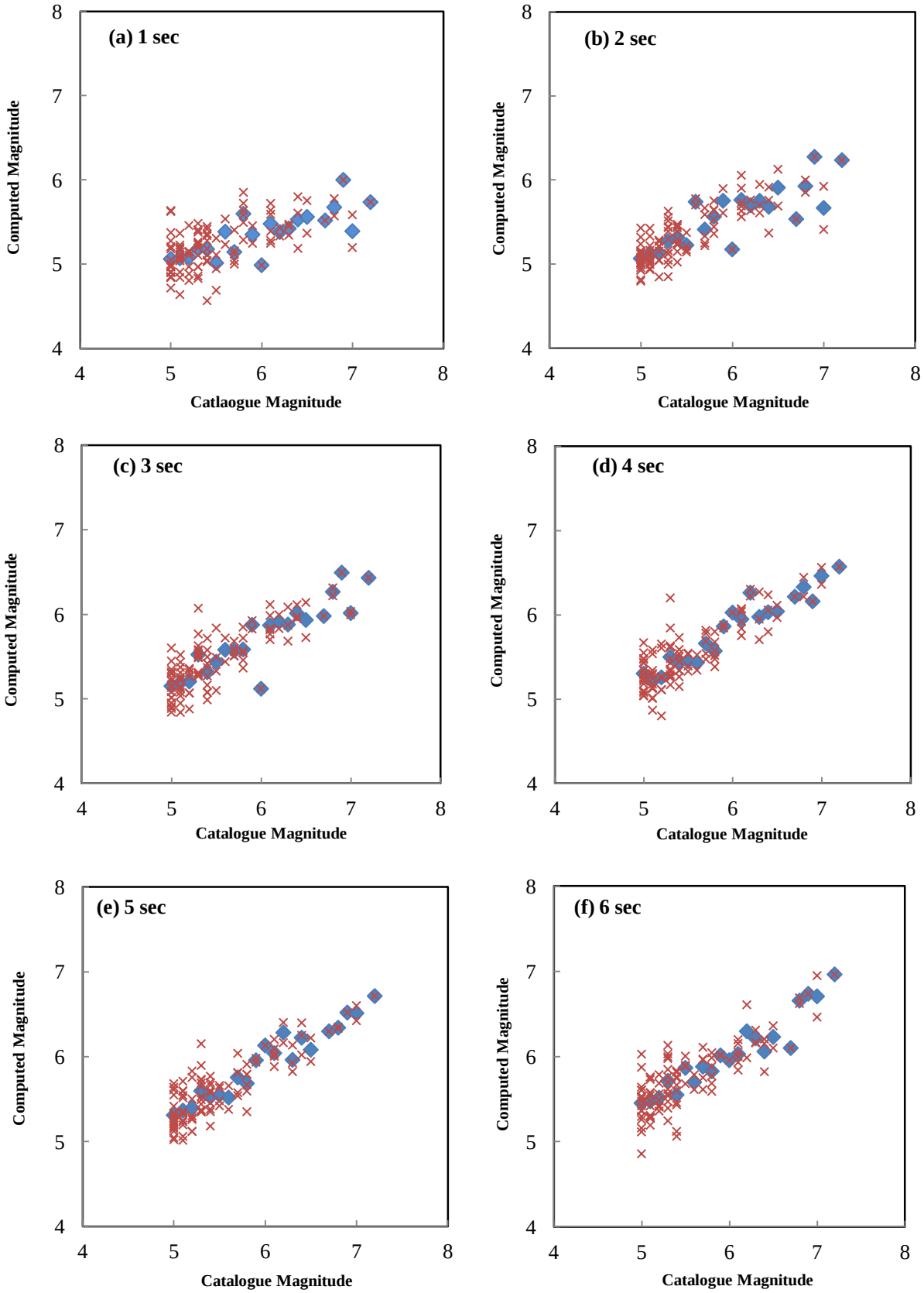

Figure 6.19 Linear relationships between the computed and catalogue magnitudes at different window lengths from 1 sec to 10 sec.

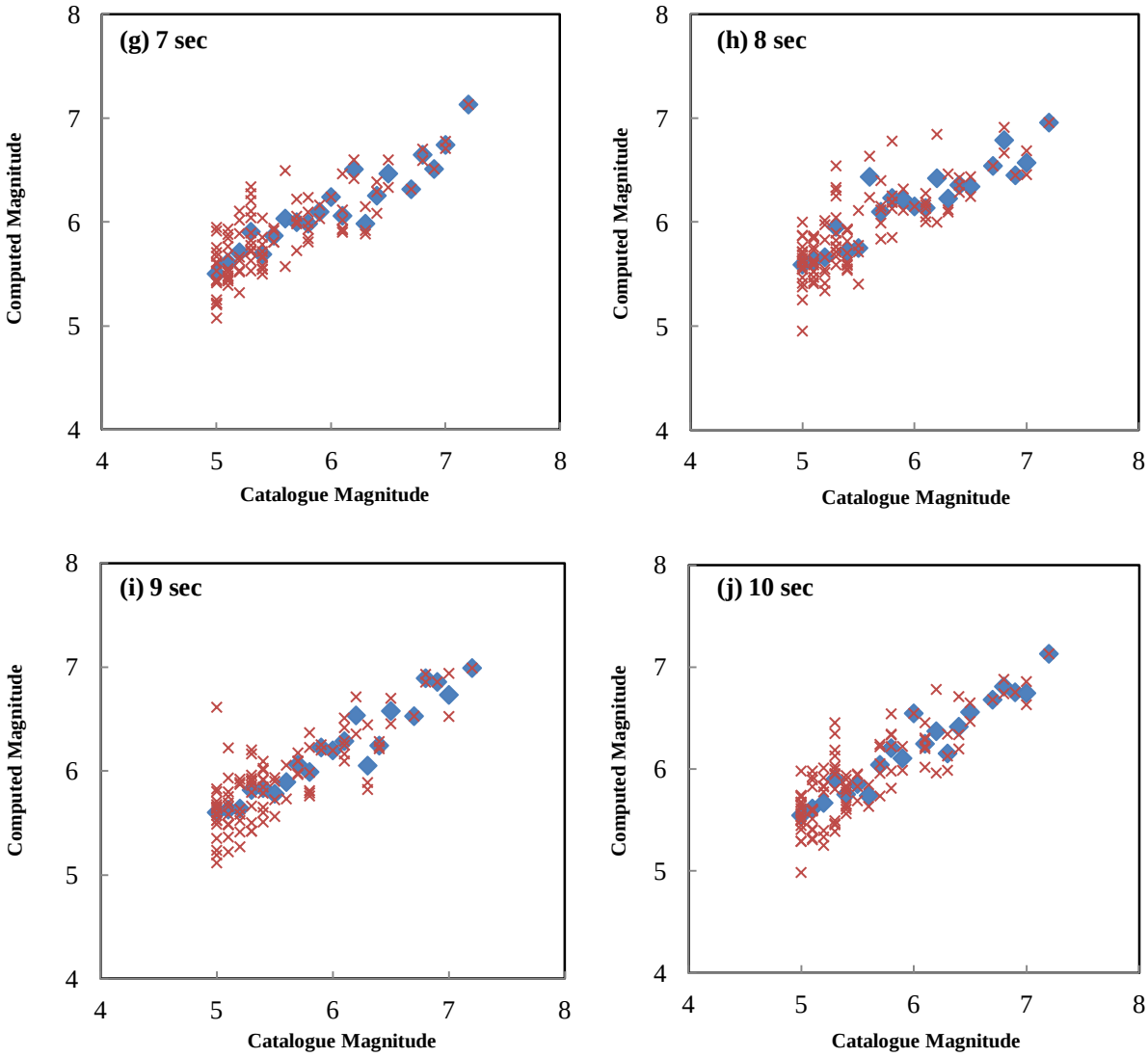

Figure 6.19 *(Continued)*

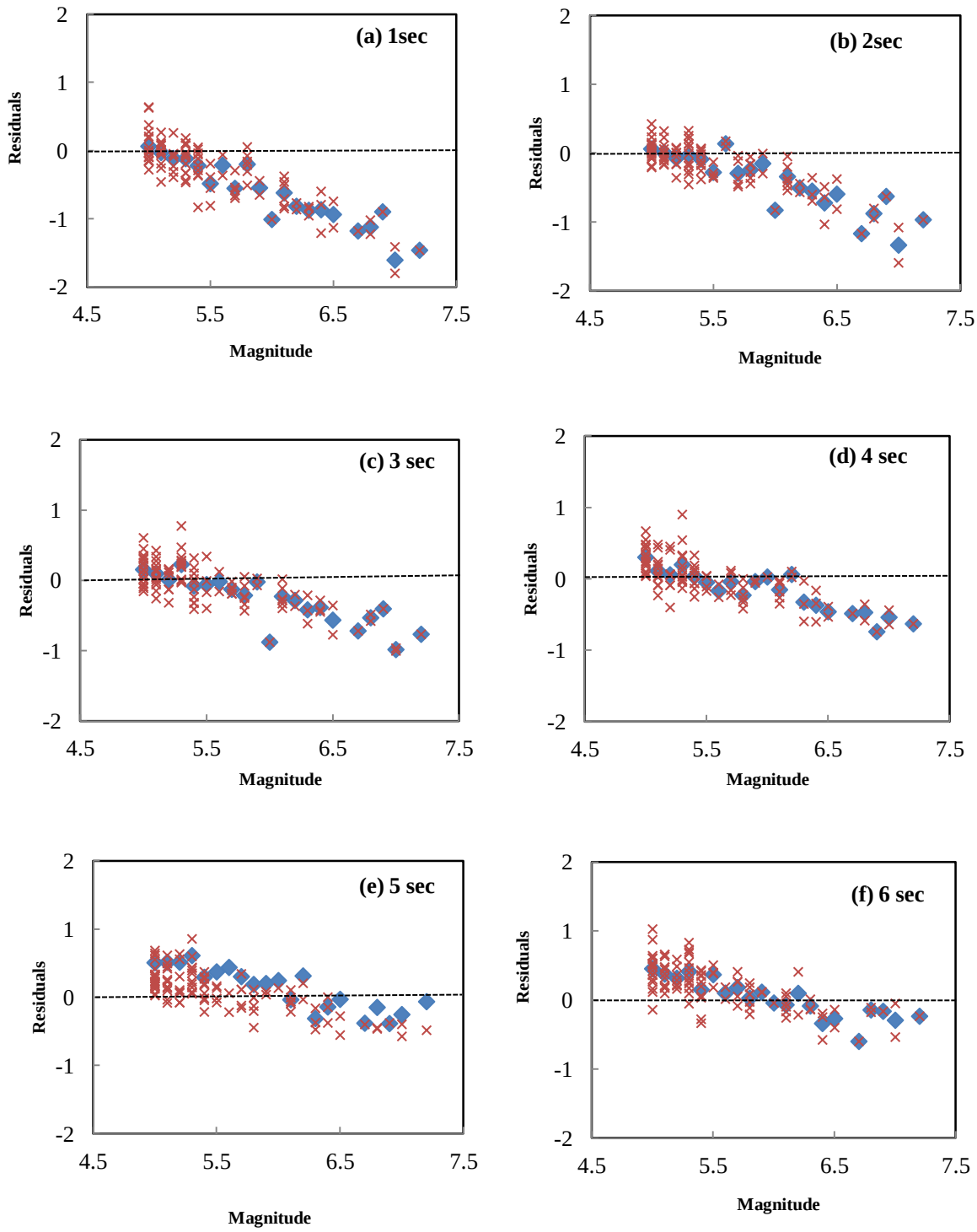

Figure 6.20 Residual v/s computed magnitude at different time windows from 1 sec to 10 sec.

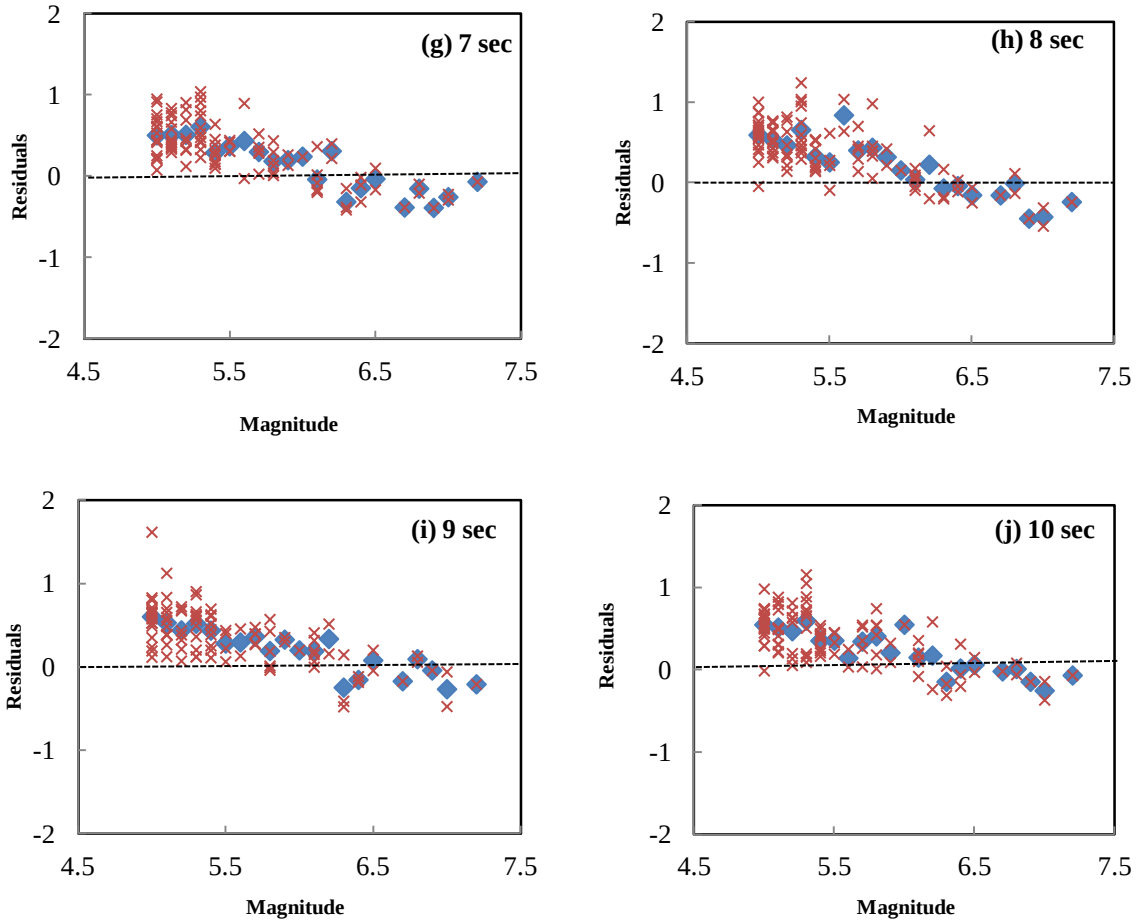

Figure 6.20 *(Continued)*

In case of EEW system there has been a tradeoff between accuracy and time. A way has to be adopted that provides reliable magnitude estimation in acceptable limits of time. On plotting the standard deviation between computed and catalogue magnitude, it has been found that at short window lengths of 1 sec, 2 sec, 3 sec and 4 sec standard deviation is much high, approximately 0.45 which starts decreasing after 4 sec and becomes 0.3 at 5 sec, thereafter it becomes almost constant for higher windows from 6 sec to 10 sec (Fig. 6.21). Mean of the differences between the computed and catalogue magnitudes at the selected time windows are shown in Fig. 6.22. In the present study, a close estimation of magnitude with an error of ±0.3 has been obtained. The mean difference becomes almost stable after 8 sec.

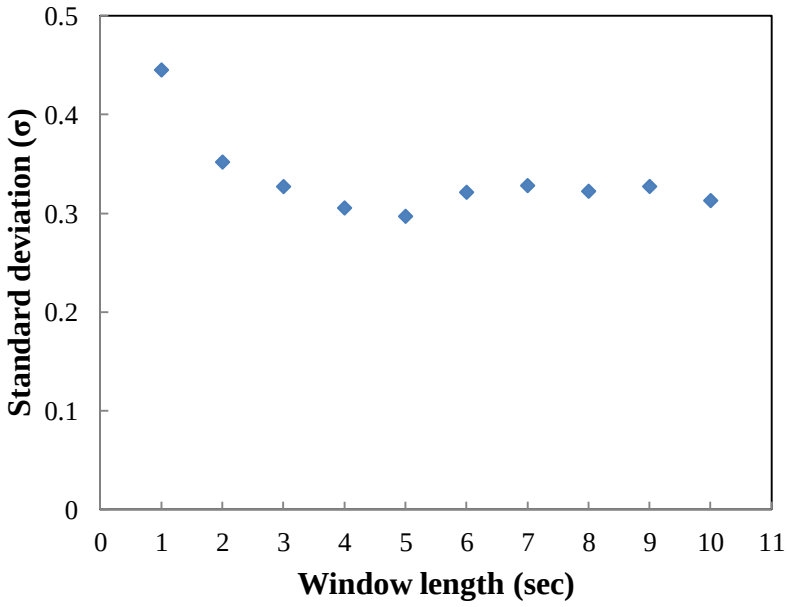

Figure 6.21 Standard deviation obtained at various window length. At 5 sec window minimum difference between computed and catalogue magnitude has been obtained.

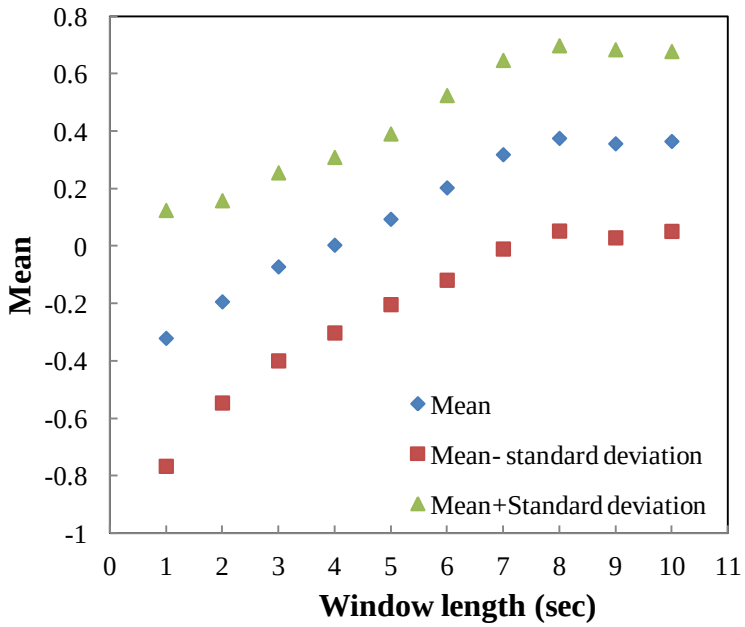

Figure 6.22 Mean of the differences between computed and catalogue magnitudes at different windows. Solid diamond represents the mean difference; solid rectangle and triangle represent the standard deviation from mean value at each time window.

The inaccuracy in terms of magnitude estimation is obvious for a larger earthquake with M ≥ 7 because its rupture time is more; the magnitude may be underestimated while the rupture is still in process (Doi 2011). Considerable uncertainties in magnitude

determination using the initial P-waves are inevitable, particularly for the large earthquakes.

The effectiveness in estimating the magnitude in EEW practice is however, supportive of the model proposed by Olson and Allen (2005) which states that the eventual size of an earthquake is mostly controlled by the initial stage of the rupture process (Wu et al. 2006). The analysis depends on earliest stage of an earthquake rupture process and also less affected by other scattering involves in other type of arrivals used in determining magnitude.

Results show that the magnitude obtained from a few initial P-wave portions agree with the well established catalogue magnitudes with an uncertainty of ± 0.3 magnitude units. The study uses variable length of time windows which results in a diversity of measurement of earthquake size (Fig. 6.19). Best results with minimum window length that can be used for magnitude estimation is 5 sec. After P-onset a time window of 5 sec may be selected for calculating the spectral parameters (Ω_o, f_c and f_{max}) by fitting Brune's model in the selected source spectra. These parameters are then used for estimating the magnitude of the earthquake. The estimated magnitude is found to be in good agreement with the catalogue magnitude with a minimum uncertainty which is due to the inherent error in M_w estimation (Das et al. 2011; Das 2013). Thus, present method is much useful in EEW systems.

6.6 EEW ALGORITHM AND MAGNITUDE ESTIMATION VALIDATION

The analyses of K-NET dataset in the earlier section of this chapter has revealed that most reliable performance of the EEW algorithm is obtainedby using three parameter preference based approach at 4 sec. Further, in case of magnitude estimation at 5 sec good magnitude estimation with small deviation from catalogue magnitude has been obtained. Thus, obtained final EEW algorithm is shown in Fig. 6.23. The proposed EEW algorithm starts initially with vertical component of time series pre-processing which includes baseline correction by fitting polynomial of 1st order and filtering of data by using fifth order high-pass Butterworth filter having cutoff frequency of 0.075 Hz. The P-onset is marked and EEW parameters: τ_p^{max}, τ_p, P_d, CAV and RSSCV are calculated at four nearest stations for a time window of 4 sec after P-onset. The calculated EEW parameters are then compared with their preset threshold values such as 1.1 sec, 1.42 sec, 0.95 cm, 23 cm/sec and 5.2 cm/sec, respectively. If the calculated parameter has value higher than the

corresponding threshold value an alarm status is set. The alarm for the event is issued only if three parameters out of five have alarm status.

Brune's model based magnitude estimation approach is used with selected time window of 5 sec for simultaneously estimating the magnitude of the event at all the triggered stations. After pre-processing cosine tapered window has been applied on the baseline corrected time series. Further, the windowed time series has been Fourier transformed to obtain velocity and displacement time series from acceleration time series. The source displacement and acceleration spectra are analyzed for calculating three spectral parameters namely Ω_o, f_c and f_{max} within 5 sec window to be used for calculating source parameter viz., M_o and in turn, M_w. The average of magnitudes estimated at various triggered stations give the final magnitude of the event. It may be noted that the magnitude estimated has been used as information only and it is not participating in issuance of alarm.

The developed EEW algorithm has been tested using Indian and PEER-NGA database for validating the proposed EEW algorithm and Brune's model based magnitude estimation approach. Indian and PEER-NGA database have been tested at specified threshold values and combination of parameters for validation of the developed algorithm. It may be noted that Indian and PEER-NGA database have been used to validate auto P-pick algorithm also.

6.6.1 Indian Dataset

Indian strong motion dataset comprised of 51 records of 28 earthquakes having magnitude range varying from 3.3 to 6.8 (as discussed Chapter 5). Out of 28 events there were 27 events having magnitude less than 6 for which no warning need to be issued. However, there has been a single event of magnitude 6.8 for which warning need to be issued.

At an epicentral distance of 60 km Indian strong motion dataset have small number of records available. On applying the proposed EEW algorithm for five different time windows the number of alarms obtained are shown in Table 6.26. It has been observed that in case of Indian dataset three EEW parameter preference based approach has found to be quite effective from 2 sec onwards.

It has been observed from Table 6.26 that at 1 sec the output has 1 (100%) CA, with 26 (96.3%) CAC, 0 (0%) MA and only 1 (3.7%) FA. Further, with the increase in time window the efficiency of the algorithm has been found to be 100%.

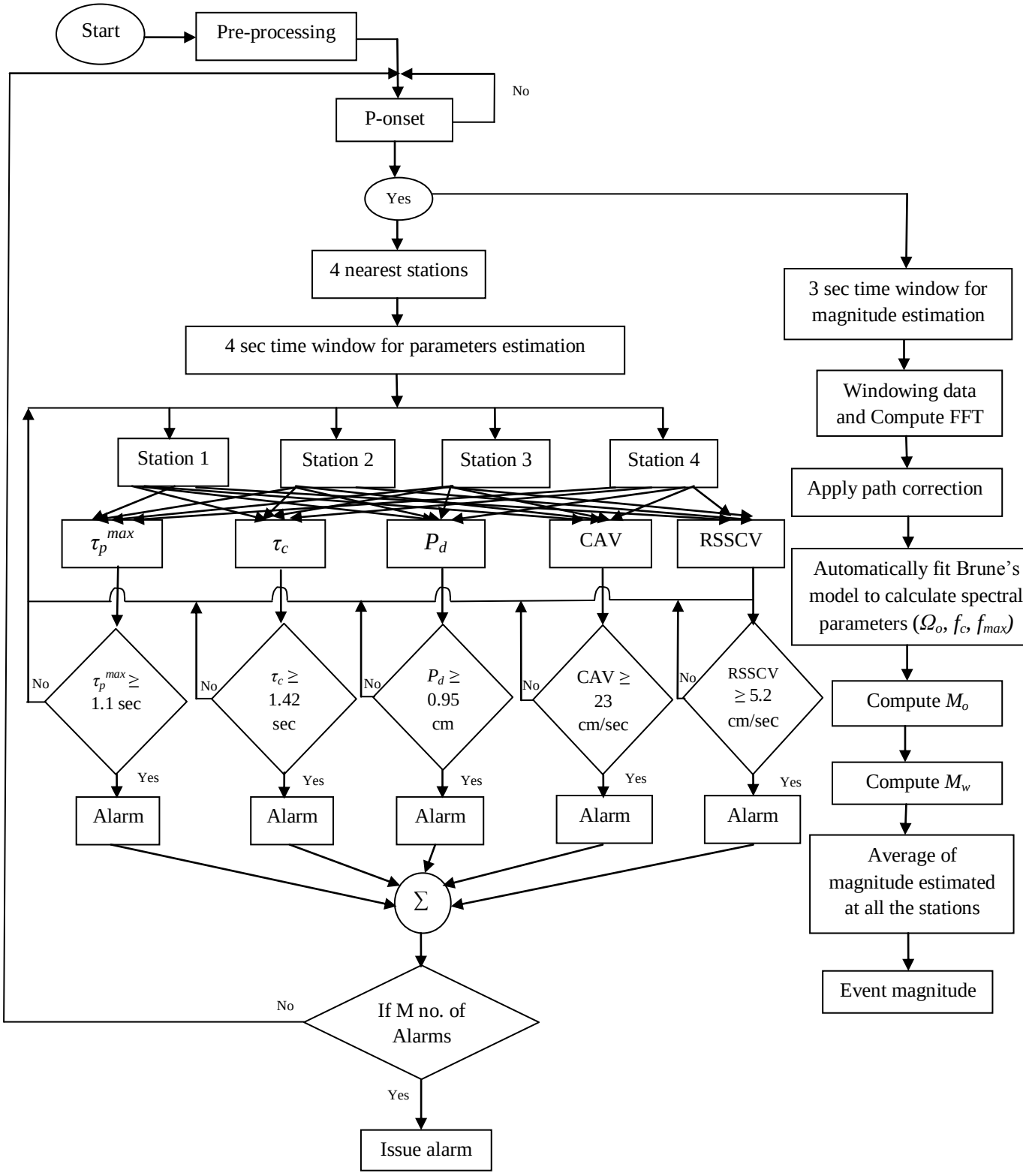

Figure 6.23 Proposed EEW algorithm, using three parameter preference based approach at 4 sec time window for issuance of warning. τ_p^{max}, τ_c, P_d, CAV and RSSCV parameters are used in the warning analysis. Brune's model based magnitude estimation approach is used for simultaneously estimating the magnitude of the event within a time window of 5 sec.

Table 6.26 Number and percentage of CA and MA obtained from an event having M ≥ 6, while CAC and FA obtained from 27 events having M < 6, using a three EEW parameter preference based approach.

Time	**CA**		**MA**		**CAC**		**FA**	
window	Numbers	%	Numbers	%	Numbers	%	Numbers	%
1 sec	1	100%	0	0%	26	96.3%	1	3.7%
2 sec	1	100%	0	0%	27	100%	0	0%
3 sec	1	100%	0	0%	27	100%	0	0%
4 sec	1	100%	0	0%	27	100%	0	0%
5 sec	1	100%	0	0%	27	100%	0	0%

The algorithm has also been explained in terms of numbers of CD and ICA in Fig. 6.24. At 1 sec, 27 events have been correctly detected with only one incorrect alarm. The results showed that the Indian dataset is in strong agreement with proposed three parameter preference based approach at 4 sec.

The magnitude estimation algorithm based on Brune's model approach has been applied on Indian strong motion dataset. The results of K-NET algorithm proposed that by using 5 sec time window after P-onset results in best magnitude estimation. Thus, the Indian dataset has been tested at 5 sec time window and the results obtained have been shown in Fig. 6.25. There are 31 individual earthquake points (marked by cross) and 19 earthquake points which represents the average of the earthquakes having same magnitude (marked by solid diamond). Less number of records have been considered in magnitude estimation due to filtration of records involved at different stages of magnitude estimation as records with $f_c = f_{max}$ are not considered.

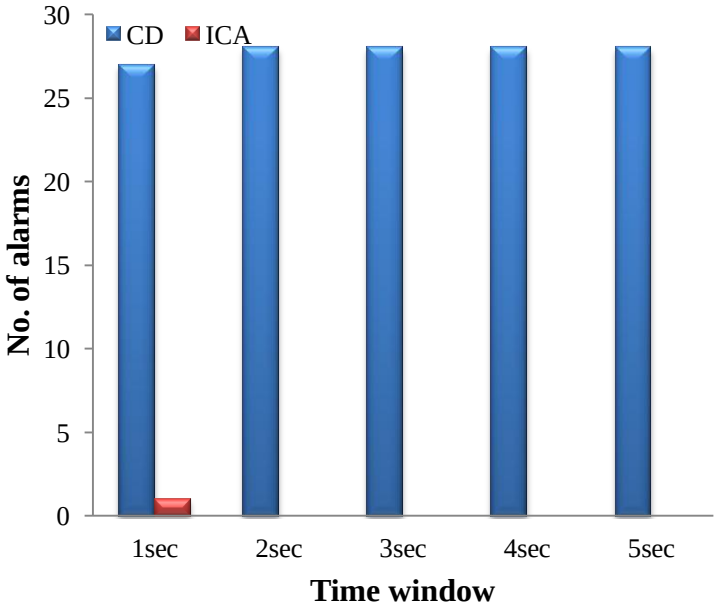

Figure 6.24 Number of CD and ICA obtained from total 28 Indian events at different time window using a three EEW parameter preference based approach.

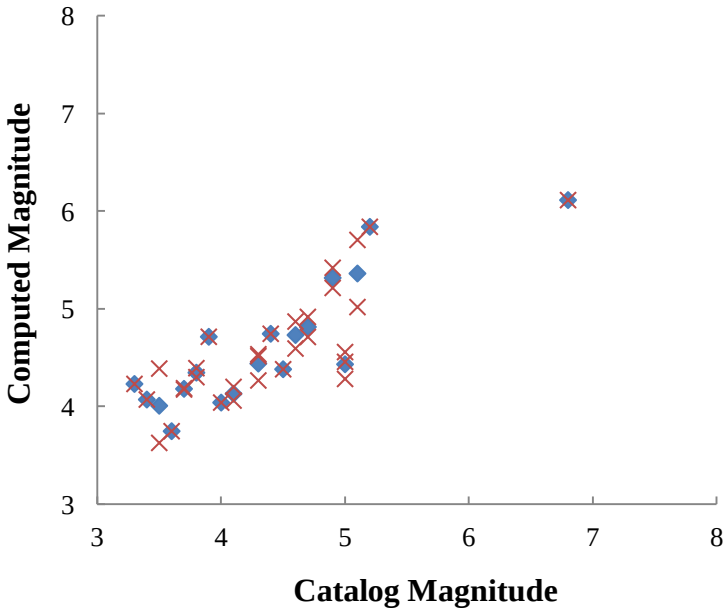

Figure 6.25 Linear relationships between the computed and catalogue magnitudes of Indian dataset at a selected time window of 5 sec with cross representing individual earthquake point and diamond represents average of the earthquakes having same magnitude.

From Fig. 6.26, the high value of residuals obtained at 5 sec time window shows that the deficiency of more records for an event provides poor average estimation and results in high scattering of the data points.

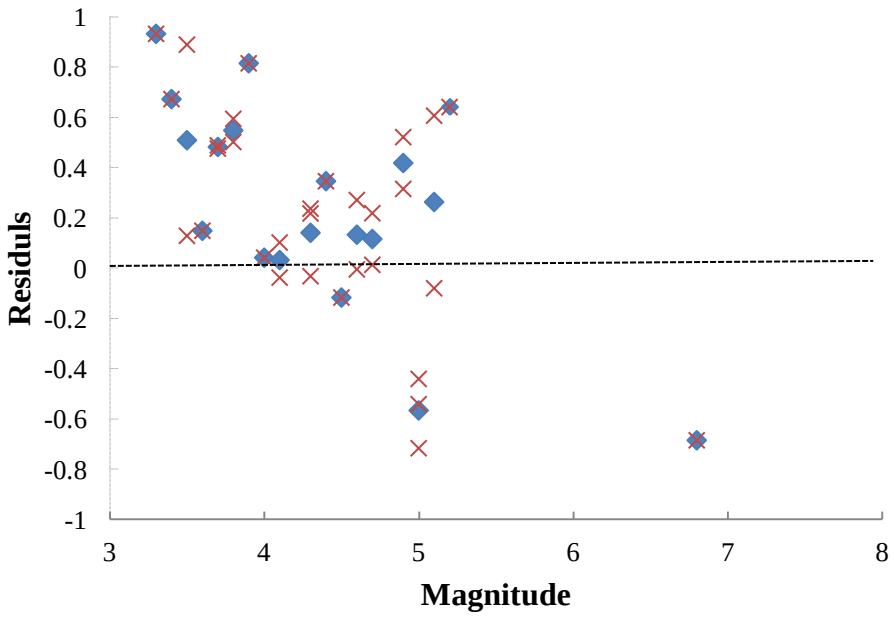

Figure 6.26 Plots of residual v/s computed magnitude at 5 sec using Indian dataset. Cross representing individual earthquake residual point and diamond represents average of residuals for the earthquakes having same magnitude.

6.6.2 PEER-NGA Dataset

The PEER–NGA dataset which consist of strong ground motion records of various countries for e.g., South California, Turkey and Taiwan (see chapter 5). There were total of 219 records of 14 earthquakes having magnitude range of 4.27 to 7.62 up to 60 km epicentral distance. In 14 events, there are equal numbers of events, i.e., 7 each, for which warning need to be issued ($M \geq 6$) and not to be issued ($M < 6$).

On applying the three parameter preference based approach on PEER-NGA database at different time windows, four different types of alarms have been estimated. The CA and MA have been calculated from 7 events with $M \geq 6$. Further, CAC and FA have been calculated from other 7 event having $M < 6$. In Table 6.27, the performance of algorithm is found to be consistently increasing with addition of each second in the considered data. At 3 sec and 4 sec, similar results have been obtained but at 5 sec further improvement in CA and MA rate took place.

Table 6.27 List of number and percentage of CA and MA obtained from 7 events having M ≥ 6, while CAC and FA obtained from 7 events having M < 6, using a three EEW parameter preference based approach. The addition of each second of data makes the algorithm more accurate.

Time	**CA**		**MA**		**CAC**		**FA**	
window	Numbers	%	Numbers	%	Numbers	%	Numbers	%
1 sec	5	71.43%	2	28.57%	4	57.14%	3	42.86%
2 sec	5	71.43%	2	28.57%	5	71.43%	2	28.57%
3 sec	6	85.71%	1	14.29%	7	100.00%	0	0.00%
4 sec	6	85.71%	1	14.29%	7	100.00%	0	0.00%
5 sec	7	100.00%	0	0.00%	7	100.00%	0	0.00%

Table 6.27 represents that at 1 sec the percentage of CA is 71.43 % which becomes 100% at 5 sec similar trend has been observed in case of CAC where at 1 sec the percentage of correct alarm has found to be 57.14% and becomes 100% at 5 sec. However, the continuous reduction in percentage of MA and FA with each additional second of time shows dependence of the proposed algorithm with time windows. Three EEW parameter preference based approach has found to be quite effective from 3 sec onwards in case of PEER-NGA database.

The algorithm has been explained in terms of number of CD and ICA in Fig. 6.27. At 1 sec, there are 9 events which are correctly detected, while 5 events are wrongly interpreted. At 2 sec, the rate of CD increases from 9 to 10 and one point drop in wrong estimation is observed. At 3 sec and 4 sec, similar numbers of CA and ICA alarms are obtained. However, at 5 sec, the three parameter preference based algorithm achieves its maximum efficiency with 14 CA and none ICA. At calculated specification of three parameter preference based approach and at time window of 4 sec, the algorithm got noticeable efficiency and thus, validation using PEER-NGA database has been achieved.

The magnitude estimation algorithm based on Brune's model approach has been applied on PEER-NGA database for validation. PEER-NGA database has been tested for 5 sec time window and the results obtained have been shown in Fig. 6.28. There are 219 individual earthquake points (marked by cross) and 14 earthquake points which represents the average of the earthquakes having same magnitude (marked by solid diamond). The linear relation between observed and catalogue magnitude shows that at 5 sec magnitude estimation algorithm has good efficiency. On comparing the PEER-NGA database results

with Indian database it has been observed that PEER-NGA database provides better linear dependence between observed and catalogue magnitude than Indian dataset.

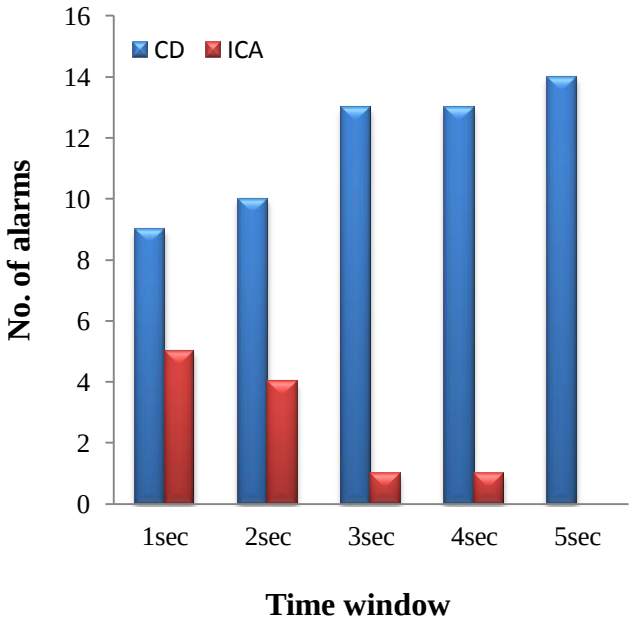

Figure 6.27 Number of CD and ICA obtained from total 14 events at different time window using a three EEW parameter preference based approach.

Fig. 6.29 quantifies the goodness of fit between the computed and the catalogue magnitude. The residuals were computed at 5 sec, time window and have been plotted with magnitude. At 5 sec window the residual at magnitude 7.6 is found to be -0.48. Small scattering has been observed at residuals value for small magnitude $M < 6$, but for higher magnitude earthquakes scattering is slightly high.

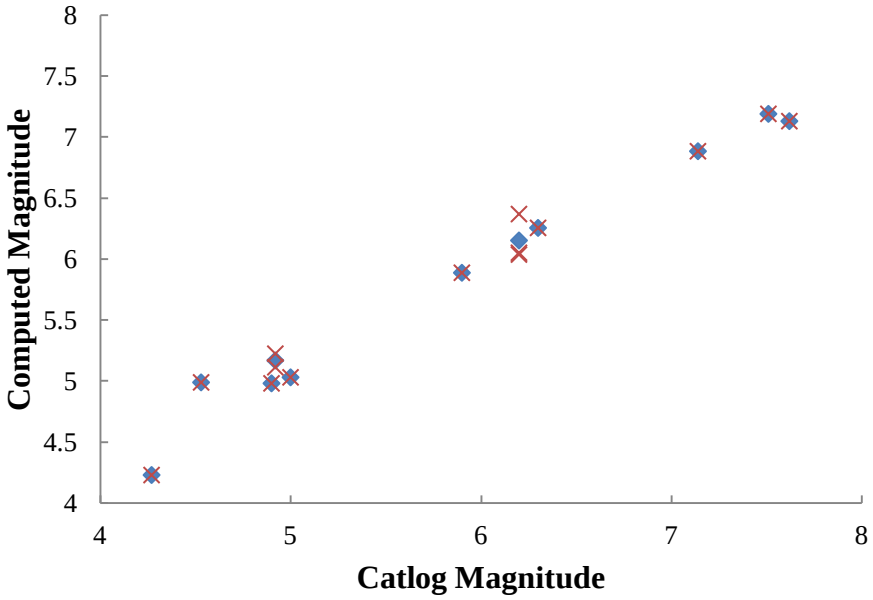

Figure 6.28 Linear relationships between the computed and catalogue magnitudes of PEER-NGA database at a selected time window of 5 sec with cross representing individual earthquake point and diamond represents average of the earthquakes having same magnitude.

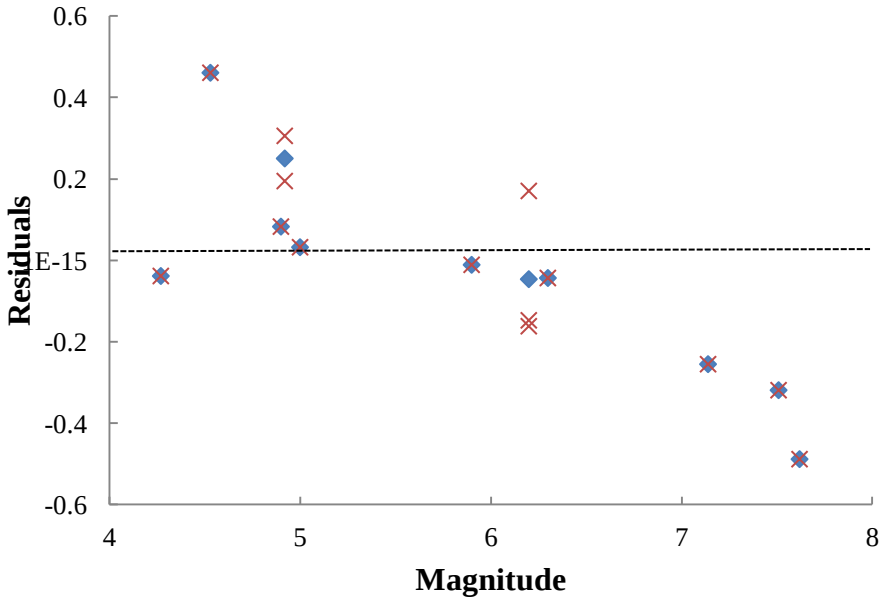

Figure 6.29 Plots of residual v/s computed magnitude at 5 sec using PEER-NGA database. Cross representing individual earthquake residual point and diamond represents average of residuals for the earthquakes having same magnitude.

6.7 SUMMARY

The chapter describes the results obtained from three different components of EEW algorithms. The first component of the algorithm deals with the auto P-pick which is RSSCV parameter based algorithm. The algorithm has been tested on K-NET 1726 earthquake records of 105 events and compared with Allen's 1978 auto P-pick algorithm.

In the second component of EEW algorithm, thresholds for issuing warning and different possible combinations of EEW parameters (τ_p^{max}, τ_c, P_d, CAV and RSSCV) have been computed and described for fast and reliable warning. EEW parameters were calculated at different stations and the regression between the average EEW parameters value for an event and magnitude have been calculated for different time windows. The analysis has been carried out at nearest four stations of an event. The warning has been issued, when out of four at least three nearest stations crosses the preset threshold level for an event. The warning has been classified in four different alarm types as Correct Alarm (CA), Missed Alarm (MA), Correct All Clear (CAC) and False Alarm (FA). Further alarm classification has been based on two types: Correct Detection (CD) and Incorrect Alarm (ICA). Based on the accurate, reliable and fast warning estimation results, the best possible combination of EEW parameter has been selected i.e., three parameter preference based approach at a time window of 4 sec. Based on performance of EEW parameters at different magnitude range, the ranking of EEW parameters is also done.

Further, in the third component of EEW algorithm Brune's model has been fitted in the initial part of P-wave at different time windows for more accurate magnitude estimation. The magnitude estimation approach based on Brune's model concludes that at a time window of 5 sec difference between observed and catalogue magnitude found to acceptably small with reliable accuracy.

The EEW algorithm for the purpose of validation has been applied on Indian and PEER-NGA database. The results obtained after analysis showed that the proposed EEW algorithm is quite reliable and accurate.

CHAPTER 7

EEW FOR NORTHERN INDIA

7.1 INTRODUCTION

The need of seismic risk mitigation technique like EEW system in seismically active regions has been established in Chapter 2 and 3 along with the methodology for EEW system described in Chapter 4. The requisite EEW parameters have been obtained using a relatively richer data set from K-NET and have been tested against the data set from Indian region. In this work, the auto P-pick algorithm, thresholds for issuing warning for potential damaging earthquake using different combination of EEW parameters at different time windows (1 sec to 5 sec) and estimation of magnitude after P-onset has been done. Further, for implementing the EEW algorithm in India, an EEW system for Northern India has been discussed in this chapter. It may be mentioned that in Northern India, potential sources of big earthquakes are located in Himalayas, whereas centers of population are few hundred kilometers away from the sources. This distance gives the centers of population, a lead time of few tens of seconds before the damaging S-wave arrive. Lead time for six cities of Northern India has been calculated on the basis of proposed EEW algorithm. Further, a lead time varying from few seconds to 1.5 minutes has been achieved for the considered cities.

7.2 NEED OF EEW IN INDIA

Economic and human losses due to natural calamities have increased exponentially worldwide and little progress has been made in reducing their rate of fatalities, this also holds for earthquake damages and is mainly due to increasing population and industrial density in high hazard and vulnerable areas. In addition to possibility of saving life, seismic early warning becomes increasingly relevant for technical infrastructure such as transportation lines (trains and airlines), gas pipelines, heavy machines, computers and nuclear power plants to avoid different hazards. If real-time seismological information becomes adequately tuned to the operational requirements of technical systems, losses can be significantly reduced.

Possibility of getting maximum advantage of EEW system in Northern India is very high due to the fact that for northern India, potential source of earthquakes are located in Himalayas, whereas centers of large population as well as big industrial hubs (including our capital Delhi) are in plains adjoining Himalayas. In Delhi itself with more than 15 million inhabitants, lies approximately 200 km from MBT and 300km from MCT, the two most active thrust planes of the Himalayas. In view of above, development of EEW can be very beneficial for northern India in large.

Delhi, the capital city of India, is situated approximately 300 km (186 miles) away from the Himalayas. Many studies have been carried out to predict strong motion in Delhi (Iyengar 2000; Parvez et al 2002; Sharma et al 2003; Sharma and Dimri 2003; Sharma and Arora 2005; Joshi and Sharma 2011a, 2011b). Singh et al. (2002) has calculated the values of PGA in Delhi for probable magnitude M 8 and M 8.5 earthquakes to be 96-140 cm/sec^2 and 174-218 cm/sec^2, respectively. Sharma et al. (2003), proposed a maximum PGA of 0.34g for Delhi. Further, Mittal et al. (2012b, 2013) provided more extensive coverage by estimating ground motion at 55 sites in Delhi for three regional and one local event. It has also been highlighted that during the earthquake the amplification may go up at certain pockets, large scale liquefaction may take place and East of Yamuna may prove to be most vulnerable area in Delhi. Delhi being the socio-political and economic nerve centre of the country it demands much more attention from the angle of disaster preparedness such as EEW system.

7.3 PROPOSED AREA FOR EEW INSTRUMENTATION

From the seismicity study of India in chapter 2, it has been concluded that in past several catastrophic events originated in Himalayas namely 1897 Shilong (M 8.7), 1905 Kangra (M 8.6), 1934 Bihar (M 8.4), 1950 Assam (M 8.7), 1991 Uttarkashi (M 6.8), 1999 Chamoli (M 6.4) and 2005 Muzaffarabad (M 7.6) adversely affected several cities in Northern India. Also, based on the past and the contemporary seismicity reported from Garhwal Himalaya region, prevalent earthquake occurrence models, plate motions and presently going on deformations in the region, presence of reported locked faults and the cities falling in the vicinity of this active region, the region between MCT and MBT has been considered as a cluster region for any seismogenic source zone in near future earthquake activity. Thus, a committee of seismologists constituted by *Ministry of Earth Science (MoES)*, the Government of India identified an area of about 100 km in length and

about 50 km wide in Uttarakhand region near MCT for EEW instrumentation as shown in Fig. 7.1 (Personal communication with Prof. Ashok Kumar, Principal Investigator, Earthquake Early Warning Project funded by MoES). An array of 100 EEW stations as shown in Fig. 7.1 has been suggested to be installed in this region. EEW instrumentation array will cover Uttarkashi, Chamoli, Rudraprayag and Tehri Garhwal regions of the Himalayas for providing EEW to cities such as Dehradun, Roorkee, Hardwar, Saharanpur, Muzaffarnagar, Meerut, Baghpat, Ghazizbad, Gautam Buddha nagar and Delhi having high population density as listed in Table 7.1. By summing the total population of Uttarkashi, Chamoli, Rudraprayag and Tehri Garhwal districts and dividing it with instrumentation area the population density per km^2 in the instrumentation area comes out to be 315 per km^2 which is much smaller than population density in individual benefited cities. From Table 7.1 it has been observed that in Delhi which is the central unit of India, if hit by an earthquake of around M 8, effect 11289 lives per km^2.

Table 7.1 List of cities included for EEW system instrumentation and for issuing warning with their population, area and population density information according to census 2011.

Cities	**Population**	**Area (km^2)**	**Population density (per km^2)**	
Uttarkashi	329686	7951	41	EEW Instrume-ntation
Chamoli	391114	7692	51	
Rudraprayag	236857	1896	125	
Tehri Garhwal	616409	4085	151	
Roorkee	118188	33	3581	Benefited cities
Dehradun	1698560	3088	550	
Hardwar	1927029	2360	817	
Saharanpur	3464228	3689	939	
Muzaffarnagar	4138605	4008	1033	
Meerut	3447405	2522	1367	
Baghpat	1302156	1345	968	
Ghaziabad	4661452	1175	3967	
Gautam Buddha Nagar	1674714	1269	1320	
Delhi	16753235	1484	11289	

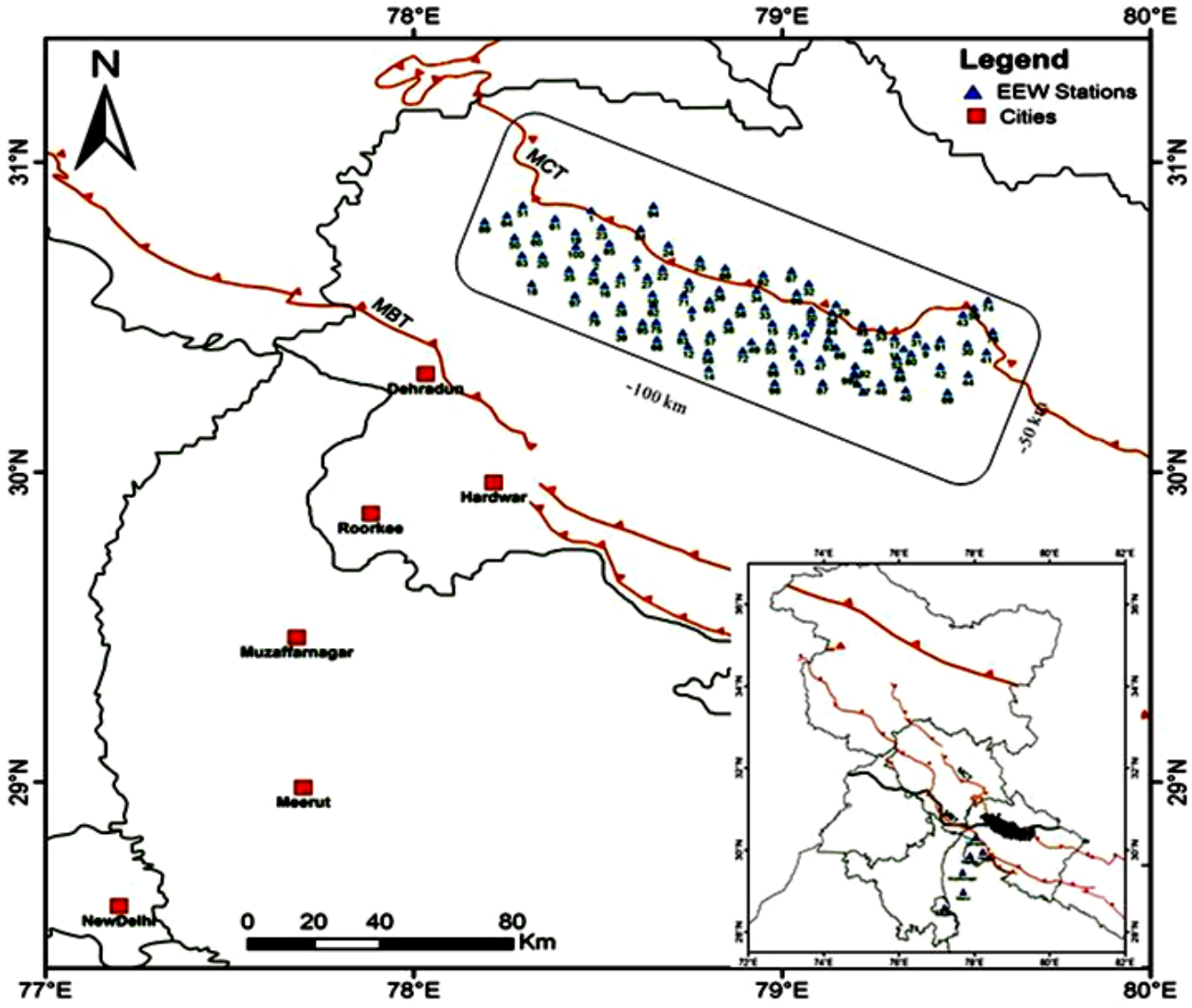

Figure 7.1 Proposed EEW instrumentation network in Uttarakhand region of Himalayas covering an area of around 5000 km^2. EEW stations marked with blue triangles and the benefited cities for which EEW will be issued are marked with solid red squares.

7.4 STEPS FOR EEW SYSTEM

For implementation of an EEW system in Northern India following steps need to be followed:

1. A dense network of sensors will be required in the vicinity of Himalayas with few km of inter station spacing (~20 km). At sensors auto P-pick algorithm like Allen (1978) or RSSCV based algorithm may be used. The sensors may stream real-time acceleration time history and also determine EEW attributes at the sensor end within few seconds after P-onset. The calculated parameters should be transmitted to the *Central Processing Center* (CPC) which may be located at Roorkee, for EEW decision. At CPC,

the developed EEW algorithm will be applied in a logical manner by using EEW parameters calculated from nearest four stations for issuing regional warning. Using electronic transmission medium, the warning can be transmitted to target site (see Fig. 7.2).

2. A network of 100 stations with EEW sensors around MCT in Uttarakhand (within about 300 km from Delhi) has been proposed (Fig. 7.1). By doing so, the nearest sensor will be within less than 20 km from epicenter of earthquakes originating from the selected area of interest. Locations of the stations are chosen by carefully inspecting the map and selecting a place which should have road connectivity. The instrument is proposed to be installed at safe places like government buildings for proper maintenance and power supply. Fig. 7.1 shows locations of all the 100 stations on topographic map of the region taken from Indian map.

3. Transmission of data from each field station to a central station in real time will be done with least possible delay. Speed of transmission of data from large number of field sensors to CPC is very crucial, as each second of delay in transmission will mean about 3 km increase of blind zone. There can be several options for transmission of data. In Taiwan, dedicated leased lines between sensors and the processing centre are in use, whereas in Japan, dedicated satellite channels are used. V-SAT connection could be used at each location for transmission of data in real time as shown in Fig. 7.2.

4. Next step is to receive and process the massive data in real time and take decision on issuing of alarm/warning. For this, there is requirement of large scale computational facility with sufficient backup systems to receive huge amount of real time streamed data. Developed EEW algorithm based software will then be applied on the received data. A schematic diagram showing flow of data is shown in Fig. 7.2.

5. Based on the developed algorithm protocol to issue alarm needs to be decided. It has been proposed that whenever four nearest stations reports the onset of an event and EEW parameters (τ_p^{max}, τ_c, P_d, CAV and RSSCV) value at any three stations out of the four crosses the preset threshold values an alarm needs to be issued. The algorithm is so designed that alarm gets updated every second after P-onset and at 4 sec it provides reliable level of alarms and at 5 sec estimation of magnitude of event can be made efficiently.

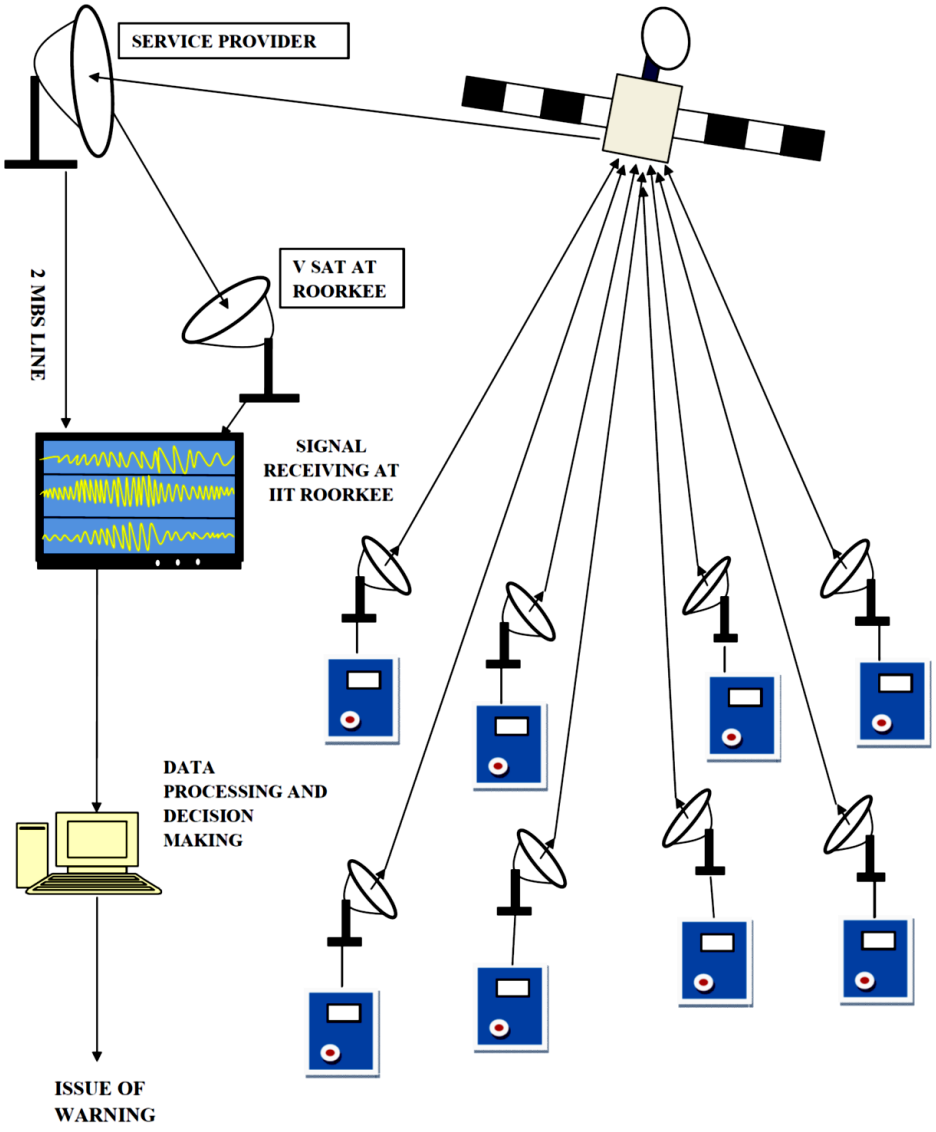

Figure 7.2 Proposed EEW network connectivity and data flow (after personal communication with Prof. Ashok Kumar, principal investigator, EEW project funded by MoES).

7.5 LEAD TIME CALCULATION FOR CITIES IN NORTHERN INDIA

Till now, in the present chapter the need of EEW system in India has been discussed. Further, the instrumentation and steps for designing EEW system have been explained. Now, the lead time for various cities such as Roorkee, Dehradun, Hardwar, Saharanpur, Muzaffarnagar, Meerut, Baghpat, Ghazizbad, Gautam Buddha Nagar and Delhi need to be calculated.

Lead time is defined as the time difference between S-wave arrivals at the user site and first P-wave arrival at the seismic network in addition with the transmission delay and

the time consumed in various processing (detection of P-onset, calculation of various EEW parameters, decision to issue an alarm for a potentially damaging earthquake). Fig. 7.3 represents how the lead time is calculated in case for a regional warning approach.

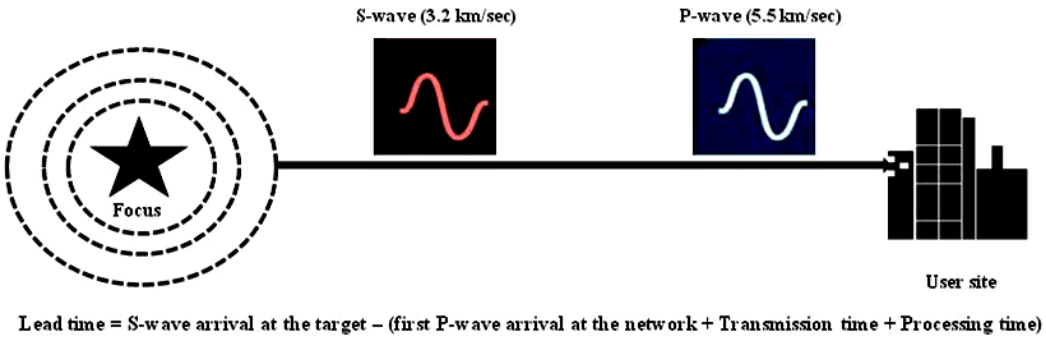

Figure 7.3 Difference in velocity of P and S-wave used for lead time calculation.

The time taken by S-wave to reach a particular place will be time available to act or to give warning. Keeping in view, the developed EEW algorithm takes 4 sec to compute EEW parameters and to make decision about the alarm with 1 sec of transmission delay and 1 sec of processing delay. Thus, the lead time is calculated as follows:

Lead time = (S-wave arrival at the target city) - (P-wave arrival at the farthest of 4 nearest EEW station +4 sec (EEW algorithm) + 1 sec (Transmission delay) + 1 sec (Processing delay)) (7.1)

In the present study, lead time has been calculated for six main cities of Northern India namely, Dehradun, Hardwar, Roorkee, Muzaffarnagar, Meerut and Delhi. The array of 100 stations with EEW sensors has been considered as the epicenter of 100 earthquakes having focal depth of 15 km originated in the selected seismic network region. The lead time for the six selected cities has been calculated for each earthquake by considering P-arrival at farthest of the nearest four stations and S-arrival at the cities along with decision time, transmission and processing delay. The P-wave and S-wave velocities considered are 5.5 km/sec and 3.2 km/sec, respectively. For example, for earthquake number 1 the nearest four stations are: 1st station itself, 23rd station, 19th station and 61th station, respectively, with corresponding hypocentral distances such as 15 km, 16.42 km, 17.29 km and 17.91 km as shown in Table 7.2. After the search of nearest four stations with their hypocentral distance calculation has been done, the longest P-arrival time at the four nearest stations

has been considered for calculating P-arrival time at the seismic network. Further, by using Heaversine formula distance between the event and the city has been determined and the time taken by the destructive S-wave to reach the particular city has been calculated. The calculated P-arrival and S-arrival time along with 4 sec of EEW algorithm decision time, 1 sec of transmission delay and 1 sec of processing delay provides the lead time for the cities by using Eq. (7.1). The lead time for each city has been calculated and listed in Table 7.3.

Table 7.2 List of 100 earthquakes (EQ) with distribution of four nearest stations and their corresponding hypocentral distance.

EQ No.	1st nearest Station	Hypo dist. 1st nearest Station	2nd nearest Station	Hypo dist. 2nd nearest Station	3rd nearest Station	Hypo dist. 3rd Station	4th nearest Station	Hypo dist. 4th nearest Station
1	1	15	23	16.42	19	17.39	61	17.91
2	2	15	26	15.94	85	16.27	100	16.48
3	3	15	27	16.46	21	16.66	22	16.72
4	4	15	73	15.46	7	15.56	6	16.27
5	5	15	65	16.02	71	16.06	83	17.28
6	6	15	13	15.96	55	16.25	4	16.27
7	7	15	4	15.56	70	15.68	73	15.8
8	8	15	99	15.03	77	15.32	92	15.39
9	9	15	91	15.67	80	15.71	31	15.74
10	10	15	62	15.5	27	16.25	71	17.07
11	11	15	80	15.23	52	15.42	17	15.71
12	12	15	83	15.84	58	15.98	57	16.67
13	13	15	6	15.96	47	16.07	98	16.45
14	14	15	58	16.16	12	17.88	72	18.6
15	15	15	73	16.05	33	16.15	55	16.51
16	16	15	26	15.94	21	15.98	28	17.02
17	17	15	53	15.7	11	15.71	31	16.1
18	18	15	20	18.26	63	18.33	35	18.61
19	19	15	100	15.85	23	16.55	61	16.63
20	20	15	63	15.93	60	16.92	35	17.21
21	21	15	16	15.98	27	16.51	26	16.62
22	22	15	27	15.84	3	16.72	37	17.15
23	23	15	85	16.16	1	16.42	19	16.55
24	24	15	22	17.22	81	17.6	3	17.84
25	25	15	66	16.68	37	17.24	24	17.85
26	26	15	16	15.94	2	15.94	35	16.33
27	27	15	22	15.84	10	16.25	3	16.46
28	28	15	79	16.93	16	17.02	62	17.21
29	29	15	54	15.31	70	16.47	84	16.55
30	30	15	41	16.07	91	16.63	78	16.99

EQ No.	1st nearest Station	Hypo dist. 1st nearest Station	2nd nearest Station	Hypo dist. 2nd nearest Station	3rd nearest Station	Hypo dist. 3rd Station	4th nearest Station	Hypo dist. 4th nearest Station
31	31	15	9	15.74	17	16.1	11	16.16
32	32	15	90	15.67	67	16.31	70	17.74
33	33	15	15	16.15	56	16.28	34	16.35
34	34	15	82	16.18	33	16.35	56	16.56
35	35	15	26	16.33	2	17.06	100	17.2
36	36	15	65	15.74	66	16.97	56	17.05
37	37	15	71	15.8	22	17.15	36	17.22
38	38	15	57	16.31	56	16.31	65	17.49
39	39	15	95	16.22	79	17.42	28	17.5
40	40	15	48	16.49	88	16.63	69	18.53
41	41	15	30	16.07	78	16.78	44	17.72
42	42	15	44	16.89	9	17.09	80	17.46
43	43	15	59	15.45	74	17.17	78	17.92
44	44	15	42	16.89	69	17.15	41	17.72
45	45	15	53	15.85	46	16.4	84	16.98
46	46	15	53	16.13	45	16.4	17	16.57
47	47	15	86	16.07	13	16.07	93	16.69
48	48	15	76	16.03	77	16.21	88	16.46
49	49	15	72	15.49	55	15.81	15	17.27
50	50	15	60	16.09	63	16.44	64	17.07
51	51	15	64	15.95	61	17.85	60	18.64
52	52	15	11	15.42	80	15.49	88	15.73
53	53	15	17	15.7	45	15.85	46	16.13
54	54	15	29	15.31	84	15.53	70	15.99
55	55	15	49	15.81	6	16.25	15	16.51
56	56	15	33	16.28	38	16.31	34	16.56
57	57	15	38	16.31	58	16.39	83	16.64
58	58	15	12	15.98	14	16.16	57	16.39
59	59	15	43	15.45	74	15.7	78	17.84
60	60	15	50	16.09	61	16.73	20	16.92
61	61	15	19	16.63	60	16.73	51	17.85
62	62	15	10	15.5	75	16.21	95	16.54
63	63	15	20	15.93	50	16.44	60	17.18
64	64	15	51	15.95	89	16.24	50	17.07
65	65	15	36	15.74	5	16.02	71	16.56
66	66	15	25	16.68	36	16.97	82	18.1
67	67	15	32	16.31	82	16.76	90	17.06
68	68	15	75	16.29	83	16.61	95	16.62
69	69	15	44	17.15	42	17.71	40	18.53
70	70	15	7	15.68	54	15.99	29	16.47
71	71	15	37	15.8	5	16.06	65	16.56
72	72	15	49	15.49	55	16.93	58	17.56

EQ No.	1st nearest Station	Hypo dist. 1st nearest Station	2nd nearest Station	Hypo dist. 2nd nearest Station	3rd nearest Station	Hypo dist. 3rd Station	4th nearest Station	Hypo dist. 4th nearest Station
73	73	15	4	15.46	7	15.8	15	16.05
74	74	15	59	15.7	43	17.17	78	18.78
75	75	15	95	15.41	62	16.21	68	16.29
76	76	15	77	15.34	48	16.03	8	16.26
77	77	15	8	15.32	76	15.34	99	15.55
78	78	15	41	16.78	30	16.99	59	17.84
79	79	15	28	16.93	97	17.24	39	17.42
80	80	15	11	15.23	52	15.49	9	15.71
81	81	15	94	17.43	24	17.6	85	17.84
82	82	15	34	16.18	67	16.76	66	18.1
83	83	15	12	15.84	68	16.61	57	16.64
84	84	15	54	15.53	7	15.97	93	16.06
85	85	15	23	16.16	2	16.27	100	17.37
86	86	15	93	15.4	47	16.07	92	17.14
87	87	15	47	17.28	99	17.49	77	17.56
88	88	15	52	15.73	80	16.41	48	16.46
89	89	15	64	16.24	50	17.85	51	18.9
90	90	15	32	15.67	70	16.62	67	17.06
91	91	15	9	15.67	31	16.33	30	16.63
92	92	15	99	15.22	8	15.39	77	16.38
93	93	15	86	15.4	84	16.06	4	16.31
94	94	15	81	17.43	24	20.88	23	21.61
95	95	15	75	15.41	39	16.22	62	16.54
96	96	15	98	16.25	13	17.73	87	19.51
97	97	15	16	17.19	79	17.24	26	17.66
98	98	15	96	16.25	13	16.45	6	16.97
99	99	15	8	15.03	92	15.22	77	15.55
100	100	15	19	15.85	2	16.48	35	17.2

Table 7.3 The calculated lead time for Dehradun, Hardwar, Roorkee, Muzaffarnagar, Meerut and Delhi for the earthquakes (EQ) originated in the selected EEW seismic network region.

EQ No.	Location of event (in degree)		Lead time in (sec)					
			Dehradun	Hardwar	Roorkee	Muzaffarnagar	Meerut	Delhi
	Latitude	Longitude						
1	30.85	78.48	14	23	30	45	60	78
2	30.69	78.5	11	18	25	40	55	74
3	30.69	78.61	13	19	27	42	56	75
4	30.45	79.06	23	22	32	45	57	77
5	30.53	78.75	14	17	26	40	53	73
6	30.4	79.03	21	20	30	43	55	75
7	30.48	79.08	23	23	33	46	58	78
8	30.31	79.2	27	23	34	46	56	76
9	30.41	79.39	32	30	40	52	62	83
10	30.58	78.65	12	16	25	40	54	73
11	30.4	79.33	30	28	39	51	61	81
12	30.41	78.75	13	14	23	37	50	70
13	30.35	79.05	22	20	30	43	54	74
14	30.33	78.8	14	13	23	36	48	68
15	30.48	78.97	20	20	30	44	56	76
16	30.6	78.52	9	15	23	38	52	71
17	30.44	79.31	30	28	39	51	61	82
18	30.61	78.32	5	14	20	35	50	68
19	30.78	78.44	12	20	27	42	57	76
20	30.7	78.35	8	17	23	38	54	72
21	30.64	78.56	11	17	25	40	54	73
22	30.66	78.68	14	19	28	42	56	75
23	30.79	78.51	13	21	28	43	59	77
24	30.74	78.69	16	21	30	45	59	78
25	30.69	78.78	17	21	30	45	59	78
26	30.64	78.49	9	16	24	39	54	72
27	30.63	78.63	12	18	26	41	55	74
28	30.54	78.56	9	14	22	37	51	70
29	30.54	79.15	26	26	36	49	61	81
30	30.42	79.5	35	33	43	55	65	85
31	30.44	79.36	31	29	40	52	62	83
32	30.61	79.07	24	25	35	49	61	81
33	30.53	78.95	20	21	31	44	57	77
34	30.59	78.93	20	22	32	45	58	78
35	30.66	78.42	8	16	23	38	53	72
36	30.59	78.83	17	20	29	43	56	76
37	30.62	78.75	15	19	28	42	56	75
38	30.49	78.85	16	18	27	41	54	73
39	30.46	78.56	8	11	20	35	49	68

EQ No.	Location of event (in degree)		Lead time in (sec)					
			Dehradun	Hardwar	Roorkee	Muzaffarnagar	Meerut	Delhi
	Latitude	Longitude						
40	30.27	79.34	30	26	37	48	58	78
41	30.39	79.56	37	34	45	56	65	86
42	30.34	79.43	33	30	40	52	61	82
43	30.51	79.49	35	34	44	56	67	87
44	30.32	79.5	35	32	42	53	62	83
45	30.48	79.22	27	26	37	49	60	80
46	30.42	79.23	27	26	36	48	59	79
47	30.37	79.1	23	21	32	44	55	75
48	30.29	79.27	28	25	35	47	57	77
49	30.42	78.92	18	18	28	41	53	73
50	30.76	78.27	8	19	24	39	55	73
51	30.86	78.3	12	22	28	43	58	76
52	30.37	79.31	30	27	38	50	60	80
53	30.46	79.27	29	27	38	50	61	81
54	30.52	79.14	25	25	35	48	60	80
55	30.42	78.97	20	19	29	42	54	74
56	30.54	78.89	18	20	30	43	56	76
57	30.45	78.81	15	16	26	39	52	72
58	30.39	78.8	15	14	24	38	50	70
59	30.53	79.52	36	35	45	57	68	88
60	30.77	78.33	10	19	25	40	56	74
61	30.82	78.38	12	21	27	42	58	76
62	30.54	78.65	12	15	24	39	52	72
63	30.7	78.29	7	17	23	38	53	71
64	30.83	78.25	10	21	26	41	57	75
65	30.56	78.8	16	18	28	42	55	75
66	30.66	78.85	18	22	31	45	59	78
67	30.65	79.03	23	25	35	49	62	81
68	30.43	78.66	11	12	22	36	49	69
69	30.26	79.45	33	29	40	51	60	80
70	30.52	79.08	24	24	34	47	59	79
71	30.57	78.73	14	17	27	41	54	74
72	30.39	78.89	17	16	26	40	52	71
73	30.47	79.03	22	21	32	45	57	77
74	30.56	79.56	37	36	47	59	69	89
75	30.49	78.66	11	14	23	37	51	70
76	30.26	79.22	27	23	34	45	55	75
77	30.29	79.21	27	23	34	46	56	76
78	30.46	79.57	37	35	46	57	67	87
79	30.51	78.49	7	12	20	35	49	68
80	30.38	79.35	31	28	39	51	61	81
81	30.79	78.62	15	22	30	45	60	78

EQ No.	Location of event (in degree)		Lead time in (sec)					
			Dehradun	Hardwar	Roorkee	Muzaffarnagar	Meerut	Delhi
	Latitude	Longitude						
82	30.64	78.95	21	23	33	47	60	79
83	30.45	78.73	13	14	24	38	51	70
84	30.48	79.14	25	24	35	48	59	79
85	30.74	78.53	12	20	27	42	57	75
86	30.4	79.15	25	23	33	46	57	77
87	30.29	79.11	23	20	31	43	53	73
88	30.33	79.32	30	27	37	49	59	79
89	30.81	78.19	9	20	25	40	56	73
90	30.58	79.04	23	24	34	47	60	79
91	30.43	79.43	33	31	42	53	64	84
92	30.34	79.2	26	24	34	46	57	77
93	30.43	79.13	24	23	34	46	57	77
94	30.86	78.65	17	24	32	47	61	80
95	30.49	78.62	10	13	22	37	50	70
96	30.29	78.98	19	16	27	39	50	70
97	30.57	78.44	7	13	21	36	50	69
98	30.35	78.98	20	18	28	41	52	72
99	30.32	79.2	26	24	34	46	56	76
100	30.73	78.44	10	19	26	41	56	74

From the Table 7.3, it has been concluded that for Dehradun, the minimum lead time is 5 sec and maximum lead time is 37 sec, for Hardwar, the minimum lead time is 11 sec and maximum lead time is 36 sec, for Roorkee, the minimum lead time is 20 sec and maximum lead time is 47 sec, for Muzaffarnagar, the minimum lead time is 35 sec and maximum lead time is 59 sec, for Meerut, the minimum lead time is 48 sec and maximum lead time is 70 sec and for Delhi, the minimum lead time is 68 sec and maximum lead time is 90 sec as shown in Fig. 7.4. Thus, the cities which are near to the epicetral region have small lead time in comparison to cities which are far from it. On calculating an average lead time for the consider cities which are as follows:

1) Dehradun - 20 sec

2) Hardwar - 22sec

3) Roorkee - 31 sec

4) Muzaffarnagar - 44 sec

5) Meerut - 57 sec

6) Delhi - 76 sec

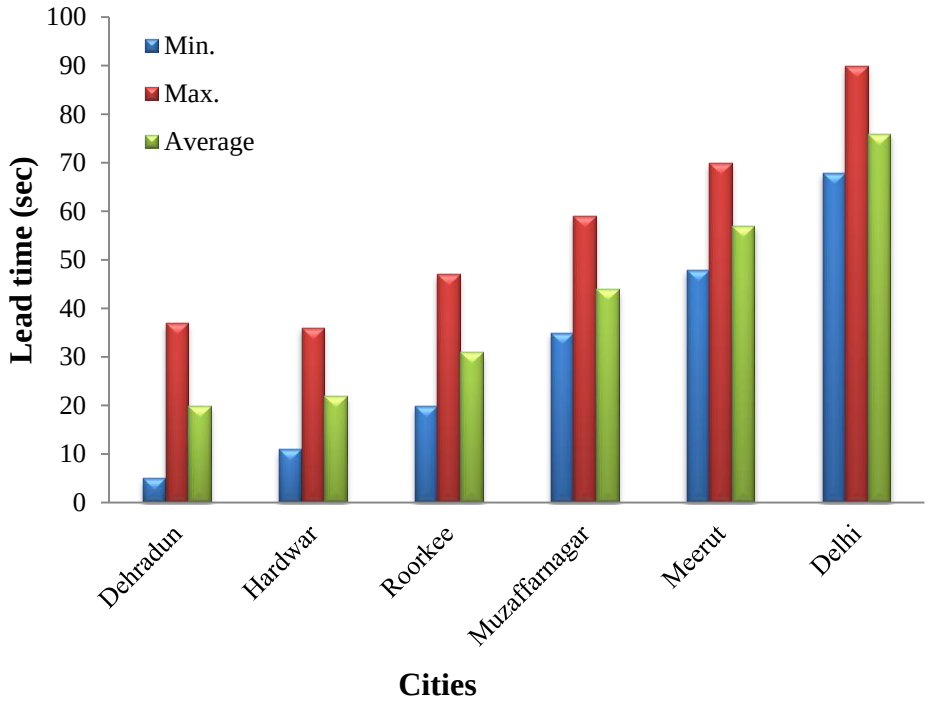

Figure 7.4 The maximum, minimum and average lead time achieved using the proposed EEW algorithm for Dehradun, Roorkee, Hardwar, Muzaffarnagar, Meerut and Delhi.

It is found that for all the cities, the time available for alarm varies from 5sec to 90 sec, i.e., from seconds to more than a minute, which is substantial time to act for saving human lives and for activation of emergency response measures such as immediate shutdown of industrial units, nuclear power plants, gas lines, pipelines, computers and slow down high speed train.

7.6 SUMMARY

This chapter describes the need of EEW system in India due to high rate of damage caused by the earthquakes in India every year. Further, the proposed area for instrumentation with benefited population area has been earmarked and defined. The EEW system designing steps in reference to Northern India are given in details. The lead time for Dehradun, Roorkee, Hardwar, Muzaffarnagar, Meerut and Delhi has been calculated using the proposed EEW algorithm. Delhi gets a lead time of 1.3 minutes to take earthquake mitigation steps to avoid loss of life and property.

CHAPTER 8

SUMMARY AND CONCLUSIONS

8.1 GENERAL

Advancement in data analyses techniques and increased public perception of seismic hazard accelerated the growth of real-time earthquake information system such as EEW system. EEW system makes use of difference in the propagation speed of seismic and electromagnetic waves to issue warning before seismic waves actually hit the potential user's site. EEW system collects data from an occurring event, analyzes them quickly, and provides estimates for location and magnitude of the event. The warning time provided by the EEW system can be used to minimize property damage, loss of lives and to aid emergency response. An attempt has been made in the present study to understand EEW, develop new EEW parameters, develop a multi-parameter based EEW algorithm for accurate and reliable EEW, size estimation during the issuance of warning and propose EEW system for disaster mitigation in seismically active Northern Indian region. The development of algorithm has been carried out using K-NET strong ground motion dataset and is indigenize using strong ground motion dataset from India and validation for data from Turkey, Taiwan and Southern California.

8.2 SUMMARY

The main objective of the present thesis is to review the existing EEW systems (such as UrEDAS, Compact UrEDAS, FREQL, SAS, SASO and ElarmS etc.) deployed in various parts of the world critically on their usability in Indian context especially with respect to data and the parameters involved in such exercises. This research work presents a multi parameter based EEW algorithm which provides more accurate and reliable EEW.

An approach based on velocity of the incoming time series (a more appropriate parameter for damageability) has been developed for P-picking and for warning threshold estimation. The conclusions have been drawn based on the regression analysis between EEW parameters (τ_p^{max}, τ_c, P_d, CAV and RSSCV) and magnitude at five different time windows starting from 1sec to 5 sec carried out on K-NET data which comprises of 1726 earthquake records of 105 events. The obtained regression relations have been used to

calculate the threshold values of the EEW parameters at the selected time window to issue warning for a potentially damaging earthquake ($M \geq 6$). The applicability of the algorithm is tested on Indian data (51 records of 28 events) followed by the stability check on data from Southern California, Taiwan and Turkey (174 records of 14 events).

An endeavor has been made to improve the size estimation during the issuance of warning and its confirmation with in stipulated usable time in EEW systems. For the purpose, Brune's model has been used with Fourier Transform usage of finite time series at ten different time windows (1 sec to 10 sec). The results reveal a better matching with the apriori known magnitudes from the catalogues.

Finally, on studying the status of seismic hazard in Northern India it has been concluded that the region has high seismicity and gets affected by the earthquakes originates in Himalayas. Thus, an EEW system in the region between MCT and MBT has been proposed to reduce the possible risk in cities around Himalayas like Dehradun, Hardwar, Saharanpur, Muzaffarnagar, Bijnor, Moradabad, Meerut, Baghpat, Ghaziabad, Gautam Buddha Nagar and Delhi. The feasibility of EEW system for northern Indian region has been completed successfully with estimations of lead times for the important cities falling in this region.

8.3 CONCLUSIONS

The following conclusions have been drawn based on the present study:

1. The past and the contemporary seismicity reported from Garhwal Himalaya region, prevalent earthquake occurrence models, plate motions and presently going on deformations in the region, the seismic hazard studies reported for this region implicitly make the northern part of Himalaya a fit case for EEW system.

2. The review of existing EEW systems deployed in various parts of the world reveals that there is further scope to develop such systems in more efficient way for fast and reliable real-time disaster mitigation

3. An approach has been developed using a new parameter namely, RSSCV as an alternative solution for auto P-picking which has been used further as a parameter proportional to damageability.

4. A multi parameter EEW algorithm has been developed for automatic P-onset detection, warning decision and magnitude estimation.

5. The EEW parameters for the multi-parameter algorithm developed under the present study have been estimated using 1726 records from K-NET data from Japan to issue EEWs

6. The set of parameters have been used to demonstrate the successful issue of EEW using Indian dataset for damaging earthquake.

7. Further, world wide dataset from Southern California, Taiwan and Turkey have also been used to demonstrate the stability of the approach and the parameters estimated for the newly developed algorithm

8. The results reveal that by using three parameter preference based approach at a time window of 4 sec after P-onset provides 96%, 100% and 93% of correct detections in case of K-NET, Indian and PEER-NGA dataset.

9. The study concludes that use of Brune's model concept improves the size estimation during the issuance of warning and its confirmation within stipulated usable time in EEW systems. At a time window of 5 sec after P-onset the developed Brune's model based magnitude estimation approach provides information regarding the size of the impending event with only ±0.3 uncertainty.

10. The region between MCT and MBT has been considered to be a cluster region for any seismogenic source zone in near future earthquake activity.

11. Based on the presence of seismogenic source and the target cities, an EEW system for Northern India has been proposed with some recommendations for the instrumentation, network connectivity and possible lead time for the cities in northern India.

12. EEW system is one of the real time risk reduction measures which should be used for Northern Indian region for disaster mitigation and management.

8.4 SCOPE FOR FUTURE WORK

The present work presents an EEW algorithm based on multi parameter analysis approach. Since the work relies on several EEW parameters as well as on the analysis time, the following recommendations have been made in order to get more realistic, accurate and fast EEW system.

1. Better understanding of seismotectonics is required for more realistic designing of an EEW system.

2. New EEW parameters are required, which are more closely related to the energy of the signal generated during an earthquake to retrieve more accurately and rapidly the location, magnitude and intensity of the event.

3. Onsite warning approach based EEW system for India should be explored with effects of source and site included.

4. As more data will be available, the better performance check can be made.

5. The proposed algorithm efficiency to be checked in Northern India and then EEW systems should also be deployed in other regions like NE Himalayas and Jammu & Kashmir.

6. More cities like Chandigarh, Jammu, Bihar, Sikkim, Guwahati and whole NE states should also be considered for such endeavors.

BIBLIOGRAPPHY

1. Aki, K. (1967). Scaling relation of seismic spectrum. *Journal of Geophysical Research* **72** (4), 1217-1231.
2. Akinci, A., A. G. Taktak, and S. Ergintav (1994). Attenuation of coda waves in Western Anatolia. *Physics of the Earth Planetary Interiors* **87** (1-2), 155-165.
3. Alcik, H., O. Ozel, N. Apaydin, and M. Erdik (2009). A study on warning algorithm for Istanbul early warning system. *Geophysical Research Letters* **36** (5), 1-3.
4. Alcik, H., O. Ozel, Y.-M. Wu, N. M. Ozel, and M. Erdik (2011). An alternative approach for the Istanbul earthquake early warning system. *Soil dynamics and Earthquake Engineering* **31** (2), 181-187.
5. Allen, R. M, and A. Ziv (2011). Application of real-time GPS to earthquake early warning. *Geophysical Research Letters* **38** (16), L16310; doi:10.1029/2011GL047947.
6. Allen, R. M. (2006). Probabilistic warning times for earthquake ground shaking in the San Francisco Bay Area. *Seismological Research Letters* **77**, 371-376.
7. Allen, R. M. (2007). The ElarmS earthquake early warning methodology and application across California. In *Earthquake Early Warning Systems*, ed. P. Gasparini, G. Manfredi, and J. Zschau, 21-44. Berlin and Heidelberg: Springer.
8. Allen, R. M. (2011). Earthquakes, Early and Strong Motion Warning. In *Encyclopedia of Solid Earth Geophysics*, ed. Harsh Gupta, 226-233. Springer.
9. Allen, R. M. (2012). Transforming earthquake detection? *Science* **335**, 297-298.
10. Allen, R. M., and H. Kanamori (2003). The potential for earthquake early warning in Southern California. *Science* **300** (5620), 786–789.
11. Allen, R. M., H. Brown, M. Hellweg, O. Khainovski, P. Lombard, and D. Neuhauser (2009). Real-time earthquake detection and hazard assessment by ElarmS across California. *Geophysical Research Letters* **36** (5), LOOB08; doi:10.1029/2008GL036766.
12. Allen, R. V. (1978). Automatic earthquake recognition and timing from single traces. *Bulletin of the Seismological Society of America* **68** (5), 1521-1532.

13. Aoi, S., T. Kunugi, and H. Fujiwara (2004). Strong-motion seismograph network operated by NIED: K-NET and KiK-net. *Journal of Japan Association for Earthquake Engineering* **4** (3), 65-74.
14. Arya, A. S. (1990). Damage scenario of a hypothetical 8.0 magnitude earthquake in Kangra region of Himachal Pradesh. *Bulletin of Indian Society of Earthquake Technology* **27** (3), 121-132.
15. Atkinson, G. M., and D. M. Boore (1995). Ground-motion relations for eastern North America. *Bulletin of the Seismological Society of America* **85** (1), 17-30.
16. Avouac, J. P., and P. Tapponnier (1993). Kinematic model of active deformation in central Asia. *Geophysical Research Letters* **20** (10), 895-898.
17. Baker, D. M., R. J. Lillie, R. S. Yeats, G. D. Johnson, M. Yousuf, and A. S. H. Zamin (1988). Development of the Himalayan frontal thrust zone: Salt Range, Pakistan. *Geology* **16**, 3-7.
18. Banerjee, P., and R. Burgmann (2002). Convergence across the Northwest Himalaya from GPS measurements. *Geophysical Research Letters* **29** (13), 1652-1655.
19. Beroza, G. C., and W. L. Ellsworth (1996). Properties of the seismic nucleation phase. *Tectonophysics* **261** (1-3)**,** 209-227.
20. Bhardwaj, R., A. Kumar, and M. L. Sharma (2010). An algorithm for automatic detection of primary wave onset for early warning system. In *14th Symposium on Earthquake Engineering*, Roorkee, India, 373-380.
21. Bhardwaj, R., A. Kumar, and M. L. Sharma (2012a). Analysis of Tauc (τ_c) and P_d attributes for earthquake early warning in India. In *Proceedings of the 15th World Conference on Earthquake Engineering*, Lisbon, paper no. 0696, 1-8.
22. Bhardwaj, R., A. Kumar, and M. L. Sharma (2012b). Effect of medium characteristics in magnitude estimation for earthquake early warning systems. *Golden Jubilee Symposium Indian Society of Earthquake Technology (ISET)*, Department of earthquake engineering building IIT Roorkee, Roorkee, paper no. H002, 1-10.
23. Bhardwaj, R., A. Kumar, and M. L. Sharma (2013a). Root sum of squares cumulative velocity: an attribute for earthquake early warning. *Disaster Advances* **6** (3), 24-31.

24. Bhardwaj, R., M. L. Sharma, and A. Kumar (2012c). P-wave time window approach for EEW systems. In *National Workshop on Engineering Geophysics for Civil Engineering and Geo-hazards* (EGCEG), CSIR- Central Building Research Institute, Roorkee.
25. Bhardwaj, R., M. L. Sharma, and A. Kumar (2013b). Earthquake magnitude prediction for real time EEW system: An automization from P-wave time window analysis. *Himalayan Geology* **34** (1), 84-91.
26. Bhardwaj, R., M. L. Sharma, and A. Kumar (2013c). Inclusion of Q-value in parameters used for earthquake early warning systems. *Disaster Advances* **6** (5), 54-60.
27. Bhatia, S. C., R. M. Kumar, and H. K. Gupta (1999). A probabilistic seismic hazard map of India and adjoining regions. *Annali di Geofisica* **42** (6), 1153-1164.
28. Bhattacharya, A., M. K. Arora, and M. L. Sharma (2012). Surface displacement measurements along Himalayan frontal fault using differential SAR interferometry. *Natural Hazards* **64** (2), 1105-1123.
29. Bhattacharya, A., M. K. Arora, M. L. Sharma, M. Vöge, and R. Bhasin (2014). Surface displacement estimation using space-borne SAR interferometry in a small portion along Himalayan Frontal Fault. *Optics and Lasers in Engineering* **53**, 164-178.
30. Bilham, R., F. Blume, R. Bendick, and V. K. Gaur (1998). Geodetic constraints on the translation and deformation of India, implications for future great Himalayan earthquakes. *Current Science* **74** (3), 213-229.
31. Bilham, R., K. Larson, and J. Freymueller (1997). GPS measurements of present-day convergence across the Nepal Himalaya. *Nature* **386**, 61-64.
32. BMPTC (Building Materials and Technology Promotion Council) vulnerability atlas of India (first revision, 2006). New Delhi, India.
33. Böse, M. (2006). Earthquake early warning for Istanbul using artificial neural networks. PhD thesis, Karlsruhe University, Karlsruhe, Germany.
34. Böse, M., C. Ionescu, and F. Wenzel (2007). Earthquake early warning for Bucharest, Romania: novel and revisited scaling relations. *Geophysical Research Letters* **34** (7), 1-4.
35. Böse, M., E. Hauksson, K. Solanki, H. Kanamori, Y.-M. Wu, and T. Heaton (2009). A new trigger criterion for improved real-time performance of on-site early warning in southern California. *Bulletin of the Seismological Society of America* **99** (2A), 897-905.

36. Böse, M., F. Wenzel, and M. Erdik (2008). PreSEIS: A neural network-based approach to earthquake early warning for finite faults. *Bulletin of the Seismological Society of America* **98** (1), 366-382.
37. Böse, M., M. Erdik, and F. Wenzel (2007). A New Approach to Earthquake Early Warning. In *Earthquake Early Warning Systems*, ed. P. Gasparini, G. Manfredi, J. Zschau, 65-83. Berlin and Heidelberg: Springer.
38. Brown, H. (2012). Evaluating and improving the ElarmS earthquake early warning algorithm. PhD thesis, University of California, Berkeley.
39. Brown, H. M., R. M. Allen, and V. F. Grasso (2009). Testing ElarmS in Japan. *Seismological Research Letters* **80** (5), 727-739.
40. Brown, H. M., R. M. Allen, M. Hellweg, O. Khainovski, D. Neuhauser, and A. Souf (2011). Development of the Elarms methodology for earthquake early warning: realtime application in California and offline testing in Japan. *Soil dynamics and Earthquake Engineering* **31** (2), 188-200.
41. Brune, J. N. (1970). Tectonic stress and the spectra of seismic shear waves from earthquake. *Journal of Geophysical Research* **75** (26), 4997-5009.
42. Brune, J. N. (1971). Correction to tectonic stress and the spectra of seismic shear waves from earthquakes. *Journal of Geophysical Research* **76** (20), 5002.
43. Bureau of Indian Standards BIS (2002). IS 1893 (Part 1): 2002, Indian standard - criteria for earthquake resistant design of structures, Part 1 - General Provisions and Buildings. ICS 91.120.25, New Delhi.
44. Böse, M., R. M. Allen, H. Brown, G. Cua, M. Fischer, E. Hauksson, T. Heaton, M. Hellweg, M. Liukis, D. Neuhauser, P. Maechling, and CISN EEW Group (2013). CISN ShakeAlert: An Earthquake Early Warning Demonstration System for California. In *Early Warning for Geological Disasters - Scientific Methods and Current Practice*, ed. F. Wenzel, and J. Zschau. Berlin Heidelberg: Springer.
45. Cabañas, L., B. Benito, and M. Herráiz (1997). An approach to the measurement of the potential structural damage of earthquake ground motions. *Earthquake Engineering & Structural Dynamics* **26** (1), 79-92.
46. Campbell, K. W., and Y. Bozorgnia (2006). Next generation attenuation (NGA) empirical ground motion models: can they be used in Europe? In *Proceedings of the*

First European Conference on Earthquake Engineering and Seismology, Geneva, Switzerland, paper no. 458.

47. Caprio, M., M. Lancieri, G. B. Cua, Zollo, and S. Wiemer (2011). An evolutionary approach to real-time moment magnitude estimation via inversion of displacement spectra. *Geophysical Research Letters* **38** (2), L02301.
48. Chamlagain, D. (2009). Earthquake scenario and recent efforts towards earthquake reduction in Nepal. *Journal of South Asia Disaster Studies* **2** (1), 57-80.
49. Chiaruttini, C., and G. Salemi (1993). Artificial intelligence techniques in the analysis of digital seismograms. *Computers and Geosciences* **19** (2)**,** 149-156.
50. Chiou, B. S.-J., and R. R. Youngs (2008). An NGA model for the average horizontal component of peak ground motion and response spectra. *Earthquake Spectra* **24** (1), 173-215.
51. Colak, O. H., C. D. Tahir, O. Sukru, A. Hasan, and C. Osman (2009). Detection of P- and S-waves arrival times using the discrete wavelet transform in real seismograms. *The Arabian Journal for Science and Engineering* **34**, 79-89.
52. Cooper, J. D. (1868). Letter to Editor, San Francisco Daily Evening Bulletin, November 3.
53. Crowell, B. W, Y. Bock, and M. B. Squibb (2009). Demonstration of earthquake early warning using total displacement waveforms from real-time GPS networks. *Seismological Research Letters* **80** (5), 772-782.
54. Cua, G. B. (2005). Creating the Virtual Seismologist: developments in ground motion characterization seismic early warning. PhD thesis, California Institute of Technology, http://etd.caltech.edu/etd/available/etd-02092005-125601.
55. Cua, G. B., and T. Heaton (2003). An envelope-based paradigm for seismic early warning. Eos. Trans. AGU, Fall Meet. Suppl. **84** (46)**.**
56. Cua, G. B., and T. Heaton (2007). The Virtual Seismologist (VS) method: a Bayesian approach to earthquake early warning. In *Earthquake Early Warning Systems*, ed. P. Gasparini, G. Manfredi, and J. Zschau, 97-132. Berlin and Heidelberg: Springer.
57. Danciu, L., and G.-A. Tselentis (2007). Engineering ground-motion parameters attenuation relationships for Greece. *Bulletin of the Seismological Society of America* **97** (1B)**,** 162-183.

58. Das, R. (2013). Probabilistic seismic hazard assessment for Northeast India region. PhD thesis, Indian Institute of Technology Roorkee, Roorkee, India.
59. Das, R., H. R. Wason, and M. L. Sharma (2011). Global regression relations for conversion of surface wave and body wave magnitudes to moment magnitude. *Natural Hazards* **59** (2), 801-810.
60. Deb, S. K. (2008). Emerging Technologies for Earthquake Risk Reduction in Construction of Buildings. In *Proceedings of Conference on Managing Earthquake Risk*, New Delhi, 251-259.
61. DeCelles, P. G., G. E. Gehrels, J. Quade, T. P. Ojha, P. A. Kapp, and B. N. Upreti (1998). Neogene foreland basin deposits, erosional unroofing, and the kinematic history of the Himalayan fold-thrust belt, western Nepal. *Bulletin of Geological Society of America* **110** (1), 2-21.
62. Dewey, J. F., and J. M. Bird (1970). Mountain belts and new global tectonics. *Journal of Geophysical Research* **75** (14), 2625-2647.
63. Dimri, V. P., and A. Chamoli (2008). Development of computational geophysics in India. *Geology Society of India: Memoir* **68**, 1-14.
64. Doi, K. (2011). The operation and performance of earthquake early warnings by the Japan meteorological agency. *Soil Dynamics and Earthquake Engineering* **31** (2), 119-126.
65. Dowla, F., S. Taylor, and R. Anderson (1990). Seismic discrimination with artificial neural networks: preliminary results with regional spectral data. *Bulletin of the Seismological Society of America* **80** (5)**,** 1346-1373.
66. Eck, T. V. (1988). Attenuation of coda waves in the Dead Sea region. *Bulletin of the Seismological Society of America* **78** (2), 770-779.
67. Ellsworth, W. L., and G. C. Beroza (1995). Seismic evidence for an earthquake nucleation phase. *Science* **268,** 851-855.
68. England, P. C., and P. Molnar (1997). Active deformation of Asia from kinematics to dynamics. *Science* **278**, 643-662.
69. EPRI-Electric Power Research Institute (1988). A criterion for determining exceedance of the operating basis earthquake: Report of Electric Power Research Institute, EPRI NP-5930, Palo Alto, California.

70. EPRI-Electric Power Research Institute (1991). Standardization of the cumulative absolute velocity: Report of Electric Power Research Institute, EPRI TR-100082, Palo Alto, California.

71. EPRI-Electric Power Research Institute (2006). Use of cumulative absolute velocity (CAV) in determining effects of small magnitude earthquakes on seismic hazard analyses. In: Electric Power Research Institute, Electric Power Research Institute, Palo Alto, California, prepared by ARES Corporation Inc and Norm A Abrahamson Inc., Report No: RS-1014099.

72. Erdik, M., Y. Fahjan, O. Ozel, H. Alcik, A. Mert, and M. Gul (2003). Istanbul earthquake rapid response and the early warning system. *Bulletin of Earthquake Engineering* **1** (1), 157-163.

73. Espinosa-Aranda, J. M., A. Cuellar, A. Garcia, G. Ibarrola, R. Islas, S. Maldonado, and F. H. Rodriguez (2009). Evolution of the Mexican seismic alert system (SASMEX). *Seismological Research Letters* **80** (5), 694-706.

74. Espinosa-Aranda, J. M., A. Jimenez, G. Ibarrola, F. Alcantar, A. Aguilar, M. Inostroza, and S. Maldonado (1995). Mexico City seismic alert system. *Seismological Research Letters* **66** (6), 42-53

75. Feldl, N., and R. Bilham (2006). Great Himalayan earthquakes and the Tibetan plateau. *Nature* **444**, 165-170.

76. Festa, G., A. Zollo and M. Lancieri (2008). Earthquake magnitude estimation from radiated energy. *Geophysical Research Letters* **35** (22), L22312; doi:10.1029/2008GL035576.

77. Festa, G., and A. Zollo (2009). Early radiation and final magnitude: insights from source kinematics. In *Proceedings of the 2nd EEW workshop in Kyoto*, Japan.

78. Fleming, K., M. Picozzi, C. Milkereit, F. Khünlenz, B. Lichtblau, J. Fischer, C. Zulfikar, O. Ozel, and the SAFER and EDIM Working Groups (2009). The Self-organizing Seismic Early Warning Information Network (SOSEWIN). *Seismological Research Letters* **80** (5)**,** 755-771.

79. Gansser, A. (1964). Geology of Himalaya. *Inter-Science,* New York, 289.

80. Giardini, D. (1999). The Global Seismic Hazard Assessment Program (GSHAP): 1992-1999. *Annali di Geofisica* **36** (3-4), 15-24.

81. Glassmoyer, G., and R. D. Borcherdt (1990). Source parameters and effects of bandwidth and local geology on high-frequency ground motions observed for aftershocks of the Northeastern Ohio earthquake of 31st January 1986. *Bulletin of the Seismological Society of America* **80** (4), 889-912.

82. Goltz, J. D., and P. J. Flores (1997). Real-time earthquake early warning and public policy: A report on Mexico City's Sistema de Alerta Sismica. *Seismological Research Letters* **68** (5), 727-733.

83. Gonzalo, G.-C., A. Muñoz-Diosdado, J. A. Peralta, J. A. Balderas-López, and F. Angulo-Brown (2012). Parameters of Higuchi's Method to characterize primary waves in some seismograms from the Mexican subduction zone. *Acta Geophysica* **60** (3), 910-927.

84. GSI (2000). Seismotectonic Atlas of India and its Environs. Geological Survey of India.

85. Gupta, H. K., N. P. Rao, B. K. Rastogi, and D. Sarkar (2001). The deadliest interplate earthquake. *Science* **291**, 2101-2102.

86. Gupta, S. C., and A. Kumar (2002). Seismic wave attenuation characteristics of three Indian regions: A comparative study. *Current Science* **82** (4), 407-413.

87. Gupta, S. C., V. N. Singh, and A. Kumar (1995). Attenuation of coda waves in the Garhwal Himalaya India. *Physics of Earth and Planetary Interiors* **87** (3)**,** 247-253.

88. H. Mittal, Kamal, A. Kumar, S.K. Singh (2013). Estimation of site effects in Delhi using standard spectral ratio. *Soil Dynamics and Earthquake Engineering* 50, 53-61.

89. Haldar, P., Y. Singh, D. H. Lang, and D. K. Paul (2013). Comparison of seismic risk assessment based on macroseismic intensity and spectrum approaches using 'SeisVARA'. *Soil Dynamics and Earthquake Engineering* **48**, 267-281.

90. Hanks, T. C. (1982). f_{max}. *Bulletin of the Seismological Society of America* **72** (6A), 1867-1879.

91. Hanks, T. C., and H. Kanamori (1979). A moment magnitude scale. *Journal of Geophysical Research* **84** (B5), 2348-2350.

92. Harbindu, A., M. L. Sharma, and Kamal (2012). Stochastic ground-motion simulation of two Himalayan earthquakes: seismic hazard assessment perspectives. *Journal of Seismology* **16**, 345-369.

93. Heaton, T. H. (1985). A model for a seismic computerized alert network. *Science* **228**, 987-990.

94. Horiuchi, S., H. Negishi, K. Abe, A. Kamimura, and Y. Fujinawa (2005). An automatic processing system for broadcasting earthquake alarms. *Bulletin of the Seismological Society of America* **95** (2)**,** 708-781.

95. Hsiao, N. C., Y.-M. Wu, L. Zhao, D. Y. Chen, W. T. Huang, K. H. Kuo, T. C. Shin, and P. L. Leu (2011). A new prototype system for earthquake early warning in Taiwan. *Soil Dynamics and Earthquake Engineering* **31** (2), 201-208.

96. Hsiao, N.-C., Y.-M. Wu, T.-C. Shin, L. Zhao, and T.-L. Teng (2009). Development of earthquake early warning system in Taiwan. *Geophysical Research Letters* **36** (5)**,** LOOB02; doi:10.1029/2008GL036596.

97. Huang, B. S., W. G. Huang, Y. L. Huang, L. C. Kuo, K. C. Chen, and J. Angelier (2009). Complex fault rupture during the 2003 Chengkung, Taiwan earthquake sequence from dense seismic array and GPS observations. *Tectonophysics* **466** (3-4), 184-204

98. Iervolino, I., V. Convertito, M. Giorgio, G. Manfredi, and A. Zollo (2006). Real-time risk analysis for hybrid earthquake early warning systems. *Journal of Earthquake Engineering* **10** (6), 867-85.

99. Iio, Y. (1992). Slow initial phase of the P-wave velocity pulse generated by microearthquakes. *Geophysical Research Letters* **19** (5), 477-480.

100. Iio, Y. (1995). Observations of the slow initial phase generated by microearthquakes: implications for earthquake nucleation and propagation. *Journal of Geophysical Research* **100** (B8), 15333-49.

101. Ionescu, C., and G. Marmureanu (2005). Rapid Early Warning System (REWS) for Bucharest and industrial facilities. Presentation at Caltech University.

102. Ionescu, C., M. Böse, F. Wenzel, A. Marmureanu, A. Grigore, and G. Marmureanu (2007). An early warning system for deep Vrancea (Romania) earthquakes. In *Earthquake Early Warning Systems*, ed. P. Gasparini, G. Manfredi, and J. Zschau, 343-349. Berlin and Heidelberg: Springer.

103. Iyengar, R. N. (2000). Seismic status of Delhi megacity. *Current Science* **78** (5), 568-574.

104. Jackson, M. E., and R. Bilham (1994). 1991-1992 GPS measurements across the Nepal Himalaya. *Geophysical Research Letters* **21** (12), 1169-1172.
105. Joshi, G. C., and M. L. Sharma (2011a). Estimation of peak ground acceleration and its uncertainty for Northern Indian region. *International Journal of Geotechnical Earthquake Engineering* **2** (1), 1-19.
106. Joshi, G. C., and M. L. Sharma (2011b). Strong ground motion prediction and uncertainties estimation for Delhi, India. *Natural Hazard* **59** (2), 617-637.
107. Joswig, M. (1990). Pattern recognition for earthquake detection. *Bulletin of the Seismological Society of America* **80** (1), 170-186.
108. Kamble, V. P., and H. M. Chaudhury (1979). Recent seismicity around Delhi and neighbourhood. *Mausam* **30** (2-3), 305-312.
109. Kamigaichi, O., M. Saito, K. Doi, T. Matsumori, S. Tsukada, K. Takeda, T. Shimoyama, K. Nakamura, M. Kiyomoto, and Y. Watanabe (2009). Earthquake early warning in Japan: warning the general public and future prospects. *Seismological Research Letters* **80** (5), 717-726.
110. Kanamori, H. (2005). Real-time seismology and earthquake damage mitigation. *Annual Review of Earth and Planetary Sciences* **33** (1), 195-214.
111. Kanamori, H., E. Hauksson, and T. Heaton (1997). Real time seismology and earthquake hazard mitigation. *Nature* **390**, 461-464.
112. Katsumata, A. (1996). Comparison of magnitudes estimated by the Japan Meteorological Agency with moment magnitudes for intermediate and deep earthquakes. *Bulletin of the Seismological Society of America* **86** (3), 832-842.
113. Kayal, J. R. (1996). Earthquake source process in Northeast India: A review. *Himalayan Geology* **17**, 53-69.
114. Kayal, J. R. (1998). Seismicity of Northeast India and surroundings development over the past 100 years. *Journal of Geophysics* **19** (1), 9-34.
115. Keiles-Borok, V. (1959). An estimation of the displacement in an earthquake source and of source dimensions. *Annali di Geofisica* **12**, 205-214.
116. Khattri, K. N., A. M. Rogers, D. M. Perkins, and S. T. Algermissen (1984). A seismic hazard map of India and adjacent areas. *Tectonophysics* **108**, 93-134.

117. Kilb, D., and J. Gomberg (1999). The initial subevent of the 1994 Northridge, California, earthquake: is earthquake size predictable? *Journal of Seismology* **3**, 409-20.

118. Kinoshita, S. (1998). Kyoshin Net (K-NET). *Seismological Research Letters* **69**, 309-332.

119. Köhler, N., G. Cua, F. Wenzel, and M. Böse (2009). Rapid source parameter estimations of Southern California earthquakes using PreSEIS. *Seismological Research Letters* **80** (5), 748-754.

120. Kostov, M. K. (2005). Site specific estimation of cumulative absolute velocity. In *Proceedings of the 18th International Conference on Structural Mechanics in Reactor Technology (SMiRT 18)*, August 7-12, 2005, Beijing, China.

121. Kramer, S. L. (2003). *Geotechnical Earthquake Engineering*, International series in Civil Engineering and Engineering Mechanics, ed. W. J. Hall. Prentice-Hall, New Jersey.

122. Kramer, S. L., and R. A. Mitchell (2006). Ground motion intensity measures for liquefaction hazard evaluation. *Earthquake Spectra* **22** (2), 413-438.

123. Kumar, A. (2011). Study of earthquake source parameters using microearthquake and strong motion data. PhD thesis, Indian Institute of Technology Roorkee, Roorkee, India.

124. Kumar, A., A. Kumar, H. Mittal, A. Kumar, and R. Bhardwaj (2012b). Software to estimate earthquake spectral and source parameters. *International Journal of Geosciences* **3** (5), 1142-1149.

125. Kumar, A., H. Mittal, R. Sachdeva, and A. Kumar (2012a). Indian Strong Motion Instrumentation Network. *Seismological Research Letters* **83** (1), 59-66.

126. Kumar, N., I. A. Parvez, and H. S. Virk (2005). Estimation of coda wave attenuation for NW Himalayan region using local earthquakes. *Physics of Earth and Planetary Interiors* **151** (3-4), 243-258.

127. Kumar, R. (2006). Earthquake occurrence in India and its use in seismic hazard estimation using probabilistic methods. DPhill thesis, Hemwati Nandan Bahuguna Garhwal University, Srinagar, India.

128. Kumar, S., and A. K. Mahajan (1990). Studies of intensities of 26th April, 1986 Dharmsala earthquake and associated tectonics. *Geological Society of India* **35**, 213-219.

129. Kumar, S., and A. K. Mahajan (2001). Seismotectonics of the Kangra region, northwest Himalaya. *Tectonophysics* **331** (4), 359-371.

130. Kumar, S., S. G. Wesnousky, and T. K. Rockwell (2003). The Himalayan frontal thrust (HFT) is not blind. *Earthquake Geology in Reverse Faulting Terrains, Seattle Annual Meeting*, Session 24, Washington.

131. Kumar, S., S. G. Wesnousky, T. H. Rockwell, D. Ragona, V. C. Thakur, and C. G. Seitz (2001). Earthquake recurrence and rupture dynamics of the Himalayan frontal thrust, India. *Science* 294, 2328-2331.

132. Kumar, S., S. G. Wesnousky, T. K. Rockwell, R. W. Briggs, V. C. Thakur, and R. Jayangondaperumal (2006). Paleoseismic evidence of great surface rupture earthquakes along the Indian Himalaya. *Journal of Geophysical Research* **330** (3), 3304-3309.

133. Kurian, S. A., S. K. Deb, and A. Dutta (2006). Seismic vulnerability assessment of a railway overbridge using fragility curves. In *Proceedings of the 2nd Indo-Taiwan Workshop on Seismic Evaluation and Retrofitting of RC buildings*, October 11-12, 2006, Taipei, 109-117.

134. Lancieri, M., and A. Zollo (2008). A Bayesian approach to the real-time estimation of magnitude from the early *P* and *S* wave displacement peaks. *Journal of Geophysical Research* **113** (B12), B12302; doi: 10.1029/ 2007JB005386.

135. Lang, D. H., and F. Vladimir Gutiérrez Corea (2010). RISe: Illustrating georeferenced data of seismic risk and loss assessment studies using Google Earth. *Earthquake Spectra* **26** (1), 295-307.

136. Lang, D. H., S. Molina, and C. D. Lindholm (2008). Towards near real-time damage estimation using a CSM-based tool for seismic risk assessment. *Journal of Earthquake Engineering* **12** (S2), 199-210.

137. Lang, D. H., Y. Singh, and J. S. R. Prasad (2012). Comparing empirical and analytical estimates of earthquake loss assessment studies for the city of Dehradun, India. *Earthquake Spectra* **28** (2), 595-619.

138. Larson, K., R. Burgmann, R. Bilham, and J. T. Freymueller (1999). Kinematics of the India-Eurasia collision zone from GPS measurements. *Journal of Geophysical Research* **104** (B1), 1077-1093.

139. Lave, J., and J. P. Avouac (2000). Active mountain building in the Himalayas of Nepal. *Journal of Geophysical Research* **105** (B3), 5735-5770.
140. Leathers, M. (1987). Balanced structural cross-section of the western Salt Range and Potwar Plateau: Deformation near the strike slip terminus of an overthrust sheet. MS thesis, Oregon State University, Corvallis, Oregon.
141. Lee, W. H. K., and J. C. Lahr (1972). HYPO71: a computer program for determining hypocenter, magnitude, and first motion pattern of local earthquakes. Open File Report, U. S. *Geological Survey*, page no.100.
142. Liu, W., and Y. Liu (2012). Commonly used earthquake source models. *Geologos* **18** (3), 197-209.
143. Lockman, A., and R. M. Allen (2005). Single-station earthquake characterization for early warning. *Bulletin of the Seismological Society of America* **95 (6)**, 2029-2039.
144. Lockman, A., and R. M. Allen (2007). Magnitude-period scaling relations for Japan and the Pacific Northwest: Implications for earthquake early warning. *Bulletin of the Seismological Society of America* **97** (1B), 140-150.
145. Lyon-Caen, H., and P. Molnar (1985). Gravity anomalies, flexure of the Indian Plate and the structure, support and evolution of the Himalaya and Ganga Basin. *Tectonics* **4** (6), 513-538.
146. Magotra, N., N. Ahmed, and E. Chael (1987). Seismic event detection and source location using single-station (three-component) data. *Bulletin of the Seismological Society of America* **77** (3), 958-971.
147. Mahajan, A. K. (2006). Seismicity, Seismotectonics and seismic hazard of 1905 Kangra Earthquake effected region (NW Himalaya), India. In *Environmental Hazards Science & Society*, ed. K. K. Sharma, S. K. Bandooni, and V. S. Negi, Research India Press, New Delhi, 65-86.
148. Mahajan, A. K., and G. K. Ghosh (2007). Statistical analysis of completeness of earthquake data of Northwest Himalayan region and its implication for seismicity evaluation.Natural hazard. In *Proceeding of the National Conference on ''Natural hazards (earthquakes and landslides): challenges, perspectives and societal dimensions with focus on the state of Uttaranchal''*, ed. O. P. Varma, A. K. Mahajan, and V. Gupta, December 26-28, Dehradun, 45-56.

149. Mahajan, A. K., and N. S. Virdi (2001). Macroseismic field generated by the 29th March Chamoli earthquake, 1999 and its seismotectonics. *Journal of Asian Earth Sciences* **19** (4), 507-512

150. Mahajan, A. K., J. J. Galiana-Merino, C. Lindholm, B. R. Arora, A. K. Mundepi, N. Chauhan, and N. Rai (2011). Characterization of the sedimentary cover at the Himalayan foothills: Characterization of the sedimentary cover at the Himalayan foothills using active and passive seismic techniques. *Journal of Applied Geophysics* **73**, 196-206.

151. Mahajan, A. K., V. C. Thakur, M. L. Sharma, and C. Mukesh (2009). Probabilistic seismic hazard map of NW Himalaya and its adjoining area, India. *Natural Hazards* **53** (3), 443-457.

152. Mahesh, P., J. K. Catherine, V. K. Gahalaut, B. Kundu, A. Ambikapathy, A. Bansal, L. Premkishore, M. Narsaiah, S. Ghavri, R. K. Chadha, P. Choudhary, D. K. Singh, S. K. Singh, S. Kumar, B. Nagarajan, B. C. Bhatt, R. P. Tiwari, Arun kumar, A. kumar, Harsh Bhu, and S. Kalifa (2012). Rigid Indian plate, constraints from GPS measurements. *Gondwana Research* **22** (3-4), 1068-1072.

153. Mandal, P., B. K. Rastogi, and H. K. Gupta (2000). Recent Indian Earthquakes. *Current science* **79** (9), 1334-1347.

154. Marmureanu, A., C. Ionescu, and C. O. Cioflan (2011). Advanced real-time acquisition of the Vrancea earthquake early warning system. *Soil dynamics and Earthquake Engineering* **31** (2), 163-169.

155. Martinez-Rueda, J. E., G. Moutsokapas, and E. Tsantali (2008). Predictive equations to estimate Arias Intensity and Cumulative Absolute Velocity as a function of Housner Intensity. In *Proceedings of Seismic Engineering Conference Commemorating the 1908 Messina and Reggio Calabria Earthquake*, Messina, Italy, 309-306.

156. Minster, J. B., and T. H. Jordan (1978). Present-day plate motions. *Journal of Geophysical Research* **83** (B11), 5331-5354.

157. Mittal H., A. Kumar, Kamal (2012b). Ground motion estimation in Delhi from postulated regional and local earthquakes. *Journal of Seismology* 17 (2), 593-605.

158. Mittal, H., A. Kumar, and Rebecca (2012a). Indian strong motion instrumentation network and its site characterization. *International Journal of Geosciences* **3** (6), 1151-1167.

159. Mohanty, W. K., R. Prakash, G. Suresh, A. K. Shukla, M. Y. Walling, and J. P. Srivastava (2009). Estimation of coda wave attenuation for the National Capital Region, Delhi, India using local earthquakes. *Pure and Applied Geophysics* **166** (3), 429-449.

160. Mohorovicic, A. (1915). Die Bestimmung des Epizentrum eines Erdbebens. Gerl. Beitr. z. *Geophysics* **14**, 199-205 (in German).

161. Molina, S., D. H. Lang, and C. D. Lindholm (2010). SELENA- An open-source tool for seismic risk and loss assessment using a logic tree computation procedure. *Computer and Geosciences* **36** (3), 257-269.

162. Molnar, P. (1990). A review of the seismicity and the rates of active underthrusting and the deformation of the Himalaya. *Journal of Himalayan Geology* **1** (2), 131-154.

163. Molnar, P., and P. Tapponnier (1975). Cenozoic tectonics of Asia: Effects of a continental collision. *Science* **189**, 419-426.

164. Molnar, P., and P. Tapponnier (1977). Relation of the tectonics of Eastern China to the India-Eurasia collision: application of slip-line field theory to large-scale control tectonics. *Geology* **5**, 212-216.

165. Mori, J., and H. Kanamori (1996). Rupture initiations of microearthquakes in the 1995 Ridgecrest, California. *Geophysical Research Letters* **23**, 2437-2440.

166. Mori, J., H. Kanamori, J. Davis, E. Hauksson, and R. Clayton et al., (1998). Major improvements in progress for Southern California earthquake monitoring. *EOS Transaction American Geophysical Union* **79**, 217-221.

167. Nakamura, Y. (1984). Development of the earthquake early-warning system for the Shinkansen, some recent earthquake engineering research and practical in Japan. In *Proceedings of the Japanese National Committee of the International Association for Earthquake Engineering*, June 1984, 224-238.

168. Nakamura, Y. (1988). On the urgent earthquake detection and alarm system (UrEDAS). In *Proceedings of the 9th World Conference on Earthquake Engineering* **7**, 673-678.

169. Nakamura, Y. (1989). Earthquake alarm system for Japan railways. *Japanese Railway Engineering* **28** (4), 3-7.

170. Nakamura, Y. (1996). Real-time information systems for hazards mitigation. In *Proceedings of the 11th World Conference on Earthquake Engineering*, paper no. 2134.
171. Nakamura, Y. (1998). A new concept for the earthquake vulnerability estimation and its application to the early warning system. In *International Conference on Early Warning Systems for Natural Disaster Reduction*, September 6-11, Potsdam, Germany.
172. Nakamura, Y. (2004). On a rational strong motion index compared with other various indices. In *Proceedings of 13th World Conference on Earthquake Engineering*, August 1-6, 2004, Vancouver, Canada.
173. Nakamura, Y., and B. E. Tucker (1988). Japan's earthquake warning system: should it be imported to California? *California Geological* **41** (2), 33-40.
174. Nakamura, Y., and J. Saita (2007a). FREQL and AcCo for a quick response to earthquakes. In *Earthquake Early Warning Systems*, ed. P. Gasparini, G. Manfredi, and J. Zschau, 307-324. Berlin and Heidelberg: Springer.
175. Nakamura, Y., and J. Saita (2007b). UrEDAS, the earthquake warning system: Today and tomorrow. In *Earthquake Early Warning Systems*, ed. P. Gasparini, G. Manfredi, and J. Zschau, 249-282. Berlin and Heidelberg: Springer.
176. Nakatani, M., S. Kaneshima S, and Y. Fukao (2000). Size-dependent microearthquake initiation inferred from high-gain and low-noise observations at Nikko district, Japan. *Journal of Geophysical Research Letters* **105** (B12), 28095-28109.
177. Nandy, D. R. (2001). Geodynamics of northeastern India and the adjoining region. *ACB Publication*, Kolkata.
178. Narayan, J. P., M. L. Sharma, and Ashwani Kumar (2002) A seismological report on the January 26, 2001 Bhuj, India earthquake. *Seismological Research Letters* **73** (3), 343-355.
179. NDMA-National Disaster Management Authority (2007). National Disaster Management Guidelines: Management of earthquakes. New Delhi, India.
180. Odaka, T., K. Ashiya, S. Tsukada, S. Sato, K. Ohtake, and D. Nozaka (2003). A new method of quickly estimating epicentral distance and magnitude from a single seismic record. *Bulletin of the Seismological Society of America* **93** (1), 526-532.
181. Oldham, T. (1883). A catalog of Indian earthquakes from the earliest times to the end of AD 1869. *Memoirs of the Geological Survey India* **19** (3), 163-215.

182. Olson, E., and R. M. Allen (2005). The deterministic nature of earthquake rupture. *Nature* **438**, 212-215.

183. Pareek, N., and M. L. Sharma (2007). Study of displacement pattern in Garhwal Kumaoun Himalaya due to Chamolli earthquake of March 29, 1999. In *Proceedings of the 8th Pacific Conference on earthquake Engineering*, December 5-7, 2007, Singapore.

184. Parkash, B., R. S. Rathor, P. Pati, R. P. Jakhmola, and S. Singh (2011). Convergence rates along the Himalayan Frontal Thrust inferred from terraces at Chandidevi Temple Hill, Hardwar, Northwestern Himalaya. *Current science* **100** (9), 1426-1432.

185. Parvez, I. A., F. Vaccari, and G. F. Panza (2003). A deterministic seismic hazard map of India and adjacent areas. *Geophysical Journal International* **155** (2), 489-508.

186. Parvez, I. A., G. F. Panza, A. A. Gusev, and F. Vaccari (2002). Strong motion amplitudes in the Himalayas and a pilot study for the deterministic first-order microzonation in a part of Delhi city. *Current Science* **82** (2), 158-166.

187. Paul, A., and M. L. Sharma (2011). Recent earthquake swarms in Garhwal Himalaya: a precursor to moderate to great earthquakes in the region. *Journal of Asian Earth Sciences* **42** (6), 1179-1186.

188. Paul, A., M. L. Sharma, and V. N. Singh (1998). Estimation of focal parameters for Uttarkashi earthquake using peak ground horizontal accelerations. *ISET Journal of Earthquake Technology* **35** (1-3), 1-8.

189. Paul, A., S. C. Gupta, and C. C. Pant (2003). Coda Q estimates for Kumaun Himalaya. *Proceeding of the Indian academy of sciences* **112** (4), 569-576.

190. Peltzer, G., and F. Saucier (1996). Present day kinematics of Asia derived from geologic fault rates. *Journal of Geophysical Research* **101** (B12), 27943-27956.

191. Powers, P. M., R. J. Lillie, and R. S. Yeats (1998). Structure and shortening of the Kangra and Dehradun re-entrants. *Bulletin of Geological Society of America* **110** (8), 1010-1027.

192. Pujol, J. (2004). Earthquake location tutorial: Graphical approach and approximate epicentral location techniques. *Seismological Research Letters* **75** (1), 63-74.

193. Pulli, J. J., and Aki, K. (1981). Attenuation of seismic waves in the lithosphere: comparison of active and stable areas. In *Earthquakes and Earthquake Engineering*:

Eastern United States, ed. J. Beavers, 129-141. Ann Arbor Science Publishers, Inc., Ann Arbor, Michigan.

194. Rastogi, B. K. (1974). Earthquake mechanisms and plate tectonics in the Himalaya region. *Tectonophysics* **21** (1), 47-56.
195. Rocker, S. W., B. Tucker, J. King, and D. Hatzfeld (1982). Estimates of Q in central Asia as a function of frequency and depth using the coda of locally recorded earthquakes. *Bulletin of the Seismological Society of America* **72** (1), 129-149.
196. Rosenberger, A. (2009). Arrival-time order location revisited. *Bulletin of the Seismological Society of America* **99** (3), 2027-2034.
197. Rydelek, P., and J. Pujol (2004). Real-time seismic warning with a 2-station subarray. *Bulletin of the Seismological Society of America* **94** (4), 1546-1550.
198. Rydelek, P., and S. Horiuchi (2006). Is earthquake rupture deterministic? *Nature* **442**, E5-E6.
199. Sato, T., and H. Kanamori (1999). Beginning of earthquakes modeled with the Griffith's fracture criterion. *Bulletin of the Seismological Society of America* **89** (1), 80-93.
200. Satriano, C., A. Lomax, and A. Zollo (2008). Real-time evolutionary earthquake location for seismic early warning. *Bulletin of the Seismological Society of America* **98** (3), 1482-1494.
201. Satriano, C., L. Elia, C. Martino, M. Lancieri, and A. Zollo (2011). Iannaccone G. PRESTo, the earthquake early warning system for Southern Italy: concepts, capabilities and future perspectives. *Soil Dynamics and Earthquake Engineering* **31** (2), 137-153.
202. Schelling, D., and K. Arita (1991). Thrust tectonics, crustal shortening and the structure of the far eastern Nepal Himalaya. *Tectonics* **10** (5), 851-862.
203. Seeber, L., and J. G. Armbruster (1981). Great detachment earthquakes along Himalayan arc and long term forecasting. In *Earthquake Prediction: An international review* **4**, ed. D. W. Simpson, and P. G. Richards, 259-279, Maurice Ewing Series. *American Geophysical Union*, Washington, United States.
204. Shanker, D., and M. L. Sharma (1998). Estimation of seismic hazard parameters for the Himalayas and its vicinity from complete data files. *Journal of Pure and Applied Geophysics* **152** (2), 267-279.

205. Sharma, M. L. (2001). Seismotectonic implications of Chamoli earthquake of March 29, 1999. In *Proceedings of Workshop on recent earthquakes of Chamoli and Bhuj* **II,** May 24-26, 2001, Roorkee, 359-368.

206. Sharma, M. L. (2003). Seismic hazard in Northern India region. *Seismological Research Letters* **74** (2), 140-146.

207. Sharma, M. L., A. Sinvhal, Y. Singh, and B. K. Maheshwari (2013). Damage survey report for Sikkim earthquake of September 18, 2013. *Seismological Research Letters* **84** (1), 49-56.

208. Sharma, M. L., and A. Tyagi (2010). Cyclic behaviour of seismogenic sources in India and use of ANN for its prediction. *Natural Hazard* **55** (2), 389-404.

209. Sharma, M. L., and C. Lindholm (2012). Earthquake hazard assessment for Dehradun, Uttarakhand, India, including a characteristic earthquake recurrence model for the Himalaya Frontal Fault (HFF). *Pure and Applied Geophysics*, **169**, 1601-1617.

210. Sharma, M. L., and H. R. Wason (1994). Occurrence of low stress drop earthquakes in the Garhwal Himalaya region. *Physics of Earth and Planetary Interiors* **85** (3-4), 265-272.

211. Sharma, M. L., and M. Arora (2005). Prediction of seismicity cycles in Himalayas using ANN. *Acta Geophysica Polonica* **53** (3), 299-309.

212. Sharma, M. L., and R. Dimri (2003). Seismic hazard estimation and seismic zonation of Northern India region for bed rock strong ground motion. *Journal of Seismology and Earthquake Engineering* **2** (2), 13-24.

213. Sharma, M. L., and R. N. Dubey (2000). Seismological Aspects, A Report on Chamoli earthquake of March 29, 1999, Published by Department of Earthquake Engineering, UOR, 1-25.

214. Sharma, M. L., H. R. Wason, and R. Dimri, (2003). Seismic zonation of Delhi for bed rock strong ground motion. *Journal of Pure and Applied Geophysics* **160**, 2381-2398.

215. Sharma, M. L., J. P. Narayan, and K. S. Rao (2004). Seismic microzonation of Delhi region in India. In *Proceedings of* the *13th World Conference Earthquake Engineering*, August 1- 6, 2004, *Vancouver*, paper no. 2046, 1-13.

216. Shieh, J. T., Y.-M. Wu, and R. M. Allen (2008). A comparison of tau-c and tau-p-max for magnitude estimation in earthquake early warning. *Geophysical Research Letters* **35** (20), L20301.

217. Shieh, J. T., Y.-M. Wu, L. Zhao, W. A. Chao, and C. F. Wu (2011). An examination of τ_c-P_d earthquake early warning method using strong motion building array. *Soil dynamics and Earthquake Engineering* **31** (2), 240-246.

218. Singh, S. K., W. K. Mohanty, B. K. Bansal, and G. S. Roonwal (2002). Ground motion in Delhi from future large/great earthquakes in the central seismic gaps of the Himalayan arc. *Bulletin of the Seismological Society of America* **92** (2), 555-569.

219. Sokolov, V., A. V. Ovcharenko, C. H. Loh, and K. L. Wen (2004). Seismic hazard assessment for the Taiwan region on the basis of recent strong-motion data and prognostic zonation of future earthquakes. *Natural Hazards* **33** (3), 319-363.

220. Sokolov, V., C. H. Loh, and K. L. Wen (2002). Comparison of the Taiwan Chi-Chi earthquake strong motion data and ground motion assessment based on spectral model from smaller earthquakes in Taiwan. *Bulletin of the Seismological Society of America*, **92** (5), 1855-1877.

221. Sokolov, V., F. Wenzel, and T. Furumura (2009). On estimation of earthquake magnitude in earthquake early warning systems. *Earth Planets Space* **61**, 1275-1285.

222. Sonley, E., and G. M. Atkinson (2001). Apparent source spectra for earthquakes in the Charlevoix seismic zone: A Comparison of direct and empirical Green's function methods. *Bulletin of the Seismological Society of America* **91** (6), 1729-1740.

223. Srivastava, H. N. (1988). The Mexican earthquake of 1985 vis-a-vis great Indian earthquakes: field and seismological aspects. *Mausam* **39**,149-158.

224. Srivastava, H. N., and P. C. S. Rao (1991). Seismicity patterns associated with earthquakes of August 1988 near Manipur Burma and Bihar Nepal regions. *Bulletin of Indian Society of Earthquake Technology* **28** (3), 13-22.

225. Srivastava, H. N., B. K., Bansal, and M. Verma (2013). Largest Earthquake in Himalaya: An Appraisal. *Journal Geological Society of India* **82** (1), 15-22.

226. Srivastava, H. N., M. Verma, and B. K. Bansal (2010). Seismological constraints for the 1905 Kangra earthquake and associated hazard in Northwest India. *Current Science* **99** (11), 1549-1559.

227. Srivastava, H. N., S. N. Bhattacharya, and G. D. Gupta (2007). *Earthquakes: Geography and Management*, New Age International Ltd., Ansari Road, Daryaganj, New Delhi-110002, paper no. 281.

228. Srivastava, P., and G. Mitra (1994). Thrust geometries and deep structure of the Outer and Lesser Himalaya, Kumaon and Garhwal (India): Implications for evolution of the Himalayan fold-and-thrust belt. *Tectonics* **13** (1), 89-109.

229. Szeliga, W., S. Hough, S. Martin, and R. Bilham (2010). Intensity, magnitude, location and attenuation in India for felt earthquakes since 1762. *Bulletin of the Seismological Society of America* **100** (2), 570-584.

230. Tandon, A. N. (1956). Zones of India liable to earthquake damage. *Indian Journal Meteorology Geophysics* **10**, 137-146.

231. Tapponnier, P., and P. Molnar (1977). Active faulting and tectonics in China. *Journal of Geophysical Research* **82** (20), 2905-2930.

232. Thakur, V. C., and S. Kumar (1995). Seismotectonics of the 20th October 1991 Uttarkashi earthquake in Garhwal Himalaya, North India. *Memoir Geological Society of India* **30,** 101-108.

233. Tsang, L., R. M. Allen, and G. Wurman (2007). Magnitude scaling relations from *P* waves in southern California. *Geophysical Research Letters* **34** (19), L19304; doi:10.1029/2007GL031077.

234. Umeda, Y. (1990). High-amplitude seismic waves radiated from the bright spot of an earthquake. *Tectonophysics* **175** (1-3), 81-92.

235. Valdiya, K. S. (1980). Geology of Kumaun Lesser Himalaya, Wadia Institute of Himalayan Geology, Dehradun, Uttaranchal. *WIHG (Wadia Institute of Himalayan Geology) Dehradun Annual Report 2003-2004*, paper no. 291.

236. Vanderkulk, W., F. Rosen, and S. Lorenz (1965). Large aperture seismic array signal processing study. *Technical report*, Rockville, Maryland.

237. Verma, R. K., and M. Mukhopadhyay (1977). An analysis of the gravity field in Northeast India. *Tectonophysics* **42** (2-4), 283-317.

238. Verma, R. K., M. Mukhopadhyay, and M. S. Ahluwalia (1976). Seismicity, gravity and tectonics of Northeast India and Northern Burma. *Bulletin of the Seismological Society of America* **66** (5), 1683-1694.

239. Wang, Q., P. Zhang, T. J. Freymueller, R. Bilham, K. M. Larson, X. Lai, X. You, Z. Niu, J. Wu, Y. Li, J. Liu, Z. Yang, and Q. Chen (2001). Present-day crustal deformation in China constrained by Global Positioning System measurements. *Science* **294**, 574-577.

240. Weber, E., V. Convertito, G. Iannaccone, A. Zollo, A. Bobbio, L. Camtore, M. Corciulo, M. Di Crosta, L. Elia, C. Martino, A. Romeo, and C. Satriano (2007). An advanced seismic network in southern Apennines (Italy) for seismicity investigations and experimentation with earthquake early warning. *Seismological Research Letters* **78** (6), 622-634.

241. Wen, K. L., C. M. Lin, H. J. Chiang, C. H. Kuo, Y. C. Huang, and H. C. Pu (2008). Effect of surface geology on ground motions: The case of station TAP056 - Chutzuhu Site. *Terrestrial, Atmospheric and Oceanic Sciences* **19** (5), 451-462.

242. Wen, K. L., T. C. Shin, Y.-M. Wu, N. C. Hsiao, and B. R. Wu (2009). Earthquake early warning technology progress in Taiwan. *Journal of Disaster Research* **4** (4), 202-210.

243. Wenzel, F., and D. Lungu (2000). Earthquake risk mitigation in Romania. In *Proceedings of Euro Conference on Global Change and Catastrophe Risk Management* **II**, Laxenburg.

244. Wenzel, F., and G. Marmureanu (2007). Rapid earthquake information for Bucharest. *Pure and Applied Geophysics* **164** (5), 929-939.

245. Wenzel, F., F. Bendimerad, and R. Sinha (2007). Megacities - megarisks. *Natural Hazards* **42**, 481-491.

246. Wenzel, F., M. Onescu, M. Baur, and F. Fiedrich (1999). An early warning system for Bucharest. *Seismological Research Letters* **70** (2), 161-169.

247. Wesnousky, S. G., S. Kumar, R. Mohindra, and V. C. Thakur (1999). Uplift and convergence along the Himalayan Frontal Thrust. *Tectonics* **18** (6), 967-976.

248. Wieland, M. (2001). Earthquake alarm, rapid response and early warning systems: Low cost systems for seismic risk reduction. In *International workshop on Disaster Reduction*, August 19-22, 2001, Reston, VA.

249. Wu, Y.-M., and H. Kanamori (2005a). Experiment on an onsite early warning method for the Taiwan early warning system. *Bulletin of the Seismological Society of America* **95** (1), 347-353.

250. Wu, Y.-M., and H. Kanamori (2005b). Rapid assessment of damage potential of earthquakes in Taiwan from the beginning of P waves. *Bulletin of the Seismological Society of America* **95** (3), 1181-1185.

251. Wu, Y.-M., and H. Kanamori (2008a). Development of an earthquake early warning system using real-time strong motion signals. *Sensors* **8** (1), 1-9.

252. Wu, Y.-M., and H. Kanamori (2008b). Exploring the feasibility of onsite earthquake early warning using close-in records of the 2007 Noto Hanto earthquake. *Earth, Planets, and Spaces* **60**, 155-160.

253. Wu, Y.-M., and L. Zhao (2006). Magnitude estimation using the first three seconds P-wave amplitude in earthquake early warning. *Geophysical Research Letters* **33** (16), L16312; doi:10.1029/2006GL026871.

254. Wu, Y.-M., H. Kanamori, R. M. Allen, and E. Hauksson (2007). Determination of earthquake early warning parameters, τ_c and P_d, for Southern California. *Geophysical Journal International* **170** (2), 711-717.

255. Wu, Y.-M., H. Y. Yen, L. Zhao, B. S. Huang, and W. T Liang (2006). Magnitude determination using initial P waves: a single-station approach. *Geophysical Research Letters* **33** (5), L05306; doi:10.1029/2005GL025395.

256. Wurman, G., R. M. Allen, and P. Lombard (2007). Toward earthquake early warning in northern California. *Journal of Geophysical Research* **112** (B8), B08311; doi:10.1029/2006JB004830.

257. Zollo A., O. Amoroso, M. Lancieri, Y-.M. Wu, and H. Kanamori (2010). A threshold-based earthquake early warning using dense accelerometer networks. *Geophysical Journal International* **183** (2), 963-974.

258. Zollo, A., G. lannaccone, M. Lancieri, L. Cantore, V. Convertito, A. Emolo, G. Festa, F. Gallovic, M. Vassallo, C. Martino, C. Satriano, and P. Gasparini (2009). Earthquake early warning system in southern Italy: Methodologies and performance evaluation. *Geophysical Research Letters* **36** (5), LOOB07; doi:10.1029/2008GL036689.

259. Zollo, A., M. Lancieri, and S. Nielsen (2006). Earthquake magnitude estimation from peak amplitudes of very early seismic signals on strong motion records. *Geophysical Research Letters* **33** (23), L23312; doi:10.1029/2006GL027795.

LIST OF PUBLICATIONS

National and International Journals

1. Bhardwaj, R., M. L. Sharma, and A. Kumar (2013). Inclusion of Q-value in parameters used for earthquake early warning systems. *Disaster Advances* **6** (5), 54-60.
2. Bhardwaj, R., M. L. Sharma, and A. Kumar (2013). Earthquake magnitude prediction for real time EEW system: An automization from P-wave time window analysis. *Himalayan Geology* **34** (1), 84-91.
3. Bhardwaj, R., A. Kumar, and M. L. Sharma (2013). Root sum of squares cumulative velocity: An attribute for earthquake early warning. *Disaster Advances* **6** (3), 24-31.
4. Kumar A., A. Kumar, H. Mittal, A. Kumar, and R. Bhardwaj (2012). Software to Estimate Earthquake Spectral and Source Parameters. *International Journal of Geosciences* **3** (5), 1142-1149.

National and International Conferences

1. Bhardwaj, R., A. Kumar, and M. L. Sharma (2012). Analysis of Tauc (τ_c) and P_d attributes for earthquake early warning in India. In *15th World Conference on Earthquake Engineering*, Lisbon, paper no. 0696, 1-8.
2. Bhardwaj, R., A. Kumar, and M. L. Sharma (2012). Effect of medium characteristics in magnitude estimation for earthquake early warning systems. In *Golden Jubilee Symposium Indian Society of Earthquake Technology (ISET)*, Department of earthquake engineering building IIT Roorkee, Roorkee, paper no. H002, 1-10.
3. Bhardwaj, R., M. L. Sharma, and A. Kumar (2012). P-wave time window approach for EEW systems. In *National Workshop on Engineering Geophysics for Civil Engineering and Geo-hazards* (EGCEG), CSIR- Central Building Research Institute, Roorkee.
4. Bhardwaj, R., A. Kumar, and M. L. Sharma (2010). An algorithm for automatic detection of primary wave onset for early warning system. In *14th Symposium on Earthquake Engineering*, Roorkee, India, 373-380.

APPENDIX (A)

Appendix (A) presents the details of all the recording stations on which the considered events from Indian, K-NET and PEER-NGA have been recorded.

A. 1 Details of Indian strong motion stations used in present study.

S. No.	Name of station	Station code	Latitude (°N)	Longitude (°E)	Region
1	BAGESHWAR	BAG	29.83	79.77	Kumaon
2	BALLABHGARH	BAL	28.34	77.32	National Capital Region
3	BARKOT	BAR	30.81	78.21	Garhwal Himalaya
4	BHAWNAGAR	BHA	31.55	77.92	Northwest Himalaya
5	CHAKRATA	CKR	30.69	77.90	Garhwal Himalaya
6	CHAMOLI	CHA	30.41	79.32	Garhwal Himalaya
7	CHAMPAWAT	CHP	29.33	80.09	Kumaon
8	DEHRADUN	DEH	30.32	78.04	Garhwal Himalaya
9	DELHI COLLEGE of ENGINEERING	DCE	28.80	77.12	National Capital Region
10	DELHI JAL BOARD	DJB	28.65	77.19	National Capital Region
11	DELHI RIDGE	RGD	28.68	77.21	National Capital Region
12	DELHI UNIVERSITY	DLU	28.69	77.21	National Capital Region
13	DHARCHULA	DHA	29.85	80.55	Kumaon
14	DHUBRI	DHU	26.02	90.00	Northeast Himalaya
15	GANGTOK	GTK	27.35	88.63	Northeast Himalaya
16	GARSAIN	GAR	30.05	79.29	Kumaon
17	GURGAON	GUR	28.45	77.03	National Capital Region
18	GURU GOVIND SINGH INDRAPRASTH UNIVERSITY	GGI	28.66	77.23	National Capital Region
19	GUWHATI	GUA	26.19	91.75	Northeast Himalaya
20	HAMIRPUR	HAM	31.69	76.52	Northwest Himalaya
21	KAPKOT	KAP	29.94	79.90	Kumaon
22	KHOKRAJHAR	KOK	26.40	90.26	Northeast Himalaya
23	KULLU	KUL	31.96	77.11	Northwest Himalaya

S. No.	Name of station	Station code	Latitude (°N)	Longitude (°E)	Region
24	LODHI ROAD DELHI	LDR	28.53	77.27	National Capital Region
25	MANDI	MAN	31.71	76.93	Northwest Himalaya
26	MUNSYARI	MUN	30.07	80.24	Kumaon
27	NAUGAON	NAU	26.35	92.69	Northeast Himalaya
28	NOIDA	NOI	28.51	77.48	National Capital Region
29	PITHORAGARH	PIT	29.58	80.21	Kumaon
30	RAJA GARDEN	RGD	28.66	77.12	National Capital Region
31	RAMPUR	RAM	28.79	79.01	Northwest Himalaya
32	REKONGPEO	PEO	31.54	78.27	Northwest Himalaya
33	ROHTAK	ROH	28.90	76.59	National Capital Region
34	SONIPAT	SON	29.00	77.00	National Capital Region
35	TEHRI	THE	30.37	78.43	Garhwal Himalaya
36	TEZPUR	TEP	26.62	92.80	Northeast Himalaya
37	TURA	TUR	25.51	90.22	Northeast Himalaya
38	UTTARKASHI	UTK	30.73	78.44	Garhwal Himalaya

A. 2 Details of strong K-NET motion stations used in present study.

S. No.	Site name	Station code	Latitude (°N)	Longitude (°E)
1	BISAI	AIC001	35.30	136.75
2	KOMAKI	AIC002	35.30	136.92
3	TSUSHIMA	AIC003	35.17	136.74
4	NAGOYA	AIC004	35.06	136.97
5	FUJIOKA	AIC005	35.20	137.21
6	TOYOTA	AIC009	35.08	137.15
7	TSUKUDE	AIC010	34.98	137.42
8	CHITA	AIC011	35.00	136.86
9	ANJOH	AIC012	34.91	137.04
10	NAGASHINO	AIC013	34.93	137.58
11	GAMAGOHRI	AIC014	34.83	137.22

S. No.	Site name	Station code	Latitude (°N)	Longitude (°E)
12	TOYOHASHI	AIC015	34.75	137.40
13	MIHAMA	AIC016	34.78	136.91
14	TAHARA	AIC017	34.67	137.26
15	OHDATE	AKT002	40.27	140.57
16	KADUNO	AKT006	40.22	140.79
17	MIYATA	AKT011	39.81	140.58
18	TAZAWAKO	AKT012	39.70	140.72
19	KYOWA	AKT013	39.61	140.32
20	KAKUNODATE	AKT014	39.60	140.56
21	HONJOH	AKT015	39.38	140.05
22	OHMAGARI	AKT016	39.45	140.48
23	YOKOTE	AKT017	39.30	140.56
24	CHOHKAI	AKT018	39.19	140.19
25	OGACHI	AKT019	39.04	140.45
26	KISAKATA	AKT020	39.20	139.91
27	ANI	AKT021	40.00	140.40
28	TAMAGAWA	AKT022	39.77	140.67
29	TSUBAKIDAI	AKT023	39.15	140.72
30	SHIROI	CHB003	35.79	140.06
31	SAWARA	CHB004	35.90	140.49
32	CHOHSHI	CHB005	35.74	140.83
33	NARITA	CHB006	35.78	140.31
34	SAKURA	CHB007	35.72	140.23
35	URAYASU	CHB008	35.65	139.90
36	CHIBA	CHB009	35.61	140.10
37	YOHKAICHIBA	CHB010	35.71	140.57
38	HASUNUMA	CHB011	35.60	140.50
39	TOHGANE	CHB012	35.57	140.33
40	MOBARA	CHB013	35.43	140.29
41	ANEZAKI	CHB014	35.48	140.05
42	KISARADU	CHB015	35.37	139.92
43	MISAKI	CHB016	35.30	140.39

S. No.	Site name	Station code	Latitude (°N)	Longitude (°E)
44	ICHIBA	CHB017	35.30	140.08
45	KATSUURA	CHB018	35.16	140.32
46	KYONAN	CHB019	35.11	139.84
47	KAMOGAWA	CHB020	35.12	140.10
48	SHIRAHAMA	CHB021	34.91	139.90
49	FUTTSU	CHB022	35.31	139.86
50	INAGE	CHB024	35.63	140.08
51	CHIKURA	CHB025	34.97	139.95
52	CHOUNAN	CHB026	35.39	140.24
53	ICHIKAWA-KITA	CHB028	35.77	139.97
54	GYOUTOKU	CHB029	35.69	139.92
55	KOSHINO	FKI002	36.04	136.01
56	FUKUI	FKI003	36.04	136.23
57	OHNO	FKI004	35.98	136.49
58	TAKEFU	FKI005	35.91	136.17
59	IMAJOH	FKI006	35.77	136.20
60	TSURUGA	FKI007	35.64	136.06
61	MIKATA	FKI008	35.55	135.91
62	OBAMA	FKI009	35.50	135.75
63	TAKAHAMA	FKI010	35.49	135.55
64	IZUMI	FKI011	35.91	136.67
65	MIKUNI	FKO001	33.85	130.51
66	KOSHINO	FKO002	33.83	130.71
67	FUKUI	FKO003	33.83	130.90
68	TAKEFU	FKO005	33.65	130.70
69	IMAJOH	FKO006	33.60	130.40
70	TSURUGA	FKO007	33.56	130.20
71	MIKATA	FKO008	33.57	130.85
72	OBAMA	FKO009	33.50	130.52
73	TAKAHAMA	FKO010	33.42	130.67
74	IZUMI	FKO011	33.32	130.51
75	UKIHA	FKO012	33.33	130.79

S. No.	Site name	Station code	Latitude (°N)	Longitude (°E)
76	YAME	FKO013	33.23	130.56
77	YANAGAWA	FKO015	33.16	130.41
78	SOHMA	FKS001	37.79	140.92
79	YANAGAWA	FKS002	37.84	140.60
80	IITATE	FKS004	37.68	140.73
81	HARAMACHI	FKS005	37.64	140.98
82	KATSURAO	FKS006	37.50	140.76
83	FUNEHIKI	FKS008	37.44	140.57
84	ONO	FKS009	37.28	140.63
85	HIRONO	FKS010	37.23	141.00
86	IWAKI	FKS011	37.09	140.90
87	NAKOSO	FKS012	36.91	140.79
88	FURUDONO	FKS013	37.09	140.56
89	YAMATSURI	FKS014	36.87	140.43
90	TANAGURA	FKS015	37.02	140.38
91	SHIRAKAWA	FKS016	37.12	140.19
92	SUKAGAWA	FKS017	37.28	140.37
93	KOHRIYAMA	FKS018	37.40	140.36
94	NIHOMMATSU	FKS019	37.60	140.44
95	INAWASHIRO	FKS020	37.55	140.11
96	KITAKATA	FKS021	37.65	139.86
97	NISHIAIDU	FKS022	37.60	139.65
98	AIDUWAKAMATSU	FKS023	37.48	139.93
99	NAKANO	FKS024	37.40	140.13
100	SHIMOGOH	FKS025	37.31	139.90
101	NANGOH	FKS026	37.27	139.54
102	TAKINOHARA	FKS027	37.07	139.68
103	TADAMI	FKS028	37.35	139.31
104	HINOEMATA	FKS029	37.02	139.38
105	KANEYAMA	FKS030	37.45	139.51
106	KAWAUCHI	FKS031	37.34	140.81
107	KAWAI	GIF002	36.27	137.03

S. No.	Site name	Station code	Latitude (°N)	Longitude (°E)
108	KAMIOKA	GIF003	36.33	137.30
109	TOCHIO	GIF004	36.25	137.52
110	TAKAYAMA	GIF005	36.15	137.25
111	TAKANE	GIF007	36.04	137.49
112	OSAKA	GIF008	35.95	137.26
113	SHIROTORI	GIF009	35.92	136.83
114	HIGASHISUGIHARA	GIF012	35.64	136.49
115	MINO	GIF015	35.55	136.91
116	IBIGAWA	GIF017	35.49	136.57
117	GIFU	GIF020	35.42	136.76
118	MINOKAMO	GIF021	35.44	137.00
119	KAMIISHIDU	GIF022	35.28	136.47
120	MIYAMA	GIF026	35.59	136.74
121	KATASHINA	GNM001	36.77	139.22
122	MINAKAMI	GNM002	36.78	138.97
123	NUMATA	GNM003	36.66	139.08
124	KUSATSU	GNM004	36.62	138.59
125	TSUMAGOI	GNM005	36.51	138.52
126	AGATSUMA	GNM006	36.51	138.75
127	SHIBUKAWA	GNM007	36.46	139.01
128	TAKANO	HRS001	35.03	132.90
129	TOHJOH	HRS002	34.90	133.28
130	MIYOSHI	HRS003	34.81	132.84
131	GEIHOKU	HRS004	34.73	132.28
132	TOYOHIRA	HRS006	34.67	132.41
133	KOHNU	HRS007	34.70	133.09
134	MUKAIHARA	HRS008	34.61	132.72
135	YUKI	HRS009	34.49	132.28
136	OHNO	HRS014	34.29	132.28
137	SAIJOH	HRS021	34.95	133.12
138	HAMASAKA	HYG001	35.62	134.45
139	KASUMI	HYG002	35.64	134.63

S. No.	Site name	Station code	Latitude (°N)	Longitude (°E)
140	IZUSHI	HYG003	35.46	134.88
141	MURAOKA	HYG004	35.46	134.57
142	WADAYAMA	HYG005	35.34	134.86
143	HAGA	HYG007	35.16	134.55
144	IKUNO	HYG008	35.15	134.79
145	KUROI	HYG009	35.17	135.10
146	TANNAN	HYG010	35.06	135.18
147	KOHDUKI	HYG011	34.98	134.32
148	YAMASAKI	HYG012	35.00	134.55
149	ICHIKAWA	HYG013	34.99	134.76
150	NISHIWAKI	HYG015	34.95	135.27
151	SANDA	HYG022	34.75	135.35
152	SUMOTO	HYG025	34.34	134.90
153	GOSHIKI	HYG026	34.41	134.79
154	NANDAN	HYG027	34.25	134.73
155	DAIGO	IBR001	36.78	140.36
156	TAKAHAGI	IBR002	36.71	140.71
157	HITACHI	IBR003	36.59	140.65
158	OHMIYA	IBR004	36.55	140.41
159	KASAMA	IBR005	36.39	140.24
160	MITO	IBR006	36.37	140.45
161	NAKAMINATO	IBR007	36.35	140.60
162	HOKOTA	IBR013	36.16	140.49
163	EDOSAKI	IBR017	35.95	140.32
164	KASHIMA	IBR018	35.98	140.63
165	OHYA	ISK001	37.50	137.18
166	SHOHIN	ISK002	37.44	137.29
167	WAJIMA	ISK003	37.39	136.91
168	NOTO	ISK004	37.31	137.15
169	ANAMIZU	ISK005	37.23	136.90
170	TOGI	ISK006	37.16	136.69
171	NANAO	ISK007	37.04	136.97

S. No.	Site name	Station code	Latitude (°N)	Longitude (°E)
172	HAKUI	ISK008	36.89	136.78
173	NANATSUKA	ISK009	36.73	136.70
174	DAITOH	IWT009	39.02	141.40
175	ICHINOSEKI	IWT010	38.93	141.12
176	MIZUSAWA	IWT011	39.15	141.15
177	KITAKAMI	IWT012	39.32	141.14
178	TOHNO	IWT013	39.34	141.54
179	ISHIDORIYA	IWT014	39.48	141.15
180	KAWAJIRI	IWT015	39.32	140.78
181	KADOMA	IWT017	39.63	141.44
182	MORIOKA	IWT018	39.70	141.15
183	YABUKAWA	IWT020	39.78	141.33
184	NISHINE	IWT021	39.92	141.08
185	KUZUMAKI	IWT023	40.04	141.45
186	OHSHIDA	IWT025	39.52	140.83
187	AISARI	IWT026	39.26	141.10
188	AZUMA	KGS001	32.19	130.18
189	IZUMI	KGS002	32.09	130.35
190	OHKUCHI	KGS003	32.06	130.59
191	AKUNE	KGS004	32.01	130.19
192	MIYANOJOH	KGS005	31.90	130.45
193	YOKOGAWA	KGS006	31.91	130.70
194	SENDAI	KGS007	31.81	130.30
195	KAMOH	KGS008	31.76	130.57
196	KOKUBU	KGS009	31.74	130.76
197	KUSHIKINO	KGS010	31.71	130.27
198	HIYOSHI	KGS011	31.59	130.35
199	KAGOSHIMA	KGS012	31.61	130.57
200	OHSAKI	KGS015	31.43	131.01
201	KASEDA	KGS016	31.42	130.32
202	UCHINOURA	KGS022	31.28	131.05
203	KAMIKOSHIKI	KGS036	31.84	129.87

S. No.	Site name	Station code	Latitude (°N)	Longitude (°E)
204	SHIMOKOSHIKI	KGS037	31.64	129.71
205	TANOURA	KMM013	32.37	130.51
206	MINAMATA	KMM015	32.22	130.40
207	HITOYOSHI	KMM016	32.22	130.73
208	RYUHGATAKE	KMM018	32.39	130.39
209	HONDO	KMM019	32.46	130.19
210	SHINWA	KMM020	32.36	130.18
211	AMAKUSA	KMM021	32.38	130.00
212	USHIBUKA	KMM022	32.19	130.03
213	YOKOSUKA	KNG003	35.27	139.66
214	MISAKI	KNG004	35.14	139.62
215	KAMAKURA	KNG005	35.32	139.55
216	FUJISAWA	KNG007	35.34	139.49
217	ATSUGI	KNG009	35.44	139.36
218	HIRATSUKA	KNG010	35.34	139.35
219	FIJINO	KNG011	35.62	139.15
220	HADANO	KNG012	35.38	139.20
221	ODAWARA	KNG013	35.26	139.15
222	HIRATSUKA-ST2	KNG202	34.74	139.84
223	HIRATSUKA-ST3	KNG203	34.80	139.64
224	HIRATSUKA-ST4	KNG204	34.89	139.57
225	HIRATSUKA-ST5	KNG205	34.94	139.42
226	HIRATSUKA-ST6	KNG206	35.10	139.38
227	KUMIHAMA	KYT002	35.60	134.89
228	MIYADU	KYT004	35.54	135.20
229	MAIDURU	KYT005	35.48	135.39
230	FUKUCHIYAMA	KYT006	35.28	135.18
231	ASHIU	KYT007	35.31	135.71
232	HONJOH	KYT008	35.26	135.40
233	HIYOSHI	KYT009	35.16	135.50
234	OHFUSE	KYT010	35.21	135.77
235	KAMEOKA	KYT011	35.02	135.56

S. No.	Site name	Station code	Latitude (°N)	Longitude (°E)
236	KYOTO	KYT012	35.00	135.82
237	UJI	KYT013	34.88	135.80
238	MINAMIYAMASHIRO	KYT014	34.77	135.99
239	FUJIWARA	MIE001	35.17	136.49
240	KOMONO	MIE002	35.03	136.51
241	YOKKAICHI	MIE003	34.97	136.64
242	KAMEYAMA	MIE004	34.86	136.45
243	UENO	MIE005	34.77	136.12
244	TSU	MIE006	34.72	136.50
245	HAKUSAN	MIE007	34.64	136.34
246	NABARI	MIE008	34.63	136.11
247	MATSUZAKA	MIE009	34.58	136.53
248	ISE	MIE010	34.49	136.73
249	IITAKA	MIE011	34.43	136.33
250	NANTOH	MIE013	34.28	136.50
251	MIYAKAWA	MIE017	34.36	136.33
252	KESENNUMA	MYG001	38.90	141.57
253	UTATSU	MYG002	38.73	141.51
254	TOHWA	MYG003	38.73	141.31
255	TSUKIDATE	MYG004	38.73	141.02
256	NARUKO	MYG005	38.80	140.65
257	FURUKAWA	MYG006	38.58	140.97
258	TOYOSATO	MYG007	38.59	141.25
259	KITAKAMI	MYG008	38.58	141.45
260	TAIWA	MYG009	38.45	140.89
261	ISHINOMAKI	MYG010	38.43	141.28
262	OSHIKA	MYG011	38.30	141.50
263	SHIOGAMA	MYG012	38.32	141.03
264	SENDAI	MYG013	38.27	140.93
265	SAKUNAMI	MYG014	38.32	140.64
266	IWANUMA	MYG015	38.10	140.87
267	SHIOISHI	MYG016	38.01	140.62

S. No.	Site name	Station code	Latitude (°N)	Longitude (°E)
268	KAKUDA	MYG017	37.98	140.78
269	TSUNO	MYZ006	32.26	131.56
270	SAITO	MYZ008	32.11	131.39
271	EBINO	MYZ009	32.05	130.81
272	KOBAYASHI	MYZ010	32.00	130.97
273	MIYAZAKI	MYZ013	31.91	131.42
274	TANO	MYZ014	31.85	131.30
275	NICHINAN	MYZ016	31.61	131.37
276	KUSHIMA	MYZ017	31.46	131.23
277	TOIMISAKI	MYZ018	31.40	131.31
278	IKOMA	NAR001	34.72	135.73
279	NARA	NAR002	34.67	135.84
280	HAIBARA	NAR004	34.53	135.95
281	GOJOH	NAR005	34.34	135.69
282	OHTOH	NAR007	34.22	135.74
283	TOTSUKAWA	NAR009	33.94	135.76
284	IIYAMA	NGN001	36.85	138.37
285	SHINANO	NGN002	36.81	138.21
286	YAMANOUCHI	NGN003	36.74	138.41
287	NAGANO	NGN004	36.65	138.19
288	HAKUBA	NGN005	36.70	137.85
289	OHMACHI	NGN006	36.51	137.85
290	KUISEKE	NGN007	36.53	138.12
291	UEDA	NGN008	36.40	138.25
292	HOTAKA	NGN009	36.34	137.87
293	NAGATO	NGN011	36.26	138.27
294	MATSUMOTO	NGN012	36.26	137.98
295	AZUMI	NGN013	36.18	137.79
296	NARAKAWA	NGN017	35.97	137.83
297	KISOFUKUSHIMA	NGN019	35.86	137.71
298	NOMOZAKI	NGS013	32.58	129.76
299	GOHNOURA	NGS023	33.75	129.69

S. No.	Site name	Station code	Latitude (°N)	Longitude (°E)
300	RYOHTSU	NIG002	38.07	138.44
301	SAWATA	NIG003	38.00	138.32
302	OGI	NIG004	37.82	138.28
303	MATSUGASAKI	NIG005	37.92	138.50
304	NIIGATA	NIG010	37.91	139.01
305	NIITSU	NIG011	37.80	139.14
306	KANOSE	NIG012	37.69	139.48
307	MAKI	NIG013	37.76	138.88
308	SANJOH	NIG014	37.64	138.96
309	MURAMATSU	NIG015	37.69	139.19
310	TERADOMARI	NIG016	37.64	138.77
311	NAGAOKA	NIG017	37.44	138.84
312	KASHIWAZAKI	NIG018	37.37	138.56
313	OJIYA	NIG019	37.30	138.81
314	KOIDE	NIG020	37.23	138.96
315	TOHKAMACHI	NIG021	37.13	138.75
316	SHIOZAWA	NIG022	37.04	138.85
317	TSUNAN	NIG023	37.01	138.65
318	YASUDUKA	NIG024	37.13	138.44
319	NAOETSU	NIG025	37.16	138.22
320	ARAI	NIG026	37.02	138.25
321	ITOIGAWA	NIG027	37.02	137.86
322	NAGAOKA-SHISHO	NIG028	37.43	138.89
323	YUBARA	OKY001	35.19	133.73
324	KAMO	OKY002	35.18	134.05
325	NISHIAWAKURA	OKY003	35.17	134.34
326	NIIMI	OKY004	34.96	133.50
327	OCHIAI	OKY005	35.01	133.73
328	TSUYAMA	OKY006	35.07	134.01
329	TAKAHASHI	OKY007	34.78	133.61
330	TAKEBE	OKY008	34.87	133.90
331	YOSHII	OKY009	34.92	134.09

S. No.	Site name	Station code	Latitude (°N)	Longitude (°E)
332	KAMISAIBARA	OKY015	35.28	133.93
333	NOSE	OSK001	34.97	135.39
334	TAKATSUKI	OSK002	34.86	135.60
335	TOYONAKA	OSK003	34.77	135.47
336	SHIJOHNAWATE	OSK004	34.74	135.64
337	OHSAKA	OSK005	34.73	135.51
338	KISHIWADA	OSK008	34.44	135.39
339	KAWACHINAGANO	OSK009	34.44	135.58
340	SENNAN	OSK010	34.38	135.25
341	CHINZEI	SAG001	33.53	129.88
342	KARATSU	SAG002	33.42	129.92
343	FUJI	SAG003	33.37	130.21
344	IMARI	SAG004	33.26	129.88
345	KYUHRAGI	SAG005	33.32	130.06
346	TAKEO	SAG006	33.19	130.03
347	SAGA	SAG007	33.26	130.30
348	YOGO	SIG001	35.54	136.21
349	IMADU	SIG002	35.42	136.02
350	NAGAHAMA	SIG003	35.38	136.26
351	KUTSUKI	SIG004	35.35	135.92
352	HIKONE	SIG005	35.25	136.24
353	SHIGA	SIG006	35.20	135.92
354	OUMIHACHIMAN	SIG007	35.14	136.09
355	EIGENJI	SIG008	35.07	136.29
356	KOHSEI	SIG009	35.01	136.09
357	OHTSU	SIG010	34.97	135.90
358	SHIGARAKI	SIG011	34.88	136.06
359	KOHGA	SIG012	34.90	136.23
360	MIHONOSEKI	SMN001	35.54	133.16
361	MATSUE	SMN002	35.47	133.07
362	YOKOTA	SMN003	35.18	133.09
363	KISUKI	SMN004	35.29	132.90

S. No.	Site name	Station code	Latitude (°N)	Longitude (°E)
364	IZUMO	SMN005	35.36	132.74
365	OHTA	SMN006	35.19	132.50
366	OOCHI	SMN007	35.08	132.59
367	MIZUHO	SMN008	34.85	132.53
368	GOHTSU	SMN009	35.01	132.22
369	HIKIMI	SMN011	34.57	132.01
370	MUIKAICHI	SMN012	34.35	131.94
371	MASUDA	SMN013	34.67	131.85
372	TSUWANO	SMN014	34.47	131.78
373	HIROSE	SMN015	35.36	133.17
374	KAKEYA	SMN016	35.20	132.81
375	ATAMI	SZO001	35.14	139.08
376	ITOH	SZO002	34.97	139.10
377	HIGASHIIZU	SZO003	34.82	139.05
378	MINAMIIZU	SZO004	34.65	138.82
379	MATSUZAKI	SZO005	34.75	138.78
380	TOI	SZO006	34.91	138.79
381	SHUZENJI	SZO007	34.98	138.95
382	NUMADU	SZO008	35.10	138.87
383	SUSONO	SZO009	35.20	138.91
384	GOTEMBA	SZO010	35.31	138.93
385	FUJINOMIYA	SZO011	35.21	138.60
386	KAMBARA	SZO012	35.13	138.62
387	SHIMIZU	SZO013	35.04	138.48
388	SHIZUOKA	SZO014	34.96	138.37
389	UMEGASHIMA	SZO015	35.24	138.34
390	YAIDU	SZO016	34.86	138.31
391	HAMAOKA	SZO017	34.64	138.13
392	HAIBARA	SZO018	34.74	138.22
393	KAKEGAWA	SZO019	34.77	138.00
394	HONKAWANE	SZO021	35.10	138.13
395	TENRYUH	SZO023	34.87	137.82

S. No.	Site name	Station code	Latitude (°N)	Longitude (°E)
396	HAMAMATSU	SZO024	34.71	137.72
397	KOSAI	SZO025	34.72	137.53
398	HARUNO	SZO026	34.98	137.90
399	NISHIIZU	SZO027	34.79	138.80
400	KAWANA	SZO028	34.95	139.14
401	KUROISO	TCG001	36.94	140.08
402	SHIOBARA	TCG002	36.99	139.80
403	FUJIWARA	TCG003	36.81	139.72
404	YUMOTO	TCG005	36.81	139.93
405	YAITA	TCG006	36.76	140.13
406	OGAWA	TCG013	36.44	140.02
407	MOTEGI	TCG014	36.55	140.17
408	KITATAKAOKA	TCG016	36.53	140.16
409	NARUTO	TKS001	34.20	134.61
410	TOKUSHIMA	TKS002	34.04	134.58
411	ANAN	TKS003	33.87	134.60
412	OKADA	TKY008	34.79	139.39
413	HABUMINATO	TKY009	34.69	139.44
414	NIIJIMA	TKY010	34.38	139.26
415	KAMITSUKI	TKY011	34.12	139.53
416	SUNAMACHI	TKY013	35.66	139.83
417	SHINONOME	TKY016	35.65	139.80
418	TATSUMI	TKY017	35.65	139.81
419	HACHIEDA	TKY018	35.66	139.81
420	SHINOZAKI	TKY025	35.71	139.90
421	UKITA	TKY026	35.67	139.86
422	MIZUE	TKY027	35.69	139.89
423	WAKASA	TTR001	35.34	134.40
424	TOTTORI	TTR002	35.49	134.22
425	MOCHIGASE	TTR003	35.34	134.21
426	SHIKANO	TTR004	35.46	134.07
427	KURAYOSHI	TTR005	35.43	133.83

S. No.	Site name	Station code	Latitude (°N)	Longitude (°E)
428	AKASAKI	TTR006	35.51	133.63
429	KOHFU	TTR007	35.28	133.49
430	YONAGO	TTR008	35.43	133.33
431	NICHINAN	TTR009	35.17	133.31
432	SAKAI	TYM001	36.98	137.63
433	HIMI	TYM002	36.87	136.97
434	UODU	TYM003	36.82	137.42
435	UNADUKI	TYM004	36.86	137.53
436	SHINMINATO	TYM005	36.78	137.08
437	TOYAMA	TYM007	36.67	137.21
438	OHYAMA	TYM008	36.61	137.28
439	YATSUO	TYM009	36.59	137.14
440	ASHIKURA	TYM011	36.58	137.39
441	TOGA	TYM012	36.44	137.04
442	WAKAYAMA	WKY001	34.23	135.17
443	NAGA	WKY002	34.28	135.43
444	ARIDA	WKY003	34.10	135.12
445	SHIMIZU	WKY004	34.08	135.43
446	RYUHJIN	WKY005	33.89	135.49
447	GOBOH	WKY006	33.89	135.15
448	HONGUH	WKY007	33.84	135.77
449	TANABE	WKY008	33.73	135.38
450	SUSAMI	WKY010	33.55	135.50
451	KOHYA	WKY013	34.22	135.59
452	KOMORI	WKY014	33.71	135.64
453	SUSA	YMG001	34.62	131.60
454	HAGI	YMG002	34.41	131.40
455	IKUMONAKA	YMG003	34.38	131.60
456	NAGATO	YMG004	34.37	131.18
457	MINE	YMG007	34.17	131.21
458	YAMAGUCHI	YMG008	34.01	131.40
459	KANO	YMG009	34.23	131.82

S. No.	Site name	Station code	Latitude (°N)	Longitude (°E)
460	MIKAWA	YMG010	34.23	131.98
461	HOHFU	YMG013	34.03	131.53
462	TOKUYAMA	YMG014	34.05	131.81
463	KUGA	YMG015	34.10	132.08
464	IWAKUNI	YMG016	34.17	132.18
465	TABAYAMA	YMN001	35.79	138.92
466	OHTSUKI	YMN002	35.61	138.95
467	FUJIYOSHIDA	YMN003	35.46	138.81
468	ENZAN	YMN004	35.70	138.73
469	KOHFU	YMN005	35.65	138.57
470	MOTOSU	YMN006	35.47	138.61
471	NAMBU	YMN007	35.28	138.46
472	HAYAKAWA	YMN008	35.43	138.33
473	ROKUGOH	YMN009	35.50	138.46
474	ASHIYASU	YMN011	35.64	138.38
475	TABAYAMA	YMT001	38.91	139.81
476	SHINJOH	YMT002	38.77	140.30
477	TSURUOKA	YMT003	38.73	139.80
478	HIJIORI	YMT005	38.61	140.16
479	OBANAZAWA	YMT006	38.60	140.41
480	HIGASHINE	YMT007	38.43	140.39
481	SAGAE	YMT009	38.39	140.27
482	YAMAGATA	YMT010	38.26	140.35
483	KAMINOYAMA	YMT011	38.15	140.27
484	KIYOKAWA	YMT016	38.79	140.02
485	SINJYO-SHISHO	YMT017	38.79	140.31

A. 3 Details of PEER-NGA strong motion stations used in present study.

S. No.	Station name	Latitude (°N)	Longitude (°E)
1	CWB 99999 KAU050	23.16	120.76
2	CWB 99999 TCU078	23.81	120.85
3	CDMG 12966 Indian Wells - Hwy111 & El Dorad	33.72	-116.338
4	CDMG 47524 Hollister - South & Pine	36.8480	-121.397
5	CWB 99999 CHY026	23.7987	120.4113
6	CWB 99999 CHY035	23.5200	120.5840
7	CWB 99999 CHY087	23.38	120.5190
8	CWB 99999 HWA037	23.45	121.3840
9	CWB 99999 TCU052	24.1980	120.7393
10	CWB 99999 TCU076	23.91	120.6757
11	CWB 99999 TCU082	24.15	120.6760
12	CWB 99999 TCU089	23.90	120.8565
13	CWB 99999 TCU107	24.07	120.5402
14	CWB 99999 TCU110	23.96	120.57
15	CWB 99999 TCU112	24.06	120.4240
16	CWB 99999 TCU116	23.86	120.58
17	CWB 99999 TCU117	24.1335	120.4598
18	CWB 99999 TCU120	23.9803	120.61
19	CWB 99999 TCU137	24.1850	120.9220
20	CWB 99999 TCU138	23.92	120.5955

S. No.	Station name	Latitude (°N)	Longitude (°E)
21	CWB 99999 TTN051	23.19	121.0168
22	CWB 9999917 ALS	23.51	120.81
23	ERD 99999 Izmit	40.7900	29.9600
24	LAMONT 1060 Lamont 1060	40.78	30.6130
25	USGS 1742 San Jose - Weather Station	37.35	-121.904
26	USGS 1760 Benicia Fire Station #1	38.05	-122.157
27	CDMG 12092 Radec - Sage & Cottonwood School	33.48	-116.911
28	CDMG 12116 Idyllwild - Hwy 243 & Pine Crest	33.75	-116.715
29	CDMG 12331 Hemet Fire Station	33.73	-116.979
30	CDMG 12636 Sage - Fire Station	33.58	-116.931
31	CDMG 12919 Beaumont - 6th & Maple	33.9300	-116.972
32	CDMG 12923 Hemet - Acacia & Stanford	33.7440	-116.931
33	CDMG 12951 La Quinta - Bermudas & Durango	33.6710	-116.300
34	CDMG 12952 Palm Desert - Country Club & Por	33.76	-116.374
35	CDMG 12953 Rancho Mirage - G Ford & B Hope	33.79	-116.41
36	CDMG 13066 Anaheim - Brookhurst & Crescent	33.84	-117.957
37	CDMG 13099 Corona - 6th & Smith	33.88	-117.593
38	CDMG 13100 Corona - Green River & Cyn Crest	33.88	-117.636
39	CDMG 13873 Brea - Central Ave Caltrans Yard	33.93	-117.896
40	CDMG 13879 Fullerton - Valencia&Brookhurst	33.87	-117.958
41	CDMG 13880 Fullerton - Hermosa & Harbor	33.9100	-117.930

S. No.	Station name	Latitude (°N)	Longitude (°E)
42	CDMG 13881 La Habra - La Habra&Monte Vista	33.93	-117.96
43	CDMG 22959 Landers - Hwy 247 & Jesse	34.2820	-116.453
44	CDMG 23542 San Bernardino - E & Hospitality	34.0650	-117.29
45	CDMG 23583 Hesperia - 4th & Palm	34.41	-117.313
46	CDMG 23780 San Bernardino - Mtn Vw & Clstr	34.10	-117.286
47	CDMG 23898 San Bernardino - Medical Center	34.1350	-117.322
48	CDMG 23920 Yucaipa Valley - Calimesa & Cnty	34.0040	-117.058
49	CDMG 47006 Gilroy - Gavilan Coll.	36.97	-121.568
50	CDMG 47381 Gilroy Array #3	36.9870	-121.536
51	CDMG 47762 Salinas - County Hospital Gnds	36.6970	-121.634
52	CDMG 57383 Gilroy Array #6	37.03	-121.484
53	CDMG 57600 San Jose - Emory & Bellrose	37.3290	-121.937
54	CWB 99999 CHY024	23.76	120.6062
55	CWB 99999 CHY025	23.78	120.5137
56	CWB 99999 CHY026	23.80	120.4113
57	CWB 99999 CHY028	23.63	120.6052
58	CWB 99999 CHY035	23.52	120.5840
59	CWB 99999 CHY036	23.61	120.48
60	CWB 99999 CHY039	23.52	120.3440
61	CWB 99999 CHY042	23.36	120.5833
62	CWB 99999 CHY046	23.4765	120.46

S. No.	Station name	Latitude (°N)	Longitude (°E)
63	CWB 99999 CHY047	23.49	120.4468
64	CWB 99999 CHY052	23.29	120.5010
65	CWB 99999 CHY074	23.51	120.8052
66	CWB 99999 CHY080	23.5972	120.68
67	CWB 99999 CHY086	23.35	120.5932
68	CWB 99999 CHY092	23.7913	120.4783
69	CWB 99999 CHY101	23.6862	120.5622
70	CWB 99999 CHY102	23.25	120.6138
71	CWB 99999 CHY104	23.67	120.4648
72	CWB 99999 HWA002	23.60	121.5122
73	CWB 99999 HWA020	23.81	121.4328
74	CWB 99999 HWA030	23.7852	121.4488
75	CWB 99999 HWA032	23.71	121.4120
76	CWB 99999 HWA035	23.73	121.4362
77	CWB 99999 HWA058	23.97	121.4840
78	CWB 99999 KAU054	23.2777	120.7128
79	CWB 99999 TCU050	24.18	120.63
80	CWB 99999 TCU053	24.1935	120.6688
81	CWB 99999 TCU054	24.16	120.6750
82	CWB 99999 TCU055	24.1392	120.6643
83	CWB 99999 TCU057	24.1732	120.6107

S. No.	Station name	Latitude (°N)	Longitude (°E)
84	CWB 99999 TCU060	24.2247	120.6440
85	CWB 99999 TCU063	24.11	120.6158
86	CWB 99999 TCU065	24.06	120.6912
87	CWB 99999 TCU071	23.99	120.7883
88	CWB 99999 TCU074	23.9622	120.9618
89	CWB 99999 TCU075	23.98	120.6778
90	CWB 99999 TCU076	23.9077	120.6757
91	CWB 99999 TCU079	23.8395	120.89
92	CWB 99999 TCU084	23.88	120.8998
93	CWB 99999 TCU088	24.2533	121.1758
94	CWB 99999 TCU089	23.90	120.8565
95	CWB 99999 TCU100	24.1858	120.62
96	CWB 99999 TCU101	24.24	120.7092
97	CWB 99999 TCU106	24.08	120.5518
98	CWB 99999 TCU107	24.07	120.5402
99	CWB 99999 TCU109	24.08	120.5713
100	CWB 99999 TCU110	23.96	120.5695
101	CWB 99999 TCU111	24.11	120.4872
102	CWB 99999 TCU113	23.8928	120.3865
103	CWB 99999 TCU115	23.96	120.4693
104	CWB 99999 TCU120	23.9803	120.6130

S. No.	Station name	Latitude (°N)	Longitude (°E)
105	CWB 99999 TCU138	23.92	120.5955
106	CWB 99999 TCU139	23.92	120.5403
107	CWB 99999 TCU141	23.8338	120.4640
108	CWB 9999917 TCU	24.15	120.6760
109	CWB 9999917 WNT	23.8783	120.6843
110	CWB 9999936 TCU129	23.88	120.6843
111	ERD 99999 Bolu	40.75	31.6100
112	ERD 99999 Gebze	40.82	29.4400
113	ERD 99999 Iznik	40.44	29.7500
114	ERD 99999 Mudurnu	40.46	31.1820
115	KOERI 99999 Yarimca	40.76	29.7620
116	LAMONT 1059 Lamont 1059	40.75	30.8720
117	LAMONT 1061 Lamont 1061	40.72	30.79
118	LAMONT 1062 Lamont 1062	40.72	30.8200
119	LAMONT 362 Lamont 362	40.67	30.6660
120	LAMONT 531 Lamont 531	40.70	30.8550
121	SCSN 99999 Hector	34.8294	-116.335
122	SGS 129 Loma Linda Univ Medical Center	34.0500	-117.26
123	USGS 1575 Hollister - City Hall Annex	36.85	-121.402
124	USGS 1590 Larkspur Ferry Terminal (FF)	37.95	-122.508
125	USGS 1722 Richmond Rod & Gun Club	37.9780	-122.366

S. No.	Station name	Latitude (°N)	Longitude (°E)
126	USGS 1737 El Cerrito - Mira Vista Country	37.9340	-122.30
127	USGS 1743 Petaluma Fire Station	38.27	-122.658
128	USGS 1749 Richmond - Point Molate	37.9500	-122.42
129	USGS 1751 Novato Fire Station #4	38.07	-122.537
130	USGS 1758 Morgan Hill - El Toro Fire Sta	37.1410	-121.663
131	USGS 1759 Vallejo Fire Station #1	38.11	-122.248
132	USGS 1761 Sonoma Fire Station #1	38.29	-122.457
133	USGS 1762 Novato Fire Station #1	38.0970	-122.565
134	USGS 1767 Santa Rosa Fire Station #1	38.44	-122.701
135	USGS 1768 Petaluma Fire Station #1	38.23	-122.636
136	USGS 1797 Hollister - Airport Bldg #3	36.89	-121.404
137	USGS 5037 Reche Canyon - Olive Dell Ranch	34.0040	-117.223
138	USGS 5043 Hurkey Creek Park	33.68	-116.680
139	USGS 5044 Anza - Pinyon Flat	33.61	-116.453
140	USGS 5069 Fun Valley	33.93	-116.389
141	USGS 5071 Morongo Valley	34.0490	-116.578
142	USGS 5072 Whitewater Trout Farm	33.99	-116.656
143	USGS 5073 Cabazon	33.92	-116.782
144	USGS 5075 Forest Falls Post Office	34.0880	-116.92
145	USGS 5076 Mill Creek Ranger Station	34.0790	-117.045
146	USGS 5160 Anza Fire Station	33.56	-116.674

S. No.	Station name	Latitude (°N)	Longitude (°E)
147	USGS 5161 Highland Fire Station	34.14	-117.213
148	USGS 5162 Mentone Fire Station #9	34.0670	-117.117
149	USGS 5220 Borrego Springs - Scripps Clinic	33.19	-116.329
150	USGS 5222 Anza - Tripp Flats Training	33.60	-116.756
151	USGS 5223 Mountain Center - Pine Mtn Rnch	33.58	-116.590
152	USGS 5232 Idyllwild - Keenwild Fire Sta.	33.71	-116.717
153	USGS 5245 San Bernardino - Co Service Bldg - Freefield	34.11	-117.287
154	USGS 5265 Devore - Devore Water Company	34.24	-117.407
155	USGS 5270 Mecca Fire Station	33.57	-116.076
156	USGS 5294 Indio - Jackson Road	33.75	-116.215
157	USGS 5295 North Palm Springs Fire Sta #36	33.93	-116.548
158	USGS 5300 Seven Oaks Dam Downstream Surf.	34.11	-117.099
159	USGS 5300 Seven Oaks Dam Right Abt.	34.11	-117.099
160	USGS 5327 San Bernardino - Fire Sta. #7	34.17	-117.288
161	USGS 5328 San Bernardino - Mont. Mem Pk	34.05	-117.277
162	USGS 5329 San Bernardino - Fire Sta. #11	34.07	-117.275
163	USGS 5330 San Bernardino - Fire Sta. #9	34.10	-117.349
164	USGS 5331 San Bernardino - Del Rosa Wk Sta	34.1663	-117.251
165	USGS 5331 San Bernardino - Del Rosa Wk Sta	34.1663	-117.251
166	USGS 5336 San Bernardino - Serrano School	34.15	-117.22

S. No.	Station name	Latitude (°N)	Longitude (°E)
167	USGS 5337 San Bernardino - Fire Sta. #4	34.14	-117.294
168	USGS 5339 San Bernardino - Fire Sta. #10	34.0910	-117.289
169	USGS 5341 Colton - Kaiser Medical Clinic	34.06	-117.305
170	USGS 5371 San Bernardino - N Verdemont Sch	34.2050	-117.365
171	USGS 5372 Idyllwild - Kenworthy Fire Sta.	33.62	-116.621
172	USGS 5373 San Bernardino - Lincoln School	34.12	-117.287
173	USGS 5375 Ocotillo Wells - Veh. Rec. Area	33.16	-116.168
174	USGS 5409 Lytle Creek Fire Station	34.2330	-117.482